An investigation into *Shaker*-like potassium channel Kv1.6 and its role in the somatosensory nervous system



Liam Peck

St John's College

University of Oxford

A thesis submitted for the degree of

Doctor of Philosophy

Trinity Term 2019

Title: An investigation into *Shaker*-like potassium channel Kv1.6 and its role in the somatosensory nervous system

Name: Liam Peck **Affiliation:** St John's College, University of Oxford

Degree: Doctor of Philosophy **Term:** Trinity Term 2019

Abstract

Pain is a fascinatingly malleable sensory percept, evoking a unique experience for each individual. Most people who have experienced pain have an inherent understanding of its unpleasantness, and under most conditions this negative affect drives short- and long-term behavioural changes, which serve to protect organisms from potential further harm relating to the offending stimulus. Most commonly, pain is short-lasting, associated with observable physical damage to the body, and reversible. Chronic pain is long-lasting, persisting even after recovery of tissue damage, which can instil societal stigma towards sufferers. 'Neuropathic' pain, associated with prior lesion of the nervous system, is typified by spontaneous pain sensation and pain evoked by non-noxious stimuli – a debilitating symptomatic experience and major global health burden.

Presently, we lack satisfactory treatments for neuropathic pain due to insufficient understanding of maladaptive structural and pathophysiological changes occurring in the nervous system. Neuronal hyperexcitability is a key feature of neuropathic pain. Potassium channels have long been known as regulators of neuronal activity – they are instrumental in ensuring appropriate generation and propagation of action potentials and regulate neural communication by influencing presynaptic neurotransmitter release. There is now a large body of evidence that K^+ channel dysfunction is mechanistically involved in the initiation and maintenance of neuropathic pain, offering novel therapeutic targets.

Ostensibly, the relative ease of genetic manipulation in mice enables us to study individual genes in isolation and assess their functions in health or disease. This thesis comprises an in-depth genetic, anatomical, physiological, and behavioural investigation of two different Kv1.6 knock-out mice. The results of the present study simultaneously reveal an unconventional role for this potassium channel in thermal nociception and a major flaw in the design of certain transgenic animals – namely, that overexpression of exogenous LacZ gene products is not necessarily benign but may induce unsolicited and confounding neurotoxic effects.

Acknowledgements

I am fortunate to have thoroughly enjoyed the four years spent conducting my DPhil research, and there are many people who deserve thanks for ensuring that this was the case. My supervisor, Prof. David Bennett, has provided me with much support and sage scientific guidance since before my DPhil began, when I joined the laboratory as an undergraduate student working under Dr John Dawes, whose mentorship and friendship have been a constant support for the duration of my research career since. The laboratory has a reputation for thorough scientific excellence among the field, yet Prof. Bennett has fostered a delightfully warm environment to work in through positive management of both projects and people in the laboratory. Everyone that has passed through the laboratory has truly been a friend as well as a colleague and they should know that I am very thankful for the fond memories shared over the past four years, and for their scientific and personal support in that time as well. Some of the research in this thesis was conducted in other laboratories, and even overseas. I am thankful to my hosts at Universidad Católica in Santiago, Chile (Associate Prof. Margarita Calvo) and University College London (Prof. Anthony Dickenson), and their laboratory members for welcoming and helping me, as well as to Prof. Andrew Todd at the University of Glasgow for advice and assistance with electron microscopy experiments.

I am also fortunate to have benefited from an OXION studentship provided by the Wellcome Trust, which has enabled the research within this thesis to be carried out. I am grateful to the OXION directors at the University of Oxford, Prof. Stephen Tucker and Prof. Frances Ashcroft, for offering me a place on this prestigious programme, and to the Wellcome Trust for their generosity and support.

Above all, I would like to thank my family and friends who have been constantly supportive throughout all of my education. Without them I would not have been able to produce this work.

Declaration

I declare that the work contained within this thesis is my own, unless otherwise specified. I performed some experiments in other laboratories, with assistance from collaborators. Notable contributions were made by:

- Luis Martín González Gómez at Universidad Católica, Chile, together with whom I performed neuroma surgeries and collected behavioural data for **Chapter III**
- Dr Ryan Patel at University College London, together with whom I collected *in vivo* electrophysiological data for **Chapter V**
- Professor Andrew Todd at the University of Glasgow, who provided electron micrographs from tissue that I collected for **Chapter V**

Contents

Chapter I – Introduction …1

i. Organisation of the somatosensory nervous system …1

a. Cutaneous receptors …2

b. Signal modulation at the first relay station …3

c. Forming the percept: the central representation of pain …6

d. Descending modulation of afferent input …10

ii. Understanding peripheral neuropathic pain …13

a. Acute pain …13

b. Chronic pain …14

iii. Heterogeneity in the dorsal root ganglia and dorsal horn …18

Classification of dorsal root and trigeminal ganglia neurons …18

a. Morphology and electrical properties …19

b. Histochemical properties …20

c. Functionally-defined populations …21

d. Transcriptomics …23

Classification of dorsal horn neurons …25

a. Projection neurons …25

b. Interneurons …26

Methods of investigating DRG and dorsal horn populations …29

iv. Potassium channels and pain …30

a. 'Leak' potassium channels …31

b. Voltage-gated potassium channels …31

Kv1 potassium channels …36

a. Kv1.1 and Kv1.2 …37

b. Kv1.6 …39

v. Aims of this thesis …42

vi. References …43

Chapter II – Characterisation of *Kcna6* expression in the mouse somatosensory axis …54

i. **Results** …57

Dorsal Root Ganglia

a. Quantification of *Kcna6* mRNA via *in situ* hybridisation probes …57

b. Subcellular distribution of Kv1.6 in DRG neurons …60

c. Expression of a *Kcna6* surrogate, β-galactosidase, in *Kcna6*^{tm1Lex} mice …60

Central Nervous system

d. Distribution of *Kcna6* expression in the mouse spinal cord …63

e. *Kcna6* in the brain …66

ii. **Conclusions** …67

iii. **Methods** …73

iv. **References** …78

Chapter III - Behavioural phenotyping of *Kcna6* ^{tm1Lex} knock-out mice …80

i. **Results** …82

Baseline Sensorimotor Behaviour

a. *Kcna6*^{tm1Lex} expressing mice exhibit normal exploratory behaviour and motor function …82

b. Hetero- and homozygous *Kcna6*^{tm1Lex} mice are hyposensitive to noxious heat …82

c. Hetero- and homozygous *Kcna6*^{tm1Lex} mice are mildly hypersensitive to the algogen formalin …84

Experimental Nerve Injury Models

d. *Kcna6*^{tm1Lex} mice sustain post-SNI mechanical hypersensitivity comparably to wild-types …85

e. *Kcna6*^{tm1Lex} homozygotes do not recover from neuroma hypersensitivity …85

f. *Kcna6* mRNA is not altered in the DRG 3 weeks after SNI …86

Chapter III – Continued

ii. **Conclusions** …88

iii. **Methods** …96

iv. **References** …101

Chapter IV– Anatomy and physiology of the *Kcna6* ^{tm1Lex} peripheral nervous system

…104

i. **Results** …107

a. Assessment of hind paw intraepidermal innervation …107

b. Quantification of DRG subpopulations …108

c. *In vitro* calcium imaging of dissociated DRG neurons …109

ii. **Conclusions** …112

iii. **Methods** …117

iv. **References** …122

Chapter V – Anatomy and physiology of the *Kcna6* ^{tm1Lex} dorsal horn …124

i. **Results** …125

a. Dorsal horn pathology in *Kcna6*^{tm1Lex} knock-out mice …125

b. Progressive morphological changes to central primary afferent projections …127

Chapter V – Continued

c. Ultrastructural analysis of degenerating terminals …129

d. *In vivo* dorsal horn physiology …132

ii. Conclusions …135

iii. Methods …140

iv. References …145

Chapter VI – Contributions of *Kcna6* loss vs. *lacZ* expression to the *Kcna6* ^{tm1Lex} phenotype

…147

i. Results …149

a. LacZ is responsible for the aberrant *Kcna6*^{tm1Lex} primary afferent terminal morphology …149

b. 'Clean' *Kcna6*$^{em1(IMPC)J}$ knock-outs also display hyposensitive behavioural tendencies …151

c. *In vitro* Ca^{2+} responses of *Kcna6*$^{em1(IMPC)J}$ DRG neurons to thermal and chemical challenges …156

ii. Conclusions …160

iii. Methods …169

iv. References …173

Chapter VII – Discussion …175

i. **LacZ/β-gal toxicity suggests a role for gangliosides in presynaptic boutons** …175

ii. **Insights into thermal sensation** …181

iii. **Why are Kv1.6 knock-out mice hyposensitive to noxious thermal stimuli?** …187

a. Genetic compensation as a driver of hyposensitivity …188

b. Subunit stoichiometry: Kv1.6 loss could produce Kv1 gain-of-function …188

c. Generic effect on thermosensitive primary afferents …189

d. Developmental loss of a thermosensitive DRG subpopulation …190

iv. **Conclusion** …191

v. **References** …193

Appendix – Antibodies and RT-qPCR primers …196

Word/Page Count:

38,947 words (excluding figure legends, references, and appendix)

197 pages (excluding title page, abstract, acknowledgements, declaration and contents)

Chapter I

Introduction

i. Organisation of the somatosensory nervous system

Somatosensory interpretation of our environment makes an important contribution to the human experience. Through contact with the skin, the body's largest organ, or the visceral epithelia, one can detect a wide dynamic range of external and internal mechanical, thermal, and chemical stimuli. Proprioceptive feedback from muscles and joints meanwhile contributes to an appreciation of our own position in space. These sensations are the product of a highly organised axis involving interactions between specialised peripheral or visceral structures, afferent neuronal activity from the peripheral nervous system, and further activation of complex central nervous system circuits. Collectively, the neuronal component of this axis is termed the somatosensory nervous system. Its activation enables us to discern environmental and internal stimuli in terms of location, modality, intensity, and temporal duration. This highly salient information allows the formation of social bonds through affective tactile stimulation, as well as detection of temperature, accurate motor performance and practical interaction with our surroundings for day-to-day activity. Encompassed within this arm of the nervous system is also the ability to detect high-intensity, noxious stimuli that either cause or pose a threat of physical harm to tissue.

Pain itself, as opposed to nociception, is a complex and malleable percept, defined by the International Association for the Study of Pain (IASP) as "an unpleasant sensory and emotional experience, associated with actual or potential tissue damage, or described in terms of such damage"[1]. This definition is suggestive of the duality of the 'pain experience' – dependent upon both stimulation of the peripheral nervous system and further interpretation or processing of this

input by the central nervous system. Theories abound as to the mechanism by which this percept forms, but through meticulous interrogation of the somatosensory nervous system's structure and function the pain research community has made great strides towards understanding the neural circuitry responsible for pain sensation. This chapter will begin by briefly attempting to unpick the pathways that sensory impulses take from detection in the fingertip to perception in the brain.

a) Cutaneous receptors

Sir Charles Sherrington, through his work on simple spinal reflex arcs, was among the first to recognise that knee extensor and flexor reflexes were mediated by distinct low- and high-threshold receptors, anatomically segregated in the deep and superficial skin, respectively[2]. The work of Sherrington thus provided early evidence for the 'specificity' theory of pain, which posits that there are distinct populations of cutaneous neurons that respond specifically to either innocuous or noxious stimuli. These are varied in their terminal specialisations and in function[3,4] – low threshold receptors are associated with specialised dermal end-organs or hair follicles while high threshold nociceptors have 'bare' nerve endings that penetrate into the epidermis. This description has recently been updated by the discovery of mechanosensitive, non-myelinating Schwann cells in close physical association with these high-threshold fibres, with apparent functional contributions to nociception[5].

Later seminal work by Edgar Adrian, who developed a technique to record from single nerve fibres, demonstrated that the intensity of sensation, including pain, is encoded in the electrical discharge of cutaneous nerve fibres[6]. This encoding manifested not as a positive correlation between stimulus intensity and the magnitude of electrical discharge, which remained constant, but as a correlation between intensity and firing frequency of stimulated fibres, also involving progressive spatial

recruitment of activity in fibres with neighbouring receptive fields. Thus, the all-or-nothing nature of the action potential was confirmed, and the concepts of temporal and spatial summation of neural activity were born. Firing frequency was often adaptive – that is, it gradually reduced as stimulus duration lengthened – and therefore Adrian reasoned that peripheral nerve terminals in the skin are sensitive to environmental *change*. With the refinement of techniques such as *ex vivo* skin-nerve preparations[7] and microneurography[8], it has been possible to further differentiate sensory fibre types by their stimulus-response functions, characteristic firing patterns, and conduction velocity. In general, nociceptors show limited adaptation while low-threshold mechanoreceptors exhibit a much greater degree of adaptation.

Information pertaining to somatosensory stimuli is therefore encoded as some combination of the types of neurons they activate, and the amount and pattern of activity they induce in such neurons. In truth, it is not known exactly how many functionally distinct populations of primary sensory neurons exist, and there is undoubtedly interspecies variation, but sensory neurons and even nociceptors are molecularly heterogeneous populations. This molecular diversity – in particular the repertoire of transducing receptors – imparts responsiveness to particular sensory modalities. Various methods of classifying sensory neurons, which have cell bodies located in the dorsal root and trigeminal ganglia (DRG/TG), will be discussed later in this chapter.

b) Signal modulation at the first relay station

The existence of primary afferent neurons which respond to specific stimulus modalities implies that there may be a 'labelled line' of sensation from the periphery to the brain. The first synapse of primary afferent neurons occurs in the grey matter of the spinal dorsal horn, which, in 1952, Rexed showed is highly organised in terms of cytoarchitecture[9]. Neurons in different Rexed laminae are

structurally distinct from one another, and nociceptive-specific second order neurons were later identified in the most superficial lamina I, the marginal zone[10]. Laminae IV, V and VI neurons were also observed by Patrick Wall to be discernible from one another based on distinct electrophysiological firing properties (including differing degrees of spontaneous activity), peripheral receptive field size and location, and susceptibility to modulation by descending pyramidal tract stimulation[11].

The central terminal projections of primary afferent neurons and the dendritic arborisation of spinal projection neurons were initially visualised via *in vivo* labelling of single cells – typically by iontophoresis of horseradish peroxidase (HRP)[12,13]. This was sometimes accompanied by paired *in vivo* electrophysiological recordings[14] from the labelled primary afferents and spinal projection neurons, which uncovered the anatomical basis of peripheral cutaneous receptive fields represented in the dorsal horn[15]. These early investigations fuelled research into the topographic organisation of the dorsal horn. It was found by Light and Perl that small-diameter fibres projected to superficial Rexed laminae, while large-diameter fibres had deeper termination sites in the simian dorsal horn, including the nucleus proprius[16]. Others such as Réthelyi[17] also identified unmyelinated fibres in the substantia gelatinosa. Within these large and small fibre categories, populations with distinct stimulus-response properties were also reported to terminate at spatially disparate sites within the dorsal horn[18]. Subsequently, histochemically and genetically-defined primary afferent populations have been shown to project to specific laminae, with peptidergic nociceptors terminating in laminae I and III-V[19,20], non-peptidergic nociceptors in lamina II[21], and low-threshold mechanoreceptors in deeper laminae[22].

Although the termination sites of different primary afferent fibre types within the dorsal horn are segregated along the dorso-ventral axis, the various afferent populations innervating similar cutaneous receptive fields project to the same dorsal horn territory on the medio-lateral axis, giving

rise to narrow medio-lateral columns that stretch dorso-ventrally and rostro-caudally within the dorsal horn[23]. These columns exist in a medial-to-lateral somatotopic arrangement at any given spinal level, such that afferent fibre columns from neighbouring receptive fields in the skin are contiguous within the dorsal horn[24,25] **Fig1.1(A)**. Unmyelinated visceral C-fibre afferents terminate over a markedly larger area in both the rostro-caudal and medio-lateral planes[26]; and this comparatively poor anatomical definition may underlie our poor capacity for spatial discrimination of visceral pain. Spatial sensory information and modality therefore appears to be mapped anatomically in the spinal cord by the topographical organisation of primary afferent termination. Taken together these revelations appear permissive for the labelled line or specificity theory.

However, Mendell and Wall had previously discovered the wide dynamic range neuron (WDR)[27]. These deep dorsal horn neurons are responsive to input from fast-conducting, low-threshold A-fibres as well as slowly conducting C-fibres. They are polymodal in that they respond to mechanical and thermal stimuli, and their firing rate directly encodes stimulus intensity and matches human psychophysical reports[28]. Presently, we lack a definitive genetic or histochemical marker for WDRs, making morphological analysis challenging. However, Woolf and King performed anatomical studies on a limited number of HRP-filled, electrophysiologically-characterised WDRs from laminae III-V and found them to be morphologically heterogeneous. The six lamina V neurons identified generally had extensive dorso-ventral, medio-lateral and rostro-caudal dendritic fields, but their axonal projections had highly variable trajectories[29]. The properties of such neurons imply that they receive convergent input from superficial- and deep-terminating primary afferent populations conveying nociceptive and non-nociceptive signals.

Additionally, supraspinal injection of cholera toxin B (CTb) retrogradely labels spinal projection neurons, and this technique has revealed that ascending projections arise from relatively few neurons located in laminae I and III-VI[30,31]. The vast majority of dorsal horn neurons are therefore

locally acting interneurons. In the superficial laminae I-III, interneurons represent >90% of neurons[32], approximately 30% of which express the inhibitory neurotransmitter, GABA[33]. The presence of inhibitory interneurons in the superficial laminae (the substantia gelatinosa) was crucial to Melzack and Wall's 'Gate Control' theory of pain, which allowed for modulation of presynaptic nociceptor input to projection neurons by activity in neighbouring low-threshold fibres[34]. An appropriate balance of spinal inhibitory and excitatory tone is considered necessary to prevent activation of ascending nociceptive pathways by low-threshold primary afferent fibres. This was demonstrated by intrathecal administration of GABA or glycine receptor antagonists, after which pain-like behaviours were evoked in response to light tactile stimulation – an effect preventable in a dose-dependent manner by prior administration of glutamatergic antagonists[35].

Wall had also previously shown that dorsal horn neuron activity could be altered by stimulation from the descending pyramidal tract[11]. Therefore, the majority of primary afferent input to projection neurons is indirect and subject to modulation, and the signal from primary afferents to supraspinal sites is carried by a diminishing number of fibres. These key observations demonstrate that there is a convergence of noxious and non-noxious input at the level of the spinal cord and this contradicts, or at least complicates, the labelled line theory.

c) Forming the percept: the central representation of pain

Even Sherrington was careful to qualify that his experiments on the decerebrate dog were not sufficient to evoke pain unless peripheral nerve endings were "still connected to the sensorium… the neural machinery to which consciousness is adjunct"[2]. Identifying the supraspinal regions that underlie the pain percept is a sought-after achievement, for the development of more targeted pain therapies but also in terms of objectifying pain metrics, which currently rely on subjective self-

reporting as the gold standard. Innocuous sensation was famously mapped to the primary somatosensory area in the post-central gyrus by Penfield and Boldrey's electrical stimulation of the cortex[36]. Stimulation of the sensory 'homunculus' faithfully reproduced spatially localised touch sensation but in general failed to produce painful sensation, nor could another cortical pain area be found. Even with recent stimulation of a more exhaustive list of deeper cortical regions, evoked pain was again scarcely achieved[37].

This is perhaps unsurprising. Indeed, pain serves a tissue-protective role requiring discriminative interpretation of the spatiotemporal aspect and intensity of the stimulus, and primal escape or withdrawal responses engaging appropriate motor units. This much is obvious and is evidenced clinically by extreme phenotypes in families exhibiting congenital insensitivity to pain (CIP). CIP exists in numerous forms and may result from mutations so far identified in genes encoding the sodium channel *SCN9A* [38,39], an epigenetic regulator *PRDM12* [40], nerve growth factor[41] or its receptor *NTRK1* [42–44], and a long non-coding RNA pseudogene *FAAH-OUT* [45]. The common feature of these mutations is complete loss of pain sensation, with preserved sensation of non-noxious touch. Patients suffer repeatedly from traumatic injuries, burns, and other forms of inadvertent self-mutilation from birth.

However, in addition to the tissue-protective function of acute pain sensation, the recurrent nature of these injuries suggests a more profound role for pain in behavioural adaptation. Pain induces negative affective responses leading to short- and long-term modulation of behaviour (e.g. withdrawal reflex versus learned avoidance), via memory formation and cue-associated recall, in order to prevent future decision-making previously associated with pain. This phenomenon is self-evident in normal human behaviour but has also been demonstrated via conditioned place avoidance (CPA) or preference (CPP) assays in animals[46,47]. These usually involve freely moving animals in a multi-chamber apparatus with distinct chamber-specific visual, tactile, or olfactory

features that become paired to, or associated with, either painful stimuli (CPA) or pain relief (CPP). The proportion of time spent in the paired chamber provides an ethological indication of pain memory (CPA) or ongoing pain (CPP). This can be exploited to screen for novel analgesic therapies, which, if successful, may bring about a reduction in CPA or analgesia-induced CPP.

One therefore expects perceived painful stimuli to simultaneously activate multiple neuroanatomical loci – sometimes rather nebulously referred to as the 'pain matrix' – and can appreciate why stimulation of any single cortical region would fail to elicit pain. This is predicted by retrograde anatomical tracing studies, which identified that the ascending fibres of dorsal horn projection neurons branch into collateral axons[48] terminating in the lateral parabrachial nucleus (which projects to, for example, the amygdala and other limbic 'emotional' areas) and the periaqueductal grey[48,49] (stimulation of which promotes profound analgesia[50] via numerous indirect descending pathways to the dorsal horn), and in the thalamus[49] (which shares bidirectional connectivity with the primary somatosensory cortex), among other nuclei[31,49].

The birth of functional magnetic resonance imaging (fMRI) has enabled researchers to assess changes in blood oxygenation (BOLD-fMRI) or perfusion (arterial spin labelling), which are a proxy for neural activity, evoked in localised brain regions by various stimulation paradigms. The difficulty with this approach in understanding pain-specific activity is that many 'pain matrix' centres are activated by any number of audio-visual or psychological influences concurrently acting in the experimental environment – notably tactile stimulation associated with the delivery of noxious stimuli[51]. Nevertheless, groups have developed algorithms to consolidate activity across the pain matrix, providing a signature pattern relating to physical pain that was distinct from emotional pain (rejection paradigms) and was reduced with analgesic treatment[52]. This neurological pain signature (NPS) comprised activity in the insula, secondary somatosensory area, thalamus, hypothalamus, and the anterior cingulate cortex, and was all but absent in one patient with CIP

secondary to *SCN9A* mutation[39], which goes some way to validating the specificity of the computed NPS.

Among the brain regions reported to show activity following noxious stimulation in human imaging studies is the amygdala[53]. This collection of nuclei is associated with fear and negative affect, and shares connectivity with the mesolimbic circuitry via input to the nucleus accumbens (NAc), where release of dopamine from ventral tegmental area (VTA) neurons is known to encode reward-prediction error indicating the salience of external stimuli[54]. Although better known for defects in long-term memory formation resulting from partial hippocampal resection, patient HM also displayed indifference to pain[55] – attributed to an almost complete removal of the amygdala upon post-mortem examination[56].

Recent work on a nociceptive neural ensemble in the basolateral amygdala has begun to dissect this central circuitry encoding the aversive quality of pain[57]. The authors used *in vivo* calcium imaging of the mouse basolateral amygdala (BLA) to identify a neuronal population activated selectively by noxious stimulation. Targeted silencing of this nociceptive neural ensemble was achieved by viral delivery of a Fos-dependent (activity-induced) Cre recombinase, mediating expression of a G_i-coupled inhibitory designer receptor activated by designer drugs (DREADD) after noxious stimulation. Mice which received an injection of clozapine-N-oxide (CNO) to activate the hM4 inhibitory DREADD receptor, and silence the nociceptive BLA neurons, were unaffected in their mechanosensory detection (withdrawal) thresholds but did have deficits in more complex pain-like behavioural components such as limb attendance and escape responses. In addition, on an unrestricted temperature gradient preference paradigm, CNO-treated mice made repeated entries to noxious temperature zones, displaying an apparently impaired ability to learn avoidance from prior exposure to noxious heat or cold.

d) Descending modulation of afferent input

Behavioural decision-making processes require computation of complex cost-benefit analyses from predicted actions and outcomes[58], based on prior experience and, importantly, competing internal cognitive or motivation states, such as potential calorific reward[59,60]. Ultimately, this renders the perceived intensity or salience of pain vulnerable to change based on environmental and emotional context. Thus, identical noxious stimuli are not always faithfully represented as identical in the pain percept. It is implicit in this understanding of pain sensation that there is a degree of bidirectional modulation of afferent sensory information, which must be underpinned by neural circuitry.

This control is mediated in part by descending tracts from the brain to the dorsal horn of the spinal cord. Patrick Wall had described the ability of descending fibres to modulate dorsal horn activity[11], and modulatory input was subsequently shown to originate in the periaqueductal grey area (PAG) via electrical stimulation in rodents, which produced sufficient analgesia for surgical procedures to be performed with no anaesthesia[50]. Involvement of the PAG and spinal cord in placebo analgesia – endogenous pain modulation – has been confirmed in human functional imaging studies[61,62]. The PAG is activated by inputs from superior cortical and subcortical sites and exerts its pain modulatory effects on the dorsal horn via relay neurons in the rostral ventromedial medulla (RVM)[63]. In animal models, analgesia mediated by stimulation or morphine application at any of these sites is be reversed by local naloxone (an opioid receptor antagonist) delivered to more caudal sites, strongly suggesting this effect is mediated by endogenous opioids[63]. Human pain conditions also engage endogenous opioidergic signalling pathways to mediate placebo analgesia, evidenced by naloxone-induced hyperalgesia[64] and PET-based receptor occupancy studies[65]. Recently, the activity of dorsal horn neurons expressing the endogenous opioid enkephalin has been shown to gate mechanical sensitivity in mice[66]; however, there is some evidence that in rats other non-opioidergic, endocannabinoid-mediated analgesic mechanisms exist[60].

As well as descending inhibitory control of afferent impulses, the RVM has the ability to facilitate pain signalling. This is largely due to descending noradrenergic and serotonergic neurons, which may exert inhibitory or excitatory neuromodulatory effects depending on their specific postsynaptic G-protein coupled receptors[67,68]. In general, noradrenaline is thought to be inhibitory, and serotonergic signalling mostly facilitative, of pain[68], and the existence of monoamine signalling in the dorsal horn potentially provides some mechanistic insight to the clinical success of serotonin/noradrenaline reuptake inhibitors (SNRIs) in treating neuropathic pain[69]. The targets expressing these monoamine receptors are among the milieu of neuronal dorsal horn populations now known to integrate, modulate, and transmit sensory input from primary afferents.

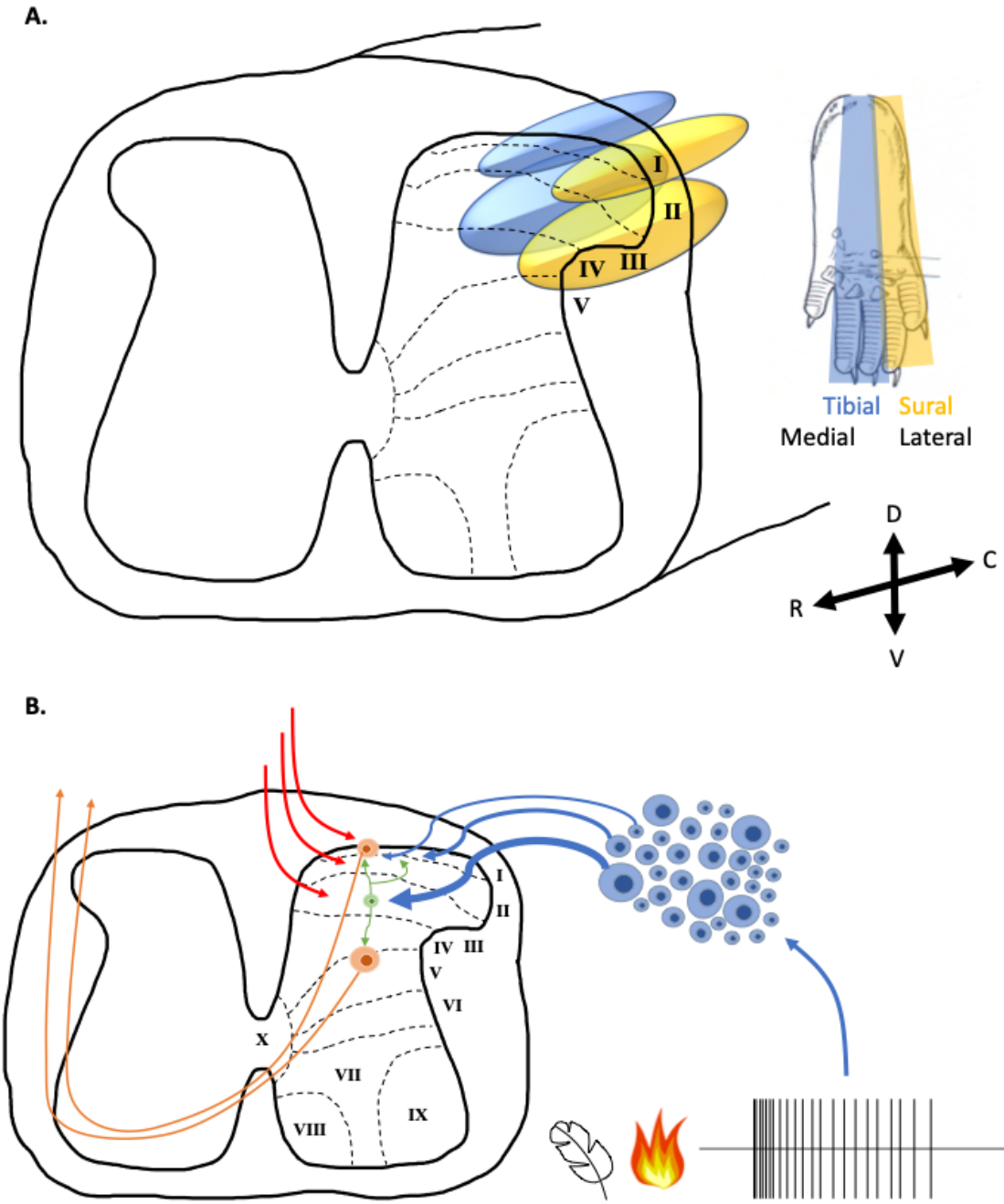

Figure 1.1 – The junction between the peripheral and central somatosensory nervous system

(A) Primary afferents terminate with somatotopic and modality-specific topography in the dorsal horn. For example, afferents from adjacent hind-paw skin territories form distinct branches of the sciatic nerve (tibial/sural) and terminate in adjacent dorso-ventral / rostro-caudal columns within the dorsal horn **(blue/yellow ellipsoid regions)**. Within these columns, nociceptive fibres **(small ellipsoid)** generally terminate in superficial laminae I-II, while low-threshold non-nociceptive afferents **(large ellipsoid)** terminate in deeper laminae.

(B) Action potentials **(black trace)** elicited in distal cutaneous or visceral primary afferent terminals propagate along axons of mechanoreceptors, thermoreceptors, and nociceptors. These neurons have cell bodies located in the DRG **(blue)** and terminate in the dorsal horn of the spinal cord. Innocuous touch is generally conveyed by large-diameter fibres projecting to deep laminae, while nociception is generally a function of medium and small-diameter fibres terminating in superficial laminae. Spinal projection neurons **(orange)** are reside in laminae I and III-IV and are the second neuronal conduit for afferent sensory information. The majority of neurons in the dorsal spinal laminae are interneurons **(green)**, which receive direct input from primary afferents and exert modulatory control over projection neurons, other interneurons, and primary afferent terminals. Afferent signals are also modulated by monoaminergic fibres **(red)** descending from supraspinal nuclei, which have facilitatory or inhibitory effects. Thus, the dorsal horn is a major site of sensory integration.

ii. Understanding neuropathic pain

Intuitively, we understand that pain takes many forms. It can be classified according to: anatomical site and pattern of radiation, temporal profile (acute versus chronic), character, alleviating or exacerbating factors including pharmacotherapy, associated symptoms, underlying aetiology, and severity. For example, pain can be local, diffuse or multifocal; transient, persistent or remitting; sharp or dull; burning; lancinating – to list but a few examples. Pain may occur as a result of damage or threatened damage to non-neural tissue (nociceptive pain), or as a result of lesion or disease to the somatosensory nervous system (neuropathic pain), or in the absence of either ('nociplastic' pain). Much emphasis has been placed on the semantics of these pain descriptors[70], and while this has been met with some scepticism[71], this is an important pursuit for standardisation of diagnoses[72] and phenotyping and stratification of patients[73–75], as well as providing patients with some validation that their symptomatic experience falls within a defined mechanistic category.

a) Acute pain

Pain is the result of a complex integration of stimulus intensity, environmental and historical context, vulnerability, motivational or emotional states, beliefs and cognition. However, when controlling for these influencing factors, acute 'nociceptive' pain is characterised as resulting from direct activation of peripheral (including visceral) nociceptors, and generally the perceived location, intensity and duration match those of the stimulus. Useful tissue-protective and informative functions, usually promoting aversion, are hallmarks of acute nociceptive pain. Pain may warn of potential injury or inform us of actual injury. In the latter case, where tissue damage has occurred, the release of inflammatory mediators and neuroactive substances from damaged tissue and peripheral nerve endings acts to sensitise nociceptors, usually through direct effects of these

sensitising agents on transduction channels and receptors. For example, the TRPV1 receptor, a transducer of noxious heat[76], is modulated by extracellular acidification and inflammatory agents[77,78]. Sensitisation takes the form of a shift in stimulus-response function towards lower activation thresholds, and results in hyperalgesia – an augmentation of the perceived intensity of suprathreshold stimuli. However, this phenomenon is usually short-lived and resolves with tissue repair.

Pharmacological relief of acute pain is usually effective[79,80] and typically involves approaches targeting components of the inflammatory response to tissue damage (e.g. non-steroidal anti-inflammatory drugs, NSAIDs), blockade of action potential conduction from the periphery via sodium channel antagonists (e.g. local anaesthetics), or the use of opioid analgesics such as codeine – with diverse mechanisms likely involving potentiation of descending inhibitory pathways and direct inhibitory effects on peripheral sensory neurons[81].

b) Chronic pain

Chronic pain, defined in the international classification of diseases (ICD-11) as that which persists in spite of treatment for greater than 3 months[82], represents a much greater clinical challenge. According to the 2013 Global Burden of Disease Study[83], chronic back pain was considered the single greatest contributor of 'years lived with disability' (YLDs)[84] – a metric which takes into account the prevalence and severity weighting of disease. Five other chronic pain conditions ranked in the top 20 causes of YLDs, including neck pain and migraine, which was the 7th most common chronic disease overall. The annual economic cost associated with chronic pain, accounting for medical costs as well as losses in the employment sector, has been calculated to exceed $600 billion,

as a conservative estimate, in the United States[85] – more than double that of cardiovascular disease ($300bn) or cancer ($250bn).

Among chronic pain disorders, neuropathic pain specifically must be associated with an anatomically plausible history of lesion or disease to the somatosensory nervous system[72]. The location of pain should be related to that of the neurological lesion, but the precise injurious aetiology may vary. For example, neuropathic pain may precipitate as a consequence of cardiovascular, metabolic or infectious disease (stroke, diabetic peripheral neuropathy, postherpetic neuralgia), Mendelian genetic mutations (inherited erythromelalgia), nerve compression (carpal tunnel syndrome), iatrogenic cancer intervention (chemotherapy-induced peripheral neuropathy, CIPN), or traumatic nerve injury, among other conditions[86]. In recent years, autoimmunity has emerged as a causal factor in examples of neuropathic pain previously considered idiopathic in nature[87–90].

As neuropathic pain is defined as persisting for at least several months after the initial injury, it is unsurprising that patients are generally refractory to the acute pain pharmacotherapeutic strategies described earlier, which usually target the immediate inflammatory consequences of injury. The understanding that neuropathic pain does not simply lie on a temporal continuum with acute pain has been an important paradigm shift in our approaches to treatment. Much work has been done to establish that neuropathic pain may manifest as a result of maladaptive, plastic changes within the somatosensory nervous system at molecular scale affecting synaptic structure and function, and at circuit and macroscopic structural levels[91]. Such changes have been observed at all levels of the somatosensory system. Through experimental procedures outlined earlier it is known that pain perception may be modulated at peripheral, spinal, and supraspinal sites and this potentially opens novel therapeutic avenues. The analgesics with greatest efficacy in neuropathic pain are those targeting monoaminergic signalling (tricyclic antidepressants, and SNRIs)[69], which have presumed

mechanisms of action within the descending pain modulatory system (DPMS). Altered functional connectivity in the DPMS correlates with chronic pain phenotypes[92], for example conferring vulnerability to pain in diabetic neuropathy[93]. However, there is a dearth of longitudinal pre- to post-treatment imaging studies in human chronic pain conditions and it is difficult to ascertain what is cause and what is effect. As an example, effective treatment of chronic low back pain was reported to reverse macroscopic volumetric loss associated with pain in prefrontal brain structures[94], so these structural changes may either be responsible for or a consequence of chronic pain induction and maintenance, or both.

Neuropathic pain may result from central or peripheral nervous system lesions. The focus of the work presented in this thesis predominantly relates to neuropathic pain precipitated by peripheral lesions. However, the site of the initial lesion does not restrict mechanisms of pain maintenance to the peripheral or central nervous system. As discussed, structural and functional plasticity may occur at any point along the sensory neuraxis. The debate over the relative importance of central and peripheral mechanisms of peripheral neuropathic pain has been long and hard fought[95]. A cardinal feature of neuropathic pain is spontaneous pain sensation, in the absence of any clear stimulus. Ectopic activity in C-fibres has been observed via microneurography recordings in patients with painful peripheral neuropathies[96]. There is also increased ectopic discharge and reduced rheobase in dissected human DRG neurons that previously innervated dermatomes affected by radicular pain, compared with both same-subject internal control neurons from pain-free dermatomes and healthy external control neurons[97]. It is easily conceivable that such examples of ongoing input from the periphery might bring about spontaneous pain, and if sufficient may induce central mechanisms of sensitisation.

In terms of maladaptive cortical plasticity in the 'absence' of peripheral input, the poster child is phantom limb pain following amputation. This unfortunate condition has been the subject of many

fanciful mechanistic theories, including the highly popularised concept that the cortical real estate once occupied by the amputated limb may infiltrate neighbouring somatosensory cortex – such that sensation in the neighbouring body part may be referred to the phantom limb[98]. This is theoretically possible, but the evidence from functional brain imaging in amputees now favours preservation of normal hand representation in the somatosensory cortex, with minimal cortical remapping[99,100]. It has also recently become clear that there is a tonic ectopic drive from axotomised primary afferents in the amputated limb, arising from both the terminal stump and cell bodies in the more proximal dorsal root ganglion (DRG)[101]. Blockade of spontaneous firing by intrathecal or intraforaminal lidocaine injection provided rapid and reversible relief from spontaneous phantom limb pain and innocuous phantom sensation, in a titratable fashion[101]. Thus, even regional pain disorders thought to manifest from central sensitisation may respond to therapies targeted to sensory neurons of the DRG, which reflects novel understanding of the peripheral mechanisms perpetuating neuropathic pain.

It is somewhat more difficult to conceive of primary afferent ectopia driving pain mediated by central lesions. However, it has also been demonstrated in a small cohort of patients that spontaneous 'central' post-stroke pain localised to one limb was completely improved by peripheral nerve block in the relevant anatomical territory with lidocaine[102]. There is additional evidence in mice that spinal cord injury can induce upregulation of sodium channel Nav1.8 in the DRG, resulting in ongoing spontaneous electrical activity; post-injury siRNA knock-down of the channel was effective in reducing Nav1.8 currents, reflexive hypersensitivity, and CPP for analgesic-paired chambers[103]. While the CNS is undoubtedly implicated in sensitising and modulating the overall pain experience, these are compelling cases for tonic peripheral input from primary afferents as a key driver of neuropathic pain – following both central and peripheral nervous system lesions. An improved understanding of DRG and dorsal horn subpopulations may therefore enable more targeted and effective treatment of neuropathic pain.

iii. Heterogeneity in the dorsal root ganglia and dorsal horn

The complexity of the perceptual experience of pain is reflected in the known anatomy for transduction, transmission, and processing of nociceptive and non-nociceptive information. The peripheral sensory neural axis relays sensory information from specialised receptor end-organs, and 'free' nerve endings in the skin and visceral organs, to various loci in the brain via the spinal cord. As the first afferent-signalling cells in the sensory neuraxis, primary sensory neurons are entirely necessary for our ability to detect environmental stimuli across the noxious and innocuous tactile, thermal and chemical modalities. This ability is underpinned by functional expression of ionotropic and G-protein-coupled receptors that transduce external stimuli to electrical signals via depolarisation of primary afferent terminals[104,105]. Subsequent successful transmission of these signals is dependent on appropriate expression of voltage-gated sodium[106], potassium[107] and calcium[108] channels. There is remarkable diversity among sensory neurons and their synaptic partners in the dorsal horn. Numerous classification systems have been applied to neurons in the dorsal root and trigeminal ganglia, and the dorsal horn, ranging from sorting by morphological and electrophysiological parameters to pharmacological, histochemical or molecular genetic profiling. There has been a concerted effort over the years to attribute function to these distinct populations in order to understand their relative contributions to the conveyance and interpretation of pain and discriminative touch in health and disease.

Classification of dorsal root and trigeminal ganglia neurons

While a 'labelled line' may not exist directly from the periphery to the brain, an expansive body of research exists to suggest that many of the distinguishing perceptual features of external stimuli are encoded at the peripheral level by activity in distinct populations of neurons. In the context of

neuropathic pain, where ectopic activity in sensory neurons maintains a chronic pain percept, non-selective inhibition of peripheral nerve signalling is an unsatisfactory therapeutic approach due to its impact on normal sensory and motor function. Thus, there is a considerable demand to identify the functional populations encoding different modalities and those responsible for the initiation and maintenance of neuropathic pain, which may inform more targeted pain therapies.

a) Morphology and electrical properties

Primary afferents can be most simply defined on the basis of size. The prevailing assumption has been that (Aβ) neurons with large-diameter somata and axons, that are thickly myelinated and conduct rapidly, convey information pertaining to touch. Meanwhile, pain is encoded in the activity of more slowly conducting medium- and small-diameter (Aδ and C) neurons with thin or no myelination, respectively[109]. Distally, large-diameter, low threshold mechanoreceptors project to the dermis where they interact with specialised end-organs and hair follicles and transduce non-noxious mechanical stimulation[3]. Nerve endings of small- to medium-diameter fibres innervate the epidermis, ensheathed by mechanosensitive Schwann cells[5] and expressing an array of ion channels and other receptors capable of transducing noxious stimuli[104,105]. There are, however, some notable exceptions to these general rules, such as Aδ-hair afferents and C-fibre low threshold mechanoreceptors (Aδ-/C-LTMRs)[3], as well as high-threshold Aβ-fibres with activity correlating with psychophysical pain reports[110]. Further sub-classifications have made within these populations on the basis of stimulus-response function and adaptation of firing frequency[7].

Some afferent populations can also be distinguished by the morphology of their central terminals. Ribeiro-da-Silva and Coimbra identified two main types of synaptic glomeruli, where primary

afferents make multiple synaptic connections, within laminae II-III[111]. Type I glomeruli are characterised by electron-dense cytoplasm with variable vesicle diameter and few mitochondria, and are thought to originate from non-peptidergic, unmyelinated nociceptors[112]. Type II glomeruli are larger, more electron-lucent, and contain numerous mitochondria; these are thought to represent terminals of A-LTMR fibres due to the occasional co-localisation of neurofilaments and their distribution in ventral lamina II and lamina III[111]. However, C-LTMR fibres labelled genetically by Tafa4 expression or by co-localisation with vesicular glutamate transporter 3 (Vglut3) have been shown to form type I[113] or type II[114] glomerular structures, respectively. Peptidergic afferents may form glomerular or non-glomerular termination structures, and typically contain dense-core vesicles[19,115].

b) Histochemical properties

One of the oldest and most common approaches to distinguish cell types in the sensory ganglia is by histochemical markers. In reality, there are potentially as many markers as there are genes expressed in sensory neurons, but the classical population-defining markers used throughout this thesis are introduced here. In rodents, neurofilament 200 (NF200) expression delineates the myelinated population, including Aβ- and Aδ-fibres[116]. One category of nociceptors is distinguished by the expression of neuropeptides such as calcitonin gene-related peptide (CGRP) and substance P (SP), which overlap to some extent with the NF200 population (these are probably Aδ-nociceptors). 'Non-peptidergic' nociceptors are instead marked by binding of *Griffonia simplicifolia* isolectin B4 (IB4)[117], although there can be significant overlap of IB4-binding with $CGRP^+$ neurons that varies between species (rat >> mice) and sensory ganglia (DRG > TG)[118]. C-LTMRs – the putative transducers of pleasant light touch[119,120] – can be identified by their expression of tyrosine hydroxylase (TH).

The majority of neurons in the spinal cord are glutamatergic, including all primary afferent neurons. However, differences in expression of presynaptic vesicular glutamate transporter (Vglut) proteins have been described between populations. Specifically, in the rat Vglut1 expression is detected in presynaptic terminals of myelinated low-threshold afferents projecting to laminae III-VI, including type II glomerular structures, as well as more ventral laminae[121,122]. Vglut2 was detected in superficially terminating myelinated and unmyelinated nociceptive populations, albeit with weak immunoreactivity – this transporter is much more strongly expressed in intrinsic excitatory interneurons of the substantia gelatinosa[121,122]. There is co-expression of these transporters in myelinated afferents[121] and these distributions are broadly the same in the mouse[123]. Within the dorsal horn, a third transporter (Vglut3) appears to be expressed specifically by C-LTMRs[124] forming type II glomerular synapses within ventral lamina II.

c) Functionally-defined populations

Among nociceptors, the presence or absence of peptides does not proffer much information *per se* regarding cell function. The identification of molecular transducers of mechanical, thermal and chemical stimuli, such as stretch-activated Piezo channels for mechanosensation[125] and the transient receptor potential (TRP) channel family for thermo- and chemosensation[126,127], has been instrumental in advancing our understanding of sensory transduction but also the contributions of discrete populations to sensation. Deletion of the Piezo2 channel in sensory neurons and Merkel cells, for example, results in loss of mechanically-evoked currents and behavioural hyposensitivity to innocuous tactile stimuli[125], with similar deficits observed in loss-of-function PIEZO2 mutations in humans[128]. Transducers of noxious mechanical stimuli are still largely unknown, although Piezo2 appears to have some involvement[129].

Trpv1, the cloned receptor for chilli pepper-derived capsaicin, was identified as a cation channel activated by >43ºC heat and potentiated by inflammatory agents; a promising molecular correlate for noxious heat but also nociceptor sensitisation[76,77]. In adult mice, this channel is largely but not exclusively restricted to peptidergic afferents[118,130,131], and either Trpv1 knock-out or ablation of $Trpv1^+$ afferents with intrathecal capsaicin or resiniferotoxin results in specific behavioural deficits for both noxious heat sensation and inflammation-induced thermal hypersensitivity[132–134]. Conversely, ablation of $Mrgprd^+$ afferents, a large subset of non-peptidergic C-fibres[135,136], causes profound mechanical hyposensitivity[133]. The two effects could be superimposed by Trpv1 ablation in Mrgprd-ablated mice, with no additive effect on mechanical sensation[133]. Meanwhile, $CGRP^+$ fibre ablation also selectively reduces noxious thermal sensitivity[137], suggesting a dichotomous relationship of heat and mechanical sensation in peptidergic and non-peptidergic fibres, respectively.

However, Trpv1 knock-out mice retain some degree of residual behavioural heat sensitivity[132] and a population of IB4-binding neurons are responsive to noxious heat[130], so there appears to be functional redundancy in the transduction of noxious heat and a potential role for non-peptidergic nociceptors. Through a combined knock-out approach, it is now proposed that Trpv1, Trpm3, and Trpa1 form a trio of channels that each are independently capable and sufficient for transducing noxious heat and inducing withdrawal behaviours, whereas loss of all three channels totally abrogates heat-evoked withdrawal responses[138]. Meanwhile, other cold-transducing ion channels such as Trpm8[139] and, paradoxically, Trpa1[140,141] are believed to underlie sensitivity to innocuous and noxious cold respectively[142]. Warmth sensation is poorly understood, but current opinion favours a role for Trpm2[143] over previous candidates Trpv3/4, which only determine thermal preference behaviour on certain genetic backgrounds[144]. The sensitivity of TRP channels to natural chemical compounds such as capsaicin (Trpv1), pregnenolone sulphate (Trpm3), menthol (Trpm8) or allyl isothiocyanate (Trpa1) provides an *in vitro* proxy for estimating

percentages of sensory neurons sensitive to thermal stimuli and their overlap, but this is an indirect approach and makes assumptions that functional TRP channel expression *in vitro* both matches that *in vivo* and guarantees thermal sensitivity. More recently, various temperature stimulation paradigms have seen more use[138,140,143,145–148], as has *in vivo* DRG imaging[149–151], but where quantifications have been made, these have individually failed to capture the entire thermal spectrum and have varied considerably in their assertions about the proportion of temperature-transducing sensory neurons.

The outcomes of various behavioural studies contributing to our understanding of the major molecular candidates and DRG populations underlying different sensory modalities have been amalgamated and summarised in **Fig1.2**.

d) Transcriptomics

With the rise in popularity and feasibility of transcriptomic analyses, sensory neuron populations are being scrutinised in ever more detail. In recent years there have been several large-scale attempts to define sensory neuron populations based on gene expression cluster analysis from single-cell RNA sequencing of DRG neurons[152–155]. These clusters have been validated with *in situ* hybridisation and largely agree with segregation of neurons based on classical histochemical markers, (NF200, CGRP, Non-peptidergic, TH) but further subdivide these populations into a total of 17 clusters at the latest count[155]. With the assumption that genetic diversity defines functional diversity in sensory neurons, there is now an impetus to seek out genes which define these clusters with high specificity, such that new mouse strains may be developed that will enable researchers to interrogate the function of smaller, better-defined populations[105,156].

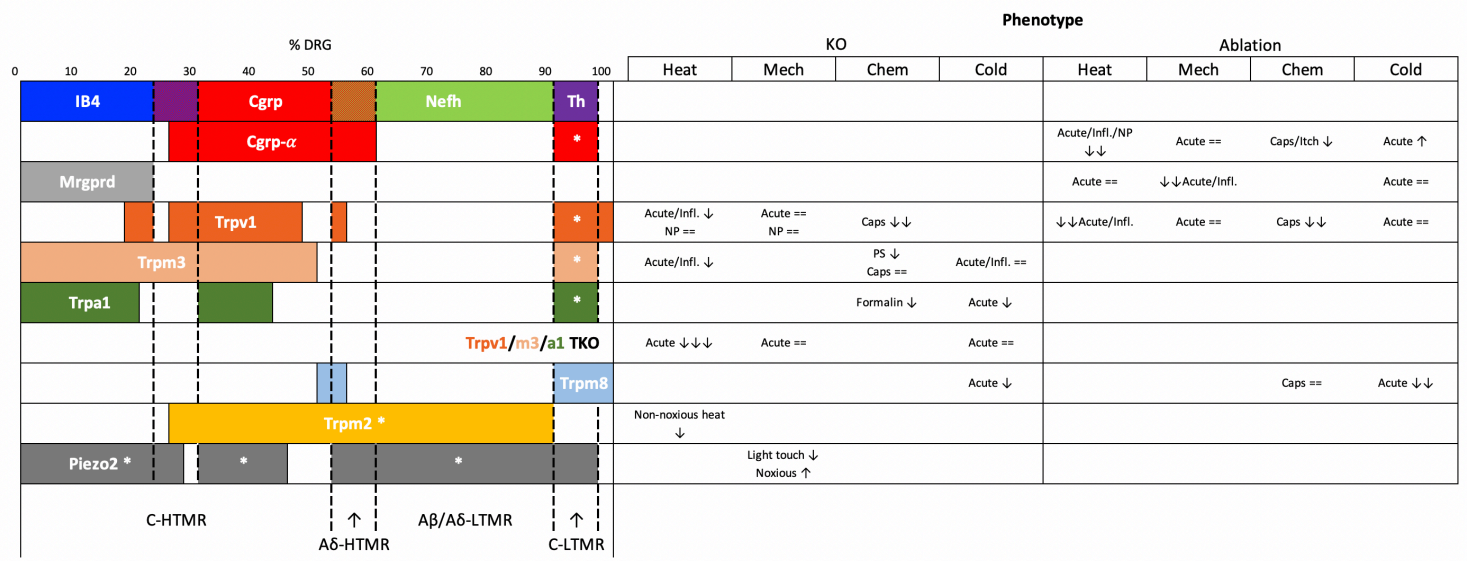

Figure 1.2 – Molecular and functional classification of DRG neurons

Numerous attempts have been made to classify of DRG neurons into populations serving distinct functions.
This figure represents an effort to consolidate reports of expression of population-defining molecular markers in the mouse DRG from studies utilising immunohistochemistry, transgenic reporter mice, *in situ* hybridisation, *in vitro* pharmacology, and bulk and single-cell RNA sequencing. Conflicting results are rife in the published literature, so the values in this figure are not simply an additive sum of evidence from each technique or each publication. Instead, an approximation has been made based on the weight of evidence available for and against expression of each marker from the various techniques used.

* Where possible, direct evidence of *functional* expression, i.e. protein or agonist-evoked response, has been used so evidence gleaned from mRNA expression alone is marked by an asterisk.
Behavioural Phenotypes: ↓ = hyposensitive; ↑ = hypersensitive, == = no change, blank = not tested
Acute = typically withdrawal threshold or similar, Infl. = inflammatory hypersensitivity, NP = neuropathic (nerve injury) hypersensitivity,
PS = pregnenolone sulphate (Trpm3 agonist), caps = capsaicin (Trpv1 agonist)

Sources

Barabas, M. E., Kossyreva, E. A. & Stucky, C. L. TRPA1 Is Functionally Expressed Primarily by IB4-Binding, Non-Peptidergic Mouse and Rat Sensory Neurons. PLoS One 7, e47988 (2012).
Bautista, D. M. et al. The menthol receptor TRPM8 is the principal detector of environmental cold. Nature 448, 204–208 (2007).
Camino, D. del et al. TRPA1 contributes to cold hypersensitivity. J. Neurosci. 30, 15165–15174 (2010).
Caterina, M. J. et al. Impaired nociception and pain sensation in mice lacking the capsaicin receptor. Science (80-.). 288, 306–313 (2000).
Cavanaugh, D. J. et al. Distinct subsets of unmyelinated primary sensory fibers mediate behavioral responses to noxious thermal and mechanical stimuli. Proc. Natl. Acad. Sci. U. S. A. 106, 9075–80 (2009).
Cavanaugh, D. J. et al. Restriction of Transient Receptor Potential Vanilloid-1 to the Peptidergic Subset of Primary Afferent Neurons Follows Its Developmental Downregulation in Nonpeptidergic Neurons. J. Neurosci. 31, 10119–10127 (2011).
Jankowski, M. P., Rau, K. K. & Koerber, H. R. Cutaneous TRPM8-expressing sensory afferents are a small population of neurons with unique firing properties. Physiol. Rep. 5, e13234 (2017).
Karashima, Y. et al. TRPA1 acts as a cold sensor in vitro and in vivo. Proc. Natl. Acad. Sci. U. S. A. 106, 1273–1278 (2009).
McCoy, E. S. et al. Peptidergic CGRPα Primary Sensory Neurons Encode Heat and Itch and Tonically Suppress Sensitivity to Cold. Neuron 78, 138–151 (2013).
McNamara, C. R. et al. TRPA1 mediates formalin-induced pain. Proc. Natl. Acad. Sci. 104, 13525–13530 (2007).
Mishra, S. K. & Hoon, M. A. Ablation of TrpV1 neurons reveals their selective role in thermal pain sensation. Mol. Cell. Neurosci. 43, 157–163 (2010).
Pogorzala, L. A., Mishra, S. K. & Hoon, M. A. The Cellular Code for Mammalian Thermosensation. J. Neurosci. 33, 5533–5541 (2013).
Price, T. J. & Flores, C. M. Critical Evaluation of the Colocalization Between Calcitonin Gene-Related Peptide, Substance P, Transient Receptor Potential Vanilloid Subfamily Type 1 Immunoreactivities, and Isolectin B4 Binding in Primary Afferent Neurons of the Rat and Mouse. J. Pain 8, 263–272 (2007).
Ranade, S. S. et al. Piezo2 is the major transducer of mechanical forces for touch sensation in mice. Nature 516, 121–125 (2014).
Takashima, Y. *et al.* Diversity in the neural circuitry of cold sensing revealed by genetic axonal labeling of transient receptor potential melastatin 8 neurons. *J. Neurosci.* **27**, 14147–14157 (2007).
Tan, C. H. & McNaughton, P. A. The TRPM2 ion channel is required for sensitivity to warmth. Nature 536, 460–463 (2016).
Teichert, R. W. et al. Functional profiling of neurons through cellular neuropharmacology. Proc. Natl. Acad. Sci. U. S. A. 109, 1388–95 (2012).
Vandewauw, I. et al. A TRP channel trio mediates acute noxious heat sensing. Nature 555, 662–666 (2018).
Vriens, J. et al. TRPM3 Is a Nociceptor Channel Involved in the Detection of Noxious Heat. Neuron 70, 482–494 (2011).
Winter, Z., Gruschwitz, P., Eger, S., Touska, F. & Zimmermann, K. Cold Temperature Encoding by Cutaneous TRPA1 and TRPM8-Carrying Fibers in the Mouse. Front. Mol. Neurosci. 10, 209 (2017).
Woodbury, C. J. et al. Nociceptors Lacking TRPV1 and TRPV2 Have Normal Heat Responses. J. Neurosci. 24, 6410–6415 (2004).
Zeisel, A. et al. Molecular Architecture of the Mouse Nervous System. Cell 174, 999-1014.e22 (2018).
Zhang, M., Wang, Y., Geng, J., Zhou, S. & Xiao, B. Mechanically Activated Piezo Channels Mediate Touch and Suppress Acute Mechanical Pain Response in Mice. Cell Rep. 26, 1419-1431.e4 (2019).
Zheng, Y. et al. Deep Sequencing of Somatosensory Neurons Reveals Molecular Determinants of Intrinsic Physiological Properties. Neuron 103, 1–19 (2019).

Classification of dorsal horn neurons

Nociceptors terminate in the ipsilateral dorsal horn of the spinal cord at or within several spinal levels of their nerve root. The importance of the dorsal horn in somatosensory and pain processing, first posited by Melzack and Wall[34], has been alluded to earlier in this chapter. The major neuronal components of the dorsal horn can be divided into the incoming primary afferent terminals, projection neurons that provide output to higher brain centres, and locally extending interneurons as well as descending axons that are both responsible for signal modulation prior to its output. The overwhelming majority of neuronal profiles in the dorsal horn are interneurons[31]. As described, primary afferent fibres appear to have high specificity for distinct modalities, and the laminar organisation of their termination sites give reason to make the logical assumption that in general superficial dorsal horn neurons relate to pain sensation and deep dorsal horn neurons respond to innocuous mechanical stimulation. These assumptions have been confirmed experimentally by electrophysiological slice recordings[10] and nociceptive c-Fos induction[157]. Discriminative touch is of course also conveyed via the ascending dorsal column-medial lemniscus pathway, but the relevance of these two distinct termination pathways for LTMRs is unclear.

a) Projection neurons

Retrograde labelling from supraspinal sites has identified populations of projection neurons that express the NK1 receptor for peptidergic nociceptor transmitter substance P in laminae I and III-V of the dorsal horn[30,48], and in the lateral spinal nucleus (LSN)[31]. Close apposition of CGRP/SP boutons to lamina I projection neurons and expression of neural activity marker c-Fos following noxious stimulation indicate that there is direct input from peptidergic nociceptors to this population[157]. However, much of the input from deeper terminals to lamina I is polysynaptic via

several interneuron populations[4,158], notably vertical cells with dendrites that extend ventrally through laminae II-III and axons projecting to lamina I, and are thus anatomically well placed to integrate input from nociceptors, LTMRs, and other interneurons[32]. Less is known of the input to deeper laminae projection neurons, although likewise there is mixed input from primary afferents and interneurons[31]. Neurons of the LSN receive minimal direct input from primary afferents and respond relatively selectively to mechanical pressure to deep tissues[159].

Wide dynamic range neurons are a curious population that are often considered to be projection neurons, although anatomical evidence for this is lacking due to an absence of histochemical markers. Few morphological analyses have been attempted via camera lucida images of filled cells following intracellular recording[29]. However, this is not routinely performed – most often these cells are recorded from with extracellular electrodes and are defined by their electrophysiological and stimulus-response properties. These cells are of interest in chronic pain as they are polymodal, encode stimulus intensity from low-threshold and nociceptive input[27,28], and exhibit morphological and electrophysiological plasticity, in the form of dendritic spine remodelling[160] after nerve injury or electrical wind-up with repetitive stimulation[27] – which are phenomena that we may expect to occur in sensitised states.

b) Interneurons

The major synaptic targets of primary afferents are interneurons. The resident interneurons of laminae I-III are most well-characterised and can be divided into excitatory (glutamatergic) and inhibitory (GABA-/glycinergic), which represent approximately 70% and 30% of interneurons in this region respectively based on stereological estimates[33]. These have predominantly been categorised based on morphological and electrophysiological properties[161], with these definitions

increasingly being matched to minimally-overlapping neurochemical expression[32,162–164] and transcriptomics-based cell clustering[165,166] to define functional populations. This genetic information is increasingly being used to identify and study populations via Cre-reporter mice, in primary afferents and the dorsal horn alike, but must be used with caution as non-inducible Cre mice can overestimate adult populations due to transient developmental expression[131,167].

Expression of neuropeptides and other proteins has been used to account for almost all inhibitory interneurons of the superficial dorsal horn, which express the inhibitory fate-determining transcription factor Pax2. In total, five populations have been identified, expressing calretinin, parvalbumin, nNOS, galanin/dynorphin, and neuropeptide Y[162]. Loss or silencing of inhibitory interneuron populations reveals that they generally impose a tonic inhibition on nociception and itch[168,169], and it has been suggested that neuropathic pain in part manifests due to disinhibition of pain signalling – immunostaining for GAD65, a GABAergic synaptic marker, shows loss of inhibitory synapses in laminae I-II after chronic constriction injury of the sciatic nerve, which correlates temporally and in magnitude with behavioural hypersensitivity[170]. However, peripheral axotomy has been shown by others to induce mechanical allodynia with no loss of GABAergic synapses[171]. *Boyle et al. (2019)* also contested the concept of structural loss of GABAergic interneurons or their synapses and instead found that parvalbumin-expressing (PV^+) interneurons remained structurally intact but were functionally defective resulting from an intrinsic reduction in membrane excitability[25]. This population forms feedback axo-axonic synapses on myelinated primary afferent terminals or vertical cell dendrites, ordinarily gating LTMR input to lamina I projection neurons via vertical cell conduits[25,172]. PV^+ axonal processes extend laterally between somatotopic boundaries in the dorsal horn; thus, disinhibition through reduced PV^+ neuron activity may partly underly 'central sensitisation' and allodynia in skin territories adjacent to injury sites. Disinhibition may also occur, for example, by nerve injury-induced KCC2 downregulation and dysfunctional chloride signalling[173]. This mechanism is common to males and females, although

the upstream activation of microglia by primary afferent-derived CSF-1[174] is only necessary in males[175].

As well as tonic inhibition of nociception from inhibitory interneurons, there are feed-forward polysynaptic mechanisms involving excitatory and inhibitory interneurons that ordinarily prevent low-threshold stimuli from activating ascending pain pathways. According to some reports, LTMR input is necessary for inflammatory and neuropathic hypersensitivity[176,177]. These polysynaptic inhibitory interneuron circuits can be altered by peripheral nerve injury[178] or capsaicin-evoked sensitisation[179] – thus permitting low-threshold innocuous signals through the dorsal horn 'gate' and facilitating hypersensitivity or allodynia.

Excitatory interneurons are more populous than their inhibitory counterparts; to date, approximately 75% of this population has been accounted for by neurochemical expression and genetic labelling[32], forming another 6 largely non-overlapping populations expressing neurokinin B, neurotensin, cholecystokinin, substance P, gastrin-releasing peptide, and neuropeptide FF[163]. Ablation of a large somatostatin^{+} population, which has considerable overlap with all of the neurochemically defined populations[32], has been shown to reduce acute and neuropathic mechanical pain, suggesting a general pain facilitatory role for excitatory interneurons[180]. Continued methodical interrogation of these complex circuits will hopefully enable more targeted treatments for neuropathic pain and its characteristic symptoms of spontaneous pain and allodynia. For example, the substance P and gastrin-releasing peptide populations have recently been described in great morphological and electrophysiological detail, exposing significant differences in synaptic inputs from primary afferent versus interneurons and responsiveness to neuromodulators such as monoamines and opioids[164].

The transcriptomic analysis of dorsal horn interneurons identified 15 glutamatergic and 15 GABAergic populations[165] that, in a similar fashion to the DRG, appear to further subdivide the known neurochemically-defined populations, and it will be interesting to see what this greater genetic resolution of the dorsal horn reveals about function.

Methods of investigating DRG and dorsal horn populations

Over the two or three preceding decades, we have tended towards classifying somatosensory neurons into more refined subpopulations in order to understand their nuanced functions. This began with histochemical and genetic definitions of subpopulations, which enabled chemical or diphtheria toxin-mediated ablation studies – generally providing quite striking results as a starting point for further interrogation of primary afferent[133,137] or dorsal horn populations[169]. Cell ablation is rather crude mechanistically and may affect anatomical connectivity within the dorsal horn or initiate inflammatory processes, not to mention that many of these early targeted populations may actually represent multiple distinct subpopulations identified by the extra resolution afforded by transcriptomic data[153–155,165,181]; this might yield exaggerated or misleading results. More refined techniques are in development, which attempt to make use of these novel transcriptomic data sets with molecular genetic toolkits to selectively and reversibly manipulate genetically-defined neuronal populations via optogenetic[182] or chemogenetic[177,183–185] control. These neuromodulatory techniques vary widely in their reversibility, temporal and spatial resolutions, route of administration and mechanism of action, all of which have been reviewed recently[186]. Together, these tools are beginning to enable us to understand the behavioural consequences of activating or inactivating individual subpopulations of primary afferent and dorsal horn neurons in an otherwise unaltered nervous system, but also might provide new therapies if combined with gene therapy strategies. Therapeutically, in the context of neuropathic pain, desirable features would include long-term duration of selective, reversible action with a tolerable route of administration.

iv. Potassium channels and pain

While transducing receptors are key for the detection of stimuli and in some respects define the function of the fibres within which they are expressed, transmission of this information is essential for the formation of a sensory percept. Conduction along axons is dependent on the action potential, shaped by highly regulated activity of ion channels which vary between different cell populations, at distinct subcellular sites, and at different stages of development[106,107,187–189]. Single-cell transcriptomic datasets are useful for predicting which genes may be relevant to the function of distinct neuronal populations, but do not offer genuine functional insight alone. Very recently, *Zheng et al.* have instead used 8 Cre-reporter mouse lines to combine detailed electrophysiological characterisation with bulk RNA sequencing for each of the genetically and functionally-defined populations[189]. This has enabled the indirect and direct investigation of ion channel contributions to each population's distinctive electrophysiological properties via analysis of relative gene expression and pharmacological responses to selective channel modulators[189].

Potassium-selective channels represent one such family of genes. Potassium currents were identified by Hodgkin and Huxley in 1952 as the key determinants of the inside-negative neuronal resting membrane potential, which provides the electrochemical gradient for sodium ion entry and action potential generation. These are mostly carried by two-pore domain 'leak' K^+ channels. Among other roles, voltage-gated potassium channels also antagonise inward sodium currents such that action potential generation only occurs after appropriate supra-threshold stimulation. Genome sequencing has identified at least 70 potassium channel genes[107,190–193], many of which are expressed throughout the nervous system and influence sensory processing. Most is known about the two-pore domain background K^+ channels and voltage-gated channels[194]. In general, potassium channels negatively modulate neuronal excitability, and downregulation of these genes is thought to be partly responsible for hyperexcitability in chronic pain models.

a) 'Leak' potassium channels

The description of two-pore domain potassium channels (K_{2P}) as 'leak' channels is somewhat of a misnomer, as their activity is a highly regulated process subject to much modulation[193]. However, they are expressed in DRG neurons[195] and provide background currents contributing to the polarised resting membrane potential in neurons, including nociceptors[196]. A recent knock-out study of K_{2P} channel Tresk has demonstrated hyperexcitable nociceptive and light-touch behavioural phenotypes, corresponding to gene (*Kcnk18*) expression in C- and Aδ-nociceptors and Aδ-hair afferents[197]. Despite expression in peptidergic and non-peptidergic trigeminal nociceptors alike, Tresk knock-out selectively decreased rheobase and increased repetitive action potential firing in $IB4^+$ neurons *in vitro*. Together with behavioural heat hypersensitivity, this also incidentally provides further evidence for the role of non-peptidergic neurons in noxious heat sensation. Decreased rheobase enables normally sub-threshold stimuli to activate sensory nerve endings, and this is thought to be a mechanism involved in pain under neuropathic conditions, when various K_{2P} channels become downregulated[194]. Clinical evidence from fully penetrant dominant-negative TRESK mutations in cases of familial migraine with aura has identified a role for these channels in human pain sensation[198].

b) Voltage-gated potassium channels

The voltage-gated, or Kv, potassium channels (VGKCs) make up a considerable (~40 genes) fraction of all potassium channels[190]. Unlike voltage-gated sodium channels, which are transcribed as a whole pore-forming channel[106], Kv channels are transcribed as discrete alpha subunits which multimerise to form functional pore-forming tetramers[199] (in reality, octomers, including beta subunits), giving rise to potential hetero-multimerisation between and within Kv families and vast

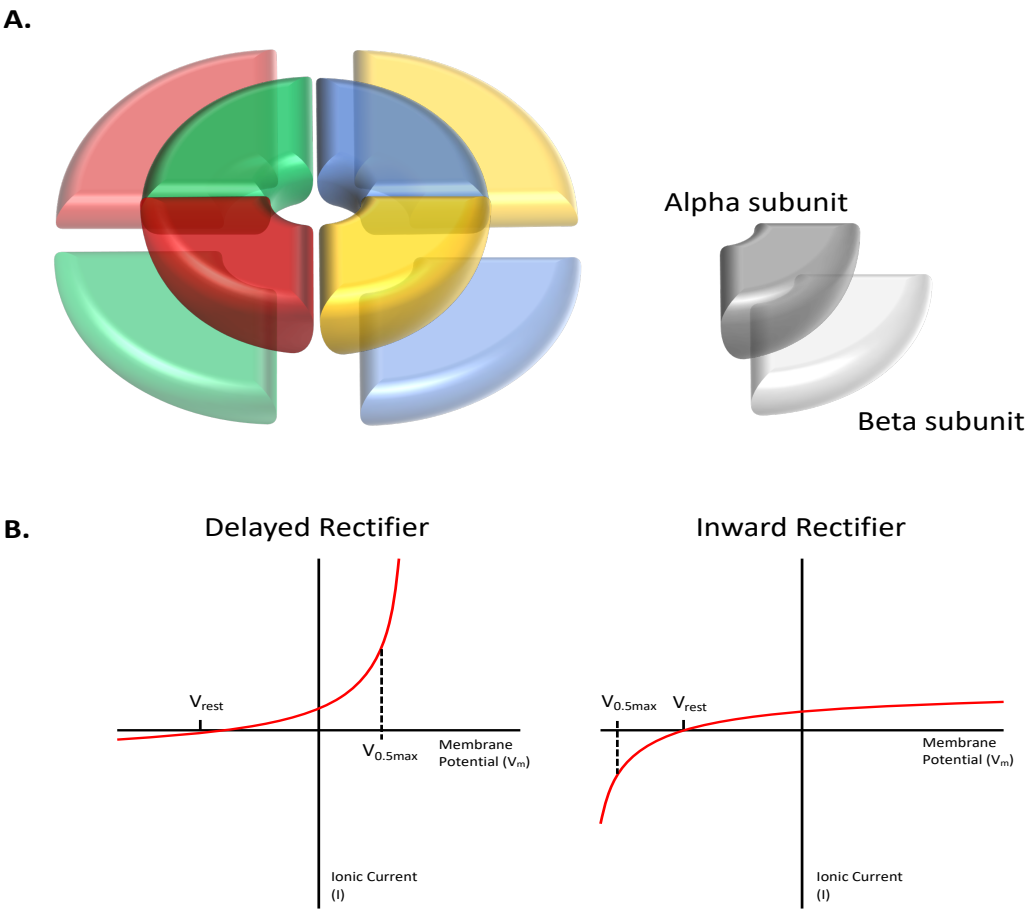

Figure 1.3 – Structural and electrical properties of VGKCs

(A) VGKCs are composed of 4 alpha and 4 beta subunits, each independently translated prior to co-assembly as an octomeric structure. This gives rise to vast opportunities for heteromultimerisation within and between the various subunit families, which ultimately determines channel properties.

(B) Typical current-voltage relationships of delayed (outward) and inward rectifying potassium channels. Delayed rectifiers vary in their membrane potential activation threshold but begin to pass considerable outward K^+ current at depolarised membrane potentials to counter e.g. Na^+ or Ca^{2+} influx. Inward rectifiers are activated at hyperpolarized potentials, e.g. immediately following the action potential downstroke, and pass inward K^+ current to depolarize the membrane back towards resting potential.

diversity in channel properties[190] **Fig1.3(A)**. Currents through these channels show a high degree of dependence on membrane voltage, and they typically 'rectify' – meaning they preferentially pass K^+ ions in one direction into or out of the cell to restore resting membrane potential **Fig1.3(B)**. The voltage-dependence of these channels indicates functionality in electrically excitable cell types and is often represented as the membrane potential at which current is half maximal ($V_{0.5max}$). This value is generally more depolarised than resting potential (delayed, outward rectification), although inwardly rectifying channels activate at more negative potentials and return hyperpolarised cells to resting potential via influx of K^+. VGKCs can be phylogenetically divided[190] into 12 families (Kv1-Kv12), and VGKC currents are generally divided based on their activation and inactivation kinetics into delayed rectifying (I_K), slowly inactivating (I_D), fast-inactivating (I_A), and non- inactivating (I_M) currents.

Not all of the 12 Kv families follow conventional mechanisms of regulating cell excitability. Four families are described as 'silent' – they are unable to form current-passing homomers when expressed alone but can exert modulatory effects on other channels from Kv families by forming functional heteromers[190,194]. Notably, the 'silent' subunit Kv9.1 is downregulated after spinal nerve transection, producing hyperexcitable DRG neurons via Kv2 channel dysregulation and corresponding with behavioural hypersensitivity[200]. Although not yet peer-reviewed work, another silent subunit Kv6.4 also directly influences Kv2.1 function; human variants in Kv6.4 appear to confer resilience to labour pain and experimentally tested cold, heat and pressure pain thresholds[201]. When expressed in mouse sensory neurons, the mutant Kv6.4 is unable to traffic to the plasma membrane and causes a depolarised shift in Kv2.1 inactivation (that is, a gain of function) and reduced excitability compared to wild-type Kv6.4 subunits. Kv2.1 and Kv2.2 themselves also have a non-canonical structural role in tethering contacts between the endoplasmic reticulum and plasma membrane via interaction with VAMP-associated proteins[202,203].

The significance of different K^+ currents in spinal processing is beginning to be revealed. I_A currents in the dorsal horn are mediated by rapidly activating and inactivating channels such as Kv4.2 and mice lacking this channel display enhanced dorsal horn excitability and pain sensitivity[204]. However, they are resistant to ERK-mediated mechanisms of inflammatory sensitisation after peripheral formalin or carrageenan injection, indicating that Kv4.2 is a target of ERK signalling[204]. These transiently active currents are well-suited to rectify brief sub-threshold depolarising stimuli and play a key role in filtering out major ongoing 'silent' Aβ-mediate input to vertical transmission interneurons, or delaying their activation by supra-threshold Aβ-input such that feed-forward inhibition can occur earlier, thus forming part of the spinal 'gate'[179].

The work in this thesis will focus on the Kv1 channel family, but there are numerous accounts of other VGKCs not described here, and their function or dysfunction in acute and chronic pain sensation have been reviewed previously[107,194].

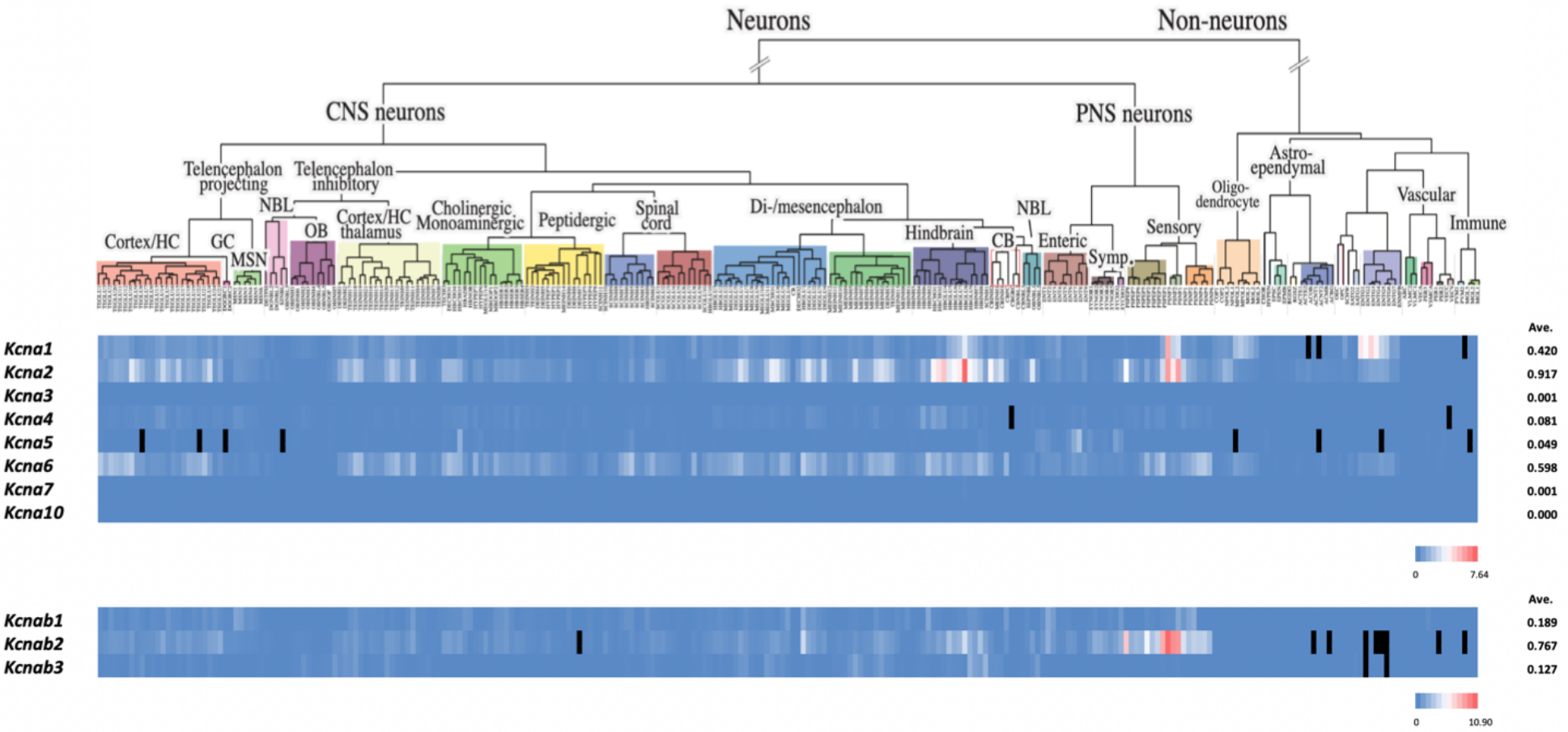

Table 1.1 – Kv1 subunit expression in the mouse nervous system

Relative mRNA expression of Kv1 alpha and beta genes in tissues of the mouse nervous system. Data represent log2 expression; values with a "≤ x" log2 score are denoted in black and were excluded from calculations of average expression (right hand column). Reproduced from public repository available at mousebrain.org

Kv1 Potassium Channels

The *Shaker*-like Kv1 family comprises 8 channels (Kv1.1-1.8), each considered a mammalian homolog of the *Shaker* channel that produced hyperexcitable sensorimotor phenotypes in *Drosophila* when mutated. Paired with evidence that human mutations in *KCNA1* (Kv1.1) cause familial episodic ataxia[205], and Kv1.1 or Kv1.2 knock-out mice suffer from major seizures[206–208], these channels are now known to be key regulators of neuronal excitability. Expression of Kv1 subunits in *Xenopus* oocytes revealed that they provide delayed rectifying currents that were slowly inactivating (I_D/I_{KD}), except for Kv1.4, which rapidly inactivates due to a mechanism involving its long N-terminus and is the only Kv1 channel capable of producing A-type currents[209]. The Kv1.6 subunit has an intriguing property; it can induce a position-dependent inhibition of this rapid inactivation in Kv1.4-containing channels when situated directly adjacent to the Kv1.4 subunit in genetically concatenated obligate tetramers[210], indicating that subunit composition affects channel properties. Each subunit when expressed as a homomer has different voltage activation thresholds. All but Kv1.7 have intronless coding regions, so functional diversity among Kv1 channels arises mainly from heteromerisation as opposed to alternative splicing[190].

Various methods of detecting Kv1 expression in sensory neurons have been attempted, including immunohistochemical approaches[187], pharmacological manipulation of *ex vivo* DRG cells with subtype specific antagonists[211], and more recently the previously described transcriptomic datasets have revealed mRNA expression[154,155,189]. These methods generally agree on high expression of Kv1.1 and 1.2 subunits in the DRG, particularly but not exclusively in large fibre mechanoreceptors. Immunohistochemistry reported that Kv1.4 was the dominant channel in small-fibre nociceptors[187], but independent transcriptomic approaches show very little expression of Kv1.4 throughout the DRG, instead revealing high expression of Kv1.6 in small-diameter neurons[154,155,189]. The discrepancy is possibly due to poor specificity of antibodies against Kv1

subunits, but also there are likely differences between rodent species as immunohistochemical studies describing Kv1.4 expression were performed in rats[187,212]. Pharmacological studies also report this reciprocal relationship of Kv1.1/2 and Kv1.6[211]. Expression data from the *Zeisel et al. (2018)* transcriptomics publication[155] has been extracted and depicted in **Table 1.1** to highlight the relative expression among Kv1 subunits in the nervous system. These highly expressed Kv1.1/1.2/1.6 subunits (incidentally, all sensitive to α-dendrotoxin) will form the main focus of this study.

a) Kv1.1 and Kv1.2

Kv1.1, but not Kv1.2 or Kv1.6, channels were convincingly shown to be intrinsically mechanically sensitive by expression in HEK cells, and in mouse DRG neurons mechanical force causes a negative shift in Kv1.1 $V_{0.5max}$ threshold[213]. Importantly, whole-cell patch clamp with subunit-specific pharmacological blockade also revealed outward mechanically-activated K^+ currents predominantly provided by Kv1.1 subunits. Loss of Kv1.1-containing channel function via pharmacological means or in Kv1.1-dominant negative mutant mice was sufficient to produce hyperexcitable A-LTMRs and C-HTMRs, as well as to reduce behavioural withdrawal thresholds to mechanical but not heat stimuli. Kv1.1-containing channels are therefore mechanically-sensitive and act as a brake on low-and high-threshold mechanoreceptor excitability, but this does not exclude a role for other Kv1 channels, as $Kv1.1^{-/-}$ mice were not affected in the same way due to compensation from other subunits[213]. Kv1.2 has also been implicated in mechanical hypersensitivity – following peripheral nerve injury in rats, there has been observed upregulation of an endogenous long non-coding RNA (lncRNA) complementary to Kv1.2 sense mRNA. This has a silencing role on the channel, as mimicry of this upregulation reduces Kv1.2 expression and causes DRG neuron hyperexcitability and neuropathic pain symptoms in rats[214].

As well as exerting 'brake' counter-currents following mechanical stimulation, the α-dendrotoxin-sensitive Kv1.1/1.2/1.6 channels produce an outward I_{KD} current in response to cooling of cold-sensitive DRG cells in vitro, and increased native I_{KD} current correlates with colder activation temperatures[148]. Blockade of this current shifts the activation temperature of cold-sensing trigeminal ganglia neurons to warmer thresholds *in vitro* and local hind-paw blockade increases nocifensive responses to cold stimuli in a Trpa1-independent manner[148]. After nerve injury, decreased I_{KD} current density is responsible for the emergence of cold allodynia via the aforementioned shifts in activation temperature, and the emergence of *de novo* cold-sensors[147].

Kv1.1 and 1.2 subunits are known to localise highly specifically to juxtaparanodal regions (JXP) of myelinated axons in numerous nervous tissues, in a process dependent on VGKC complex protein Caspr2[215]. The functional relevance of this specific expression pattern is unknown, as in this location channels are electrically isolated by the overlaying membrane wraps of myelinating glial cells, but nevertheless this distribution is lost with Caspr2 knock-out[216] and these mice display behavioural and peripheral nerve fibre hypersensitivity[89]. Similarly, Kv1.1/1.2 staining at the JXP is lost acutely after peripheral nerve injury, and this phenomenon corresponds well with the time course of acquired mechanical hypersensitivity[212]. These complex proteins, CASPR2 and LGI1, have been identified as targets of autoantibodies in patients with clinical syndromes typified by neuronal hyperexcitability – such as limbic encephalitis, Morvan's syndrome and Isaac's syndrome[217–219]. Neuropathic pain is a common feature of these disorders[220], and passive transfer of patient-derived CASPR2 autoantibodies to mice has a causative role in the development of sensory hypersensitivity via dysregulation of Kv1.1/1.2 channels at the DRG soma[89]. With increased screening for VGKC complex antibodies in patient serum, there has been a growth in antibodies detected against the channel subunits themselves – interestingly, against intracellular epitopes. The Kv1 subunit with autoantibodies that most commonly associated with neuropathic pain was in fact Kv1.6[221].

b) Kv1.6

Potassium channel Kv1.6 has enjoyed some 'cameo' appearances in neuroscience literature since the gene, *Kcna6*, was cloned from rat tissue in 1990[222]. Typically, references to this Kv1 alpha subunit are fleeting and exist as cursory footnotes on more comprehensive analyses of the historically preferred candidates, Kv1.1 and 1.2. Together these studies do provide some insight into Kv1.6 expression both within and external to the nervous system: various reports have described *Kcna6* expression in cardiac progenitor cells[223] and the atrioventricular node[224], vascular tissues[225,226], the nephron[227], chondrocytes[228], as well as glial cells[229–233] and neuronal tissue of the central[234–236] and peripheral[212,237–239] nervous systems. A recent, ambitious effort to characterise the transcriptome of the mouse nervous system with single cell resolution[155] describes widespread expression of *Kcna6*. In fact, on average across all cell clusters *Kcna6* was expressed to a greater degree than *Kcna1* and was the second most abundant Kv1 alpha subunit, behind *Kcna2* **Table 1**. Within the mouse DRG, *Kcna6* is the second most abundantly transcribed of all VGKC alpha subunits in peptidergic and non-peptidergic nociceptors, behind Kv4.1[189]. An independent transcriptomic analysis of human DRG confirmed *KCNA6* expression, which was enriched in the DRG when compared to previous expression datasets from other human neuronal and non-neuronal tissues[240].

The dominance of *Kcna6* expression in nociceptors is a relatively recent discovery, and fittingly there are few reports of Kv1.6 in pain literature. Using the streptozotocin model of diabetic neuropathy, *Wang et al. (2015)* attributed reduced C-fibre conduction failure following stimulation of the rat coccygeal nerve to downregulation of Kv1.2 and 1.6[239]. However, the immunohistochemical evidence for this downregulation was poor, again most likely due to sub-optimal commercial antibodies. The authors relied mostly on α-dendrotoxin effects to infer Kv1.6 involvement, but this affects Kv1.1/1.2/1.6-containing channels in any combination. Most

publications that have studied Kv1.6 channels in a pain context indicate the contrary; while the majority of Kv1 channels undergo downregulation after neuropathy or nerve injury, *Kcna6* mRNA appears resilient to this change across the whole DRG and remains expressed at a constant level[238,241].

Recently, *Calvo et al. (2016)* reported on neuronal Kv1 expression and distribution in a neuropathic pain model[212]. They found that, following peripheral nerve axotomy, juxtaparanodal Kv1.1 and 1.2 channels are downregulated within the injured fibres, resulting in increased spontaneous electrical discharge from the injured nerve and evoked mechanical hypersensitivity. Chronically after injury, the lost subunits are replaced by Kv1.6 and 1.4 at juxtaparanodes within the neuroma that forms after injury. The upregulation of Kv1.6/1.4 is temporally associated with a reduction in axotomy-induced spontaneous electrical activity in the transected nerve and amelioration of hypersensitive mechanical withdrawal thresholds observed post-surgery. Both of these recovery effects were reversed by local administration of α-dendrotoxin to the neuroma – which is suggestive of a compensatory and restorative role for Kv1.6-containing channels in neuropathic states.

The mechanism of this upregulation is unknown but given previous reports of stable *Kcna6* mRNA after axotomy it may not involve increased gene expression[238,241]. Using a method of purifying ribosomal-associated mRNA molecules (translating ribosome affinity purification, TRAP), *Megat et al. (2019)* performed translational profiling of DRGs from mice with chemotherapy-induced neuropathy[242]. This publication produced a dataset of ribosome-bound and unbound mRNAs from mice treated with either vehicle or paclitaxel to induce neuropathy, providing a dataset that discriminated between genome-wide transcription and translation in a model of neuropathy. The results for selected Kv1 α- and β-subunits have been extracted and represented in **Fig1.4**, and appear to indicate that, in CIPN, Kv1.6 is upregulated by means of increased translation but has stable transcription. It is possible that the same mechanism exists for traumatic neuropathy.

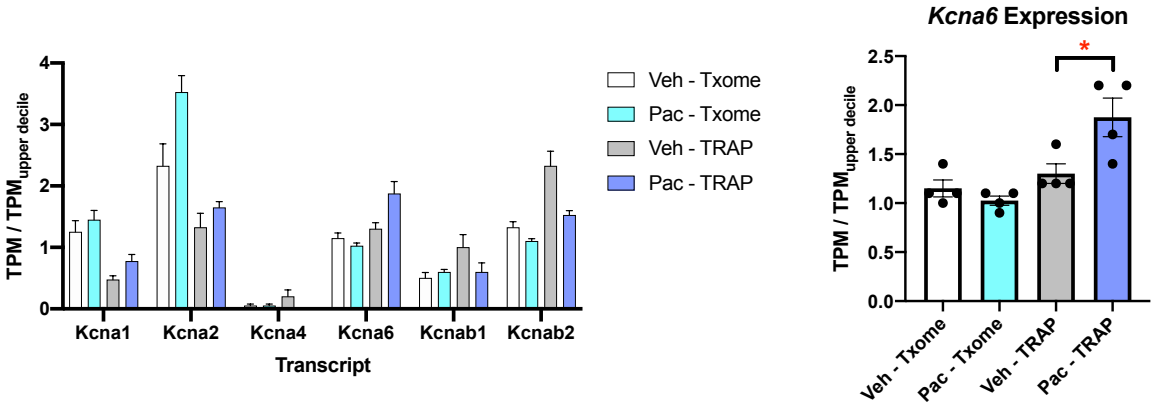

Figure 1.4 – Variations in Kv1 subunit expression after chemotherapy-induced peripheral neuropathy

Data extracted from *Megat et al. (2019).* Kv1 channel expression may be regulated by transcriptional (Txome) or translational (TRAP) changes in the context of neuropathy. For paclitaxel-induced CIPN, the Kv1.6 subunit appears to be upregulated by means of increased translation.
***** = $p<0.05$ (Pac – TRAP vs Veh – TRAP) after unpaired two-tailed Student's t-test, n = 4 Veh, 4 Paclitaxel. Statistical tests only performed for the *Kcna6* subunit.

v. Aims of this thesis

VGKCs are important regulators of neuronal excitability throughout the nervous system and regulate pain sensitivity at numerous anatomical sites along the sensory neuraxis. The naïve and neuropathic expression profile of *Kcna6* compared to other Kv1 subunits suggests that it might be an interesting target for pain therapeutics, and there is growing evidence for a demonstrable functional role in the context of animal neuropathic pain models[212] and painful autoimmune neuropathies in humans[221]. The Kv1.6 channel was therefore selected for much-needed and more rigorous analysis within peripheral sensory neurons and the dorsal horn. The data collected for this thesis are herein mostly presented in chronological order. As such, conclusions drawn at the end of each chapter were interim, and subject to change with accumulating experimental evidence. Nonetheless, my aims at the outset were, and remained:

- To explore the expression of *Kcna6* within the mouse somatosensory nervous system, primarily in order to understand its distribution across the various defined subpopulations of primary afferent sensory neurons as this may help to verify existing data or predict unexplored roles in each of the different sensory modalities.
- To ascertain whether loss of Kv1.6 subunit function impacts on sensation in 'naïve' and neuropathic states, by assessing an array of sensorimotor behavioural outcomes on global Kv1.6 knock-out mice before and after experimentally induced neuropathy.
- To provide anatomical or physiological evidence for mechanistic relationships between Kv1.6 function and sensation, where any impact of Kv1.6 knock-out is found.

It is hoped that in pursuing these aims, I will have provided the community with novel information pertaining to the processes involved in mammalian somatosensation and nociception. This information may be useful in fuelling further research in this field, or indeed in revealing novel pharmacological therapies, particularly for neuropathic pain.

vi. References

1. IASP. Subcommittee on taxonomy. Classification of chronic pain. Descriptions of chronic pain syndromes and definitions of pain terms. *Pain* **3 (Supp)**, S1–S225 (1986).
2. Sherrington, C. S. Qualitative difference of spinal reflex corresponding with qualitative difference of cutaneous stimulus. *J. Physiol.* **30**, 39–46 (1903).
3. Abraira, V. E. & Ginty, D. D. The sensory neurons of touch. *Neuron* **79**, 618–639 (2013).
4. Moehring, F., Halder, P., Seal, R. P. & Stucky, C. L. Uncovering the Cells and Circuits of Touch in Normal and Pathological Settings. *Neuron* **100**, 349–360 (2018).
5. Abdo, H. *et al.* Specialized cutaneous Schwann cells initiate pain sensation. *Science (80-.).* **365**, 695–699 (2019).
6. Adrian, E. D. The impulses produced by sensory nerve-endings: Part 4. Impulses from Pain Receptors. *J. Physiol.* **62**, 33–51 (1926).
7. Zimmermann, K. *et al.* Phenotyping sensory nerve endings in vitro in the mouse. *Nat. Protoc.* **4**, 174–196 (2009).
8. Vallbo, Å. B. Microneurography: how it started and how it works. *J. Neurophysiol.* **120**, 1415–1427 (2018).
9. Rexed, B. The cytoarchitectonic organization of the spinal cord in the cat. *J. Comp. Neurol.* **96**, 414–495 (1952).
10. Christensen, B. N. & Perl, E. R. Spinal neurons specifically excited by noxious or thermal stimuli: marginal zone of the dorsal horn. *J. Neurophysiol.* **33**, 293–307 (1970).
11. Wall, P. D. The laminar organization of dorsal horn and effects of descending impulses. *J. Physiol.* **188**, 403–423 (1967).
12. Snow, P. J., Rose, P. K. & Brown, A. G. Tracing axons and axon collaterals of spinal neurons using intracellular injection of horseradish peroxidase. *Science (80-.).* **191**, 312–313 (1976).
13. Brown, A. G. Cutaneous Axons and Sensory Neurones in the Spinal Cord. *Br. Med. Bull.* **33**, 109–112 (1977).
14. Light, A. R. & Durkovic, R. G. Horseradish peroxidase: An improvement in intracellular staining of single, electrophysiologically characterized neurons. *Exp. Neurol.* **53**, 847–853 (1976).
15. Brown, A. G. & Noble, R. Connexions between hair follicle afferent fibres and spinocervical tract neurones in the cat: the synthesis of receptive fields. *J. Physiol.* **323**, 77–91 (1982).
16. Light, A. R. & Perl, E. R. Differential termination of large-diameter and small-diameter primary afferent fibers in the spinal dorsal gray matter as indicated by labeling with horseradish peroxidase. *Neurosci. Lett.* **6**, 59–63 (1977).
17. Réthelyi, M. Preterminal and terminal axon arborizations in the substantia gelatinosa of cat's spinal cord. *J. Comp. Neurol.* **172**, 511–527 (1977).
18. Sugiura, Y., Lee, C. L. & Perl, E. R. Central projections of identified, unmyelinated (C) afferent fibers innervating mammalian skin. *Science (80-.).* **234**, 358–361 (1986).
19. McNeill, D. L., Coggeshall, R. E. & Carlton, S. M. A light and electron microscopic study of calcitonin gene-related peptide in the spinal cord of the rat. *Exp. Neurol.* **99**, 699–708 (1988).
20. Jakab, G., Salamon, I., Petrusz, P. & Réthelyi, M. Termination patterns of calcitonin gene-related peptide-immunoreactive nerve fibers in the dorsal horn of the human spinal cord. *Exp. Brain Res.* **80**, 609–617 (1990).
21. Zylka, M. J., Rice, F. L. & Anderson, D. J. Topographically distinct epidermal nociceptive circuits revealed by axonal tracers targeted to Mrgprd. *Neuron* **45**, 17–25 (2005).
22. Abraira, V. E. *et al.* The Cellular and Synaptic Architecture of the Mechanosensory Dorsal

Horn. *Cell* **168**, 295-310.e19 (2016).
23. Li, L. *et al.* The functional organization of cutaneous low-threshold mechanosensory neurons. *Cell* **147**, 1615–1627 (2011).
24. Swett, J. E. & Woolf, C. J. The somatotopic organization of primary afferent terminals in the superficial laminae of the dorsal horn of the rat spinal cord. *J. Comp. Neurol.* **231**, 66–77 (1985).
25. Boyle, K. A. *et al.* Defining a Spinal Microcircuit that Gates Myelinated Afferent Input: Implications for Tactile Allodynia. *Cell Rep.* **28**, 526-540.e6 (2019).
26. Sugiura, Y., Terui, N. & Hosoya, Y. Difference in distribution of central terminals between visceral and somatic unmyelinated (C) primary afferent fibers. *J. Neurophysiol.* **62**, 834–840 (1989).
27. Mendell, L. M. & Wall, P. D. Responses of single dorsal cord cells to peripheral cutaneous unmyelinated fibres. *Nature* **206**, 97–99 (1965).
28. Sikandar, S., Ronga, I., Iannetti, G. D. & Dickenson, A. H. Neural coding of nociceptive stimuli - From rat spinal neurones to human perception. *Pain* **154**, 1263–1273 (2013).
29. Woolf, C. J. & King, A. E. Physiology and morphology of multireceptive neurons with C-afferent fiber inputs in the deep dorsal horn of the rat lumbar spinal cord. *J. Neurophysiol.* **58**, 460–479 (1987).
30. Todd, A. J., McGill, M. M. & Shehab, S. A. S. Neurokinin 1 receptor expression by neurons in laminae I, III and IV of the rat spinal dorsal horn that project to the brainstem. *Eur. J. Neurosci.* **12**, 689–700 (2000).
31. Todd, A. J. Neuronal circuitry for pain processing in the dorsal horn. *Nat. Rev. Neurosci.* **11**, 823–836 (2010).
32. Todd, A. J. Identifying functional populations among the interneurons in laminae I-III of the spinal dorsal horn. *Mol. Pain* **13**, 1–19 (2017).
33. Polgár, E., Durrieux, C., Hughes, D. I. & Todd, A. J. A Quantitative Study of Inhibitory Interneurons in Laminae I-III of the Mouse Spinal Dorsal Horn. *PLoS One* **8**, e78309 (2013).
34. Melzack, R. & Wall, P. D. Pain Mechanisms: A New Theory. *Science (80-.).* **150**, 971–978 (1965).
35. Yaksh, T. L. Behavioral and autonomic correlates of the tactile evoked allodynia produced by spinal glycine inhibition: effects of modulatory receptor systems and excitatory amino acid antagonists. *Pain* **37**, 111–123 (1989).
36. Penfield, W. & Boldrey, E. Somatic motor and sensory representation in the cerebral cortex of man as studied by electrical stimulation. *Brain* **60**, 389–443 (1937).
37. Mazzola, L., Isnard, J., Peyron, R. & Mauguire, F. Stimulation of the human cortex and the experience of pain: Wilder Penfield's observations revisited. *Brain* **135**, 631–640 (2012).
38. Cox, J. J. *et al.* An SCN9A channelopathy causes congenital inability to experience pain. *Nature* **444**, 894–898 (2006).
39. McDermott, L. A. *et al.* Defining the Functional Role of NaV1.7 in Human Nociception. *Neuron* **101**, 905-919.e8 (2019).
40. Chen, Y. C. *et al.* Transcriptional regulator PRDM12 is essential for human pain perception. *Nat. Genet.* **47**, 803–808 (2015).
41. Einarsdottir, E. *et al.* A mutation in the nerve growth factor beta gene (NGFB) causes loss of pain perception. *Hum. Mol. Genet.* **13**, 799–805 (2004).
42. Indo, Y. *et al.* Mutations in the TRKA/NGF receptor gene in patients with congenital insensitivity to pain with anhidrosis. *Nat. Genet.* **13**, 485–488 (1996).
43. Houlden, H. *et al.* A novel TRK A (NTRK1) mutation associated with hereditary sensory and autonomic neuropathy type V. *Ann. Neurol.* **49**, 521–525 (2001).
44. Chen, Y.-C. *et al.* A Comprehensive Functional Analysis of NTRK1 Missense Mutations Causing Hereditary Sensory and Autonomic Neuropathy Type IV (HSAN IV). *Hum.*

Mutat. **38**, 55–63 (2016).
45. Habib, A. M. *et al.* Microdeletion in a FAAH pseudogene identified in a patient with high anandamide concentrations and pain insensitivity. *Br. J. Anaesth.* **0**, 1–5 (2019).
46. King, T. *et al.* Unmasking the tonic-aversive state in neuropathic pain. *Nat. Neurosci.* **12**, 1364–1366 (2009).
47. Navratilova, E. *et al.* Pain relief produces negative reinforcement through activation of mesolimbic reward-valuation circuitry. *Proc. Natl. Acad. Sci.* **109**, 20709–20713 (2012).
48. Al-Khater, K. M. & Todd, A. J. Collateral projections of neurons in laminae I, III, and IV of rat spinal cord to thalamus, periaqueductal gray matter, and lateral parabrachial area. *J. Comp. Neurol.* **515**, 629–646 (2009).
49. Polgár, E., Wright, L. L. & Todd, A. J. A quantitative study of brainstem projections from lamina I neurons in the cervical and lumbar enlargement of the rat. *Brain Res.* **1308**, 58–67 (2010).
50. Reynolds, D. V. Surgery in the rat during electrical analgesia induced by focal brain stimulation. *Science (80-.).* **164**, 444–445 (1969).
51. Büchel, C., Geuter, S. & Sprenger, C. Comparing Painful Stimulation vs Rest in Studies of Pain. *JAMA Neurol.* **73**, 1258 (2016).
52. Wager, T. D. *et al.* An fMRI-Based Neurologic Signature of Physical Pain. *N. Engl. J. Med.* **368**, 1388–1397 (2013).
53. Simons, L. E. *et al.* The human amygdala and pain: Evidence from neuroimaging. *Hum. Brain Mapp.* **35**, 527–538 (2014).
54. Navratilova, E. & Porreca, F. Reward and motivation in pain and pain relief. *Nat. Neurosci.* **17**, 1304–1312 (2014).
55. Hebben, N., Corkin, S., Eichenbaum, H. & Shedlack, K. Diminished ability to interpret and report internal states after bilateral medial temporal resection: Case H.M. *Behav. Neurosci.* **99**, 1031–1039 (1985).
56. Annese, J. *et al.* Postmortem examination of patient H.M.'s brain based on histological sectioning and digital 3D reconstruction. *Nat. Commun.* **5**, 3122 (2014).
57. Schnitzer, M. J. *et al.* An amygdalar neural ensemble that encodes the unpleasantness of pain. *Science (80-.).* **363**, 276–281 (2019).
58. Fields, H. L. How expectations influence pain. *Pain* **159**, S3–S10 (2018).
59. Alhadeff, A. L. *et al.* A Neural Circuit for the Suppression of Pain by a Competing Need State. *Cell* **173**, 140-152.e15 (2018).
60. Davies, A. J. *et al.* Hedonic drinking engages a supraspinal inhibition of thermal nociception in adult rats. *Pain* **160**, 1059–1069 (2019).
61. Eippert, F. *et al.* Activation of the Opioidergic Descending Pain Control System Underlies Placebo Analgesia. *Neuron* **63**, 533–543 (2009).
62. Eippert, F., Finsterbusch, J., Bingel, U. & Büchel, C. Direct evidence for spinal cord involvement in placebo analgesia. *Science (80-.).* **326**, 404 (2009).
63. Fields, H. State-dependent opioid control of pain. *Nature Reviews Neuroscience* **5**, 565–575 (2004).
64. Levine, J. D., Gordon, N. C., Jones, R. T. & Fields, H. L. The narcotic antagonist naloxone enhances clinical pain. *Nature* **272**, 826–827 (1978).
65. Scott, D. J. *et al.* Placebo and Nocebo Effects Are Defined by Opposite Opioid and Dopaminergic Responses. *Arch. Gen. Psychiatry* **65**, 220 (2008).
66. François, A. *et al.* A Brainstem-Spinal Cord Inhibitory Circuit for Mechanical Pain Modulation by GABA and Enkephalins. *Neuron* **93**, 822-839.e6 (2017).
67. Ossipov, M. H., Morimura, K. & Porreca, F. Descending pain modulation and chronification of pain. *Current Opinion in Supportive and Palliative Care* **8**, 143–151 (2014).
68. Bannister, K. & Dickenson, A. H. What do monoamines do in pain modulation? *Current Opinion in Supportive and Palliative Care* **10**, 143–148 (2016).

69. Finnerup, N. B. *et al.* Pharmacotherapy for neuropathic pain in adults: A systematic review and meta-analysis. *Lancet Neurol.* **14**, 162–173 (2015).
70. Kosek, E. *et al.* Do we need a third mechanistic descriptor for chronic pain states? *Pain* **157**, 1382–6 (2016).
71. Granan, L. P. We do not need a third mechanistic descriptor for chronic pain states! Not yet. *Pain* **158**, 179 (2017).
72. Finnerup, N. B. *et al.* Neuropathic pain: An updated grading system for research and clinical practice. *Pain* **157**, 1599–1606 (2016).
73. Baron, R. *et al.* Peripheral neuropathic pain: a mechanism-related organizing principle based on sensory profiles. *Pain* **158**, 261–272 (2017).
74. Uceyler, N. *et al.* Sensory profiles and skin innervation of patients with painful and painless neuropathies. *Pain* **159**, (2018).
75. Themistocleous, A. C., Crombez, G., Baskozos, G. & Bennett, D. L. Using stratified medicine to understand, diagnose, and treat neuropathic pain. *Pain* **159**, S31–S42 (2018).
76. Caterina, M. J. *et al.* The capsaicin receptor: A heat-activated ion channel in the pain pathway. *Nature* **389**, 816–824 (1997).
77. Tominaga, M. *et al.* The cloned capsaicin receptor integrates multiple pain-producing stimuli. *Neuron* **21**, 531–543 (1998).
78. Aneiros, E. *et al.* The biophysical and molecular basis of TRPV1 proton gating. *EMBO J.* **30**, 994–1002 (2011).
79. Moore, R. A. *et al.* Non-prescription (OTC) oral analgesics for acute pain- an overview of Cochrane reviews. *Cochrane Database Syst. Rev.* (2015). doi:10.1002/14651858.CD010794
80. Moore, R. A., Derry, S., Aldington, D. & Wiffen, P. J. Single dose oral analgesics for acute postoperative pain in adults - an overview of Cochrane reviews. *Cochrane Database of Systematic Reviews* **2017**, (2015).
81. Stein, C., Schäfer, M. & Machelska, H. Attacking pain at its source: new perspectives on opioids. *Nature Medicine* **9**, 1003–1008 (2003).
82. Treede, R.-D. *et al.* A classification of chronic pain for ICD-11. *Pain* **156**, 1003–7 (2015).
83. Vos, T. *et al.* Global, regional, and national incidence, prevalence, and years lived with disability for 301 acute and chronic diseases and injuries in 188 countries, 1990-2013: A systematic analysis for the Global Burden of Disease Study 2013. *Lancet* **386**, 743–800 (2015).
84. Rice, A. S. C., Smith, B. H. & Blyth, F. M. Pain and the global burden of disease. *Pain* **157**, 791–796 (2016).
85. Gaskin, D. J. & Richard, P. The economic costs of pain in the United States. *J. Pain* **13**, 715–724 (2012).
86. Colloca, L. *et al.* Neuropathic pain. *Nat. Rev. Dis. Prim.* **3**, 17002 (2017).
87. Bennett, D. L. H. & Vincent, A. Autoimmune pain; An emerging concept. *Neurology* **79**, 1080–1081 (2012).
88. Dawes, J. M. & Vincent, A. Autoantibodies and pain. *Curr. Opin. Support. Palliat. Care* **10**, 137–142 (2016).
89. Dawes, J. M. *et al.* Immune or Genetic-Mediated Disruption of CASPR2 Causes Pain Hypersensitivity Due to Enhanced Primary Afferent Excitability. *Neuron* **97**, 806–822 (2018).
90. Cuhadar, U. *et al.* Autoantibodies produce pain in Complex Regional Pain Syndrome by sensitizing nociceptors. *Pain* (2019). doi:10.1097/j.pain.0000000000001662
91. Kuner, R. & Flor, H. Structural plasticity and reorganisation in chronic pain. *Nature Reviews Neuroscience* **18**, 20–30 (2017).
92. Denk, F., McMahon, S. B. & Tracey, I. Pain vulnerability: a neurobiological perspective. *Nature Neuroscience* **17**, 192–200 (2014).
93. Segerdahl, A. R., Themistocleous, A. C., Fido, D., Bennett, D. L. & Tracey, I. A brain-

based pain facilitation mechanism contributes to painful diabetic polyneuropathy. *Brain* **141**, 357–364 (2018).
94. Seminowicz, D. A. *et al.* Effective Treatment of Chronic Low Back Pain in Humans Reverses Abnormal Brain Anatomy and Function. *J. Neurosci.* **31**, 7540–7550 (2011).
95. Meacham, K., Shepherd, A., Mohapatra, D. P. & Haroutounian, S. Neuropathic Pain: Central vs. Peripheral Mechanisms. *Current Pain and Headache Reports* **21**, 28 (2017).
96. Serra, J. *et al.* Microneurographic identification of spontaneous activity in C-nociceptors in neuropathic pain states in humans and rats. *Pain* **153**, 42–55 (2012).
97. North, R. Y. *et al.* Electrophysiological and transcriptomic correlates of neuropathic pain in human dorsal root ganglion neurons. *Brain* **142**, 1215–1226 (2019).
98. Ramachandran, V. S. & Rogers-Ramachandran, D. Phantom limbs and neural plasticity. *Archives of Neurology* **57**, 317–320 (2000).
99. Makin, T. R., Scholz, J., Henderson Slater, D., Johansen-Berg, H. & Tracey, I. Reassessing cortical reorganization in the primary sensorimotor cortex following arm amputation. *Brain* **138**, 2140–2146 (2015).
100. Kikkert, S., Johansen-Berg, H., Tracey, I. & Makin, T. R. Reaffirming the link between chronic phantom limb pain and maintained missing hand representation. *Cortex* **106**, 174–184 (2018).
101. Vaso, A. *et al.* Peripheral nervous system origin of phantom limb pain. *Pain* **155**, 1384–1391 (2014).
102. Haroutounian, S. *et al.* How central is central poststroke pain? The role of afferent input in poststroke neuropathic pain: a prospective, open-label pilot study. *Pain* **159**, 1317–1324 (2018).
103. Yang, Q. *et al.* Persistent Pain after Spinal Cord Injury Is Maintained by Primary Afferent Activity. *J. Neurosci.* **34**, 10765–10769 (2014).
104. Basbaum, A. I., Bautista, D. M., Scherrer, G. & Julius, D. Cellular and Molecular Mechanisms of Pain. *Cell* **139**, 267–284 (2009).
105. Le Pichon, C. E. & Chesler, A. T. The functional and anatomical dissection of somatosensory subpopulations using mouse genetics. *Front. Neuroanat.* **8**, 21 (2014).
106. Bennett, D. L., Clark, A. J., Huang, J., Waxman, S. G. & Dib-Hajj, S. D. The Role of Voltage-Gated Sodium Channels in Pain Signaling. *Physiol. Rev.* **99**, 1079–1151 (2019).
107. Tsantoulas, C. & McMahon, S. B. Opening paths to novel analgesics: The role of potassium channels in chronic pain. *Trends Neurosci.* **37**, 146–158 (2014).
108. Katz, B. & Miledi, R. Ionic requirements of synaptic transmitter release. *Nature* **215**, 651 (1967).
109. Fang, X., McMullan, S., Lawson, S. N. & Djouhri, L. Electrophysiological differences between nociceptive and non-nociceptive dorsal root ganglion neurones in the rat in vivo. *J. Physiol.* **565**, 927–943 (2005).
110. Nagi, S. S. *et al.* An ultrafast system for signaling mechanical pain in human skin. *Sci. Adv.* **5**, eaaw1297 (2019).
111. Ribeiro-Da-Silva, A. & Coimbra, A. Two types of synaptic glomeruli and their distribution in laminae I–III of the rat spinal cord. *J. Comp. Neurol.* **209**, 176–186 (1982).
112. Gerke, M. B. & Plenderleith, M. B. Ultrastructural analysis of the central terminals of primary sensory neurones labelled by transganglionic transport of Bandeiraea simplicifolia I-isolectin B4. *Neuroscience* **127**, 165–175 (2004).
113. Kambrun, C. *et al.* TAFA4 Reverses Mechanical Allodynia through Activation of GABAergic Transmission and Microglial Process Retraction. *CellReports* **22**, 2886–2897 (2018).
114. Larsson, M. & Broman, J. Synaptic Organization of VGLUT3 Expressing Low-Threshold Mechanosensitive C Fiber Terminals in the Rodent Spinal Cord. *eNeuro* **6**, ENEURO.0007-19.2019 (2019).

115. Ribeiro-da-silva, A., Tagari, P. & Cuello, A. C. Morphological characterization of substance P-like immunoreactive glomeruli in the superficial dorsal horn of the rat spinal cord and trigeminal subnucleus caudalis: A quantitative study. *J. Comp. Neurol.* **281**, 497–515 (1989).
116. Lawson, S. N. & Waddell, P. J. Soma neurofilament immunoreactivity is related to cell size and fibre conduction velocity in rat primary sensory neurons. *J. Physiol.* **435**, 41–63 (1991).
117. Silverman, J. D. & Kruger, L. Selective neuronal glycoconjugate expression in sensory and autonomic ganglia: relation of lectin reactivity to peptide and enzyme markers. *J. Neurocytol.* **19**, 789–801 (1990).
118. Price, T. J. & Flores, C. M. Critical Evaluation of the Colocalization Between Calcitonin Gene-Related Peptide, Substance P, Transient Receptor Potential Vanilloid Subfamily Type 1 Immunoreactivities, and Isolectin B4 Binding in Primary Afferent Neurons of the Rat and Mouse. *J. Pain* **8**, 263–272 (2007).
119. Löken, L. S., Wessberg, J., Morrison, I., McGlone, F. & Olausson, H. Coding of pleasant touch by unmyelinated afferents in humans. *Nat. Neurosci.* **12**, 547–548 (2009).
120. Liljencrantz, J. & Olausson, H. Tactile C fibers and their contributions to pleasant sensations and to tactile allodynia. *Front. Behav. Neurosci.* **8**, 37 (2014).
121. Todd, A. J. *et al.* The expression of vesicular glutamate transporters VGLUT1 and VGLUT2 in neurochemically defined axonal populations in the rat spinal cord with emphasis on the dorsal horn. *Eur. J. Neurosci.* **17**, 13–27 (2003).
122. Alvarez, F. J., Villalba, R. M., Zerda, R. & Schneider, S. P. Vesicular Glutamate Transporters in the Spinal Cord, with Special Reference to Sensory Primary Afferent Synapses. *J. Comp. Neurol.* **472**, 257–280 (2004).
123. Gutierrez-Mecinas, M. *et al.* Immunostaining for Homer reveals the majority of excitatory synapses in laminae I-III of the mouse spinal dorsal horn. *Neuroscience* **329**, 171–181 (2016).
124. Seal, R. P. *et al.* Injury-induced mechanical hypersensitivity requires C-low threshold mechanoreceptors. *Nature* **462**, 651–655 (2009).
125. Ranade, S. S. *et al.* Piezo2 is the major transducer of mechanical forces for touch sensation in mice. *Nature* **516**, 121–125 (2014).
126. Julius, D. TRP Channels and Pain. *Annu. Rev. Cell Dev. Biol.* **29**, 355–384 (2013).
127. Vriens, J., Nilius, B. & Voets, T. Peripheral thermosensation in mammals. *Nature Reviews Neuroscience* **15**, 573–589 (2014).
128. Chesler, A. T. *et al.* The Role of PIEZO2 in Human Mechanosensation. *N. Engl. J. Med.* **375**, 1355–1364 (2016).
129. Murthy, S. E. *et al.* The mechanosensitive ion channel Piezo2 mediates sensitivity to mechanical pain in mice. *Sci. Transl. Med.* **10**, eaat9897 (2018).
130. Woodbury, C. J. *et al.* Nociceptors Lacking TRPV1 and TRPV2 Have Normal Heat Responses. *J. Neurosci.* **24**, 6410–6415 (2004).
131. Cavanaugh, D. J. *et al.* Restriction of Transient Receptor Potential Vanilloid-1 to the Peptidergic Subset of Primary Afferent Neurons Follows Its Developmental Downregulation in Nonpeptidergic Neurons. *J. Neurosci.* **31**, 10119–10127 (2011).
132. Caterina, M. J. *et al.* Impaired nociception and pain sensation in mice lacking the capsaicin receptor. *Science (80-.).* **288**, 306–313 (2000).
133. Cavanaugh, D. J. *et al.* Distinct subsets of unmyelinated primary sensory fibers mediate behavioral responses to noxious thermal and mechanical stimuli. *Proc. Natl. Acad. Sci. U. S. A.* **106**, 9075–80 (2009).
134. Mishra, S. K. & Hoon, M. A. Ablation of TrpV1 neurons reveals their selective role in thermal pain sensation. *Mol. Cell. Neurosci.* **43**, 157–163 (2010).
135. Dong, X., Han, S. kyou, Zylka, M. J., Simon, M. I. & Anderson, D. J. A diverse family of GPCRs expressed in specific subsets of nociceptive sensory neurons. *Cell* **106**, 619–632

(2001).
136. Zylka, M. J., Rice, F. L. & Anderson, D. J. Topographically distinct epidermal nociceptive circuits revealed by axonal tracers targeted to Mrgprd. *Neuron* **45**, 17–25 (2005).
137. McCoy, E. S. *et al.* Peptidergic CGRPα Primary Sensory Neurons Encode Heat and Itch and Tonically Suppress Sensitivity to Cold. *Neuron* **78**, 138–151 (2013).
138. Vandewauw, I. *et al.* A TRP channel trio mediates acute noxious heat sensing. *Nature* **555**, 662–666 (2018).
139. Peier, A. M. *et al.* A TRP channel that senses cold stimuli and menthol. *Cell* **108**, 705–715 (2002).
140. Karashima, Y. *et al.* TRPA1 acts as a cold sensor in vitro and in vivo. *Proc. Natl. Acad. Sci. U. S. A.* **106**, 1273–1278 (2009).
141. Camino, D. del *et al.* TRPA1 contributes to cold hypersensitivity. *J. Neurosci.* **30**, 15165–15174 (2010).
142. Winter, Z., Gruschwitz, P., Eger, S., Touska, F. & Zimmermann, K. Cold Temperature Encoding by Cutaneous TRPA1 and TRPM8-Carrying Fibers in the Mouse. *Front. Mol. Neurosci.* **10**, 209 (2017).
143. Tan, C. H. & McNaughton, P. A. The TRPM2 ion channel is required for sensitivity to warmth. *Nature* **536**, 460–463 (2016).
144. Huang, S. M., Li, X., Yu, Y., Wang, J. & Caterina, M. J. TRPV3 and TRPV4 ion channels are not major contributors to mouse heat sensation. *Mol. Pain* **7**, 37 (2011).
145. Vriens, J. *et al.* TRPM3 Is a Nociceptor Channel Involved in the Detection of Noxious Heat. *Neuron* **70**, 482–494 (2011).
146. Vastani, N. *et al.* Impaired nociception in the diabetic Ins2 +/Akita mouse. *Diabetes* **67**, 1650–1662 (2018).
147. González, A. *et al.* Role of the excitability brake potassium current I KD in cold allodynia induced by chronic peripheral nerve injury. *J. Neurosci.* **37**, 3553–16 (2017).
148. Madrid, R., De La Peña, E., Donovan-Rodriguez, T., Belmonte, C. & Viana, F. Variable threshold of trigeminal cold-thermosensitive neurons is determined by a balance between TRPM8 and Kv1 potassium channels. *J. Neurosci.* **29**, 3120–3131 (2009).
149. Chisholm, K. I., Khovanov, N., Lopes, D. M., La Russa, F. & McMahon, S. B. Large scale in vivo recording of sensory neuron activity with GCaMP6. *eNeuro* **5**, e0417-17.2018 1–14 (2018).
150. Emery, E. C. *et al.* In vivo characterization of distinct modality-specific subsets of somatosensory neurons using GCaMP. *Sci. Adv.* **2**, e1600990–e1600990 (2016).
151. Luiz, A. P. *et al.* Cold sensing by Nav1.8-positive and Nav1.8-negative sensory neurons. *Proc. Natl. Acad. Sci.* 201814545 (2019). doi:10.1073/pnas.1814545116
152. Li, C.-L. *et al.* Somatosensory neuron types identified by high-coverage single-cell RNA-sequencing and functional heterogeneity. *Cell Res.* **26**, 83–102 (2016).
153. Li, C., Wang, S., Chen, Y. & Zhang, X. Somatosensory Neuron Typing with High-Coverage Single-Cell RNA Sequencing and Functional Analysis. *Neuroscience Bulletin* **34**, 200–207 (2018).
154. Usoskin, D. *et al.* Unbiased classification of sensory neuron types by large-scale single-cell RNA sequencing. *Nat. Neurosci.* **18**, 145–153 (2015).
155. Zeisel, A. *et al.* Molecular Architecture of the Mouse Nervous System. *Cell* **174**, 999-1014.e22 (2018).
156. Emery, E. C., Ernfors, P., Emery, E. C. & Ernfors, P. Dorsal Root Ganglion Neuron Types and Their Functional Specialization. *Oxford Handb. Neurobiol. Pain* 1–30 (2018). doi:10.1093/oxfordhb/9780190860509.013.4
157. Todd, A. J. *et al.* Projection neurons in lamina I of rat spinal cord with the neurokinin 1 receptor are selectively innervated by substance p-containing afferents and respond to noxious stimulation. *J. Neurosci.* **22**, 4103–13 (2002).

158. Peirs, C. & Seal, R. P. Neural circuits for pain: Recent advances and current views. *Science* **354**, 578–584 (2016).
159. Sikandar, S., West, S. J., McMahon, S. B., Bennett, D. L. & Dickenson, A. H. Sensory processing of deep tissue nociception in the rat spinal cord and thalamic ventrobasal complex. *Physiol. Rep.* **5**, e13323 (2017).
160. Tan, A. M., Chang, Y.-W., Zhao, P., Hains, B. C. & Waxman, S. G. Rac1-regulated dendritic spine remodeling contributes to neuropathic pain after peripheral nerve injury. *Exp. Neurol.* **232**, 222–233 (2011).
161. Grudt, T. J. & Perl, E. R. Correlations between neuronal morphology and electrophysiological features in the rodent superficial dorsal horn. *J. Physiol.* **540**, 189–207 (2002).
162. Boyle, K. A. *et al.* A quantitative study of neurochemically defined populations of inhibitory interneurons in the superficial dorsal horn of the mouse spinal cord. *Neuroscience* **363**, 120–133 (2017).
163. Gutierrez-Mecinas, M., Bell, A., Polgár, E., Watanabe, M. & Todd, A. J. Expression of Neuropeptide FF Defines a Population of Excitatory Interneurons in the Superficial Dorsal Horn of the Mouse Spinal Cord that Respond to Noxious and Pruritic Stimuli. *Neuroscience* **416**, 281–293 (2019).
164. Dickie, A. C. *et al.* Morphological and functional properties distinguish the substance P and gastrin-releasing peptide subsets of excitatory interneuron in the spinal cord dorsal horn. *Pain* **160**, 442–462 (2019).
165. Häring, M. *et al.* Neuronal atlas of the dorsal horn defines its architecture and links sensory input to transcriptional cell types. *Nat. Neurosci.* **21**, 869–880 (2018).
166. Sathyamurthy, A. *et al.* Massively Parallel Single Nucleus Transcriptional Profiling Defines Spinal Cord Neurons and Their Activity during Behavior. *Cell Rep.* **22**, 2216–2225 (2018).
167. Graham, B. A. & Hughes, D. I. Rewards, perils and pitfalls of untangling spinal pain circuits. *Current Opinion in Physiology* **11**, 35–41 (2019).
168. Ross, S. E. *et al.* Loss of Inhibitory Interneurons in the Dorsal Spinal Cord and Elevated Itch in Bhlhb5 Mutant Mice. *Neuron* **65**, 886–898 (2010).
169. Foster, E. *et al.* Targeted ablation, silencing, and activation establish glycinergic dorsal horn neurons as key components of a spinal gate for pain and itch. *Neuron* **85**, 1289–1304 (2015).
170. Lorenzo, L. E. *et al.* Spatial and temporal pattern of changes in the number of GAD65-immunoreactive inhibitory terminals in the rat superficial dorsal horn following peripheral nerve injury. *Mol. Pain* **10**, 1744-8069-10–57 (2014).
171. Polgár, E. & Todd, A. J. Tactile allodynia can occur in the spared nerve injury model in the rat without selective loss of GABA or GABAA receptors from synapses in laminae I-II of the ipsilateral spinal dorsal horn. *Neuroscience* **156**, 193–202 (2008).
172. Hughes, D. I. *et al.* Morphological, neurochemical and electrophysiological features of parvalbumin-expressing cells: A likely source of axo-axonic inputs in the mouse spinal dorsal horn. *J. Physiol.* **590**, 3927–3951 (2012).
173. Mapplebeck, J. C. S. *et al.* Chloride Dysregulation through Downregulation of KCC2 Mediates Neuropathic Pain in Both Sexes. *Cell Rep.* **28**, 590-596.e4 (2019).
174. Guan, Z. *et al.* Injured sensory neuron-derived CSF1 induces microglial proliferation and DAP12-dependent pain. *Nat. Neurosci.* **19**, 94–101 (2015).
175. Mapplebeck, J. C. S. *et al.* Microglial P2X4R-evoked pain hypersensitivity is sexually dimorphic in rats. *Pain* **159**, 1752–1763 (2018).
176. Seal, R. P. *et al.* Injury-induced mechanical hypersensitivity requires C-low threshold mechanoreceptors. *Nature* **462**, 651–655 (2009).
177. Dhandapani, R. *et al.* Control of mechanical pain hypersensitivity in mice through ligand-targeted photoablation of TrkB-positive sensory neurons. *Nat. Commun.* **9**, (2018).
178. Lu, Y. *et al.* A feed-forward spinal cord glycinergic neural circuit gates mechanical

allodynia. *J. Clin. Invest.* **123**, 4050–4062 (2013).
179. Zhang, Y. *et al.* Timing Mechanisms Underlying Gate Control by Feedforward Inhibition. *Neuron* **99**, 941-955.e4 (2018).
180. Duan, B. *et al.* Identification of spinal circuits transmitting and gating mechanical pain. *Cell* **159**, 1417–1432 (2014).
181. Li, C. L. *et al.* Somatosensory neuron types identified by high-coverage single-cell RNA-sequencing and functional heterogeneity. *Cell Res.* **26**, 83–102 (2016).
182. Arcourt, A. *et al.* Touch Receptor-Derived Sensory Information Alleviates Acute Pain Signaling and Fine-Tunes Nociceptive Reflex Coordination. *Neuron* **93**, 179–193 (2016).
183. Weir, G. A. *et al.* Using an engineered glutamate-gated chloride channel to silence sensory neurons and treat neuropathic pain at the source. *Brain* **140**, 2570–2585 (2017).
184. Saloman, J. L. *et al.* Gi-DREADD Expression in Peripheral Nerves Produces Ligand-Dependent Analgesia, as well as Ligand-Independent Functional Changes in Sensory Neurons. *J. Neurosci.* **36**, 10769–10781 (2016).
185. Koga, K. *et al.* Chemogenetic silencing of GABAergic dorsal horn interneurons induces morphine-resistant spontaneous nocifensive behaviours. *Sci. Rep.* **7**, 4739 (2017).
186. Wiegert, J. S., Mahn, M., Prigge, M., Printz, Y. & Yizhar, O. Silencing Neurons: Tools, Applications, and Experimental Constraints. *Neuron* **95**, 504–529 (2017).
187. Rasband, M. N. *et al.* Distinct potassium channels on pain-sensing neurons. *Proc. Natl. Acad. Sci.* **98**, 13373–13378 (2001).
188. Trimmer, J. S. Subcellular localization of K+ channels in mammalian brain neurons: Remarkable precision in the midst of extraordinary complexity. *Neuron* **85**, 238–256 (2015).
189. Zheng, Y. *et al.* Deep Sequencing of Somatosensory Neurons Reveals Molecular Determinants of Intrinsic Physiological Properties. *Neuron* **103**, 1–19 (2019).
190. Gutman, G. A. *et al.* International Union of Pharmacology. LIII. Nomenclature and molecular relationships of voltage-gated potassium channels. *Pharmacol. Rev.* **57**, 473–508 (2005).
191. Wei, A. D. *et al.* International Union of Pharmacology. LII. Nomenclature and molecular relationships of calcium-activated potassium channels. *Pharmacological Reviews* **57**, 463–472 (2005).
192. Kubo, Y. *et al.* International Union of Pharmacology. LIV. Nomenclature and Molecular Relationships of Inwardly Rectifying Potassium Channels. *Pharmacol. Rev.* **57**, (2005).
193. Goldstein, S. a N., Bayliss, D. a, Kim, D., Lesage, F. & Plant, L. D. International Union of Pharmacology. LV. Nomenclature andmolecular relationships of two-P potassium channels. *Pharmacol. Rev.* **57**, 527–540 (2005).
194. Busserolles, J., Tsantoulas, C., Eschalier, A. & García, J. A. L. Potassium channels in neuropathic pain: Advances, challenges, and emerging ideas. in *Pain* **157**, S7–S14 (2016).
195. Mathie, A. & Veale, E. L. Two-pore domain potassium channels: Potential therapeutic targets for the treatment of pain. *Pflugers Archiv European Journal of Physiology* **467**, 931–943 (2015).
196. Du, X. *et al.* Control of somatic membrane potential in nociceptive neurons and its implications for peripheral nociceptive transmission. *Pain* **155**, 2306–2322 (2014).
197. Weir, G. A. *et al.* The Role of TRESK in Discrete Sensory Neuron Populations and Somatosensory Processing. *Front. Mol. Neurosci.* **12**, 170 (2019).
198. Lafrenière, R. G. *et al.* A dominant-negative mutation in the TRESK potassium channel is linked to familial migraine with aura. *Nat. Med.* **16**, 1157–1160 (2010).
199. MacKinnon, R. Determination of the subunit stoichiometry of a voltage-activated potassium channel. *Nature* **350**, 232–235 (1991).
200. Tsantoulas, C. *et al.* Sensory Neuron Downregulation of the Kv9.1 Potassium Channel Subunit Mediates Neuropathic Pain following Nerve Injury. *J. Neurosci.* **32**, 17502–17513

(2012).
201. Lee, M. C. *et al.* Human labor pain is influenced by the voltage-gated potassium channel KV6.4 subunit. *bioRxiv* 489310 (2018). doi:10.1101/489310
202. Fox, P. D. *et al.* Induction of stable ER-plasma-membrane junctions by Kv2.1 potassium channels. *J. Cell Sci.* **128**, 2096–2105 (2015).
203. Johnson, B. *et al.* Kv2 potassium channels form endoplasmic reticulum/plasma membrane junctions via interaction with VAPA and VAPB. *Proc. Natl. Acad. Sci. U. S. A.* **115**, E7331–E7340 (2018).
204. Hu, H. J. *et al.* The Kv4.2 Potassium Channel Subunit Is Required for Pain Plasticity. *Neuron* **50**, 89–100 (2006).
205. Browne, D. L. *et al.* Episodic ataxia/myokymia syndrome is associated with point mutations in the human potassium channel gene, KCNA1. *Nat. Genet.* **8**, 136–140 (1994).
206. Smart, S. L. *et al.* Deletion of the K(v)1.1 Potassium channel causes epilepsy in mice. *Neuron* **20**, 809–819 (1998).
207. Wang, H., Kunkel, D. O., Schwartzkroin, P. A. & Tempel, B. L. Localization of Kv1.1 and Kv1.2, two K channel proteins, to synaptic terminals, somata, and dendrites in the mouse brain. *J. Neurosci.* **14**, 4588–4599 (1994).
208. Robbins, C. A. & Tempel, B. L. Kv1.1 and Kv1.2: Similar channels, different seizure models. *Epilepsia* **53**, 134–141 (2012).
209. Bertoli, A., Moran, O. & Conti, F. Activation and deactivation properties of rat brain K+ channels of the Shaker-related subfamily. *Eur. Biophys. J.* **23**, 379–384 (1994).
210. Al-Sabi, A. *et al.* Position-dependent attenuation by Kv1.6 of N-type inactivation of Kv1.4-containing channels. *Biochem. J.* **438**, 389–96 (2011).
211. Teichert, R. W. *et al.* Functional profiling of neurons through cellular neuropharmacology. *Proc. Natl. Acad. Sci. U. S. A.* **109**, 1388–95 (2012).
212. Calvo, M. *et al.* Altered potassium channel distribution and composition in myelinated axons suppresses hyperexcitability following injury. *Elife* **5**, 1–26 (2016).
213. Hao, J. *et al.* Kv1.1 channels act as mechanical brake in the senses of touch and pain. *Neuron* **77**, 899–914 (2013).
214. Zhao, X. *et al.* A long noncoding RNA contributes to neuropathic pain by silencing Kcna2 in primary afferent neurons. *Nat. Neurosci.* **16**, 1024–1031 (2013).
215. Poliak, S. *et al.* Juxtaparanodal clustering of Shaker-like K+ channels in myelinated axons depends on Caspr2 and TAG-1. *J. Cell Biol.* **162**, 1149–1160 (2003).
216. Poliak, S. & Peles, E. The local differentiation of myelinated axons at nodes of Ranvier. *Nat. Rev. Neurosci.* **4**, 968–980 (2003).
217. Irani, S. R. *et al.* Antibodies to Kv1 potassium channel-complex proteins leucine-rich, glioma inactivated 1 protein and contactin-associated protein-2 in limbic encephalitis, Morvan's syndrome and acquired neuromyotonia. *Brain* **133**, 2734–2748 (2010).
218. Irani, S. R. *et al.* Morvan syndrome: Clinical and serological observations in 29 cases. *Ann. Neurol.* **72**, 241–255 (2012).
219. Arimura, K. *et al.* Isaacs' syndrome as a potassium channelopathy of the nerve. *Muscle Nerve* **Suppl 11**, S55–S58 (2002).
220. Klein, C. J., Lennon, V. a., Aston, P. a., McKeon, A. & Pittock, S. J. Chronic pain as a manifestation of potassium channel-complex autoimmunity. *Neurology* **79**, 1136–1144 (2012).
221. Lang, B. *et al.* Intracellular and non-neuronal targets of voltage-gated potassium channel complex antibodies. *J. Neurol. Neurosurg. Psychiatry* **88**, 353–361 (2017).
222. Grupe, A. *et al.* Cloning and expression of a human voltage-gated potassium channel. A novel member of the RCK potassium channel family. *EMBO J.* **9**, 1749–1756 (1990).
223. Han, Y. *et al.* Functional ion channels in mouse cardiac c-kit(+) cells. *Am. J. Physiol. Cell Physiol.* **298**, C1109–C1117 (2010).

224. Marionneau, C. *et al.* Specific pattern of ionic channel gene expression associated with pacemaker activity in the mouse heart. *J. Physiol.* **562**, 223–234 (2005).
225. Hong, D. H. *et al.* Alterations of voltage-dependent K + channels in the mesenteric artery during the early and chronic phases of diabetes. *Clin. Exp. Pharmacol. Physiol.* **43**, 808–817 (2016).
226. Kim, E., Park, W. S. & Hong, S.-H. Expression of Ion Channels in Perivascular Stem Cells derived from Human Umbilical Cords. *Dev. Reprod.* **21**, 11–18 (2017).
227. Carrisoza-Gaytán, R., Salvador, C., Diaz-Bello, B. & Escobar, L. I. Differential expression of the Kv1 voltage-gated potassium channel family in the rat nephron. *J. Mol. Histol.* **45**, 583–597 (2014).
228. Clark, R. B. *et al.* Voltage-gated K+ currents in mouse articular chondrocytes regulate membrane potential. *Channels (Austin).* **4**, 179–191 (2010).
229. Smart, S. L., Bosma, M. M. & Tempel, B. L. Identification of the delayed rectifier potassium channel, Kv1.6, in cultured astrocytes. *Glia* **20**, 127–34 (1997).
230. Attali, B. *et al.* Characterization of delayed rectifier Kv channels in oligodendrocytes and progenitor cells. *J. Neurosci.* **17**, 8234–8245 (1997).
231. Zhu, J., Yan, J. & Thornhill, W. B. The Kv1.3 potassium channel is localized to the cis-Golgi and Kv1.6 is localized to the endoplasmic reticulum in rat astrocytes. *FEBS J.* **281**, 3433–3445 (2014).
232. Chittajallu, R. *et al.* Regulation of Kv1 subunit expression in oligodendrocyte progenitor cells and their role in G1/S phase progression of the cell cycle. *Proc. Natl. Acad. Sci. U. S. A.* **99**, 2350–2355 (2002).
233. Sobko, A. *et al.* Heteromultimeric delayed-rectifier K+ channels in schwann cells: developmental expression and role in cell proliferation. *J. Neurosci.* **18**, 10398–408 (1998).
234. Chung, Y. H., Shin, C., Kim, M. J. & Cha, C. I. Immunohistochemical study on the distribution of six members of the Kv1 channel subunits in the rat basal ganglia. *Brain Res.* **875**, 164–170 (2000).
235. Chung, Y. H., Shin, C.-M., Kim, M. J., Lee, B. K. & Cha, C. I. Immunohistochemical study on the distribution of six members of the Kv1 channel subunits in the rat cerebellum. *Brain Res.* **895**, 173–177 (2001).
236. Matus-Leibovitch, N. *et al.* Chronic morphine administration enhances the expression of Kv1.5 and Kv1.6 voltage-gated K+ channels in rat spinal cord. *Mol. Brain Res.* **40**, 261–70 (1996).
237. Glazebrook, P. A. *et al.* Potassium channels Kv1.1, Kv1.2 and Kv1.6 influence excitability of rat visceral sensory neurons. *J. Physiol.* **541**, 467–482 (2002).
238. Yang, E.-K., Takimoto, K., Hayashi, Y., de Groat, W. C. & Yoshimura, N. Altered expression of potassium channel subunit mRNA and alpha-dendrotoxin sensitivity of potassium currents in rat dorsal root ganglion neurons after axotomy. *Neuroscience* **123**, 867–74 (2004).
239. Wang, X.-C. *et al.* α-dendrotoxin sensitive Kv1 channels contribute to conduction failure of polymodal nociceptive C-fibers from rat coccygeal nerve. *J. Neurophysiol.* **115**, 947–957 (2015).
240. Ray, P. *et al.* Comparative transcriptome profiling of the human and mouse dorsal root ganglia. *Pain* **159**, 1325–1345 (2018).
241. Ishikawa, K., Tanaka, M., Black, J. a & Waxman, S. G. Changes in expression of voltage-gated potassium channels in dorsal root ganglion neurons following axotomy. *Muscle Nerve* **22**, 502–507 (1999).
242. Megat, S. *et al.* Nociceptor translational profiling reveals the ragulator-rag gtpase complex as a critical generator of neuropathic pain. *J. Neurosci.* **39**, 393–411 (2019).

Chapter II

Characterisation of *Kcna6* expression in the mouse somatosensory axis

Recent research[1] has provided a rationale for studying the contribution of Kv1.6 to somatosensation and pain, particularly in the context of traumatic nerve injury. Large-scale single-cell[2,3] and bulk[4] RNA sequencing projects using dissociated cells have already identified *Kcna6* expression within distinct DRG populations, but these experiments are not without their caveats. Isolation of individual cells is a traumatic process involving major axotomy, and we know that Kv1.6 is upregulated after axotomy, at the very least in sensory neurons[1]. While deservedly lauded for their considerable effort, these experiments are perhaps more representative of an injured nervous system and it is possible that *Kcna6* expression is overestimated in some neuronal populations. Also, limitations of sequencing depth may give false negative results for some genes with low expression counts, which may also include *Kcna6* in other neuronal populations.

Arguably, rapid tissue fixation followed by *in situ* hybridisation is more likely to preserve and accurately report mRNA expression as close to the naïve state as possible and is therefore a preferable but low-throughput approach to study expression of individual or small numbers of genes. Indeed, *in situ* hybridisation was used as a gold standard to validate much of the single-cell RNA sequencing data from DRGs[2], spinal cord interneurons[5], and the rest of the mouse nervous system[3].

I have employed a combined fluorescent *in situ* hybridisation and immunohistochemistry approach to directly visualise expression of *Kcna6* mRNA in classical immunohistochemically defined DRG subpopulations, and in the spinal cord, of wild type mice. Counter-intuitively, it is also possible to indirectly study *Kcna6* expression in knock-out tissue, using the *Kcna6*^{tm1Lex}/Mmucd mouse. This

knock-out line was created by insertion of the bacterial (*E. coli*) *lacZ* transgene (featuring a downstream neomycin phosphotransferase selection cassette), encoding β-galactosidase. The transgene was introduced via homologous recombination in place of a 1640bp region encompassing more than the entire 1587bp (529aa) translated region of *Kcna6* exon 1 – the sole protein-coding exon from a total of 2. Thus, β-galactosidase functions as a reporter protein in carriers of this allele. This reporter mouse has been useful for validation of *in situ* hybridisation data and screening for *Kcna6* expression in other CNS regions.

As distinct sensory functions are progressively ascribed to genetically defined neuronal populations along the somatosensory neuraxis **Fig1.2**, knowledge of ion channel expression across these populations may enable us to predict contributions of individual ion channels to sensation. Kv1 subunits, including Kv1.6, are understood to fulfil functions in sensory neurons by regulating plasma membrane potential, evidenced by observation of Kv1 currents with patch-clamp electrophysiology[4,6]. However, this does not exclude the possibility of functions elsewhere in the cell, involving regulation of organelle membrane potential or other unknown mechanisms. I therefore sought to directly visualise and confirm plasma membrane Kv1.6 expression in dissociated DRGs, and to investigate other subcellular localisations of this channel.

In this chapter, I present the first targeted, systematic analysis of *Kcna6* expression within the somatosensory nervous system. The most comprehensive investigation focuses on expression in peripheral sensory neurons of the dorsal root ganglia.

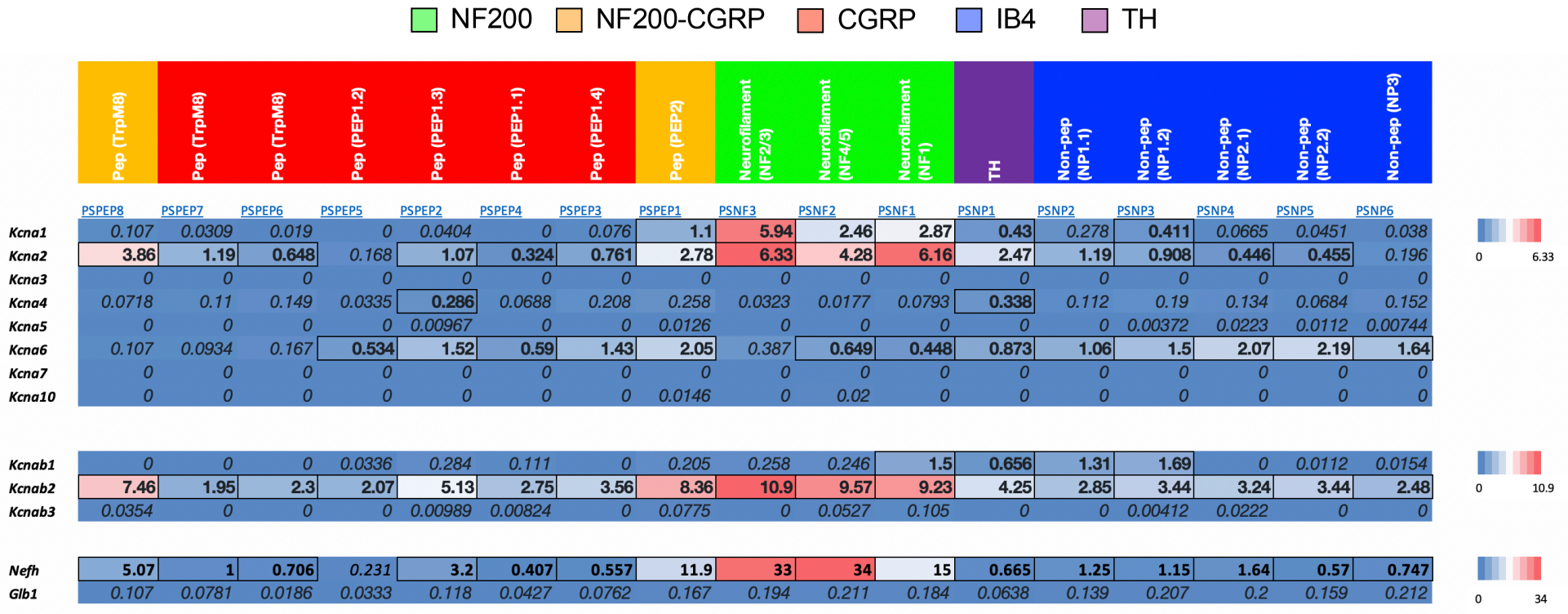

	Pep (TrpM8)	Pep (TrpM8)	Pep (TrpM8)	Pep (PEP1.2)	Pep (PEP1.3)	Pep (PEP1.1)	Pep (PEP1.4)	Pep (PEP2)	Neurofilament (NF2/3)	Neurofilament (NF4/5)	Neurofilament (NF1)	TH	Non-pep (NP1.1)	Non-pep (NP1.2)	Non-pep (NP2.1)	Non-pep (NP2.2)	Non-pep (NP3)
	PSPEP8	PSPEP7	PSPEP6	PSPEP5	PSPEP2	PSPEP4	PSPEP3	PSPEP1	PSNF3	PSNF2	PSNF1	PSNP1	PSNP2	PSNP3	PSNP4	PSNP5	PSNP6
Kcna1	*0.107*	*0.0309*	*0.019*	*0*	*0.0404*	*0*	*0.076*	1.1	5.94	2.46	2.87	0.43	*0.278*	0.411	*0.0665*	*0.0451*	*0.038*
Kcna2	3.86	1.19	0.648	*0.168*	1.07	0.324	0.761	2.78	6.33	4.28	6.16	2.47	1.19	0.908	0.446	0.455	*0.196*
Kcna3	*0*	*0*	*0*	*0*	*0*	*0*	*0*	*0*	*0*	*0*	*0*	*0*	*0*	*0*	*0*	*0*	*0*
Kcna4	*0.0718*	*0.11*	*0.149*	*0.0335*	0.286	*0.0688*	*0.208*	*0.258*	*0.0323*	*0.0177*	*0.0793*	0.338	*0.112*	*0.19*	*0.134*	*0.0684*	*0.152*
Kcna5	*0*	*0*	*0*	*0*	*0.00967*	*0*	*0*	*0.0126*	*0*	*0*	*0*	*0*	*0*	*0.00372*	*0.0223*	*0.0112*	*0.00744*
Kcna6	*0.107*	*0.0934*	*0.167*	0.534	1.52	0.59	1.43	2.05	*0.387*	0.649	0.448	0.873	1.06	1.5	2.07	2.19	1.64
Kcna7	*0*	*0*	*0*	*0*	*0*	*0*	*0*	*0*	*0*	*0*	*0*	*0*	*0*	*0*	*0*	*0*	*0*
Kcna10	*0*	*0*	*0*	*0*	*0*	*0*	*0*	*0.0146*	*0*	*0.02*	*0*	*0*	*0*	*0*	*0*	*0*	*0*
Kcnab1	*0*	*0*	*0*	*0.0336*	*0.284*	*0.111*	*0*	*0.205*	*0.258*	*0.246*	1.5	0.656	1.31	1.69	*0*	*0.0112*	*0.0154*
Kcnab2	7.46	1.95	2.3	2.07	5.13	2.75	3.56	8.36	10.9	9.57	9.23	4.25	2.85	3.44	3.24	3.44	2.48
Kcnab3	*0.0354*	*0*	*0*	*0*	*0.00989*	*0.00824*	*0*	*0.0775*	*0*	*0.0527*	*0.105*	*0*	*0*	*0.00412*	*0.0222*	*0*	*0*
Nefh	5.07	1	0.706	*0.231*	3.2	0.407	0.557	11.9	33	34	15	0.665	1.25	1.15	1.64	0.57	0.747
Glb1	*0.107*	*0.0781*	*0.0186*	*0.0333*	*0.118*	*0.0427*	*0.0762*	*0.167*	*0.194*	*0.211*	*0.184*	*0.0638*	*0.139*	*0.207*	*0.2*	*0.159*	*0.212*

0 6.33

0 10.9

0 34

Table 2.1 – Kv1 subunit expression in DRG populations

Extracted from *Zeisel et al. (2018)* at *mousebrain.org*. Log2 expression values of Kv1 alpha and beta subunits in 17 DRG subpopulations defined by transcriptomic clustering. Populations have been colour coded to match those defined by classical immunohistochemical staining in **Fig.1**, with the CGRP/NF200 (orange) population defined as peptidergic clusters with high (>5) expression of the heavy neurofilament *Nefh*. Values formatted with outlines and bold text represent genes with trinarisation scores of >0.95 in the relevant population, as reported at mousebrain.org, which can be considered to have a high probability of expression in the respective cluster. Italicised values fall below the 0.95 probability score.

Endogenous β-galactosidase (*Glb1*) expression is low in all populations.

i. Results

Dorsal Root Ganglia

a) Quantification of *Kcna6* mRNA via *in situ* hybridisation probes

Using a chromogenic *in situ* hybridisation protocol, with commercially produced probes targeting base pairs 101-1399 of the *Kcna6* transcript, I have been able to visualise *Kcna6* mRNA expression in wild type mouse L4 DRG neurons for the first time. Classical immunohistochemical markers for myelinated neurons (NF200), peptidergic (CGRP) and non-peptidergic (IB4) nociceptors, and C-LTMRs (TH) were used as neuronal counter-stains, as well as a marker of satellite glia (glutamine synthetase[7]) **Fig2.1(A)**. Compiling mean red-channel pixel intensity from all stained cells with nuclei, there is a significant negative correlation of *Kcna6* mRNA intensity with neuronal cell size (non-parametric Spearman correlation coefficient $r = -0.2817$, $p<0.0001$) **Fig2.1(B.i)**. Taking into account variation between biological replicates (where n = number of animals), on average the *Kcna6* transcript was most abundant per unit of cell area in small ($<500\mu m^2$) neurons (small 21.98 ± 2.78a.u.*****, medium 19.34 ± 0.31a.u., large 13.65 ± 0.81a.u., ***** = $p<0.05$ vs. large, One-Way ANOVA with Tukey's post-hoc multiple comparisons test) **Fig2.1(B.ii)**. Arbitrary units of quantification (a.u.) represent mean pixel intensity on a percentage scale, defined in the "image acquisition" methods.

Using immunohistochemical markers for classical DRG subpopulations, I also identified that *Kcna6* expression was greater in nociceptors than non-nociceptive neurons. Analysis of all nucleated cells showed that the vast majority of neurons in the $NF200^+$ population of LTMRs had very low mean *Kcna6* intensity values **Fig2.1(C.i)**. In contrast, neurons of other populations have higher *Kcna6* expression, and the violin distribution plots **Fig2.1(C.i)** even suggest that *Kcna6* expression may

be differentially regulated in subpopulations within some histochemically-defined populations. This would be expected in line with varied *Kcna6* mRNA expression reported across single-cell transcriptomic clusters[3] within each classical population **Table 2.1**. Definitions of 'positive' expression signal are discussed in the conclusion of this chapter.

When average expression in each population was calculated per animal, the statistically greatest expression was in neurons co-expressing both CGRP and NF200 **Fig2.1(C.ii)**. This population is thought to represent thinly myelinated, peptidergic Aδ-fibres including Aδ-nociceptors. The Aδ population is known to comprise medium-diameter DRG neurons; indeed, the majority of CGRP/NF200 double-positive neurons were found to have a somal area between 500-1000μm^2 (data not shown). *Kcna6* expression was also statistically higher than background signal in CGRP$^+$ and IB4$^+$ neurons, but not in NF200$^+$ or TH$^+$ neurons **Fig2.1(C.ii)**. However, some NF200$^+$ and TH$^+$ neurons do visibly express *Kcna6* **Fig2.1(A, C.i)**. These are confirmatory findings to the expression analysis based on size alone, in that nociceptive (small-to-medium diameter) populations clearly express *Kcna6* to a greater degree than large-diameter, NF200-expressing Aβ-fibres. Additionally, positive mRNA signal was observed in cell bodies of satellite glia **Fig2.1(A, arrow/asterisk)**, demarcated by their expression of the glutamate-recycling enzyme glutamine synthetase, previously identified in satellite glial cells[7].

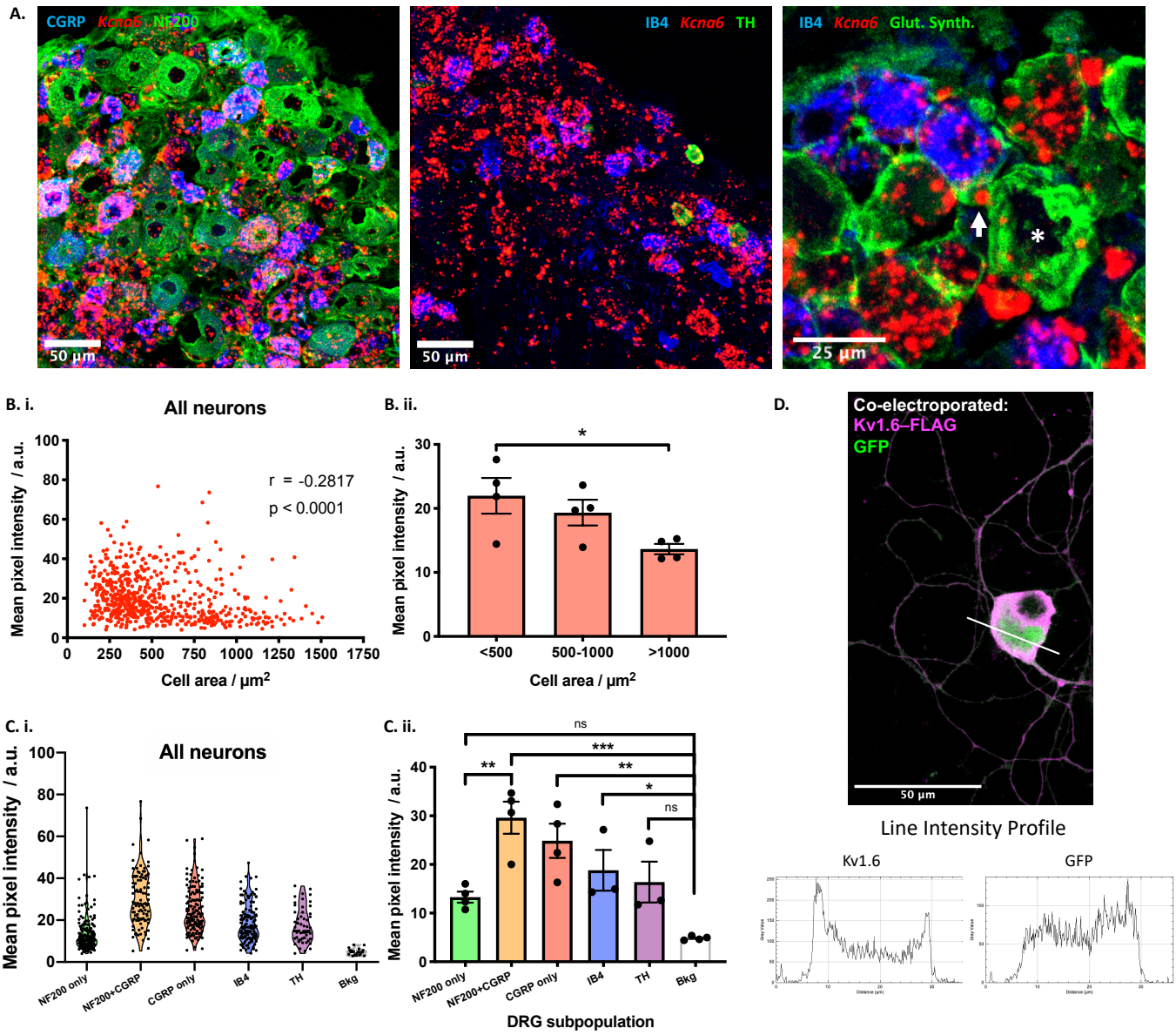

Figure 2.1 – *Kcna6* mRNA is expressed in DRG neurons

(A) Combined fluorescent *in situ* hybridisation and immunohistochemistry reveals *Kcna6* mRNA expression in the lumbar (L4) dorsal root ganglia. *Kcna6 in situ* signal intensity was analysed in L4 DRGs immunostained for neuronal markers NF200 and CGRP or IB4 and TH, or with IB4 and satellite glial marker glutamine synthetase. Some expression in satellite glial cells ensheathing an IB4-labelled neuron (arrow) and a larger, IB4-negative neuron (asterisk) are indicated.
(B.i.) *Kcna6* expression across all neurons analysed from 4 animals is negatively correlated with cell size (non-parametric two-tailed Spearman's correlation, r = -0.2817, p<0.0001). **(B.ii.)** On per-animal analysis small (<500µm^2) compared to large (>1000µm^2) diameter DRG neurons had higher expression. n = 4 WT animals per category,
***** = p<0.05 <500 vs. >1000 (small vs. large) (Ordinary One-Way ANOVA with Tukey's post-hoc multiple comparisons test).
(C.i.) Differentiating DRG populations by histochemical markers reveals generally very low *Kcna6* expression in the majority of myelinated (NF200$^+$) neurons analysed. Data points represent individual neurons, combined from all DRG sections from all animals. Bkg = background signal from attached nerve root.
(C.ii.) On per-animal analysis, expression is highest in nociceptive populations. Data points are mean values from individual replicates, plotted with overall WT mean ± SEM. n = 4 or 3 WT animals per category, */**/*** = p<0.05/0.01/0.001 (One-way ANOVA with Tukey's post hoc multiple comparisons test).
(D) Co-electroporation of a FLAG/Myc-tagged Kv1.6 plasmid with a GFP plasmid in dissociated wild-type mouse DRG neurons. Intensity values for each colour channel along the white line drawn through the cell are displayed. Kv1.6 intensity has peaks at cell extremities indicating membrane trafficking. GFP signal is constant throughout the cytoplasm.

b) Subcellular distribution of Kv1.6 in DRG neurons

Unfortunately, several commercial antibodies against mouse Kv1.6 were not reliable in detecting Kv1.6 expression in fixed tissue, dissociated cells, or protein extracts for Western blotting (not shown). To understand the function of this particular subunit, an appreciation of subcellular protein localisation is imperative, in addition to the distribution of *Kcna6* mRNA transcripts across DRG populations described previously. In pursuit of sound pharmacological targets, proteins expressed at the plasma membrane are also more appealing. Thus, I sought an alternative approach to study the subcellular trafficking of this subunit and validate its presence in the plasma membrane. DRGs were extracted from adult wild-type mice and were cultured *in vitro* after electroporation with FLAG/Myc-tagged Kv1.6 and unconjugated GFP constructs. Immunostaining for the FLAG tag revealed trafficking of Kv1.6 to the plasma membrane, identifiable by the two fluorescence peaks along the line intensity profile depicted in **Fig2.1(D)**. There was also evidence of perinuclear staining, indicating enrichment in the endoplasmic reticulum (ER). In contrast, GFP fluorescence was dispersed throughout the cytoplasm as expected.

c) Expression of a *Kcna6* surrogate, β-galactosidase, in *Kcna6*^{tm1Lex} mice

DRGs from homozygous *Kcna6*^{tm1Lex} mice were also used to validate *in situ* hybridisation data. The *Kcna6*^{tm1Lex} allele contains a *lacZ* cassette knocked in to the sole protein coding exon **Fig2.2(A)**, which is expressed under the endogenous *Kcna6* promoter, and hereon in treated as a surrogate for *Kcna6* expression. Knock-out of *Kcna6* was confirmed via quantitative reverse-transcriptase PCR (RT-qPCR), revealing a <tm1Lex> zygosity-dependent reduction in *Kcna6* transcript expression in RNA extracted from brain tissue **Fig2.2(A)**. Incidentally, expression of *Kcna1* and *Kcna2* transcripts were not affected by knock-out of *Kcna6*. Knock-out was also confirmed by *de novo* β-galactosidase

protein expression in DRG neurons **Fig2.2(B)**, identifiable by immunohistochemistry in knock-out but not wild-type tissue, demonstrating integration of the <tm1Lex> allele into the *Kcna6* locus. This approach confirmed suspicions of *Kcna6* expression in satellite glia **Fig2.2(C.i, C.ii, D)**, and validated *in situ* hybridisation findings in the same $NF200^+/CGRP^+$, $CGRP^+$, $IB4^+$, and TH^+ DRG populations **Fig2.2(E, F)**. I have also identified *Kcna6* promoter-driven expression in the DRG using an X-GAL staining protocol for β-galactosidase enzymatic activity **Fig2.2(G)**. It was possible to identify the reporter in small- to medium-diameter neurons, with large *Kcna6*-negative neurons made apparent by positive staining of surrounding satellite glia **Fig2.2(G, arrows)**. Within the attached nerve root, there was some positive staining, either depicting axons emanating from positive DRG cells, or Schwann cell expression of *Kcna6*.

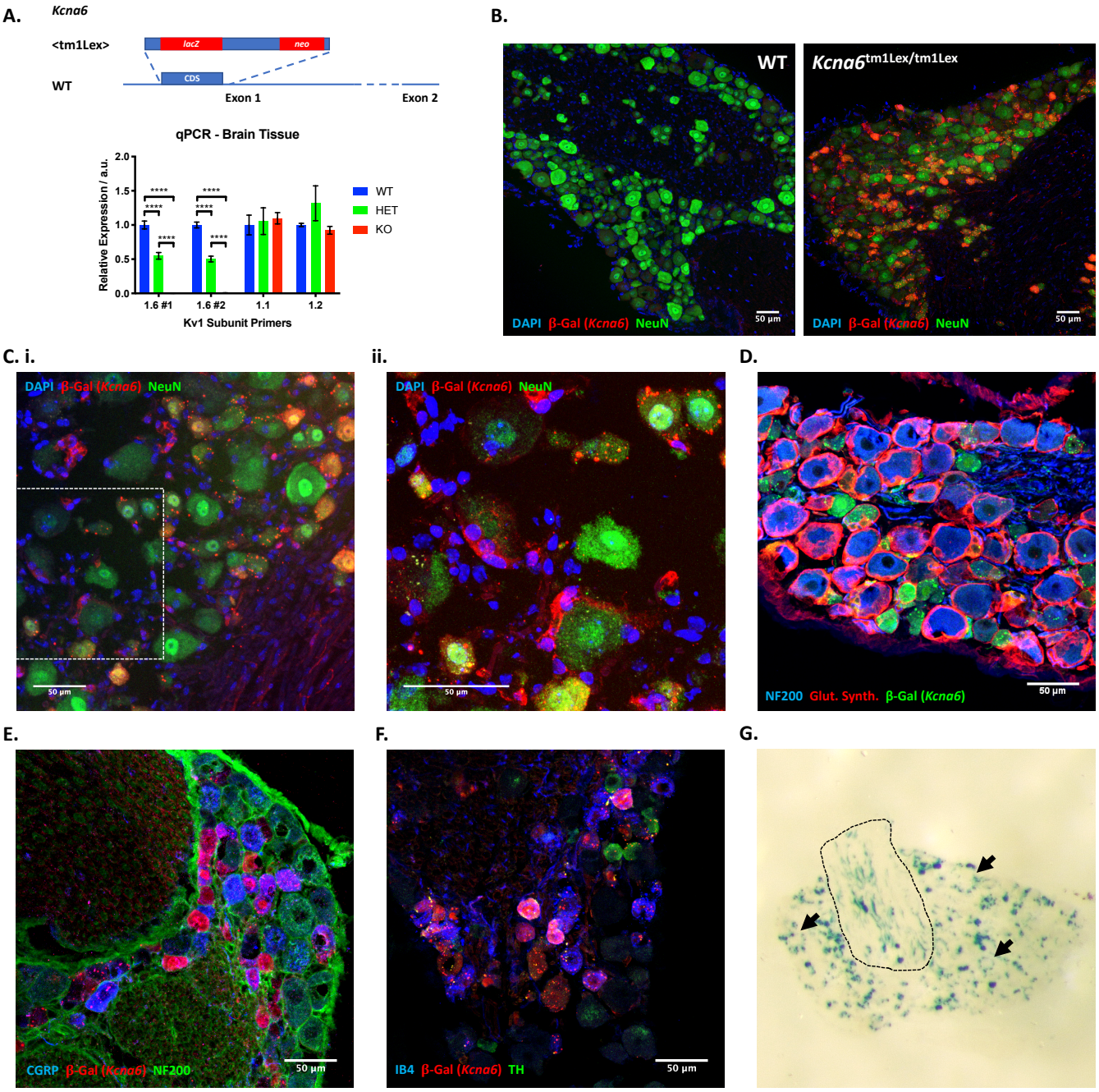

Figure 2.2 – *lacZ* (β-galactosidase) expression in *Kcna6*^{tm1Lex} DRG

(A) *Kcna6*^{tm1Lex} mice have a large deletion of *Kcna6* exon 1 via homologous recombination with the ~5kb <tm1Lex> cassette containing an open reading frame for *E.coli* β-galactosidase gene *lacZ*, and a neomycin resistance sequence. Knock-out was confirmed by quantitative RT-PCR of brain-derived RNA with primer pairs within the WT coding sequence (CDS). n = 4 WT, 3 HET, 4 KO, ******** = p<0.0001 (Ordinary One-Way ANOVA with Tukey's post hoc multiple comparisons test).
(B) *Kcna6*^{tm1Lex} carriers, but not wild-type littermates, express β-galactosidase under the *Kcna6* promoter, detectable in DRG cells by immunostaining.
(C.i-ii.) In addition to prominent β-galactosidase immunoreactivity in small neurons, staining revealed *lacZ*-expressing satellite glia ensheathing DRG neurons, confirmed with an antibody raised against satellite glial marker, glutamine synthetase **(D)**. **(E, F)** The CGRP (± NF200), IB4 and TH populations were all positive for β-galactosidase.
(G) X-GAL staining reveals β-galactosidase activity in: DRG neurons, presumed satellite glia surrounding large neurons devoid of β-galactosidase (arrows), and seemingly in axons or Schwann cells within the nerve root (dashed perimeter).

Central Nervous System

d) Distribution of *Kcna6* expression in the mouse spinal cord

Information about noxious stimuli transduced by primary sensory neurons is transmitted to diffuse ascending somatosensory pathways for processing via spinal cord projection neurons, which are heavily influenced by modulatory interneurons and descending inputs. The sensory dorsal horn of the spinal cord is therefore a promising region to identify ion channels and other mediators that may contribute to pain sensation. However, attempts to characterise *Kcna6* expression in the central nervous system have been somewhat less fruitful than in the DRG thus far. Spinal cord sections were more prone to high background fluorescence after development of the fast-red reaction for *in situ* hybridisation, which decreases fidelity in discerning genuine mRNA signal. Despite this, it is still possible to identify *Kcna6* mRNA with some degree of confidence.

Initially, it was predicted that Kv1.6 would be present in neuronal populations of the dorsal horn as a generic regulator of neuronal excitability. Unexpectedly, it appears that *Kcna6* mRNA signal only infrequently co-localises with NeuN antibodies used as a pan-neuronal counterstain **Fig2.3(A)**. Of these few *Kcna6*-positive neurons, a number are located in the lateral spinal nucleus (LSN) **Fig2.3(A, arrowheads)** – a nucleus of the dorsal horn, ventrolateral to the most superficial Rexed laminae, which is poorly understood but nonetheless is activated by nociceptive input[8], including noxious heat[9]. Additionally, there is *Kcna6* mRNA present in the attached dorsal root **Fig2.3(A, dashed perimeter)**. Aside from neuronal expression, there is *Kcna6* signal spread diffusely throughout the grey and white matter of the spinal cord. This is highly suggestive of broad glial expression. In numerous cases mRNA surrounds neuronal cell bodies **Fig2.3(A, circled)**, perhaps indicating presence in astrocytes or microglia. Immunoreactivity for an astrocyte marker, glutamine synthetase, has a very similar distribution pattern including close perineuronal

localisation **Fig2.3(B, circled)**. *Kcna6 in situ* hybridisation will be combined with this counter-stain in future experiments to confirm astrocyte expression.

X-GAL-stained *Kcna6*$^{tm1Lex/tm1Lex}$ spinal cord showed a largely similar distribution of signal in small cells diffusely scattered throughout grey and white matter **Fig2.3(C)**, assumed to be glia, as well as enrichment in the corticospinal tract (CST), which has been shown to modulate tactile and neuropathic pain sensitivity[10]. There was also nebulous X-GAL reactivity in the dorsal horn (with a notable absence from lamina II), which probably represents β-galactosidase filling unresolvable fine neurite processes of unknown origin. Given the apparent lack of *Kcna6* mRNA expression in dorsal horn neurons, the staining may depict terminal projections of *Kcna6*-positive primary afferents.

Generally, *Kcna6* expression within the spinal cord appears to be limited mostly to primary afferent terminals and non-neuronal cells. Some *Kcna6* neurons are present in deeper laminae (IV-V) and the LSN **Fig2.3(A)**, but X-GAL staining on *Kcna6*^{tm1Lex} tissue shows quite convincingly that the substantia gelatinosa (lamina II), comprising mostly interneurons, is largely devoid of cells with β-galactosidase activity and therefore lacks *Kcna6* expression **Fig2.3(C)**.

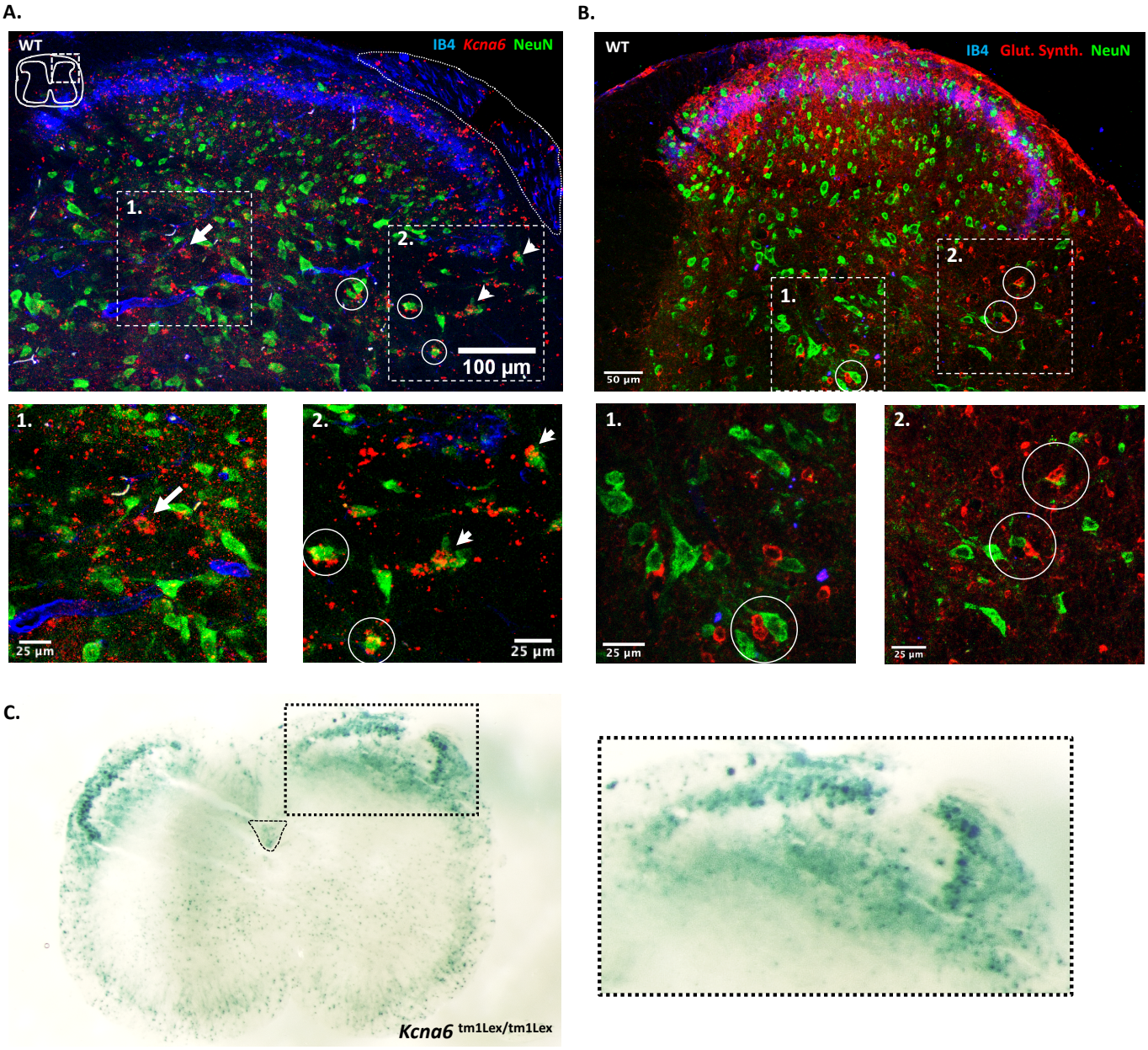

Figure 2.3 – *Kcna6* expression in the lumbar spinal cord

(A) *Kcna6* mRNA detected by *in situ* hybridisation shows infrequent co-localisation with neuronal marker NeuN (arrows, arrowheads), but expression in non-neuronal regions, suggesting expression in astrocytes, microglia, or oligodendrocytes. Often, mRNA was detected very closely apposed to NeuN-positive profiles but not within the NeuN stained region (circles). The IB4 neuropil appears to contain some positive signal, as does the attached dorsal root (marked by dotted perimeter).

(B) Immunostaining for astrocyte marker, glutamine synthetase, reveals a similar distribution to *Kcna6* mRNA in the IB4 neuropil and non-neuronal regions. Some examples of closely apposed astrocytes and NeuN-positive neurons have been indicated by circles, similar in location and appearance to structures circled in **(A)**.

(C) Blue precipitate formed by X-GAL reactivity with β-galactosidase in *Kcna6*^{tm1Lex} spinal cord appears to show a largely non-neuronal distribution of *Kcna6* expression in grey and white matter, and enrichment in the corticospinal tract (dashed perimeter).

e) *Kcna6* in the brain

So far, I have used the X-GAL staining approach as a rapid screening tool for *Kcna6* expression in the brain. After submersion in the staining solution for 24 hours, the cortex of both cerebrum and cerebellum were converted to a strikingly ubiquitous blue shade by the β-galactosidase-catalysed reaction, although upon midline sagittal sectioning it was apparent that the solution had not penetrated the tissue fully **Fig2.4(A)**. Sub-cortical structures were therefore not identified. On the contrary, the cerebellar distribution of *Kcna6* showed striking fidelity for the Purkinje cell layer with some diffuse (neurite) staining in the superficial molecular layer **Fig2.4(B)**. Rabbit Kv1.6 antiserum has previously been applied to cerebellar sections, with reactivity in Purkinje cell perikarya, co-localising with VGKC autoantibodies from Morvan syndrome patients[11]. *Zeisel et al. (2018)* also identified *Kcna6* mRNA in Purkinje cells[3]. Together, these results provide evidence for the validity and specificity of the X-GAL reporter approach.

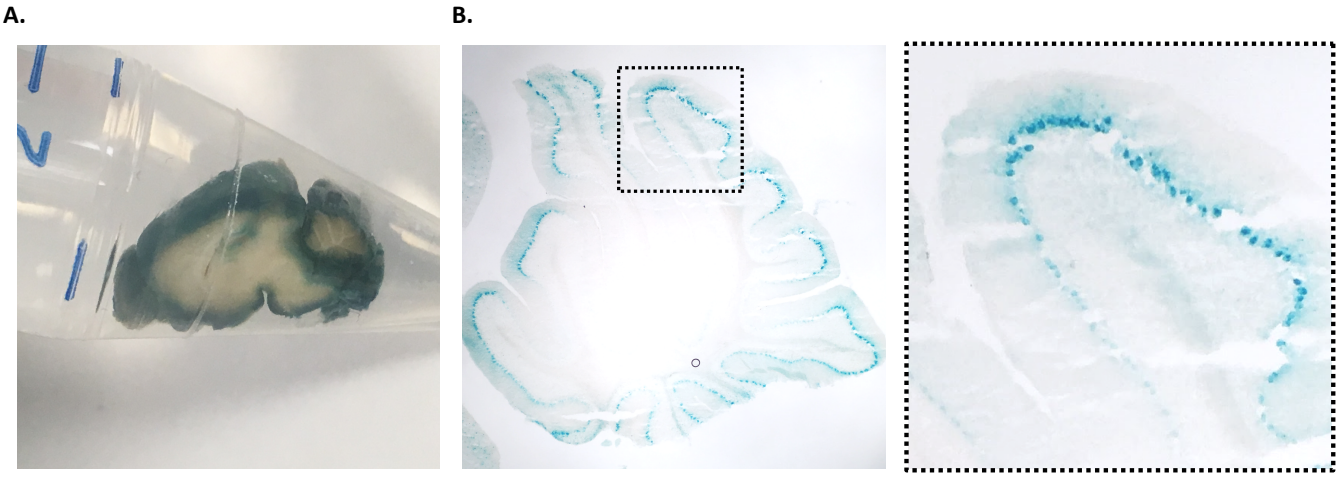

Figure 2.4 – *Kcna6*^{tm1Lex} *lacZ* reporter expression in the brain
(A) β-galactosidase reactivity was identified in cerebral and cerebellar cortices after 24hr submersion in X-GAL solution. **(B)** Microscopic analysis of the cerebellum unveiled X-GAL precipitate, and therefore *Kcna6* expression, very specific to the Purkinje cell layer.

ii. Conclusions

Expression of *Shaker*-like potassium channel *Kcna6* has been studied previously with various approaches detailed in the introductory chapter. Transcriptomic datasets[2–4] have begun to identify expression of this subunit in distinct dorsal root ganglia (DRG) subpopulations, including C-, Aδ- and potentially some Aβ-fibres **Table 2.1**, as well as dorsal horn interneurons[5] (though expression here is weak). However, there has been a lack of validation of these results in fixed tissue, which is more likely to represent the *in vivo* expression.

In this chapter, various staining methods have provided tangible visual evidence of *Kcna6* expression throughout the mouse somatosensory axis. Specifically, within the DRG there is preferential expression of this subunit in peptidergic and non-peptidergic nociceptors, as well as some expression in C-LTMRs. Meanwhile, although a complete characterisation within CNS structures has admittedly not yet been fully realised, CNS expression has been identified in a small number of spinal projection neurons in deep dorsal horn laminae and the LSN, non-neuronal cells, and the Purkinje cell layer of the cerebellum.

a) Which DRG cell populations express *Kcna6* mRNA?

I have used fluorescent *in situ* hybridisation to depict *Kcna6* mRNA expression *in situ* for the first time, within known nociceptive neuronal populations of the DRG **Fig2.1**. Quantitative analysis of such mRNA expression signals is somewhat challenging for several reasons. In my view, it is improper to designate cells as 'positive' or 'negative' for a particular gene on the basis of *in situ* mRNA visualisation alone – gene expression may be transient throughout developmental periods or occur in temporal cycles; mRNA may be trafficked away from the cell soma[12–18]; sparse mRNA signals in low-expressing cells may be outside the imaged sectioning plane; and in cells where for

example only 1 fluorescent punctum is visible, this *technically* demonstrates gene expression but is unlikely to be detected above the average background signal. Nonetheless, binary expression analyses have been reported using the same RNAscope® technology, employing arbitrary thresholds of '3 x background' [19] or 'background + 2 standard deviations' [20], for example.

In doing so, much information regarding the magnitude of expression is lost, so I have sought to retain this information by instead comparing mean signal intensity between DRG populations and background signal. This revealed significant *Kcna6* expression above background in $NF200^+/CGRP^+$, $CGRP^+$, and $IB4^+$ neurons, as well as trends towards differences in the extent of *Kcna6* expression between DRG populations **Fig2.1(C.ii)**. Information is also lost when single cell expression is condensed into an average expression value per population per animal, which was the rationale for including single-cell data in **Fig2.1(B.i & C.i)**.

By recent standards, basic histochemical definition of DRG neurons is a relatively crude means of differentiating sensory neurons – between 9 and 17 molecularly distinct subpopulations are now thought to exist that largely sub-divide the 4 to 5 populations defined here by immuno-staining[2,3,21,22]. Analysis of these novel sub-populations from *Zeisel et al. (2018)* suggests that the extent of *Kcna6* expression does indeed vary between clusters within the broad peptidergic and non-peptidergic (i.e. CGRP- and IB4-staining) populations **Table 2.1**. The violin distribution plots combined from multiple animals in **Fig2.1(C.i)** are similarly suggestive of discrete subpopulation clusters within histochemically defined populations, on the basis of variation in single-cell *Kcna6* expression, so there is value in transparently reporting data in this fashion. In addition, numerous TH^+ and potentially some $NF200^+$ neurons do appear to express *Kcna6*, for example **Fig2.1(A & C.i)**, despite on average not differing from baseline **Fig2.1(C.ii)**. However, for statistical robustness, between-animal variation must be taken into account, hence the inclusion of per-animal analyses **Fig2.1(B.ii & C.ii)**.

A binary screening approach was also employed, making use of *Kcna6*-driven LacZ expression in *Kcna6*^{tm1Lex} knock-out mice **Fig2.2**. This is a valid reporter mouse because: *lacZ* is expressed under the control of the preserved endogenous upstream *Kcna6* promoter; endogenous β-galactosidase (*Glb1*) is not highly expressed in mouse DRG neurons **Table 2.1**; and the chosen antibody used to detect β-galactosidase in this thesis is reactive only against the *E.coli* isoform which only has 28% protein sequence homology with *Mus musculus* Glb1. It is noticeable that β-galactosidase expression in DRG neurons typically manifests with two possible staining distributions. Some cells harbour β-galactosidase throughout the cytoplasm and nucleus, while others sequester the enzyme into a more punctate localisation pattern. Such distribution patterns have been observed before, in BDNF-driven LacZ reporter mice[23], and were posited to represent a correlate of gene expression (i.e. greater expression resulting in more cytoplasmic protein, lower expression presenting as more punctate), but the evidence for this is lacking.

β-galactosidase expressed from the *Kcna6*^{tm1Lex} transgene is an exogenous bacterial enzyme; it therefore may simply lack targeting motifs and be nondescriptly dispersed in certain cell types (cytoplasmic), or perhaps is recognised as foreign in other cells and targeted for proteasomal degradation (punctate). Nevertheless, presence of β-galactosidase in either form provides a binary screening tool for *Kcna6* expression that is validated by absence of β-galactosidase in wild type littermate controls **Fig2.2(B)**, consistent with low RNA sequencing reads for the endogenous mouse *Glb1* transcript in DRG neurons[3] **Table 2.1**. The <tm1Lex> reporter allele thus confirms *Kcna6* expression in NF200$^+$/CGRP$^+$, CGRP$^+$, IB4$^+$, and TH$^+$ sensory neurons, and absence in NF200$^+$ neurons **Fig2.2(E, F)**. This corresponds exactly with the *Kcna6* expression profile from bulk RNA sequencing of DRG populations defined genetically by Cre-recombinase reporter mice[4], and with my own *in situ* hybridisation results.

b) To which cellular compartments is Kv1.6 protein trafficked within DRG neurons?

In addition to identifying *Kcna6* gene expression in discrete DRG populations, which may be informative of a role in specific sensory modalities, I also tried to investigate the subcellular distribution of Kv1.6 protein in sensory neurons. Subcellular localisation of potassium channels in neurons is highly organised and determines the functional consequences of their activation or inactivation[24]. Overexpressed Kv1.6 was localised to the plasma membrane of dissociated DRG neurons *in vitro* **Fig2.1(D)**. It was important to confirm this before making the assumption that Kv1.6 is likely to influence plasma membrane potential, consistent with known functions of other Kv1 channels. However, it is also important to note that overexpression may not reflect the true endogenous localisation of Kv1.6-containing channels, as variations in the relative Kv1 alpha subunit stoichiometry can affect the distribution of Kv1 channels between endoplasmic reticulum and cell surface membrane[25]. Interestingly, perinuclear ER expression of Kv1.6 was also observed. This may represent transient, *en passant*, localisation during the post-translation protein trafficking process, or may indicate a more permanent anchoring of Kv1.6 to the ER. Kv1.1/1.2/1.6 channels are indeed known to possess ER retention motifs between their S5/S6 transmembrane loops[26], but the functional relevance of these is not currently known. However, ER expression of Kv1.6 has been observed in cultured rat astrocytes[27], so perhaps this subunit does have an intrinsic role in ER function.

c) A role for *Kcna6* in the central nervous system?

Analyses of transcriptomic datasets[3,28] have reported *Kcna6* expression in the neurons of the mouse spinal cord and numerous other CNS regions **Table 1.1**. DRG expression of *Kcna6* in this chapter largely corroborated prior transcriptomic data, and X-GAL staining was also able to replicate some of these transcriptomic results, such as *Kcna6* expression in cerebellar Purkinje cells **Fig2.4**. I am

therefore somewhat reluctant to discount the possibility of *Kcna6* expression within spinal cord neurons of mice. However, the visual data that I have presented in this chapter depict very sparse expression of *Kcna6* in mouse spinal cord neurons **Fig2.3**. A mostly glial expression profile appears to be more likely. However, *Kcna6* does appear to be expressed in occasional deeper laminae (IV-V) neurons and in neurons of the lateral spinal nucleus (LSN). This latter population is known to fire action potentials and express c-Fos evoked by deep noxious stimulation, but not radiant heat[8]. However, some unpublished results demonstrate that direct unilateral application of 55ºC water to the hind paw does induce Fos expression bilaterally in the LSN[9]. Kv1.6 may influence nociception via actions at this anatomical locus.

A retrospective, comparative analysis of novel human DRG transcriptomic data versus previously acquired data from other CNS regions (spinal cord, nucleus accumbens, caudate/striatum, hippocampus, and frontal cortex) indicated that *KCNA6* expression was low in the human CNS, including the spinal cord, but relatively enriched in the DRG[28]. Of course, transcriptomic data from cadaveric tissue also suffers from limitations, such as relatively long windows from death to tissue harvesting to RNA extraction with ample opportunity for transcriptional change to occur[29]. However, the conclusions from this work support the hypothesis that *Kcna6* expression is low in spinal cord neurons. Thus, any contribution of Kv1.6 to pain sensation is likely to be mostly, but not exclusively, mediated via its clear presence in primary nociceptive neurons of the dorsal root ganglia.

d) Concluding remarks

Overall, it is hoped that the combined approaches here satisfactorily demonstrate plasma membrane *Kcna6* expression in peptidergic and non-peptidergic nociceptors, as well as TH-positive C-fibre low threshold mechanoreceptors. This corroborates RNA sequencing data that determine

Kcna6 to be expressed in peptidergic, non-peptidergic and TH sub-populations, and to a much lower degree in heavy neurofilament populations[2–4] **Table 2.1**. Unexpectedly, these transcriptomic data show that *Kcna6* has a largely reciprocal distribution to *Kcna2* and particularly *Kcna1* within the DRG, which appear to have expression enriched in non-nociceptive NF200 neurons. Paired with extant knowledge of Kv1 channel function, I propose that this subunit is likely to regulate neuronal responses to noxious stimuli and is a good candidate for further study in the context of pain.

iii. Methods

Animals

Male and female adult (>8wks) mice were used throughout. *Kcna6*^{tm1Lex} mice were purchased from MMRRC (stock number: 011729-UCD) on a mixed C57BL/6J;129S5 background, with wild-type littermates used as controls in all experiments. The *Kcna6*^{tm1Lex} allele was produced by Lexicon Genetics, Inc. (now Lexicon Pharmaceuticals, Inc.) by homologous recombination of a gene trap cassette, containing *lacZ*/*neo* selection genes, with the coding sequence of *Kcna6* exon 1, depicted in **Fig2.2(A)**. All animal work was performed in compliance with the Animals (Scientific Procedures) Act 1986, under project licenses 30/3015 and P1DBEBAB9 held by Prof David Bennett at the University of Oxford.

Tissue preparation

To extract tissue for cryo-sectioning, animals were culled by overdose of pentobarbital delivered via intraperitoneal injection, followed by transcardial perfusion with 15ml sterile 0.9% w/v saline, then 20ml 4% paraformaldehyde (PFA) in 0.1M phosphate buffer (PB). Dissected tissues were post-fixed in 4% PFA for varied duration depending on tissue, as determined previously in our laboratory[20]: L4 DRG – 2hrs (room temperature, RT), spinal cord – 24hrs (4ºC), brain – 24hrs (4ºC). After fixation, tissue was transferred to 30% sucrose in 0.1M PB for at least 24 hours. Subsequently, tissue was embedded in OCT medium (TissueTek), rapidly frozen with liquid nitrogen, and stored at -80ºC prior to cryo-sectioning. Tissue prepared for X-GAL staining was treated in the same manner but perfused and post-fixed in 1% PFA to preserve enzyme activity. Sections were slide-mounted on Thermo Scientific™ SuperFrost Plus™ slides – with sections cut using a Leica cryostat, at tissue-dependent thickness: nerve and DRG – 10μm; spinal cord and brain – 20μm.

N.B. The protocols for dissection of fresh non-fixed tissue collected for primary cell culture or RT-qPCR are detailed below.

In situ hybridisation

Expression of *Kcna6* mRNA was investigated using a chromogenic *in situ* hybridisation assay (RNAScope 2.5-RED, Advanced Cell Diagnostics). For DRG analysis, fixed tissue was analysed from 4 (NF200/CGRP) or 3 (IB4/TH) animals. In brief, slides were removed from -80ºC storage and allowed to equilibrate to room temperature prior to removal of OCT by submersion in DNAase/RNAase-free phosphate-buffered saline (PBS). Slides were pre-treated with a 10-minute application of H_2O_2 at room temperature, washed with double de-ionised Milli-Q water, submerged in 100% EtOH and allowed to dry (20 mins) before a 10-minute application of protease plus in a humidified chamber at 40ºC, followed by a further Milli-Q wash. The target detection probe (Cat No. 462821) was warmed in a 40ºC water bath prior to a 2-hour incubation on slides at 40ºC, and the amplification steps and fast red reaction were performed according to the manufacturer's instructions. Following development of the red signal, slides were counter-stained using the protocol described below.

Primary DRG Culture

Adult (>8wks) mice were culled by rising CO_2 concentration and the vertebral column was rapidly dissected and placed into ice cold Hank's Balanced Salt Solution, HBSS (Invitrogen). After performing a complete dorsal laminectomy, DRGs were dissected from the intervertebral foramina, placed into fresh HBSS, and then enzymatically digested in collagenase II (Lorne Laboratory) and dispase (Sigma) at 37ºC for 1hr45mins with occasional agitation. DRGs were then washed in fresh HBSS and manually dissociated by 4 repetitive pipetting steps with a Gilson P1000 pipette (x2) followed by a P200 (x2). The supernatant containing the cell suspension was removed each time and ultimately centrifuged at 1000rpm for 3mins to produce a pellet of DRG cells. Cells were then electroporated with 1μg Kv1.6-FLAG/Myc plasmid (Origene cat. # MR208478) and 1μg GFP plasmid (in 10μl Buffer R) using the Neon electroporation system (ThermoFisher Scientific). The protocol involved 3x10ms pulses of 1500mV. Electroporated cells were spun down

again and resuspended in Neurobasal medium (Invitrogen) supplemented with B27 (Invitrogen), Glutamax (Invitrogen), and murine NGF/GDNF (Peprotech, 1:1000). Typically, 10µl of this cell suspension was placed into a 15µl droplet of laminin (R&D Systems) on sterile glass coverslips previously coated with poly-D-lysine (Sigma) in a 24-well plate. After allowing cells to adhere to the coverslips at 37ºC for 2 hours, wells were flooded with the supplemented Neurobasal medium and returned to the incubator. After several days *in vitro*, once there was evidence of neurite outgrowth and expression of electroporated GFP determined by fluorescent microscopy, cells were fixed on coverslips for 25 minutes in 1% EM-grade PFA (VWR) diluted in sterile distilled water (Invitrogen) and prepared for immunostaining.

Immunohistochemistry

Two immunohistochemical approaches were used in this chapter – staining of PFA-fixed sections on slides and staining of PFA-fixed cultured cells on glass coverslips. For slides, before antibody application, slides were washed and sections concurrently permeabilised in PBS+0.3% Triton X-100. Primary antibodies were diluted in PBS containing 0.3% Triton X-100 and 5% goat or donkey blocking serum and incubated on sections overnight in a humidified chamber. The next day, unbound primary antibodies were washed off with PBS, and secondary antibodies were applied to sections for 2-3 hours, followed by further washing in PBS and, in some instances where a biotinylated secondary antibody was used, a tertiary antibody incubation for up to 2 hours. Finally, slides were mounted with glass coverslips and Vectashield mounting medium for fluorescence, and air-sealed with nail polish. For staining of dissociated DRG cells after fixation, following 3 washes in distilled water, cells were permeabilised and immuno-stained in the same manner as cryo-sectioned tissue. An anti-FLAG primary antibody was used to label electroporated FLAG-tagged Kv1.6, whereas endogenous GFP fluorescence was sufficient without immuno-staining in **Fig2.1**. Exact antibodies and dilutions used are detailed in the **Appendix**.

Image acquisition

Fluorescence imaging was performed with a Zeiss LSM700 confocal microscope. For quantification, images were generally acquired using a 20x objective to capture randomly chosen, representative fields of view from 3-4 sections per slide (i.e. per animal). Maximum intensity projections were produced from z-stacks encompassing the entire section depth. For *in situ* hybridisation experiments, image acquisition settings were kept the same for all quantified images in order to make signal comparable across sections. Expression of target mRNA was quantified by calculating the mean red channel pixel intensity (converted from 0-255 8-bit colour value to a percentage scale) in regions of interest (ROIs) drawn in imageJ software around cells with identifiable nuclei, thus expression is normalised to cell size (sum of pixel intensities ÷ number of pixels). 'Background' was from ROIs containing nerve root across 7 images from multiple animals.

X-GAL enzymatic reporter assay

1% PFA-perfused tissue was treated with X-GAL staining solution: PBS (1X), 20mM Tris-HCl (pH7.3), 5mM $K_3[Fe(CN)_6]$, 5mM $K_4[Fe(CN)_6]$, 0.01% Na-deoxycholate, 0.02% NP40/IGEPAL (Sigma), 2mM $MgCl_2$, 1mg/ml X-GAL. Spinal cord and brain samples were submerged whole at for 24 hours at 37ºC prior to blocking in OCT and cryo-sectioning. Sections were subsequently stained again on slides to recover signal lost due to poor penetration of the X-GAL solution. DRGs were stained after sectioning on Thermo Scientific™ SuperFrost Plus™ slides.

RNA extraction and cDNA synthesis

Mice were culled by rising CO_2 concentration in a sealed chamber. Brains were rapidly dissected, immediately frozen in liquid nitrogen, and stored at -80ºC. Tissue was homogenised in TriPure (Roche) and then treated with chloroform prior to column purification using a High Pure RNA isolation kit (Roche). RNA was eluted in RNAase-free water. Synthesis of cDNA was achieved

using Transcriptor reverse transcriptase (Roche) with random hexamers (Invitrogen) and dNTPs (Roche).

RT-qPCR

Quantitative analysis of mRNA expression was carried out on a LightCycler 480 II system (Roche), using SYBR green fluorescence for detection. Primers were designed using Primer-BLAST (https://www.ncbi.nlm.nih.gov/tools/primer-blast/) and were assessed for specificity and efficiency by gel and melting curve analysis, and by serial dilution. Primers (0.5μM) and cDNA (5ng) were mixed with LightCycler 480 SYBR Green master mix (Roche) in a 1:1 ratio in 384-well plates and run on a 45-cycle protocol. All experimental samples were run in triplicate. Quantitation of expression was performed using the delta delta CT method[30], and Kv1 gene products were first normalised to 'housekeeping' genes (*Gapdh* and *Hprt1*) and then normalised to average wild-type expression per gene.

Statistics

In situ – For comparison of mRNA expression between DRG subpopulations or size categories after *in situ* hybridisation, the unit of statistical analysis was the animal **Fig2.1(B.ii, C.ii)**. Mean expression per animal was assessed for normality using the Shapiro-Wilk test and compared between categories by Ordinary One-Way ANOVA with Tukey's post-hoc multiple comparisons test.

RT-qPCR – Comparison of Kv1 subunit mRNA expression between *Kcna6*^{tm1Lex} genotypes was performed using Ordinary One-Way ANOVA independently for each gene, with Tukey's post-hoc multiple comparisons test. Again, the unit of analysis was the individual animal.

Calculations were performed in GraphPad Prism software.

iv. References

1. Calvo, M. *et al.* Altered potassium channel distribution and composition in myelinated axons suppresses hyperexcitability following injury. *Elife* **5**, 1–26 (2016).
2. Usoskin, D. *et al.* Unbiased classification of sensory neuron types by large-scale single-cell RNA sequencing. *Nat. Neurosci.* **18**, 145–153 (2015).
3. Zeisel, A. *et al.* Molecular Architecture of the Mouse Nervous System. *Cell* **174**, 999-1014.e22 (2018).
4. Zheng, Y. *et al.* Deep Sequencing of Somatosensory Neurons Reveals Molecular Determinants of Intrinsic Physiological Properties. *Neuron* **103**, 1–19 (2019).
5. Häring, M. *et al.* Neuronal atlas of the dorsal horn defines its architecture and links sensory input to transcriptional cell types. *Nat. Neurosci.* **21**, 869–880 (2018).
6. Hao, J. *et al.* Kv1.1 channels act as mechanical brake in the senses of touch and pain. *Neuron* **77**, 899–914 (2013).
7. George, D., Ahrens, P. & Lambert, S. Satellite glial cells represent a population of developmentally arrested Schwann cells. *Glia* **66**, 1496–1506 (2018).
8. Sikandar, S., West, S. J., McMahon, S. B., Bennett, D. L. & Dickenson, A. H. Sensory processing of deep tissue nociception in the rat spinal cord and thalamic ventrobasal complex. *Physiol. Rep.* **5**, e13323 (2017).
9. Rae, P. M. The Role of the Lateral Spinal Nucleus in Nociception (PhD Thesis). (University of Glasgow, 2009).
10. Liu, Y. *et al.* Touch and tactile neuropathic pain sensitivity are set by corticospinal projections. *Nature* **561**, 547–550 (2018).
11. Kleopa, K. A., Elman, L. B., Lang, B., Vincent, A. & Scherer, S. S. Neuromyotonia and limbic encephalitis sera target mature Shaker-type K + channels: Subunit specificity correlates with clinical manifestations. *Brain* **129**, 1570–1584 (2006).
12. tom Dieck, S., Hanus, C. & Schuman, E. M. SnapShot: Local Protein Translation in Dendrites. *Neuron* **81**, 958-958.e1 (2014).
13. Glock, C., Heumüller, M. & Schuman, E. M. mRNA transport & local translation in neurons. *Current Opinion in Neurobiology* **45**, 169–177 (2017).
14. Tushev, G. *et al.* Alternative 3' UTRs Modify the Localization, Regulatory Potential, Stability, and Plasticity of mRNAs in Neuronal Compartments. *Neuron* **98**, 495-511.e6 (2018).
15. Suter, B. RNA localization and transport. *Biochimica et Biophysica Acta - Gene Regulatory Mechanisms* **1861**, 938–951 (2018).
16. Cioni, J. M. *et al.* Late Endosomes Act as mRNA Translation Platforms and Sustain Mitochondria in Axons. *Cell* **176**, 56-72.e15 (2019).
17. Rangaraju, V., Lauterbach, M. & Schuman, E. M. Spatially Stable Mitochondrial Compartments Fuel Local Translation during Plasticity. *Cell* **176**, 73-84.e15 (2019).
18. Biever, A., Donlin-Asp, P. G. & Schuman, E. M. Local translation in neuronal processes. *Current Opinion in Neurobiology* **57**, 141–148 (2019).
19. Weir, G. A. *et al.* The Role of TRESK in Discrete Sensory Neuron Populations and Somatosensory Processing. *Front. Mol. Neurosci.* **12**, 170 (2019).
20. Dawes, J. M. *et al.* Immune or Genetic-Mediated Disruption of CASPR2 Causes Pain Hypersensitivity Due to Enhanced Primary Afferent Excitability. *Neuron* **97**, 806–822 (2018).
21. Li, C.-L. *et al.* Somatosensory neuron types identified by high-coverage single-cell RNA-sequencing and functional heterogeneity. *Cell Res.* **26**, 83–102 (2016).
22. Li, C., Wang, S., Chen, Y. & Zhang, X. Somatosensory Neuron Typing with High-Coverage Single-Cell RNA Sequencing and Functional Analysis. *Neuroscience Bulletin* **34**,

200–207 (2018).
23. Dembo, T., Braz, J. M., Hamel, K. A., Kuhn, J. A. & Basbaum, A. I. Primary Afferent-Derived BDNF Contributes Minimally to the Processing of Pain and Itch. *eneuro* **5**, ENEURO.0402-18.2018 (2018).
24. Trimmer, J. S. Subcellular localization of K+ channels in mammalian brain neurons: Remarkable precision in the midst of extraordinary complexity. *Neuron* **85**, 238–256 (2015).
25. Manganas, L. N. & Trimmer, J. S. Subunit composition determines Kv1 potassium channel surface expression. *J. Biol. Chem.* **275**, 29685–29693 (2000).
26. Misonou, H. & Trimmer, J. S. Determinants of Voltage-Gated Potassium Channel Surface Expression and Localization in Mammalian Neurons. *Crit. Rev. Biochem. Mol. Biol.* **393**, 125–145 (2004).
27. Zhu, J., Yan, J. & Thornhill, W. B. The Kv1.3 potassium channel is localized to the cis-Golgi and Kv1.6 is localized to the endoplasmic reticulum in rat astrocytes. *FEBS J.* **281**, 3433–3445 (2014).
28. Ray, P. *et al.* Comparative transcriptome profiling of the human and mouse dorsal root ganglia. *Pain* **159**, 1325–1345 (2018).
29. Zhu, Y., Wang, L., Yin, Y. & Yang, E. Systematic analysis of gene expression patterns associated with postmortem interval in human tissues. *Sci. Rep.* **7**, 5435 (2017).
30. Livak, K. J. & Schmittgen, T. D. Analysis of relative gene expression data using real-time quantitative PCR and the 2-ΔΔCT method. *Methods* **25**, 402–408 (2001).

Chapter III

Behavioural phenotyping of *Kcna6* ^{tm1Lex} knock-out mice

I had inferred from published literature[1] and expression data in the previous chapter that delayed rectifier Kv1.6 might make an important contribution to pain sensation, either in post-traumatic neuropathic states or in naïve, acute pain scenarios. Given the observed expression of *Kcna6* mRNA in peptidergic and non-peptidergic nociceptors, I studied the behaviour of a global knock-out mouse line *Kcna6*^{tm1Lex}, introduced in **Chapter II**, with intent to assess a possible contribution of this channel to sensory function, specifically nociception. The behavioural phenotyping of Kv1.6-null animals has indeed demonstrated this, in a reproducible manner across independent cohorts.

Firstly, I made baseline observations with an array of sensorimotor assays performed on mice in the naïve (uninjured) state. Behavioural paradigms were designed to assay a range of sensory modalities, including punctate mechanical pressure, noxious heat, and chemically (formalin) induced inflammatory pain. It is important to assess motor as well as sensory phenotypes, not least because the original descriptions of the Shaker and Shaker-like channels in Drosophila[3] or mice[4,5] pertain to their role in motor control, but also because proprioceptive sensory neurons are additionally important for control of muscle movement via positional or stretch feedback from muscle spindles and Golgi tendon organs. However, my (and others')[6–8] expression data would not suggest that Kv1.6 plays a major role in large-diameter proprioceptive primary afferents in the naïve, uninjured state.

In neuropathic mice, expression of Kv1.6 is upregulated[1,2] and contributes to restoration of normal mechanical sensitivity thresholds, demonstrated by immunohistochemical/behavioural analysis

paired with pharmacological inhibition[1]. I also sought to validate this finding by means of genetic ablation. I analysed sensory behavioural responses of *Kcna6*^{tm1Lex} mice following two experimentally induced nerve injury models – the spared nerve injury (SNI)[9] and the neuroma model[1], both described in detail in the methods section of this chapter. These two models assess sensitivity in different populations of neurons by virtue of the behavioural stimulation protocol. SNI involves 'sparing' the sural nerve from injury and mechanically probing the intact cutaneous afferents in the sural nerve territory of the paw to elicit behavioural responses. The neuroma model involves total transection of the sciatic nerve, and direct mechanical stimulation of the cut nerve endings. We still have a poor understanding of the relative contributions of injured versus spared afferents to chronic pain after traumatic nerve injury, and of the mechanisms involved in the generation of hypersensitivity in these two populations. By comparing the effect of Kv1.6 channel knock-out in these two models, it may be possible to identify different mechanisms in these two populations.

i. Results

Baseline Sensorimotor Behaviour

a) *Kcna6*^{tm1Lex} expressing mice exhibit normal exploratory behaviour and motor function

The open field test assesses general locomotor (gridline crossing) and more complex exploratory activity (rearing behaviour), in which we may expect to observe differences on genetically altered somatosensory backgrounds[10]. Here, I have reported no deficit in either of these behaviours for *Kcna6*^{tm1Lex} hetero- or homozygous mice compared with wild-type littermates **Fig3.1(A, B)**. Similarly, when challenged with more demanding proprioceptive/motor tasks such as the rota-rod or beam test, performance was comparable to that of wild-types **Fig3.1(C, D)**.

b) Hetero- and homozygous *Kcna6*^{tm1Lex} mice are hyposensitive to noxious heat

I have identified a clear phenotype in knock-out animals of hyposensitivity to noxious heat with the hot plate apparatus, at temperatures of both 50˚C (KO 19.63±0.16s********, HET 14.35±0.71s, WT 15.07±0.77s, ********$p<0.0001$ vs WT and HET) and 53˚C (KO 14.04±0.44s********, HET 8.54±0.43s, WT 8.26±0.46s, ******** = $p<0.0001$ vs WT and HET) **Fig3.1(E, F)**. The maximum duration of exposure to the hot plate permitted to avoid tissue damage was 20 seconds; at 50˚C it is noticeable that the homozygous mice tended to last until this maximum limit without exhibiting pain-like behaviour. Elongated latency to withdrawal was also evident in both hetero- and homozygous knock-outs with the Hargreaves radiant heat test (KO 10.83±0.39s*******, HET 11.09±0.36s*******, WT 8.69±0.32s, ******* = $p<0.001$ vs WT) **Fig3.1(G)**. No difference was observed between genotypes in 50% withdrawal threshold for punctate mechanical stimulation with Von Frey hairs (KO 0.83±0.05g, HET 0.78±0.05g, WT 0.72±0.04g) **Fig3.1(H)**.

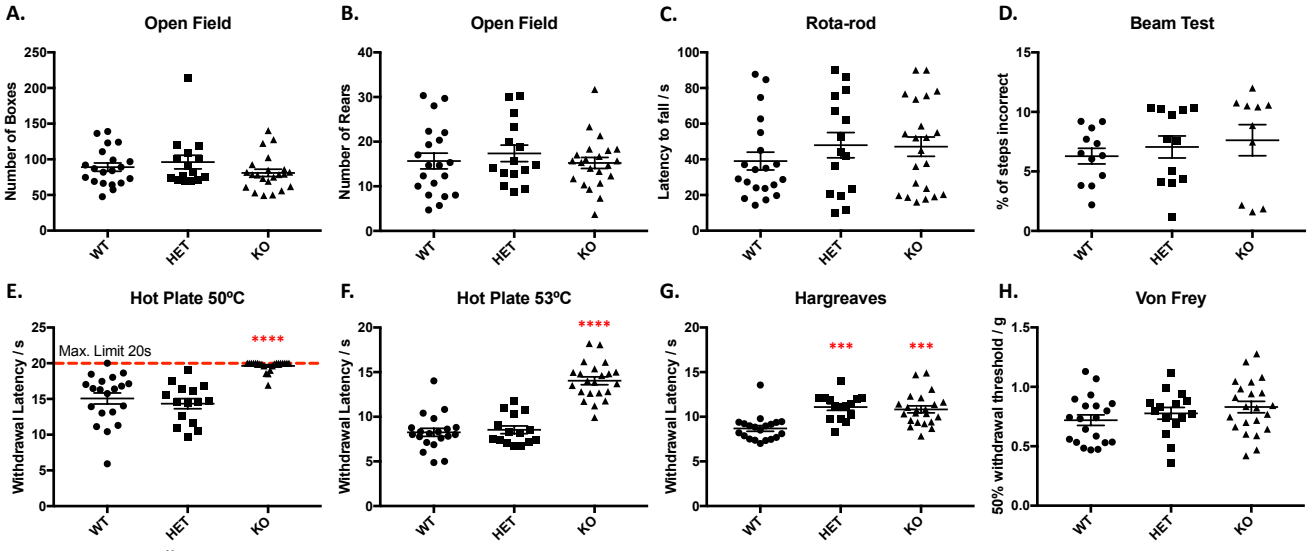

Figure 3.1 – *Kcna6*^{tm1Lex} mice are hyposensitive to noxious heat

Kcna6$^{+/-}$ and $^{-/-}$ mice perform normally on open field **(A, B)** and motor function tests **(C, D)**. *Kcna6*$^{-/-}$ mice are hyposensitive on 50°C and 53°C hot plate assays **(E, F)**, while both heterozygous and homozygous mutants are hyposensitive on the Hargreaves radiant heat assay **(G)**. Neither groups differ from wild types in their response to mechanical stimulation by Von Frey hairs **(H)**.

Data points are individual animal mean values from 2 **(D)**, 3 **(A-C, E, F)** or 4 **(G, H)** baseline experiments performed on different days, plotted with group mean ± SEM.

n = 20 WT, 15 HET, 22 KO (combined from two separate cohorts) apart from the beam test **(D)** which was performed on only one cohort (n = 12 WT, 12 HET, 10 KO).

*** = p<0.001, **** = p<0.0001 versus WT and HET **(E,F)** or versus WT **(G)** (One-Way ANOVA with Tukey's post hoc multiple comparisons test)

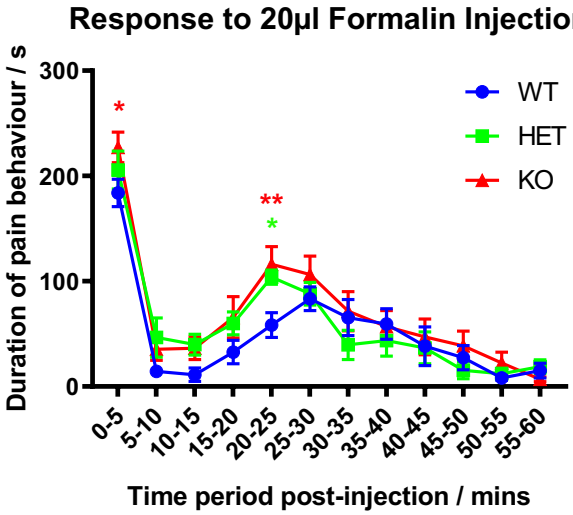

Figure 3.2 – *Kcna6*^{tm1Lex} mice are hypersensitive to the algogenic chemical formalin

Data presented as group mean ± SEM

n = 10 WT, 10 HET, 10 KO (combined from two separate cohorts).

* = p<0.05, ** = p<0.01 versus WT (Two-Way Repeated Measures ANOVA with Dunnett's post hoc multiple comparisons test)

c) Hetero- and homozygous *Kcna6*^{tm1Lex} mice are mildly hypersensitive to the algogen formalin

Mice received an intraplantar injection of 5% formalin solution to the left hind paw, which produces a biphasic pain response canonically attributed to peripheral nociception followed by a centrally mediated sensitisation. Duration of pain behaviour in homozygotes was mildly though significantly increased compared to wild-types in the first phase between 0-5mins (KO 227.03±14.47s*****, HET 205.60±17.94s, WT 183.91±12.91s, *****p<0.05 vs WT). Both *Kcna6*$^{tm1Lex/+}$ and *Kcna6*$^{tm1Lex/tm1Lex}$ mice also displayed more pain-related behaviour at the start of the second phase between 20-25mins post-injection (KO 116.06±16.80s******, HET 103.85±6.82s*****, WT 58.41±11.69s, ******/***** = p <0.01/0.05 vs WT) **Fig3.2**.

*** * ***

While sex differences in pain perception are well established[11], there were no observed differences in baseline behavioural outcomes between male and female mice within each genotype.

Experimental Nerve Injury Models

d) *Kcna6*^{tm1Lex} mice sustain post-SNI mechanical hypersensitivity comparably to wild-types

Following SNI, ipsilateral sural nerve afferents are acutely hyperexcitable, which manifests behaviourally as a reduction in threshold for paw withdrawal after mechanical stimulation of the sural nerve terminals. Both wild type and *Kcna6*^{tm1Lex} mice exhibited mechanical hypersensitivity within 3 days post-surgery, and this effect lasted until termination of the experiment at 21 days with minimal recovery in either genotype **Fig3.3(A)**. On baseline Hargreaves assessment, thermal hyposensitivity was observed in knock-out ipsi- and contralateral hind paws compared to wild type contralateral thresholds (KO ipsi 10.84±0.35s*****, KO contra 10.72±0.58s*****, WT ipsi 8.16±0.43s, WT contra 7.67±0.59s, ***** = $p<0.05$ vs WT contra). This thermal hyposensitivity was observed for the duration of the 21-day analysis; however, significance was not maintained **Fig3.3(B)**. This is due to an expected increase in the variance of responses post-injury; in knock-outs and wild types alike the standard deviation of the mean (ipsi/contra) increased from 1.21s/2.02s at baseline to 2.79s/2.76s at day 7 (KO) and from 1.13s/1.55s to 3.01s/2.20s (WT). This effect was maintained for the subsequent 14 days as well. No thermal hypersensitivity associated with SNI developed, consistent with original observations that Hargreaves response latency does not change after SNI[9].

e) *Kcna6*^{tm1Lex} homozygotes do not recover from neuroma hypersensitivity

An alternative nerve injury paradigm has been used previously to assess axotomy-induced changes in Kv1 (including Kv1.6) channel expression and function[1]. I used the neuroma model in *Kcna6* knock-outs to corroborate the authors' findings that Kv1.6 in primary afferents has a causal role in long-term recovery from neuroma hypersensitivity following sciatic nerve transection. On this occasion, non-littermate wild type mice were used as controls, which were on a pure C57BL/6J

background and thus differed slightly from the mixed BL6/129S background *Kcna6*^{tm1Lex} carriers. 5 weeks post-surgery, mechanical withdrawal thresholds in *Kcna6*^{tm1Lex} heterozygotes and C57BL/6J wild type controls began to increase. By 10 weeks after injury, mechanical sensitivity in *Kcna6*^{tm1Lex} homozygotes had still not improved (KO 0.025±0.00g******, HET 0.47±0.11g********, WT 0.19±0.04g, ******/******** = p<0.01/0.0001 vs WT) **Fig3.3(C)**.

f) *Kcna6* mRNA is not altered in the DRG 3 weeks after SNI

A key finding from the previous neuroma study was that Kv1.6-containing channels were upregulated after injury and became localised to juxtaparanode (JXP) and paranode regions, compensating for axotomy-induced loss of Kv1.1 and Kv1.2 channels[1]. Local pharmacological blockade (or genetic deletion **Fig.3(C)**) of this Kv1.6 subunit reverses or prevents recovery from acute hypersensitivity, suggesting that the upregulated Kv1.6 channels are functional. The mechanism of upregulation is unclear. In L3-5 DRGs from wild-type animals 3 weeks after SNI, there was no significant difference in *Kcna6* mRNA expression in ipsilateral compared to contralateral DRGs, relative to housekeeping gene expression, as detected by RT-qPCR **Fig3.3(D)**.

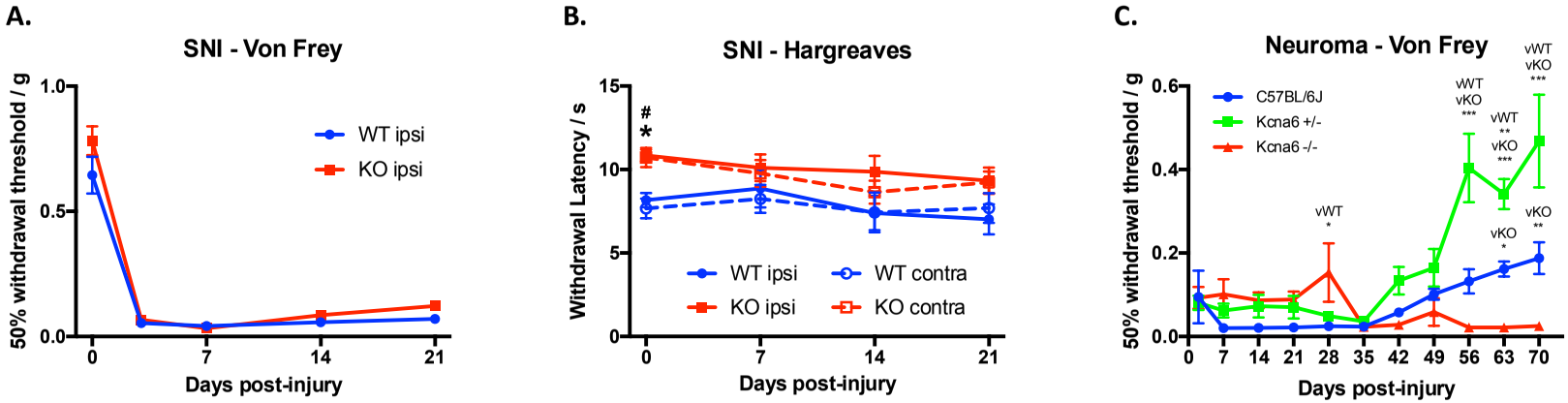

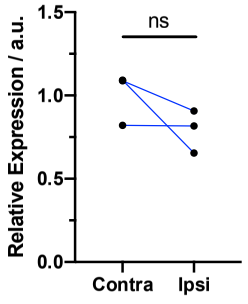

Figure 3.3 – *Kcna6*^{tm1Lex} *mice have altered recovery kinetics after sciatic nerve transection*

(A) Mechanical but not thermal withdrawal thresholds are reduced in mice following spared nerve injury (SNI). No differences in ipsilateral mechanical threshold were observed between genotypes at any time point.
(B) Thermal thresholds differed significantly at baseline and knock-outs remained hyposensitive, albeit lacking significance, during the post-surgery period.

(C) After complete sciatic nerve transection, injured afferents were directly stimulated with von Frey filaments. Non-littermate C57BL/6J wild types and *Kcna6*^{tm1Lex} heterozygote littermate controls both began recovering from mechanical hypersensitivity 5 weeks following surgery, whereas homozygote knock-outs showed no signs of recovery up to 70 days post-injury.

(D) *Kcna6* mRNA expression was not significantly altered in injured wild-type DRGs 3 weeks post-SNI.

(A) n = 8 WT, 12 KO **(B)** n = 7 WT, 12 KO ***/#** = p<0.05 KO ipsi/contra versus WT contra (Two-Way RM ANOVA with Dunnett's post hoc multiple comparisons test)
(C) n = 11 BL6 WT, 12 HET, 10 KO ***/**/***** = p<0.05/0.01/0.001 (Two-Way RM ANOVA with Tukey's post hoc multiple comparisons test)
(D) n = 3 WT contra, 3 WT ipsi (Wilcoxon matched-pairs signed rank test)

ii. Conclusions

a) Kv1.6 appears to influence thermal nociceptive thresholds

Firstly, I have shown that uninjured mice lacking Kv1.6 have thermal nociceptive deficits, evidenced by delayed responses on hot plate and Hargreaves apparatuses **Fig3.1(E-G)**. This finding is curious. Loss of Kv1 channel function is known to remove a component of the repolarising outward current activated by neuronal depolarisation. This results in reduced rheobase and thus sensory neuron hyperexcitability, which drives sensory behavioural hypersensitivity[12–14]. Noxious thermal hyposensitivity is therefore an unexpected phenotype. However, this phenomenon is not entirely without precedent, in that auditory neurons from global Kv1.2 knock-out mice are hypoexcitable compared to wild type controls, with a negative shift in I_{Kv1} activation potential, ostensibly due to dominance of Kv1.1 alpha subunit contribution in the absence of Kv1.2[15]. Thus, Kv1 channel activity is nuanced and influenced significantly by subunit composition.

Furthermore, there are subtle behavioural differences between *Kcna6*^{tm1Lex} hetero- and homozygotes. Kv1.6 heterozygotes appear to be haplo-sufficient for normal responses to the hot plate assay but do share the hyposensitive Hargreaves phenotype to infrared plantar stimulation. This pertains to the observation that hot plate stimulation engages supra-spinal brainstem circuitry to initiate a co-ordinated response of limb shaking, lifting, licking, tending and ultimately escape (jumping)[16]. On the contrary, the Hargreaves assay tends to elicit simpler limb withdrawal responses. These represent 'unconscious' activity in spinal reflex circuits, which persists in decerebrate mice with thoracic spinal transection[16], so the two assays likely probe different functions of the nervous system.

There is in fact some evidence now that different components of a response to noxious stimuli are seemingly reliant on distinct primary afferent populations and ascending projection pathways from the spinal cord. *Huang et al. (2019)* found that coping responses (for example, paw licking) to sustained, extreme mechanical, heat or cold stimuli were impaired after ablation of either $Trpv1^+$ primary afferent fibres or spinal Tac1 neurons co-expressing Lbx1[17]. In both cases, reflexive withdrawal responses were not affected by ablation, with the exception of prolonged noxious heat withdrawal latency after $Trpv1^+$ ablation, as reported previously[18]. $Tac1^+/Lbx1^+$ neurons include a population of projection neurons which project to distinct parabrachial and thalamic nuclei from Tac1/Lbx1-negative neurons[17], and a population of propriospinal interneurons which have been proposed to integrate signals across multiple spinal levels and nuclei including the LSN[19] – a characteristic which hypothetically fits well with the circuitry expected to underly complex locomotor or coping behaviours[20]. Ablation of $Mrgprd^+$ fibres delayed reflexive responses to mechanical stimuli, as described by previous research[18], but did not affect coping responses[17]. Trpv1 fibre ablation reduced pinch-evoked Fos induction in $Tac1^+/Lbx1^+$ spinal neurons, suggestive of direct or indirect connectivity in the ascending pathways of $Trpv1^+$ afferents and $Tac1^+/Lbx1^+$ projection neurons. Despite this apparent connectivity, $Tac1^+/Lbx1^+$ ablation did not affect licking responses after intraplantar capsaicin injection, so some signalling from $Trpv1^+$ afferents is presumably conveyed by other projection pathways.

Monoallelic loss of Kv1.6 may therefore be irrelevant or compensated for by other ion channels in afferent populations, ascending projection neurons, or supraspinal regions relating to the 'coping pathway', but important in more caudal reflex pathways, leading to differences between the hot plate and Hargreaves phenotype. There is some emerging evidence that 'reflex' withdrawal responses are in fact associated with simultaneous synchronised activity in the primary somatosensory cortex[21] and influenced by descending corticospinal input[22]. However, it remains

that decerebrate rodents are capable of withdrawal reflexes to thermal and punctate mechanical stimuli[16,23].

Coping behaviours have not specifically been addressed here in such a systematic manner, but the spontaneous pain-like responses evoked by formalin injection are often more akin to coping responses than to withdrawal reflexes. In addition to thermal hyposensitivity, these *Kcna6* knock-out mice display mildly but significantly increased pain-like behaviour in response to 5% formalin injection to the hind paw, during both acute (peripheral) and secondary (central) phases **Fig3.2**. This dichotomy of behavioural phenotypes, in a modality-specific manner, is perhaps suggestive of discrete effects on distinct sensory neuron populations. It is largely accepted that certain molecularly defined afferent populations convey sensory information specific to certain modalities – a concept discussed in **Introduction (Fig1.2)**. A commonly cited example of this is the dependence of normal mechanical and heat sensation on intact Mrgprd$^+$ and Trpv1$^+$ afferents, respectively[18]. The publication by *Huang et al. (2019)* somewhat exposes a shortcoming of this study, as Trpv1$^+$ afferents were in fact shown to contribute to coping responses following mechanical stimulation[17], whereas *Cavanaugh et al. (2009)* only assessed withdrawal thresholds[18].

Noxious heat above 43ºC is transduced by Trpv1[24–27], among other ion channel candidates Ano1[28], Trpm3[29,30], and Trpa1[31]. Trpa1 is also putatively the molecular target of formalin for its algogenic action on sensory neurons[32]. A recently generated public library of single-cell transcriptomic data from the mouse nervous system[7] suggests that *Kcna6* is expressed in all *Trpa1*-expressing neuronal clusters of dorsal root ganglia neurons (non-peptidergic PSNP2 and PSNP3), and all but one *Trpv1*-positive clusters (peptidergic PSPEP1-5, non-peptidergic PSNP5 and PSNP6, excluding *Trpv1*-positive PSPEP8) **Table 3.1**. According to this single-cell sequencing data, the *Trpv1* and *Trpa1* populations are largely non-overlapping, so it is conceivable that a global, indiscriminate knock-out of *Kcna6* might have divergent effects on thermal and formalin behaviour via, for example,

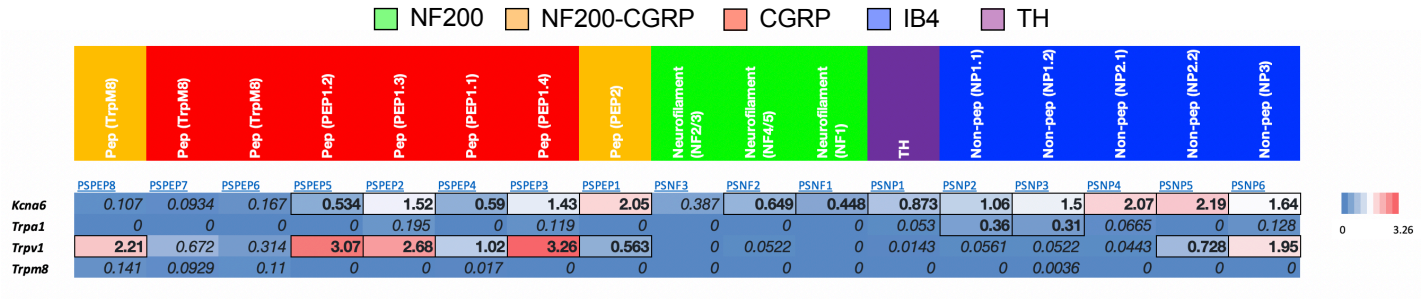

Table 3.1 – *Kcna6* expression in thermosensitive populations

Comparison of Kv1.6 and thermosensitive TRP channel expression log2 expression values of Kv1.6 alpha subunit in DRG subpopulations. Values formatted with outlines and bold text represent genes with trinarisation scores of >0.95 in the relevant population, as reported at mousebrain.org, which can be considered to have a high probability of expression in the respective cluster. Italicised values fall below the 0.95 probability score.

differential alteration of excitability in the *Trpv1* and *Trpa1* populations – dependent upon the specific repertoire of Kv1 subunits or other ion channels present in these genetically and presumably functionally distinct neurons. However, other publications have suggested that Trpv1, Trpm3 and Trpa1 are co-expressed in nociceptive populations[8,31] and are all functionally redundant with regards to acute noxious heat sensation, as only triple knock-out mice exhibit complete noxious heat insensitivity[31]. Ablation of GINIP-expressing C-LTMRs, shown to express *Trpa1*[8], significantly attenuates formalin-induced pain behaviours[33], so hypersensitivity to formalin in *Kcna6* knock-outs may be mediated by effects on C-LTMRs, many of which express *Kcna6* [8] **Chapter II**.

It remains interesting that there is no impact of *Kcna6* knock-out on mechanical sensitivity **Fig3.1(H)**, given that *Kcna6* is expressed in non-peptidergic nociceptors **Chapter II**. *Kcna6* is reportedly the second most abundant VGKC transcript in this population[8], and pharmacological blockade of Kv1.6-containing channels via α-dendrotoxin (α-DTx) application in isolated Mrgprd$^+$ neurons renders them hyperexcitable – evidenced by augmented repetitive firing responses to suprathreshold stimuli[8]. It is arguable that Von Frey filaments are not noxious mechanical stimuli and that *Kcna6* knock-out would not be expected to impact on withdrawal thresholds as it is not highly expressed in A- LTMRs **Chapter II**. However, ablation of Mrgprd$^+$ afferents does

dramatically increase Von Frey withdrawal threshold[18] indicating that non-peptidergic nociceptive fibres are indeed involved in the Von Frey response.

Aside from primary afferent-mediated effects of Kv1.6 knock-out, potential changes in CNS activity cannot be discounted. Despite a relative dearth of *Kcna6* expression in spinal cord neurons, observed in **Chapter II**, others have identified weak expression of *Kcna6* in all excitatory and inhibitory interneuron populations defined by single-cell transcriptomic clustering[34]. This could very conceivably be a locus at which loss of Kv1.6 function may have a significant impact on nociceptive thresholds, either through increased GABA-/glycinergic tone driven by hyperexcitability in inhibitory interneurons, or through more complex methods.

b) Kv1.6 influences neuropathic pain behaviour

In the context of nerve injury, Kv1.6 appears to fulfil a much more conventional role as a delayed rectifier, limiting ectopic electrical activity and tactile hypersensitivity[1]. Local application of α-DTx was used previously to confirm functional upregulation of Kv1.6 in neuroma juxtaparanodes[1], but this is an efficacious inhibitor of channels containing either Kv1.1, Kv1.2, or Kv1.6 subunits[35]. As Kv1.1 and Kv1.2 were reported to be downregulated but not totally absent from the injured nerve and DRG[1], the hypersensitivity- and hyperexcitability-inducing effect of α-DTx may have been mediated in part by inhibition on residual Kv1.1/1.2 channels. Genetic manipulation of Kv1.6 is therefore a more specific approach to assess the function of this subunit in isolation.

Pleasingly, using *Kcna6*^{tm1Lex} mice I was able to reproduce the findings that Kv1.6 is required for amelioration of neuroma sensitivity to direct tactile stimulation. Recovery was observed previously at 21 days after complete sciatic nerve transection, whereas in this study improvement in behavioural outcomes was delayed by at least 14 days **Fig3.3(C)**. This may highlight fundamental

inter-species differences, as the original study by *Calvo et al. (2016)* was performed in rats. It is also notable that heterozygote littermates recovered to a greater extent than wild-types. This result might simply reflect the fact that non-littermate, wild-type C57BL/6J mice were used as a control – whereas the *Kcna6*^{tm1Lex} mice were of a mixed C57BL/6J;129S5 background. It is known that genetic background influences behavioural outcomes[36], including sensory thresholds and responsiveness to analgesia in models of nerve injury[37].

In contrast, after spared nerve injury, no differences were observed in the development or maintenance of tactile hypersensitivity between genotypes **Fig3.3(A)**. This is perhaps unsurprising, considering that, even 6 months after surgery[9], there is little scope in this model for the type of behavioural recovery that Kv1.6 might mediate. There are fundamental differences between the two models; notably that behavioural follow-up after SNI probes mechanical sensitivity in the intact sural nerve at the lateral plantar hind-paw, whereas the neuroma model features complete transection of the proximal sciatic nerve and stimulation of axotomised afferents sutured beneath the proximal thigh skin. Perhaps in spared neurons of the sural nerve, there are different mechanisms inducing hypersensitivity, not involving dysregulation of Kv1 channels. Alternatively, if native Kv1 channels are lost in these uninjured afferents, perhaps without direct axotomy the compensatory transcriptional or translational response involving Kv1.6 upregulation is not initiated, and this results in prolonged hypersensitivity.

While *Kcna6* mRNA was unaltered in the DRG 3 weeks after SNI **Fig3.3(D)**, this is an average across all DRG cell types and there may be subtle or opposing changes in different subpopulations which cancel out. Additionally, there may be sampling errors in this analysis as L2 DRGs, which are also supplied by injured tibial and common peroneal nerves, were not extracted, and L4/5 DRGs are supplied by both injured nerves as well as uninjured sural nerve[38]. Next, I aim to compare transcriptional responses of injured versus uninjured neurons directly by using *in situ* hybridisation

for *Kcna6* in injured DRG sections, using markers of injured neurons such as ATF3[39] as a counter-stain.

Western blotting previously demonstrated that Kv1.6 protein levels in the DRG were maintained at a constant level after complete sciatic transection[1], consistent with other reports that *Kcna6* mRNA and protein is maintained at normal levels in the DRG after peripheral nerve injury (unlike *Kcna1* and *Kcna2*, which are downregulated)[40,41]. However, *Calvo et al. (2016)* found that Kv1.6 protein expression in the injured nerve was increased[1]. Similarly, in an *in vitro* model of peripheral nociceptor axotomy using microfluidic chambers, sodium channel Nav1.8 was found to be upregulated in distal terminals despite normal expression at the soma[42]. Whilst mechanisms involving antisense long non-coding RNA have provided some explanation for injury-induced loss of Kv1.2 subunits[43], there is a lack of evidence for how exactly Kv1.6 and other ion channels may come to be appear in the nerve after axotomy, especially without gross somal upregulation.

It is possible that Kv1.6 is upregulated via increased translation rather than transcription, as was shown recently in a model of chemotherapy-induced neuropathy[2] **Introduction (Fig1.4)**. This increase in translation may even occur locally within axons; the existence of axonal or dendritic mRNA is no longer in doubt[44,45] and has been reviewed extensively in recent years[46–48]. This would likely be an energy-efficient adaptation as I suggest that there would be greater metabolic cost in trafficking protein from the soma to a distal injury site, compared with axonal translation of protein from few (or single) mRNA transcripts tethered locally. Again, *in situ* hybridisation of injured nerve tissue is a worthwhile future experiment that I will perform.

Additionally, Kv1 channels have been discovered in Schwann cells[49–51], and there are unpublished reports of *Kcna6* transcripts in Schwann cell-derived exosomes from *in vitro* injury models. Possibly, Schwann cell-to-neuron transfer of mRNA (or protein) exists as a compensatory mechanism after

nerve injury[52–54]. I have already demonstrated *Kcna6* gene expression in satellite glia (supposedly a developmentally arrested form of Schwann cell in the DRG[55]) via LacZ immunoreactivity in *Kcna6*^{tm1Lex} mice **Chapter II**, and this is an approach that could be used in nerve sections along with *in situ* hybridisation to confirm Schwann cell expression and potential upregulation after injury.

c) Concluding remarks

Overall, Kv1.6 appears to play an unconventional role in acute thermal sensory processing, evidenced by marked hyposensitivity in *Kcna6*^{tm1Lex} knock-out mice. In other contexts, such as following formalin injection or nerve injury, Kv1.6 seems to suppress nociceptive activity, as genetic deletion of the channel results in hypersensitivity compared to wild type animals. This is a more canonical property of Kv1 channels, consistent with known consequences of Kv1.1 and Kv1.2 loss of function[12–14,43]. Given the unusual impact of Kv1.6 knock-out on thermosensation, what follows in the next two chapters is predominantly an exploration of the underlying mechanisms within the peripheral and central nervous systems that may have precipitated this sensory phenotype relating to acute noxious heat stimulation.

iii. Methods

Animals

Male and female adult (>8wks) mice were used throughout. *Kcna6*^{tm1Lex} mice were as described in **Chapter II**, with wild-type littermates used as controls in all experiments except for neuroma surgery, in which non-littermate wild-type C57BL/6J controls were used.

Ethico-legal considerations

All experiments performed in the UK on protected animals complied with the Animals (Scientific Procedures) Act 1986, specifically under the PPL 30/3015. The neuroma model was performed at Pontificia Universidad Católica de Chile, in Santiago, Chile in collaboration with Associate Prof. Margarita Calvo and her PhD student Luis Martin Gonzalez Gomez. This experimental protocol was approved by 'Coordinación de Ética, Bioética y Seguridad de las investigaciones UC'. All experiments were designed, conducted and reported with reference to the ARRIVE guidelines[56].

Behavioural assays

Mice were housed in individually ventilated cages with typically no more than 6 or no fewer than 2 mice per cage. The light-dark cycle period was 12 hours, and behavioural experiments were performed during the light cycle. Multiple different behavioural assays were performed each day, but the time of day for each behavioural assay was kept constant.

Baseline experiments were performed on age- and sex-matched mice where breeding success allowed (WT – 11 males, 9 females; HET – 13 males, 2 females; KO – 11 males, 11 females). These data were combined from 2 experimental cohorts, one of which received intraplantar formalin as a terminal assay, and one underwent spared nerve injury. Mice that underwent neuroma surgery were similarly age- and sex-matched to the previous cohorts (WT – 6 males, 5 females; HET – 12 males, 0 females; KO – 6 females, 4 males).

N.B. Prior to all experiments, animals were habituated to equipment so that the experimental environment was not novel. Unless otherwise stated, baseline results were averaged from 3 baseline recordings. Data from left and right hind limb paws were combined and averaged for naïve Hargreaves and Von Frey results. Experimenter was blinded to genotype at all times during behavioural testing.

a) Open field

Mice were placed in the corner of a wooden box with a 5x3 grid marked on the base and allowed to move freely for 3 minutes. During this time, the number of grid lines crossed and hind limb rearing episodes were recorded.

b) Beam test

Mice were filmed from behind walking between two points along a thin cylindrical beam (approximately 1.5cm in diameter). The video footage was used to calculate the percentage of 'incorrect' hind limb steps (that is, where hind paws either slip or hop on the beam) from the total number of steps.

c) Rota-rod

Mice were required to climb/walk against the direction of the platform (Ugo Basile) rotating at 28rpm beneath them. The designated end point of this experiment was when the animal falls off the equipment, or at the 90 second mark, or when they cling to and rotate with the platform for 2 full revolutions cumulatively throughout the 90 second period.

d) Hot plate

Animals were placed on the hot plate (Ugo Basile) set to either 50˚C or 53˚C, at which point a timer was started by depression of a foot switch. The time was recorded, and the animal

removed, when the animal displayed visible pain behaviour (hind paw licking, biting, shaking, or jumping) or after a maximum of 20 seconds to avoid tissue injury. Baseline measurements were made on 4 occasions, with only recordings 2-4 used for analysis.

e) Von Frey

Mice were housed individually in plexiglass enclosures on a metallic grille platform. After an acclimation period of between 30 minutes to 1 hour, 50% mechanical withdrawal thresholds were derived using the Dixon up-and-down method[57]. Baseline measurements were averaged from left and right paw taken on 4 occasions, with only recordings 2-4 used for analysis.

f) Hargreaves

Mice were housed individually in plexiglass enclosures on a glass platform. An infrared heat source (Ugo Basile) was placed under the animal, targeted through the glass at the hind paw. Switching on the heat source begins a timer, which turns off once the animal responds to the stimulus by relocating its paw. Otherwise, the test was stopped at a maximum of 20 seconds. Baseline recordings were taken on 4 separate occasions for each animal. On each of these occasions, between 1 and 3 recordings were taken per hind paw, generating a maximum total of 24 readings per animal from which mean withdrawal latency was calculated.

g) Intraplantar formalin

Mice received a 20μl intradermal injection of formalin solution (5% in saline) to the plantar surface of the left hind paw and were placed in a transparent plexiglass enclosure. Immediately following the injection, duration of pain behaviour (for example; paw licking, lifting, biting, shaking, flinching) was recorded during each 5-minute period for 60 minutes. Mice were culled by intraperitoneal pentobarbital overdose 2 hours following completion of the test.

Surgery

Spared nerve injury (SNI)[9] and neuroma[1] surgeries were performed as described previously under isoflurane anaesthesia. Briefly, a small incision was made to the skin over the left hind limb and blunt dissection of the muscle layer performed to expose the sciatic nerve either distal (SNI) or proximal (neuroma) to its trifurcation. For SNI, the tibial and common peroneal branches were ligated and transected distally, leaving the sural nerve intact, with subsequent Von Frey testing performed on the sural territory – that is, the lateral aspect – of the plantar hind paw. These experiments were performed at the University of Oxford. For neuroma surgery, a ligature was tied to the sciatic nerve prior to complete distal transection; the injured nerve was then attached via the intact ligature to the subcutaneous fascia, such that the truncated nerve ending could be stimulated percutaneously with Von Frey filaments to assess mechanical sensitivity in injured neuroma afferents. The neuroma experiment and corresponding behavioural assessment were performed at Universidad Católica, Santiago, Chile, jointly by myself, Associate Prof. Margarita Calvo and her PhD student Luis Martín González Gómez.

RT-qPCR

Quantitative PCR of *Kcna6* transcripts was performed as in **Chapter II**, on ipsilateral and contralateral L3-5 DRGs extracted 3 weeks after spared nerve injury. On this occasion, only *Hprt1* was used as a housekeeping gene, and an exon-spanning primer pair for *Kcna6* was used instead of a pair targeting the coding sequence as the purpose was quantitation of *bona fide* mRNA, not validation of gene knock-out. This experiment was assisted by an undergraduate medical student, Yolanda Wintle, under my supervision at the University of Oxford.

Statistical Analyses

Behaviour – data are presented as group mean (grouped by genotype and/or time point) ± standard error of the mean (SEM) unless otherwise stated and may include data points from individual animals in some instances. Data were first assessed for normality using the Shapiro-Wilk test. Baseline sensorimotor performance was compared between genotypes by One-Way ANOVA. Assays comparing genotypes over several time points were analysed by Two-Way Repeated Measures ANOVA. I used Dunnett's post hoc multiple comparisons test to identify differences relative to wild type controls, or Tukey's post hoc test when reporting differences with all possible comparisons between genotypes. The unit of statistical analysis was the animal, and significance was reported as multiplicity-adjusted p-values. Group sizes were determined by prior power calculations regarding 10 animals as the minimum required to show a 25% difference in mechanical sensitivity with a power of 80% and an alpha error of 5%.

RT-qPCR – the unit of analysis was the animal. Contralateral DRG samples failed a Shapiro-Wilk normality test, presumably due to small sample size, so a Wilcoxon matched-pairs signed rank test was performed.

Calculations were performed in GraphPad Prism software.

iv. References

1. Calvo, M. *et al.* Altered potassium channel distribution and composition in myelinated axons suppresses hyperexcitability following injury. *Elife* **5**, 1–26 (2016).
2. Megat, S. *et al.* Nociceptor translational profiling reveals the ragulator-rag gtpase complex as a critical generator of neuropathic pain. *J. Neurosci.* **39**, 393–411 (2019).
3. Kaplan, W. D. & Trout, W. E. The behavior of four neurological mutants of Drosophila. *Genetics* **61**, 399–409 (1969).
4. Smart, S. L. *et al.* Deletion of the K(v)1.1 Potassium channel causes epilepsy in mice. *Neuron* **20**, 809–819 (1998).
5. Robbins, C. A. & Tempel, B. L. Kv1.1 and Kv1.2: Similar channels, different seizure models. *Epilepsia* **53**, 134–141 (2012).
6. Usoskin, D. *et al.* Unbiased classification of sensory neuron types by large-scale single-cell RNA sequencing. *Nat. Neurosci.* **18**, 145–153 (2015).
7. Zeisel, A. *et al.* Molecular Architecture of the Mouse Nervous System. *Cell* **174**, 999-1014.e22 (2018).
8. Zheng, Y. *et al.* Deep Sequencing of Somatosensory Neurons Reveals Molecular Determinants of Intrinsic Physiological Properties. *Neuron* **103**, 1–19 (2019).
9. Decosterd, I. & Woolf, C. J. Spared nerve injury: An animal model of persistent peripheral neuropathic pain. *Pain* **87**, 149–158 (2000).
10. Orefice, L. L. L. *et al.* Peripheral Mechanosensory Neuron Dysfunction Underlies Tactile and Behavioral Deficits in Mouse Models of ASDs. *Cell* **166**, 299–313 (2016).
11. Sorge, R. E. & Strath, L. J. Sex differences in pain responses. *Current Opinion in Physiology* **6**, 75–81 (2018).
12. Hao, J. *et al.* Kv1.1 channels act as mechanical brake in the senses of touch and pain. *Neuron* **77**, 899–914 (2013).
13. González, A. *et al.* Role of the excitability brake potassium current I KD in cold allodynia induced by chronic peripheral nerve injury. *J. Neurosci.* **37**, 3553–16 (2017).
14. Dawes, J. M. *et al.* Immune or Genetic-Mediated Disruption of CASPR2 Causes Pain Hypersensitivity Due to Enhanced Primary Afferent Excitability. *Neuron* **97**, 806–822 (2018).
15. Wang, H., Kunkel, D. O., Schwartzkroin, P. A. & Tempel, B. L. Localization of Kv1.1 and Kv1.2, two K channel proteins, to synaptic terminals, somata, and dendrites in the mouse brain. *J. Neurosci.* **14**, 4588–4599 (1994).
16. Barik, A., Thompson, J. H., Seltzer, M., Ghitani, N. & Chesler, A. T. A Brainstem-Spinal Circuit Controlling Nocifensive Behavior. *Neuron* **100**, 1491-1503.e3 (2018).
17. Huang, T. *et al.* Identifying the pathways required for coping behaviours associated with sustained pain. *Nature* **565**, 86–90 (2019).
18. Cavanaugh, D. J. *et al.* Distinct subsets of unmyelinated primary sensory fibers mediate behavioral responses to noxious thermal and mechanical stimuli. *Proc. Natl. Acad. Sci. U. S. A.* **106**, 9075–80 (2009).
19. Gutierrez-Mecinas, M., Polgár, E., Bell, A. M., Herau, M. & Todd, A. J. Substance P-expressing excitatory interneurons in the mouse superficial dorsal horn provide a propriospinal input to the lateral spinal nucleus. *Brain Struct. Funct.* **223**, 2377–2392 (2018).
20. Laliberte, A. M., Goltash, S., Lalonde, N. R. & Bui, T. V. Propriospinal Neurons: Essential Elements of Locomotor Control in the Intact and Possibly the Injured Spinal Cord. *Front. Cell. Neurosci.* **13**, 512 (2019).
21. Tan, L. L. *et al.* Gamma oscillations in somatosensory cortex recruit prefrontal and descending serotonergic pathways in aversion and nociception. *Nat. Commun.* **10**, 983 (2019).

22. Liu, Y. *et al.* Touch and tactile neuropathic pain sensitivity are set by corticospinal projections. *Nature* **561**, 547–550 (2018).
23. Woolf, C. J. Long term alterations in the excitability of the flexion reflex produced by peripheral tissue injury in the chronic decerebrate rat. *Pain* **18**, 325–343 (1984).
24. Caterina, M. J. *et al.* The capsaicin receptor: A heat-activated ion channel in the pain pathway. *Nature* **389**, 816–824 (1997).
25. Tominaga, M. *et al.* The cloned capsaicin receptor integrates multiple pain-producing stimuli. *Neuron* **21**, 531–543 (1998).
26. Caterina, M. J. *et al.* Impaired nociception and pain sensation in mice lacking the capsaicin receptor. *Science (80-.).* **288**, 306–313 (2000).
27. Cao, E., Cordero-Morales, J. F., Liu, B., Qin, F. & Julius, D. TRPV1 Channels Are Intrinsically Heat Sensitive and Negatively Regulated by Phosphoinositide Lipids. *Neuron* **77**, 667–679 (2013).
28. Cho, H. *et al.* The calcium-activated chloride channel anoctamin 1 acts as a heat sensor in nociceptive neurons. *Nat. Neurosci.* **15**, 1015–1021 (2012).
29. Vriens, J. *et al.* TRPM3 Is a Nociceptor Channel Involved in the Detection of Noxious Heat. *Neuron* **70**, 482–494 (2011).
30. Vriens, J. & Voets, T. Sensing the heat with TRPM3. *Pflügers Arch. - Eur. J. Physiol.* **470**, 799–807 (2018).
31. Vandewauw, I. *et al.* A TRP channel trio mediates acute noxious heat sensing. *Nature* **555**, 662–666 (2018).
32. McNamara, C. R. *et al.* TRPA1 mediates formalin-induced pain. *Proc. Natl. Acad. Sci.* **104**, 13525–13530 (2007).
33. Urien, L. *et al.* Genetic ablation of GINIP-expressing primary sensory neurons strongly impairs formalin-evoked pain. *Sci. Rep.* **7**, 43493 (2017).
34. Häring, M. *et al.* Neuronal atlas of the dorsal horn defines its architecture and links sensory input to transcriptional cell types. *Nat. Neurosci.* **21**, 869–880 (2018).
35. Harvey, A. L. Twenty years of dendrotoxins. *Toxicon* **39**, 15–26 (2001).
36. Lacroix-Fralish, M. L. & Mogil, J. S. Progress in genetic studies of pain and analgesia. *Annu. Rev. Pharmacol. Toxicol.* **49**, 97–121 (2009).
37. Rode, F. *et al.* The importance of genetic background on pain behaviours and pharmacological sensitivity in the rat spared serve injury model of peripheral neuropathic pain. *Eur. J. Pharmacol.* **564**, 103–111 (2007).
38. Laedermann, C. J., Pertin, M., Suter, M. R. & Decosterd, I. Voltage-gated sodium channel expression in mouse DRG after SNI leads to re-evaluation of projections of injured fibers. *Mol. Pain* **10**, 1744-8069-10–19 (2014).
39. Tsujino, H. *et al.* Activating transcription factor 3 (ATF3) induction by axotomy in sensory and motoneurons: A novel neuronal marker of nerve injury. *Mol. Cell. Neurosci.* **15**, 170–182 (2000).
40. Ishikawa, K., Tanaka, M., Black, J. a & Waxman, S. G. Changes in expression of voltage-gated potassium channels in dorsal root ganglion neurons following axotomy. *Muscle Nerve* **22**, 502–507 (1999).
41. Yang, E.-K., Takimoto, K., Hayashi, Y., de Groat, W. C. & Yoshimura, N. Altered expression of potassium channel subunit mRNA and alpha-dendrotoxin sensitivity of potassium currents in rat dorsal root ganglion neurons after axotomy. *Neuroscience* **123**, 867–74 (2004).
42. Tsantoulas, C. *et al.* Probing functional properties of nociceptive axons using a microfluidic culture system. *PLoS One* **8**, e80722 (2013).
43. Zhao, X. *et al.* A long noncoding RNA contributes to neuropathic pain by silencing Kcna2 in primary afferent neurons. *Nat. Neurosci.* **16**, 1024–1031 (2013).
44. Cioni, J. M. *et al.* Late Endosomes Act as mRNA Translation Platforms and Sustain

Mitochondria in Axons. *Cell* **176**, 56-72.e15 (2019).
45. Rangaraju, V., Lauterbach, M. & Schuman, E. M. Spatially Stable Mitochondrial Compartments Fuel Local Translation during Plasticity. *Cell* **176**, 73-84.e15 (2019).
46. Glock, C., Heumüller, M. & Schuman, E. M. mRNA transport & local translation in neurons. *Current Opinion in Neurobiology* **45**, 169–177 (2017).
47. Rossoll, W. & Bassell, G. J. Crosstalk of Local Translation and Mitochondria: Powering Plasticity in Axons and Dendrites. *Neuron* **101**, 204–206 (2019).
48. Biever, A., Donlin-Asp, P. G. & Schuman, E. M. Local translation in neuronal processes. *Current Opinion in Neurobiology* **57**, 141–148 (2019).
49. Sobko, A. *et al.* Heteromultimeric delayed-rectifier K+ channels in schwann cells: developmental expression and role in cell proliferation. *J. Neurosci.* **18**, 10398–408 (1998).
50. Mi, H., Deerinck, T. J., Ellisman, M. H. & Schwarz, T. L. Differential distribution of closely related potassium channels in rat Schwann cells. *J. Neurosci.* **15**, 3761–3774 (1995).
51. Baker, M. D. Electrophysiology of mammalian Schwann cells. *Progress in Biophysics and Molecular Biology* **78**, 83–103 (2002).
52. Court, F. A., Hendriks, W. T. J., MacGillavry, H. D., Alvarez, J. & Van Minnen, J. Schwann cell to axon transfer of ribosomes: Toward a novel understanding of the role of glia in the nervous system. *J. Neurosci.* **28**, 11024–11029 (2008).
53. Lopez-Verrilli, M. A. & Court, F. A. Transfer of vesicles from Schwann cells to axons: A novel mechanism of communication in the peripheral nervous system. *Frontiers in Physiology* **3 JUN**, 205 (2012).
54. López-Leal, R., Alvarez, J. & Court, F. A. Origin of axonal proteins: Is the axon-schwann cell unit a functional syncytium? *Cytoskeleton* **73**, 629–639 (2016).
55. George, D., Ahrens, P. & Lambert, S. Satellite glial cells represent a population of developmentally arrested Schwann cells. *Glia* **66**, 1496–1506 (2018).
56. Kilkenny, C., Browne, W. J., Cuthill, I. C., Emerson, M. & Altman, D. G. Improving Bioscience Research Reporting: The ARRIVE Guidelines for Reporting Animal Research. *PLoS Biol.* **8**, e1000412 (2010).
57. Dixon, W. J. The up-and-down method for small samples. *J. Am. Stat. Assoc.* **60**, 967–978 (1965).

Chapter IV

Anatomy and physiology of the *Kcna6* ^{tm1Lex} peripheral nervous system

In search of a mechanistic explanation for the modality-specific alterations of pain sensitivity in *Kcna6*^{tm1Lex} carriers, I conducted an in-depth analysis of peripheral nervous system structure and function in this mouse line. This included histochemical assessment of small fibre integrity and developmental differentiation, and a live Ca^{2+} imaging assay to investigate the responsiveness of adult DRG neurons to thermal stimulation *in vitro*.

Under healthy conditions, activation of the sensory neuraxis is firstly achieved by ion channels and receptors capable of transducing stimuli at the distal-most terminals of peripheral sensory neurons in the skin or visceral organs. Factors affecting these terminals are posited to impact on sensation. Specifically, thermal detection thresholds, measured by quantitative sensory testing, have been shown to correlate with intraepidermal nerve fibre density (IENFD) of the proximal thigh in healthy subjects[1]. Thermal hypoesthesia is also feature of conditions in which there is a reduction of epidermal nerve fibres, such as polyneuropathy (PNP) and small fibre neuropathy (SFN)[1], or congenital insensitivity to pain (CIP) mediated by loss of function mutations in *PRDM12* [2], *SCN9A* (Nav1.7)[3], or more commonly nerve growth factor (NGF) and its receptor *NTRK1* [4–6]. CIP patients with *SCN9A* loss of function have an almost complete absence of epidermal nerve fibres at all testing sites (thigh and distal leg) and are totally insensitive to suprathreshold thermal pain stimuli, as well as having deficits in non-noxious temperature detection thresholds[3]. Therefore, in the context of thermal hypoesthesia **Chapter III**, one important strategy to employ was assessment of IENFD in *Kcna6*^{tm1Lex} mice as there is experimental precedent to justify loss of cutaneous nerve fibres as a hypothetical mechanism of hyposensitivity in these mice.

Our ability to detect a diverse array of mechanical, thermal and chemical stimuli mirrors the heterogeneity among dorsal root ganglion neurons. Indeed, modality-specific function has been ascribed to histochemically-, genetically- and pharmacologically-defined DRG subpopulations via ablation and optogenetic experiments in mice[7–12]. Regarding thermal sensitivity, it has been shown that ablation of capsaicin-sensitive (Trpv1-expressing) afferents, via intrathecal capsaicin injection, results in impaired noxious heat sensation[7]. In contrast, ablation of Mrgprd-expressing, non-peptidergic afferents reduces mechanical sensitivity to Von Frey hairs[7,13]. Furthermore, destruction of Trpv1$^+$ fibres in Mrgprd-ablated mice had no additive impact on mechanosensation[7]. In mice, Trpv1$^+$ fibres are largely confined to the peptidergic population[14], and these results have informed the prevailing dogma that the broadly categorised peptidergic and non-peptidergic DRG neurons convey information about thermal and mechanical stimuli, respectively.

However, pharmacological silencing of Trpv1$^+$ afferents in rats (by co-administration of capsaicin with membrane-impermeant lidocaine derivative QX-314) resulted in mechanical as well as thermal hyposensitivity[15]. This is possibly explained by the considerably greater overlap of both Trpv1 and CGRP expression with IB4-binding neurons in rat versus mouse DRG[16]. Nevertheless, *Trpv1* mRNA has also recently been identified in mouse 'non-peptidergic'[17,18] and C-LTMR[19] neurons, so even in mice there is not such a clear dichotomy as is often presented regarding these populations. Additionally, Trpv1$^+$ fibre ablation by intrathecal capsaicin has recently been shown to attenuate 'coping' responses in mice – such as licking following noxious mechanical stimulation[13] – implying that some peptidergic primary afferents could indeed contribute to some aspects of pain elicited by mechanical stimuli. There was therefore a need to confirm the relative proportions of DRG subpopulations in *Kcna6*^{tm1Lex} knock-outs, as a selective deficiency could evidently impact selectively on behavioural sensitivity.

Finally, there may have been a physiological change in primary afferent responsiveness to thermal stimuli relating to loss of the Kv1.6 channel. This was investigated using *in vitro* calcium imaging of dissociated adult DRG neurons – a relatively high-throughput approach that involved stimulating DRG neurons with a temperature ramp from ambient temperature to approximately 45ºC. All ion channels have some degree of heat dependence in their activity, and evoked firing rate in most neurons will be temperature-dependent as a result, but *bona fide* temperature-sensing neurons display robust increases in intracellular calcium at specific temperatures due to the repertoire of transducing receptors they express[20].

The latest evidence suggests that noxious heat is transduced by functionally redundant expression of Trpv1, Trpm3, and Trpa1, which are all independently sufficient for behavioural heat sensation[21]. In this experimental preparation, simultaneous recording of perfusate temperature and intracellular calcium concentration enabled the identification of activation temperature thresholds for individual DRG neurons across the 25-45ºC range. In addition, the magnitude of temperature-evoked calcium responses was measured as a proxy for neuronal excitability. As such, thermal activation of primary sensory neurons from wild-types and *Kcna6* knock-outs could be modelled *in vitro* and compared in a quantitative manner, to search for a peripheral mechanism resulting in heat-evoked behavioural hyposensitivity.

The aims of this chapter are to identify and rationalise any anatomical or physiological changes in the peripheral nervous system that may contribute to the dampened noxious thermal sensation apparent in *Kcna6*^{tm1Lex} mice.

i. Results

a) Assessment of hind paw intraepidermal innervation

All sensory behavioural assays described in **Chapter III** involve application of stimuli to the glabrous skin of the hind paw. This was therefore the most anatomically relevant site to investigate changes in epidermal innervation as a potential explanation for thermal hyposensitivity observed in *Kcna6*^{tm1Lex} mice. Although there was a slight reduction in mean intraepidermal nerve fibre density (WT 24.03 ± 3.87 mm^{-1}, KO 20.09 ± 2.84 mm^{-1}), this did not reach significance (p=0.44, unpaired two-tailed Student's t-test, n = 4 WT, 4 KO) **Fig4.1(B)**. In homozygous *Kcna6*^{tm1Lex} knock-out animals, the LacZ reporter product, β-galactosidase, was clearly visible in the dermal nerve plexus – counter-stained for PGP9.5 to mark nerve fibres **Fig4.1(A)**.

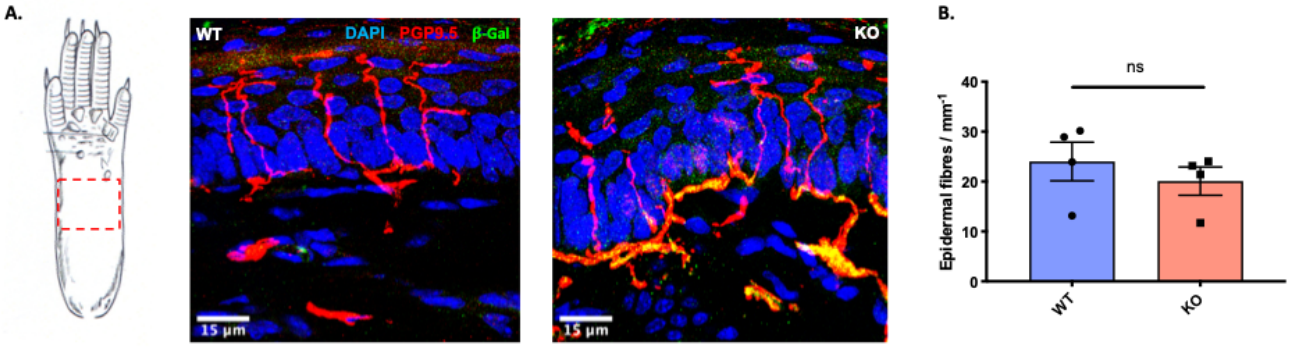

Figure 4.1 – Intraepidermal nerve fibre density is unaltered in *Kcna6*^{tm1Lex} mice

(A) Representative images of epidermal innervation from the indicated hind paw region of *Kcna6*$^{tm1/tm1}$ mice and wild type littermates. In knock-out mice, β-galactosidase immunoreactivity colocalises with the pan neuronal marker PGP9.5 in the dermal nerve plexus.
(B) Nerve fibre density in the epidermis did not differ significantly between knock-out and wild type mice. Data presented as mean ± SEM, plus mean values from individual animals (n = 4 WT, 4 KO). p = 0.4427 by unpaired, two-tailed t-test.

A.

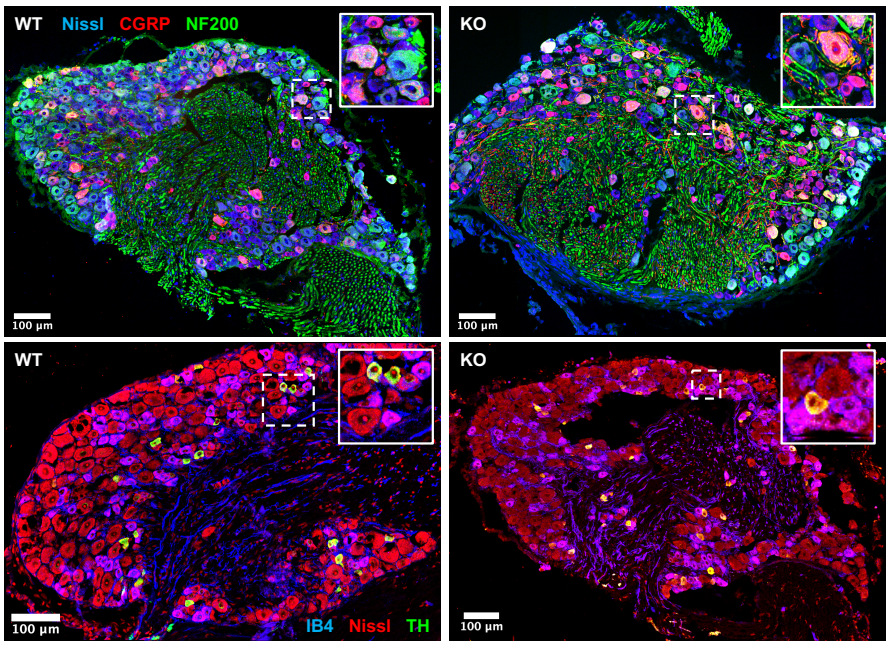

B.

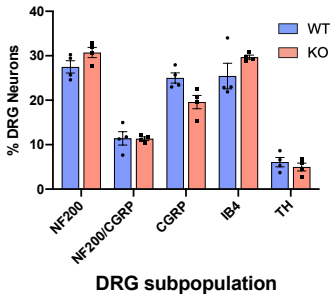

C.

DRG Subpopulation	WT	KO	FDR Adjusted p-value
NF200 only	27.49 ± 1.39 %	30.73 ± 1.16 %	0.197893
NF200/CGRP	11.42 ± 1.50 %	11.36 ± 0.41 %	>0.999999
CGRP only	25.00 ± 1.15 %	19.58 ± 1.51 %	0.054648
IB4	25.44 ± 2.88 %	29.69 ± 0.46 %	0.104730
TH	6.07 ± 1.05 %	4.98 ± 0.88 %	0.771910

Figure 4.2 – Subpopulations of dorsal root ganglion neurons in adult *Kcna6*^{tm1Lex} mice

(A) Representative images of whole dorsal root ganglia sections *Kcna6*$^{tm1/tm1}$ mice and wild type littermates. Inset: magnification of dashed region of interest.
(B) No subpopulation was differentially represented within the DRG in *Kcna6* knock-out mice. Data presented in as mean ± SEM, plus individual animal values (n = 4 WT, 4 KO).
(C) Mean ± SEM percentages from **(B)** calculated as a proportion of Neurotrace (Nissl)-positive neurons. Adjusted p-values comparing genotypes are indicated from multiple unpaired t-tests, performed with 5% False Discovery Rate using the Benjamini, Krieger and Yekutieli two-stage set-up method.

b) Quantification of DRG subpopulations

The ability to discern noxious stimuli across multiple modalities relies upon appropriate development or post-natal maintenance of nociceptive DRG subpopulations[2,3,22,23]. It is known that genetic diversity between subpopulations relates to their ability to transduce and encode different modalities of stimuli. The identified behavioural phenotype in mice carrying the *Kcna6*^{tm1Lex} allele was highly modality-specific, suggesting a peripherally-mediated effect possibly restricted to some of the specific DRG subpopulations shown to express *Kcna6* in naïve mice **Chapter II**.

I immunostained 10µm sections of naïve L4 DRGs from adult *Kcna6*^{tm1Lex} homozygotes, using classical markers of DRG neuron subpopulations (NF200, CGRP, IB4, TH) to compare the relative proportions of sensory neuron subtypes with wild type littermates. Quantification in single

DRG sections is biased towards smaller cells, so these results do not reflect absolute proportions of DRG neurons, which requires stereological analysis such as serial sectioning or staining of cleared whole-mount tissue. Hence, I have quantified 'neuronal profiles'. Both wild type and *Kcna6*^{tm1Lex} DRGs had values within the accepted reference ranges for each subpopulation **Fig4.2(B, C)**, and there were no significant differences between genotypes for any subpopulation. However, non-myelinated peptidergic neuronal profiles ('CGRP only') represented approximately 5-6% less of the total DRG population in knock-outs compared to wild type, which was approaching significance with an FDR adjusted p-value of 0.055 (2s.f.) **Fig4.2(B, C)**. The false discovery rate correction was performed because multiple t-tests were performed to assess proportional representation of DRG subpopulations belonging to the same overall sample population and therefore the likelihood of false positives increases with each hypothesis testing.

c) *In vitro* calcium imaging of dissociated DRG neurons

With no clear effect of Kv1.6 knock-out on peripheral terminals of sensory neurons, I decided to probe DRG function using calcium imaging. Heat-sensitive neurons were identified by intracellular calcium signals elicited by a thermal ramp stimulus from room temperature to >45ºC **Fig4.3(A, B)**. The mean proportion of dissociated DRG neurons responding to this stimulus was 42.07 ± 1.40% for wild type animals and 38.08 ± 2.24% for homozygous *Kcna6*^{tm1Lex} mice, which did not differ significantly (p=0.21, unpaired two-tailed Student's t-test, n = 3 WT, 3 KO) **Fig4.3(C)**.

The distributions of activation temperatures from all heat-sensitive neurons per genotype – 369 WT and 381 KO combined from 3 animals – were both non-Gaussian (p<0.0001 for Shapiro-Wilk normality test) **Fig4.3(D.i)**. The range was similar for both genotypes (WT 23.16 – 45.63ºC, KO 23.52 – 46.25ºC), but the wild type responses had more negative skew compared to knock-outs (WT -0.54 vs. KO -0.29) and less negative kurtosis (WT -0.34 vs KO -0.91). Together these metrics

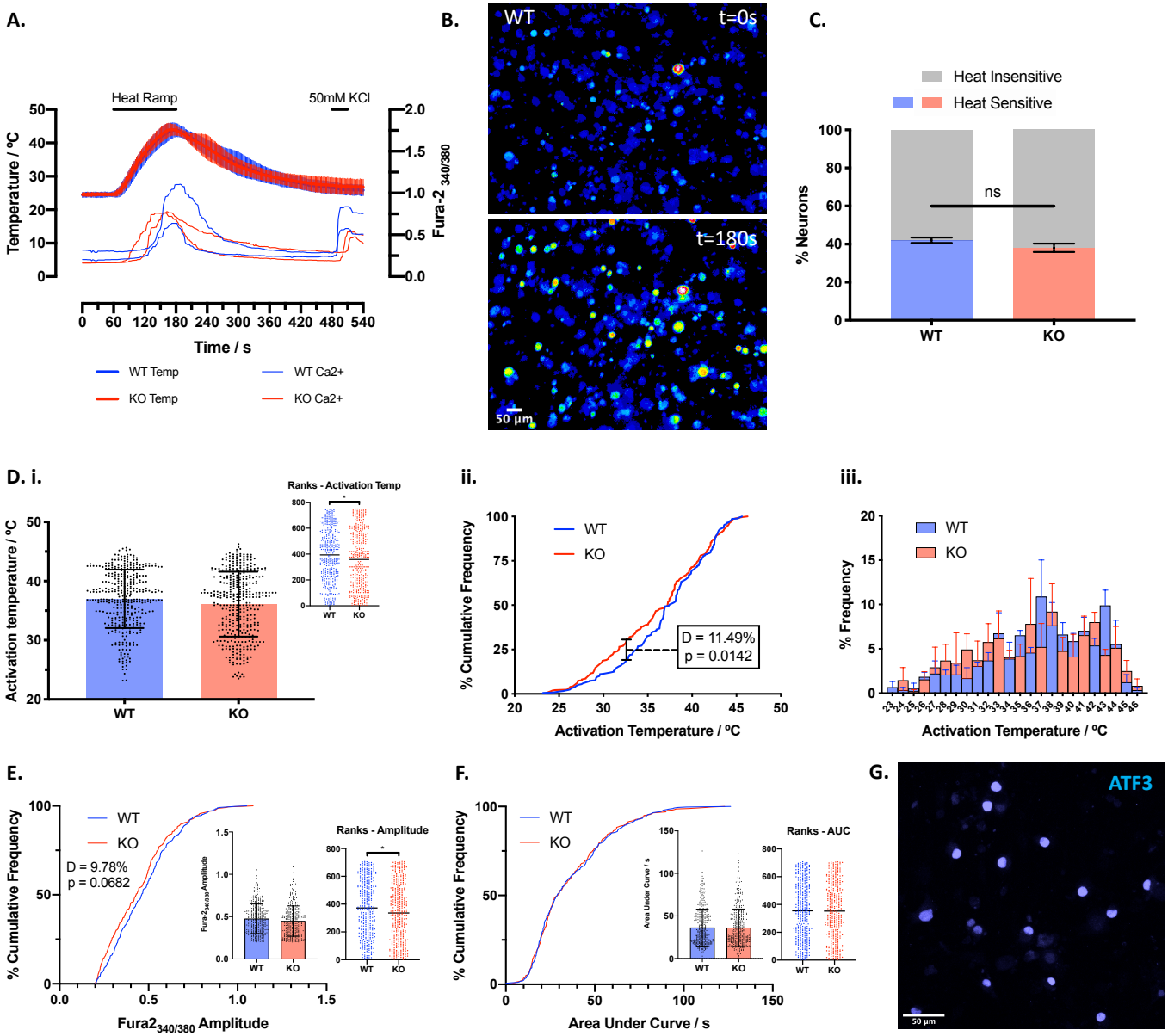

Figure 4.3 – *In vitro* calcium imaging of *Kcna6*^{tm1Lex} DRG neurons

(A, B) Intracellular calcium transients are induced in dissociated neurons by thermal ramp from 25-45°C. Temperature curves in **(A)** are presented as mean ± SD calculated from 12 coverslips (3 animals x 4 coverslips) per genotype, but N.B. activation temperatures were always derived from the exact temperature on the relevant coverslip.
(B) Isolated frames from a representative imaging experiment on WT DRG cells. Fura2-AM 340/380 ratio represented on 16-colour scale ImageJ Look-up table (LUT).
(C) The average percentage of neurons responding to heat did not differ between genotypes (n = 3 WT, 3 KO animals, unpaired two-tailed Student's t-test).
(D.i) Combined activation temperatures of heat-sensitive wild type and Kv1.6 knock-out neurons sampled across all animals and coverslips (n = 369 WT, 381 KO). The average knock-out activation temperature was slightly, but significantly, lower according to a two-tailed Mann-Whitney test to compare ranks (inset – *p<0.05).
(D.ii) The distributions also differed significantly when analysed by Kolmogorov-Smirnov test which revealed a maximum difference in cumulative distributions of 11.49% (p<0.05) found in the lower temperature range. A binned frequency histogram is provided in **(D.iii)** to show inter-replicate variation (n = 3 WT, 3 KO animals) with mean ± SEM values superimposed in front of each other (not stacked).
(E) The difference in wild type and knock-out distributions of heat-response amplitudes was approaching significance via Kolmogorov-Smirnov test, and was significantly different according to a two-tailed Mann-Whitney test (inset – *p<0.05).
(F) The distribution of areas under the curve for wild type and knock-out neurons were almost identical.
(G) Expression of injury marker, ATF3, in cultured DRG neurons.

indicate that the activation of wild type neurons was weighted more towards the noxious temperature range while knock-out animals had more even distribution between the two extremes. A Mann-Whitney test was performed to compare ranks, and this revealed a slight but significant reduction in mean activation temperature (WT 37.01ºC vs KO 36.10ºC*****, *****$p<0.05$) **Fig4.3(D.i)**. Therefore, activation at high temperatures was more common than at warm temperatures, as has been reported previously[24], in both genotypes but to a greater extent in wild types.

Comparing the cumulative distributions via a two-sample Kolmogorov-Smirnov test, the computed 'D statistic' showed a maximum difference of 11.49 % between cumulative frequency distributions and had a p-value of 0.0142, indicating that the wild type and knock-out samples represent populations with different distributions **Fig4.3(D.ii)**. Knock-outs had proportionally more neurons than wild types activating at warm temperatures between 26.5 – 32.5ºC. For transparency, a binned frequency histogram is provided in **Fig4.3(D.iii)** to depict variation between biological replicates (n = 3 WT, 3 KO animals) with mean ± SEM values superimposed in front of each other (not stacked). These binned values were far from statistically significant between genotypes when analysed by multiple t-tests with 5% FDR correction. The Ca^{2+} peak amplitude and the area under the curve for the duration of the heat stimulation (60s-470s) were calculated for each heat-sensitive neuron to provide further detail about response magnitude. Comparing distributions of combined Kv1.6 knock-out neurons to wild types showed that there was a slight reduction in Ca^{2+} response amplitude in *Kcna6*^{tm1Lex} neurons (WT 0.48 vs KO 0.45*****, *****$p<0.05$ Mann-Whitney test) but no change in area under the curve **Fig4.3(E, F)**. It is worth noting that dissociated DRG neurons have suffered major axotomy and other physical and chemical stresses during the dissociation and cell culture protocol, evidenced by their widespread expression of injury marker ATF3 **Fig4.3(G)**, so recorded calcium responses and activation temperatures may reflect a somewhat sensitised state.

ii. Conclusions

a) No evidence of reduction of intraepidermal nerve fibre density in *Kcna6*^{tm1Lex} mice

Despite stronger correlations in human subjects between thermal sensitivity and proximal rather than distal thigh innervation[1], the hind paw was chosen here as the site of analysis due to its direct stimulation by all of the sensory behavioural assays performed previously **Chapter III**. Small-diameter fibres crossing into the epidermis were present at a similar density in age-matched adult wild types and knock-outs, so there is no evidence of either developmental or adult-onset loss of nociceptive nerve fibres **Fig4.1(B)**. β-galactosidase (LacZ) was detected by immunohistochemistry in *Kcna6*^{tm1Lex} homozygote skin sections, which provides further evidence for *Kcna6* expression in peripheral afferents **Fig4.1(A)**. For reasons unknown, there was strong co-localisation with PGP9.5 in the dermal nerve plexus but notably poorer co-localisation within the epidermis. On the basis of prior expression data indicating enrichment of *Kcna6* in small-diameter DRG populations **Chapter II**, the assumption is made that the LacZ^{+} fibres in the dermis give rise to epidermal nerve endings but that there is insufficient β-galactosidase product in these narrow terminals to be detected by antibodies. An alternative interpretation is that the sub-epidermal localisation of LacZ could also reflect *Kcna6* expression in the novel class of Schwann cells recently shown to ensheath nociceptive nerve terminals and influence pain-like sensation in mice[25].

b) *Kcna6*^{tm1Lex} mice have a small, potentially significant loss of CGRP neurons in the DRG

Molecularly distinct populations of DRG neurons have been shown to serve specific functions across sensory modalities. This concept has been introduced already, but briefly regarding pain, peptidergic sensory neurons (including those expressing Trpv1[7]) are thought to transduce and convey noxious heat[12,26], while non-peptidergic neurons are required for appropriate mechanical

sensation[7]. Given the modality specificity of the *Kcna6*^{tm1Lex} phenotype, it was necessary to assess the relative proportions of these DRG populations in wild-types and *Kcna6* knock-outs, in case developmental loss of a specific neuronal class underlies the observed *Kcna6*^{tm1Lex} thermal deficit. This was achieved by immunostaining naïve (uninjured) DRG sections from adult mice.

Such a result was unexpected, as global knock-out of Caspr2 – a Kv1 channel chaperone protein that is expressed in the majority of DRG neurons – leads to a generic loss of Kv1 function but has no impact on the differentiation of sensory neurons into appropriate subpopulations, or intraepidermal nerve fibre density[27]. However, despite not quite reaching statistical significance, *Kcna6* knock-outs did appear to have a small reduction in unmyelinated peptidergic DRG profiles compared to wild types **Fig4.2**. This could be highly significant in terms of thermal sensation, as CGRP-α fibre ablation decreases responsiveness to noxious heat[12]. This analysis will be extended by assessing tissue from more animals to confirm whether this loss is genuine.

c) A physiological correlate in the DRG for behavioural thermal hyposensitivity in *Kcna6*^{tm1Lex} mice

Although the periphery was mostly structurally intact, the possibility remained that genetic deletion of Kv1.6 might have effects on excitability of DRG neurons, albeit with the opposite end-effect of hypoexcitability than would be expected from previous literature[27–29]. I was able to investigate responses of DRG neurons to 'natural' heat stimulation, as opposed to pharmacological stimulation of TRP channels, via live Fura2-based calcium imaging with a Peltier device used to heat artificial extracellular fluid. Across 4 coverslips each from 3 animals per genotype, calcium transients were evoked in 369 of 873 WT and 381 of 1021 KO neurons during the heating phase as detected by a custom-written MATLAB programme detailed in the methods section of this chapter. Per animal, when normalised to total neurons there was no difference in the proportion of heat responders between genotypes **Fig4.3(C)**.

Simultaneous recording of the bath temperature allowed derivation of the activation temperature of these heat-sensitive neurons. Firstly, this revealed interesting information about the heat sensitivity of wild type DRG neurons. The distribution was non-Gaussian – negatively skewed with a long lower tail – revealing a bias towards activation by temperatures >35ºC **Fig4.3(D)**. This pattern has been reported previously[24]. However, for technical reasons it was difficult to achieve bath temperatures much above 46ºC so it is possible that a proportion of heat-sensitive neurons with activation thresholds above this temperature were unidentified, contributing to the skew.

Due to the non-Gaussian distribution in activation temperature, response amplitude and area under the curve, for the rest of the analysis the decision was taken to combine neurons from each animal and compare overall wild type and knock-out distributions using non-parametric tests. It was found that there was a slight negative shift in activation temperature **Fig4.3(D)**. The open probability of, and therefore current carried by, noxious heat transducers such as Trpv1 is not binary but varies in a sigmoidal relationship with temperature[30]. These transducer channels are responsible for producing generator potentials which, if sufficient, depolarise the neuronal plasma membrane such that feed-forward activation of voltage gated sodium channels and action potentials may occur. If Kv1 currents act as a generic 'brake'[28,29] on excitability in sensory neurons, heat-transducing ion channels could potentially induce action potential firing at slightly lower open probabilities – that is, at lower temperatures – in Kv1.6 knock-out neurons.

This could explain the subtle shift towards cooler activation temperatures on a population level. It is tempting to draw the conclusion that this relates to thermal hyposensitivity in *Kcna6*^{tm1Lex} mice, but if temperature is encoded by activation of distinct fibre populations, this mechanism would actually describe a gain of function in thermal nociceptors. It is possible that a slight loss of CGRP fibres **Fig4.2** reduces heat-activated nociceptive input to the dorsal horn sufficiently to cause delayed behavioural responses. Behavioural assays were performed at >50ºC so it is also possible

that there may be physiological effects of *Kcna6* knock-out on other neurons responsible for detection of these more extreme temperatures, which were not activated by the maximum temperature achieved in the calcium imaging protocol.

There was also a negative shift in peak Ca^{2+} signal amplitude **Fig4.3(E)**. This is an interesting finding as again one might expect increased excitability and therefore more calcium influx in Kv1 channel knock-out neurons. Calcium influx at presynaptic terminals is directly responsible for neurotransmitter release[31] so this reduction of maximal calcium concentration in *Kcna6*^{tm1Lex} DRG neurons is possibly of mechanistic importance regarding the behavioural phenotype in this mouse line. However, it is important to consider that this is an *in vitro* preparation, and these are measurements from the cell soma with immature or absent neurites and presynaptic specialisations, so it is dangerous to extrapolate this result to *in vivo* neurotransmission. It is now possible to measure glutamate release by neurons using fluorescence-based glutamate sensors[32,33], but these experiments have not yet been performed in *Kcna6* knock-out DRG neurons.

d) Limitations of the primary cell culture approach

As mentioned, the dissociation process necessarily inflicts major axotomy on cultured neurons. This is followed by widespread expression of injury marker[34] ATF3 in cultures[35] **Fig4.3(G)**, which is known to initiate changes in the transcriptional profile of neurons, for example to stimulate neurite outgrowth[36]. These neurons are thus in a highly sensitised state. There is evidence that Kv1 channels are downregulated in DRG cultures over a period of 3 to 5 days[27,37], which could contribute to sensitisation of neurons *in vitro* and exacerbate hyperexcitable phenotypes or, more relevantly, mask suspected hypoexcitable phenotypes. If Kv1.6 follows the same pattern of downregulation, this would also render wild type neurons equivalent to knock-outs in terms of Kv1.6 expression and make comparisons between genotypes difficult. For these reasons imaging

experiments were performed 12-24 hours after cell plating to retain the *in vivo* transcriptional state as closely as possible. A preferable experiment would be to make use of *in vivo* DRG imaging with genetically encoded calcium indicators (GECIs), but these are technically challenging and expensive experiments, and come with their own controversies. Some *in vivo* imaging experiments have even suggested that polymodality of DRG neurons is a phenomenon only induced by the insult of dissociation and culture[38]. However, the interpretation of results in this publication has been recently contested[39,40] and polymodality most likely is a common endogenous property of DRG neurons.

e) Concluding remarks

The experiments detailed here attempted to provide a comprehensive characterisation of peripheral nervous system structure and function in Kv1.6 knock-out mice, particularly with regards to thermal sensation. Despite very reproducible behavioural hyposensitivity to noxious heat, this chapter's results only revealed quite subtle distinctions between wild type and *Kcna6*^{tm1Lex} homozygous mice, which are unlikely to completely explain the profound behavioural phenotype.

iii. Methods

Animals

All animal work was performed in compliance with the Animals (Scientific Procedures) Act 1986, under project licenses 30/3015 and P1DBEBAB9 held by Prof David Bennett at the University of Oxford. The experimenter was blind to genotype throughout all experiments that required manual data analysis (IENFD and DRG subpopulation quantification). Calcium imaging analysis was automated, and the experimenter was therefore not blinded to genotype during imaging experiments. For IENFD and DRG subpopulation quantification, age- and sex-matched male and female mice were used (WT – 2 males, 2 females; KO – 2 males, 2 females), all between 17-27 weeks of age. For calcium imaging experiments, only male mice were used (3 per genotype), aged between 8-11 weeks.

Tissue preparation

Animals were perfused, tissue harvested, and cells fixed as described in **Chapter II**. For analysis of epidermal nerve fibres, skin was dissected from the glabrous region of the hind paw proximal to the most proximal touch dome, as depicted in **Fig4.1(A)**. The duration of skin post-fixation (4% PFA in 0.1M PB) was 0.5hrs, and vertical sections were cut at 14μm thickness sequentially from the distal end of the tissue block on a Leica cryostat.

Immunohistochemistry

Staining of fixed tissue sections and dissociated cells was performed as described in **Chapter II**.

IENFD counts

Following immunostaining, 3 sections each from 4 animals per genotype were analysed on a Zeiss LSM700 confocal microscope. Using DAPI to mark the dermis/epidermis boundary, the number of PGP9.5 immunoreactive fibres that could be visualised crossing from dermis to epidermis was

counted through the viewfinder with a 63x oil immersion lens. A post hoc overview image was taken, and the length of epidermis analysed was measured in ZEN Black software; across all sections this ranged between 2.1-3.3mm.

DRG subpopulation counts

Naïve (uninjured) L4 DRGs were dissected from wild type and *Kcna6*^{tm1Lex} homozygote animals and fixation was performed as described in **Chapter II**. DRGs were subsequently sectioned at 10μm thickness for immunostaining, performed as described in **Chapter II**. At least 2 whole DRG sections were imaged and analysed per animal. DRG 'profiles' were defined as being Neurotrace-positive and nucleated. Profiles were designated positive or negative for histochemical markers by eye on images of whole DRG sections taken with identical acquisition settings, and their abundance was calculated as a percentage of Neurotrace-positive profiles (fluorescent Nissl stain). This experiment was performed by an undergraduate medical student, Yolanda Wintle, under my supervision at the University of Oxford.

Primary DRG culture

Primary cell culture of DRG neurons was performed as in **Chapter II**, with no electroporation.

In vitro Ca^{2+} imaging

On each occasion, DRG cultures were prepared from one wild type and one knock-out mouse simultaneously. In total, 4 coverslips each from 3 animals per genotype were imaged. After 12-24 hours *in vitro*, coverslips were chosen for calcium imaging. Coverslips were incubated for 45mins at 37ºC with 2μM Fura-2AM (Invitrogen) and 80μM pluronic acid in Neurobasal medium supplemented as above. After incubation coverslips were transferred to artificial extracellular fluid (140mM NaCl, 5mM KCl, 2mM $CaCl_2$, 1mM $MgCl_2$, 10mM D-Glucose, 10mM HEPES in distilled water). Coverslips were imaged every 2s with 4x4 binning for 540s on a Zeiss inverted fluorescence

microscope with a 10x objective, dichroic LP 409 mirror, BP 340/30 and BP 387/15 excitation and 510/90 emission filters. ZEN Blue software was used for image acquisition and selection of regions of interest (ROIs).

ECF was superfused continuously over the cells. After 60s of baseline recording a Peltier device (Warner Instruments, Harvard Apparatus – CL-100 bipolar temperature controller with SC-20 dual in-line heater/cooler) was used to heat the ECF from room temperature to >45ºC over a period of approximately 2 minutes. Perfusate temperature was recorded using a thermistor placed close to the Peltier outlet and as close to recorded cells as possible, with a USB DrDAQ and Picolog data acquisition software (Picosystems). After passive cooling, 30s of high K+ (100mM NaCl, 50mM KCl, 2mM $CaCl_2$, 1mM $MgCl_2$, 10mM D-Glucose, 10mM HEPES) was used to depolarise neurons, to discern them from other non-excitable cells also present in the culture, followed by 30s washout.

Ca^{2+} imaging – analysis workflow

I produced bespoke MATLAB scripts to automate analysis of calcium imaging fluorescence ratio data from pre-selected ROIs and to quantify the number of heat sensitive and insensitive neurons per animal. Briefly, the workflow firstly applies data smoothing for each ROI trace by selecting the moving median sequentially across each 11 adjacent data points. The script then calculates a baseline value from the mean ratio signal prior to the first stimulus (first 60 seconds). The subsequent process for designating heat responders is explained overleaf:

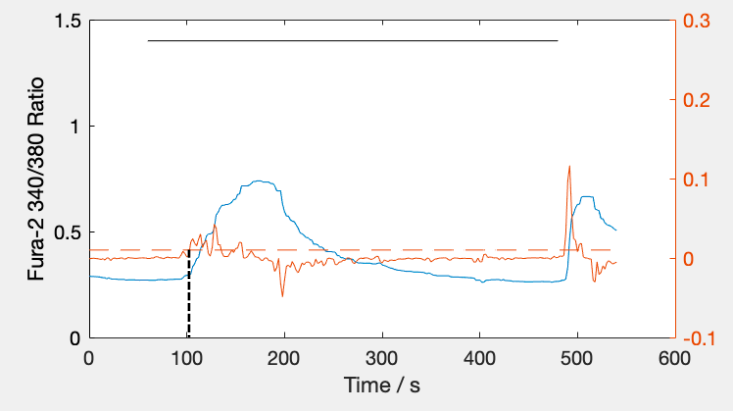

1. The first derivative of the ratio trace is computed – if there is a *bona fide* calcium 'peak', there is a positive deflection in the first derivative as the rate of change in the ratio increases.
2. The magnitude of this deflection indicates the rate of increase in the original calcium ratio. The threshold for deflections considered a true peak was determined arbitrarily by plotting the ratio data (blue trace) together with the first derivative (orange trace, unbroken line). The minimum value considered to represent most *bona fide* heat responses was 0.01 ratio units per frame (orange trace, dotted line).
3. The script computes the first time point at which the rate of change exceeds the 0.01 threshold for each trace (black vertical dotted line), signifying the beginning of the calcium peak, and cross-references this to a file containing the coverslip temperature log for each time point. Thus, the 'activation temperature' for each ROI is derived.
4. Genuine heat responses must satisfy two further conditions:
    a. maximum heat response amplitude > baseline + 0.2 ratio units
    b. maximum first derivative value during the KCl response > 0.02 units per frame (threshold determined as in point 2)
5. ROIs satisfying both conditions were heat responsive neurons and their 'activation temperatures' were recorded.

6. ROIs satisfying only condition 4.b. were considered heat-insensitive neurons due to a positive response to KCl but no heat response, thus their 'activation temperature' was excluded from temperature analysis.
7. ROIs not satisfying either condition 4.a. or 4.b. were non-neuronal and were removed.

The total number of heat sensitive and insensitive neurons per animal were combined from 4 coverslips and used to calculate the percentage of heat responders per biological replicate. Amplitude and area under the curve for heat responses were calculated relative to the mean baseline value calculated from 0-60s.

Statistics

IENFD – samples were assessed for normality by Shapiro-Wilk test and means compared with a two-tailed, unpaired Student's t-test. The unit of analysis was the animal (n = 4 per genotype).

DRG populations – samples were again assessed for normality, within each subpopulation. Multiple t-tests were performed to compare wild type and knock-out values for each subpopulation, corrected for with a false discovery rate of 5% using the recommended Benjamini, Krieger and Yekutieli method in GraphPad Prism. The unit of analysis was the animal (n = 4 per genotype).

Calcium imaging – the percentage of neurons responding to heat was calculated for each animal from combined data from 4 coverslips. The means of 3 animals in each genotype were compared by two-tailed, unpaired Student's t-test. For the rest of the analysis, data from all wild type or knock-out neurons were combined to form a single sample population per genotype, where the unit of analysis was the number of neurons. The distribution of activation temperatures, response amplitude and area under the curve was non-Gaussian in each case and genotypes were compared by Mann-Whitney and Kolmogorov-Smirnov tests in GraphPad Prism.

iv. References

1. Uceyler, N. *et al.* Sensory profiles and skin innervation of patients with painful and painless neuropathies. *Pain* **159**, (2018).
2. Chen, Y. C. *et al.* Transcriptional regulator PRDM12 is essential for human pain perception. *Nat. Genet.* **47**, 803–808 (2015).
3. McDermott, L. A. *et al.* Defining the Functional Role of NaV1.7 in Human Nociception. *Neuron* **101**, 905-919.e8 (2019).
4. Indo, Y. *et al.* Mutations in the TRKA/NGF receptor gene in patients with congenital insensitivity to pain with anhidrosis. *Nat. Genet.* **13**, 485–488 (1996).
5. Houlden, H. *et al.* A novel TRK A (NTRK1) mutation associated with hereditary sensory and autonomic neuropathy type V. *Ann. Neurol.* **49**, 521–525 (2001).
6. Einarsdottir, E. *et al.* A mutation in the nerve growth factor beta gene (NGFB) causes loss of pain perception. *Hum. Mol. Genet.* **13**, 799–805 (2004).
7. Cavanaugh, D. J. *et al.* Distinct subsets of unmyelinated primary sensory fibers mediate behavioral responses to noxious thermal and mechanical stimuli. *Proc. Natl. Acad. Sci. U. S. A.* **106**, 9075–80 (2009).
8. Arcourt, A. *et al.* Touch Receptor-Derived Sensory Information Alleviates Acute Pain Signaling and Fine-Tunes Nociceptive Reflex Coordination. *Neuron* **93**, 179–193 (2016).
9. Dhandapani, R. *et al.* Control of mechanical pain hypersensitivity in mice through ligand-targeted photoablation of TrkB-positive sensory neurons. *Nat. Commun.* **9**, (2018).
10. Mishra, S. K., Tisel, S. M., Orestes, P., Bhangoo, S. K. & Hoon, M. A. TRPV1-lineage neurons are required for thermal sensation. *EMBO J.* **30**, 582–593 (2011).
11. Pogorzala, L. A., Mishra, S. K. & Hoon, M. A. The Cellular Code for Mammalian Thermosensation. *J. Neurosci.* **33**, 5533–5541 (2013).
12. McCoy, E. S. *et al.* Peptidergic CGRPα Primary Sensory Neurons Encode Heat and Itch and Tonically Suppress Sensitivity to Cold. *Neuron* **78**, 138–151 (2013).
13. Huang, T. *et al.* Identifying the pathways required for coping behaviours associated with sustained pain. *Nature* **565**, 86–90 (2019).
14. Cavanaugh, D. J. *et al.* Restriction of Transient Receptor Potential Vanilloid-1 to the Peptidergic Subset of Primary Afferent Neurons Follows Its Developmental Downregulation in Nonpeptidergic Neurons. *J. Neurosci.* **31**, 10119–10127 (2011).
15. Binshtok, A. M., Bean, B. P. & Woolf, C. J. Inhibition of nociceptors by TRPV1-mediated entry of impermeant sodium channel blockers. *Nature* **449**, 607–610 (2007).
16. Price, T. J. & Flores, C. M. Critical Evaluation of the Colocalization Between Calcitonin Gene-Related Peptide, Substance P, Transient Receptor Potential Vanilloid Subfamily Type 1 Immunoreactivities, and Isolectin B4 Binding in Primary Afferent Neurons of the Rat and Mouse. *J. Pain* **8**, 263–272 (2007).
17. Zeisel, A. *et al.* Molecular Architecture of the Mouse Nervous System. *Cell* **174**, 999-1014.e22 (2018).
18. Usoskin, D. *et al.* Unbiased classification of sensory neuron types by large-scale single-cell RNA sequencing. *Nat. Neurosci.* **18**, 145–153 (2015).
19. Zheng, Y. *et al.* Deep Sequencing of Somatosensory Neurons Reveals Molecular Determinants of Intrinsic Physiological Properties. *Neuron* **103**, 1–19 (2019).
20. Vriens, J., Nilius, B. & Voets, T. Peripheral thermosensation in mammals. *Nature Reviews Neuroscience* **15**, 573–589 (2014).
21. Vandewauw, I. *et al.* A TRP channel trio mediates acute noxious heat sensing. *Nature* **555**, 662–666 (2018).
22. Bartesaghi, L. *et al.* PRDM12 Is Required for Initiation of the Nociceptive Neuron Lineage during Neurogenesis. *Cell Rep.* **26**, 3484-3492.e4 (2019).

23. Desiderio, S. *et al.* Prdm12 Directs Nociceptive Sensory Neuron Development by Regulating the Expression of the NGF Receptor TrkA. *Cell Rep.* **26**, 3522-3536.e5 (2019).
24. Vastani, N. *et al.* Impaired nociception in the diabetic Ins2 +/Akita mouse. *Diabetes* **67**, 1650–1662 (2018).
25. Abdo, H. *et al.* Specialized cutaneous Schwann cells initiate pain sensation. *Science (80-.).* **365**, 695–699 (2019).
26. McCoy, E. S., Taylor-Blake, B. & Zylka, M. J. CGRPα-expressing sensory neurons respond to stimuli that evoke sensations of pain and itch. *PLoS One* **7**, e36355 (2012).
27. Dawes, J. M. *et al.* Immune or Genetic-Mediated Disruption of CASPR2 Causes Pain Hypersensitivity Due to Enhanced Primary Afferent Excitability. *Neuron* **97**, 806–822 (2018).
28. González, A. *et al.* Role of the excitability brake potassium current I KD in cold allodynia induced by chronic peripheral nerve injury. *J. Neurosci.* **37**, 3553–16 (2017).
29. Hao, J. *et al.* Kv1.1 channels act as mechanical brake in the senses of touch and pain. *Neuron* **77**, 899–914 (2013).
30. Sánchez-Moreno, A. *et al.* Irreversible temperature gating in trpv1 sheds light on channel activation. *Elife* **7**, (2018).
31. Katz, B. & Miledi, R. Ionic requirements of synaptic transmitter release. *Nature* **215**, 651 (1967).
32. Marvin, J. S. *et al.* An optimized fluorescent probe for visualizing glutamate neurotransmission. *Nat. Methods* **10**, 162–170 (2013).
33. Marvin, J. S. *et al.* Stability, affinity, and chromatic variants of the glutamate sensor iGluSnFR. *Nat. Methods* **15**, 936–939 (2018).
34. Tsujino, H. *et al.* Activating transcription factor 3 (ATF3) induction by axotomy in sensory and motoneurons: A novel neuronal marker of nerve injury. *Mol. Cell. Neurosci.* **15**, 170–182 (2000).
35. Dussor, G. O., Price, T. J. & Flores, C. M. Activating transcription factor 3 mRNA is upregulated in primary cultures of trigeminal ganglion neurons. *Mol. Brain Res.* **118**, 156–159 (2003).
36. Seijffers, R., Mills, C. D. & Woolf, C. J. ATF3 Increases the Intrinsic Growth State of DRG Neurons to Enhance Peripheral Nerve Regeneration. *J. Neurosci.* **27**, 7911–7920 (2007).
37. Tsantoulas, C. *et al.* Sensory Neuron Downregulation of the Kv9.1 Potassium Channel Subunit Mediates Neuropathic Pain following Nerve Injury. *J. Neurosci.* **32**, 17502–17513 (2012).
38. Emery, E. C. *et al.* In vivo characterization of distinct modality-specific subsets of somatosensory neurons using GCaMP. *Sci. Adv.* **2**, e1600990–e1600990 (2016).
39. Chisholm, K. I., Khovanov, N., Lopes, D. M., La Russa, F. & McMahon, S. B. Large scale in vivo recording of sensory neuron activity with GCaMP6. *eNeuro* **5**, e0417-17.2018 1–14 (2018).
40. Wang, F. *et al.* Sensory Afferents Use Different Coding Strategies for Heat and Cold. *Cell Rep.* **23**, 2001–2013 (2018).

Chapter V

Anatomy and physiology of the *Kcna6* ^{tm1Lex} dorsal horn

There were no major anatomical or functional differences within the peripheral nervous system between *Kcna6*^{tm1Lex} mice and their wild type littermates that I believed could fully account for the striking behavioural phenotype of these knock-out mice. The next logical site to assess somatosensory processing was the interface between primary afferent neurons and the central nervous system. I therefore began to investigate the dorsal horn of the spinal cord, a key region for integration and modulation of sensory information[1,2]. Within the dorsal horn, likely sites where loss of *Kcna6* may impinge on sensation would be: the presynaptic terminals of the primary afferent populations shown by myself, and others[3–5], to express *Kcna6* in abundance; interneurons reportedly expressing small amounts of *Kcna6*[6]; or other spinal neurons (e.g. in the LSN) or glial cell populations expressing *Kcna6* **Chapter II**.

The complex relationships between these cellular components of the dorsal horn are challenging to investigate. As in **Chapter IV**, a combined structural and functional approach was deemed most appropriate to achieve an insightful analysis of dorsal horn circuitry and physiology. Firstly, *Kcna6*^{tm1Lex} spinal cord anatomy was analysed using immunohistochemistry and subsequently transmission electron microscopy to reveal ultrastructural details within the substantia gelatinosa. Finally, wide dynamic range neurons (WDRs) were characterised by *in vivo* extracellular electrophysiological recordings. WDR excitability represented a proxy for overall dorsal horn output in response to noxious stimulation of intact peripheral sensory neuron receptive fields, which is dependent on both direct primary afferent input and indirect input via interneurons, and intrinsic WDR neuron excitability. Thus, WDR function is a good screening tool for identifying any aberrant activity in any of the aforementioned neuronal components of dorsal horn circuitry.

i. Results

a) Dorsal horn pathology in *Kcna6*^{tm1Lex} knock-out mice

In **Chapter II**, I introduced the use of β-galactosidase immunoreactivity as a method of investigating *Kcna6* expression in *Kcna6*^{tm1Lex}-carrying knock-out mice. While employing this technique on spinal cord tissue, most strikingly, the superficial laminae I-II of adult homozygous *Kcna6*^{tm1Lex} mice contained an abundance of large amorphous LacZ-positive profiles **Fig5.1(A)**. Interestingly, LacZ immunoreactivity that was not contained within these abnormal inclusions did mark some other small profiles scattered through the grey and white matter. This was a reproducible finding **Fig5.1(A, B) & Fig.3(F)** but the smaller profiles did not co-localise with neuronal (NeuN or Pax2) markers and therefore most likely represents glial *Kcna6* expression, as suspected from *in situ* hybridisation and X-GAL staining in **Chapter II**.

Several co-stains were attempted in order to identify the origin of the unusual inclusions. Counter-stains that showed no co-localisation with the abnormal LacZ$^+$ profiles included markers of neuronal cell bodies such as NeuN (pan-neuronal) **Fig5.1(A)** and PAX2 (inhibitory interneurons) **Fig5.1(B)**, as well as markers of glial populations **Fig5.1(C)** including GFAP (astrocytes) and IBA1 (microglia). There appeared to be some form of glial activation in regions neighbouring the LacZ$^+$ profiles, evidenced by GFAP staining and activated morphology of microglia **Fig5.1(C)**. The profiles were also DAPI-negative **Fig5.1(A)**, further suggesting that they were not cell bodies either of intrinsic cells of the spinal cord or an infiltrating non-neuronal cell type. The restricted location of these objects was reminiscent of small-diameter DRG fibre termination sites within the dorsal horn. In fact, the histochemical markers most faithfully co-localising with the LacZ$^+$ profiles were markers of primary afferent populations shown to express the *Kcna6*^{tm1Lex} allele at the level of the DRG in **Chapter II**. Binding of IB4 to these abnormal structures was particularly strong, but some

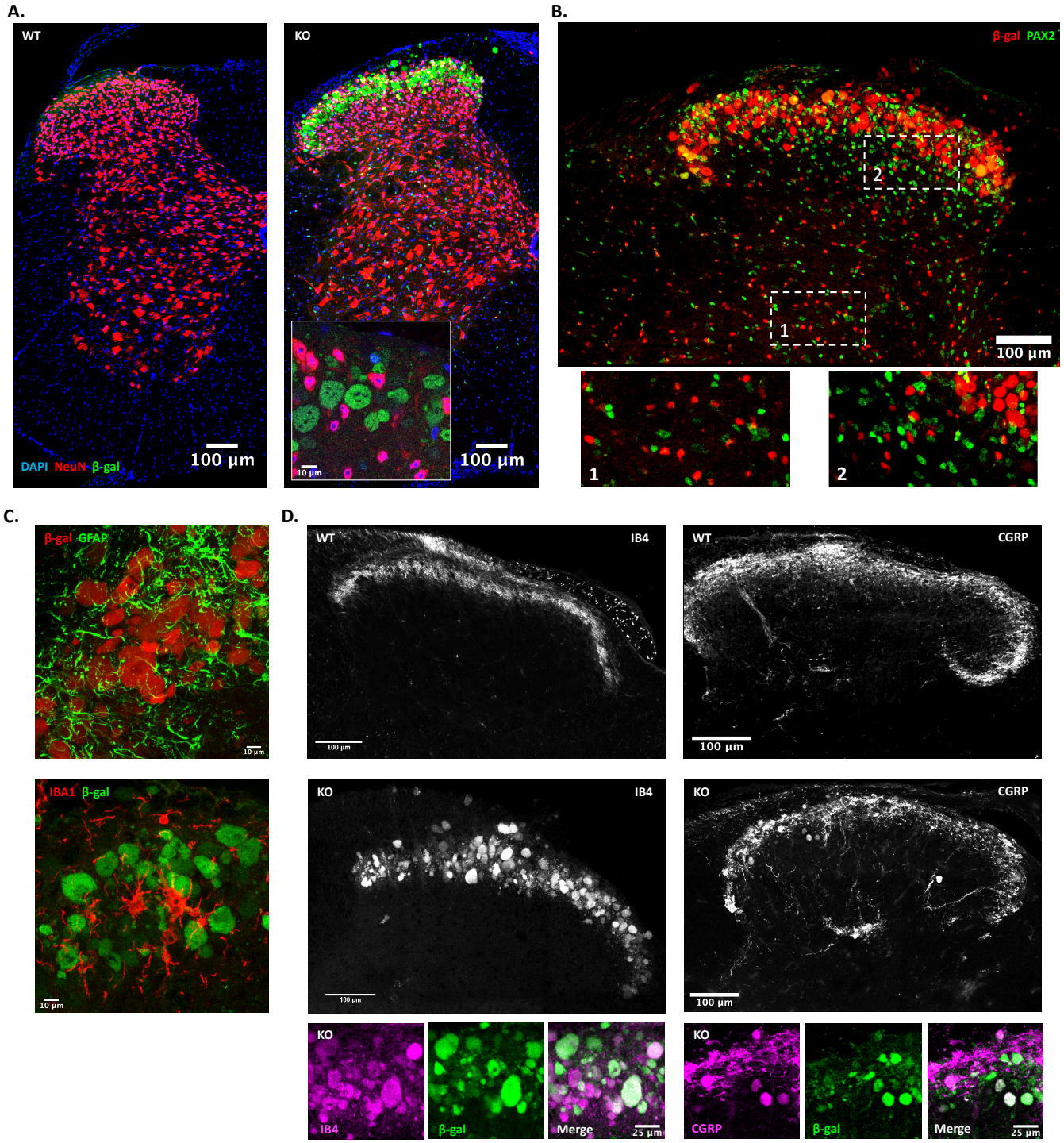

Figure 5.1 – Abnormal anatomy in the *Kcna6*^{tm1Lex} dorsal horn

(A) LacZ (β-gal) staining in *Kcna6*^{tm1Lex} homozygote spinal cord sections revealed striking abnormal, large profiles within superficial dorsal laminae. LacZ immunoreactivity also co-localised with smaller NeuN-negative, DAPI-positive profiles throughout grey and white matter. **Inset:** high power (63x objective) single z-slice image of abnormal swollen LacZ^{+} profiles in laminae I-II.

(B) Abnormal LacZ^{+} profiles do not co-localise with Pax2 (a marker of inhibitory interneurons), nor do smaller LacZ^{+} profiles in deeper grey and white matter.

(C) In superficial laminae, LacZ does not colocalise with markers of astrocytes (GFAP) or microglia (IBA1), but glial activation is often observed in close apposition to the abnormal LacZ^{+} profiles.

(D) Markers of non-peptidergic (IB4) and peptidergic (CGRP) nociceptive populations known to terminate in superficial laminae show strong co-localisation with enlarged profiles in *Kcna6*^{tm1Lex} homozygote spinal cord sections.

profiles were also CGRP-immunoreactive **Fig5.1(D)**. To confirm that the origin of these abnormalities was primary afferent nociceptors, I used a transgenic mouse expressing a bacterial artificial chromosome (BAC) encoding enhanced green fluorescent protein (EGFP) under the *Advillin* promoter, hence termed *Adv*^{EGFP}. Advillin, and therefore EGFP in this instance, is expressed in most sensory DRG neurons in mice[7] **Fig5.2(A)**. This transgenic was crossed with *Kcna6*^{tm1Lex} mice to produce a compound *Adv*$^{EGFP/+}$;*Kcna6*$^{tm1Lex/tm1Lex}$ strain. The dorsal horn of these mice resembled that of *Kcna6*^{tm1Lex} homozygotes analysed previously and, as expected, the swollen profiles also co-localised with EGFP signal **Fig.2(B)**. Despite confirmation of primary afferent pathology, there was no induction of ATF3 expression in *Kcna6* knock-out DRGs **Fig5.2(C)**.

b) Progressive morphological changes to central primary afferent projections

Six-week-old *Adv*$^{EGFP/+}$;*Kcna6*$^{tm1Lex/tm1Lex}$ mice presented with clear swollen terminals, although the profiles were much reduced in size compared to at 24 weeks **Fig5.2(B)**. Meanwhile, heterozygous *Kcna6*^{tm1Lex} mice appeared to have a degree of protection against the development of this central terminal pathology **Fig5.2(D)**, so I sought to clarify whether the condition was a progressive degenerative process. While few LacZ^{+} profiles were present in heterozygotes at 8 weeks of age **Fig5.2(D. i)**, by 18 weeks the condition had worsened **Fig5.2(D. ii)**, and at 11 months IB4^{+} terminals had deteriorated considerably **Fig5.2(D. iii)**. No evidence of degeneration was found in wild type littermates at 11 months old **Fig5.2(D. iv)**. Interestingly, compared to age-matched wild types there was no accompanying thermal hyposensitivity in these Kv1.6 heterozygotes **Fig5.2(E)** despite exhibiting a comparable state of pathology to *Kcna6*^{tm1Lex} homozygotes analysed previously.

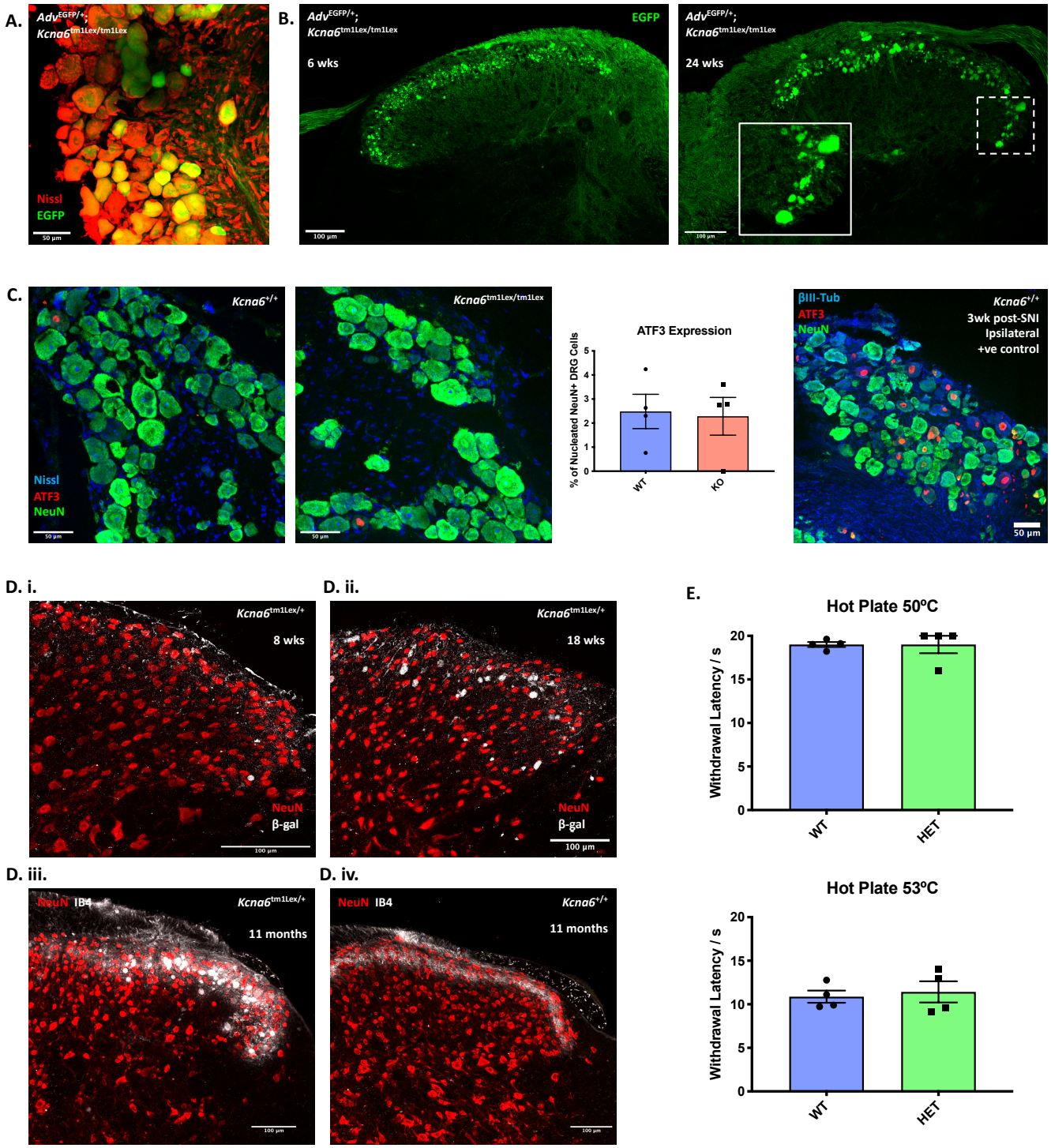

Figure 5.2 – Progressive degeneration in *Kcna6*^{tm1Lex} primary afferents

(A) *Advillin*-driven EGFP reporter mouse was crossed to the *Kcna6*^{tm1Lex} homozygotes to label primary afferents marked by Nissl staining. **(B)** EGFP co-localized with the abnormal spinal profiles, confirming that they are primary afferent in origin. The pathology was present by 6 weeks postnatally, but also appeared to worsen with age.
(C) Despite pathology of primary afferent terminals, a lack of ATF3 upregulation suggests that injury-related gene-expression changes are not initiated in *Kcna6* KO DRGs.
(D) *Kcna6*^{tm1Lex} heterozygotes had a late-onset, slowly progressing pathology over a period of 11 months, evidenced by LacZ **(D.i-ii.)** or IB4 **(D.iii**.) staining, whereas wild-types were unaffected at 11 months **(D.iv.)**
(E) At 11 months, despite developing primary afferent terminal pathology, *Kcna6* heterozygote mice did not display any behavioural hyposensitivity to noxious heat compared to wild-type age-matched controls.

c) Ultrastructural analysis of degenerating terminals

Standard confocal microscopy was useful in identifying the source of this unusual dorsal horn morphology; however, it provided little insight to the pathophysiological processes affecting nociceptive fibres. To understand how Kv1.6 knock-out might affect the structural integrity of primary afferent axons, it was necessary to view these structures at nanoscale resolution using transmission electron microscopy (TEM). After osmication, 60μm transverse sections from lumbar cord were viewed by light microscopy and the superficial profiles were stained strongly in knock-out tissue, which suggested the presence of a high concentration of lipids **Fig5.3(A)**. Closer inspection revealed densely packed, lipid-rich vesicular bodies contained within membrane-delimited profiles **Fig5.3(B)**. Both the abnormal profiles and the vesicles within were highly variable in size and electron density **Fig5.3(C)**. Some profiles were ensheathed by myelin, within or in close proximity to Lissauer's tract **Fig5.3(D)**. Others made clear synaptic contacts with adjacent dendrites containing post synaptic densities, and often appeared to send out multiple cytoplasmic projections from their swollen region – tentatively designated as inter-varicose axons **Fig5.3(E)**.

Homer$^+$ puncta, post-synaptic markers of excitatory synapses, were also found via immunohistochemistry to neighbour LacZ$^+$ profiles, which generally lacked the presynaptic marker synaptophysin **Fig5.3(F)**. While some normal synaptic boutons (of unknown origin) could be found in the superficial laminae **Fig5.3(G)**, there was a notable reduction of normal type I (C_1) and type II (C_2) glomerular central boutons[8], originating from IB4$^+$ neurons[2] and Aδ-[2] or C-LTMRs[9], respectively. The few examples of central glomerular boutons appeared highly irregular in form and content. Type I central boutons (C_1) are described by *Ribeiro-da-Silva & Coimbra (1982)* as having "a dark small central terminal of indented contour with closely packed spherical vesicles of variable diameter and few mitochondria"[10], but the example in **Fig5.3(H)** lacks vesicles and is

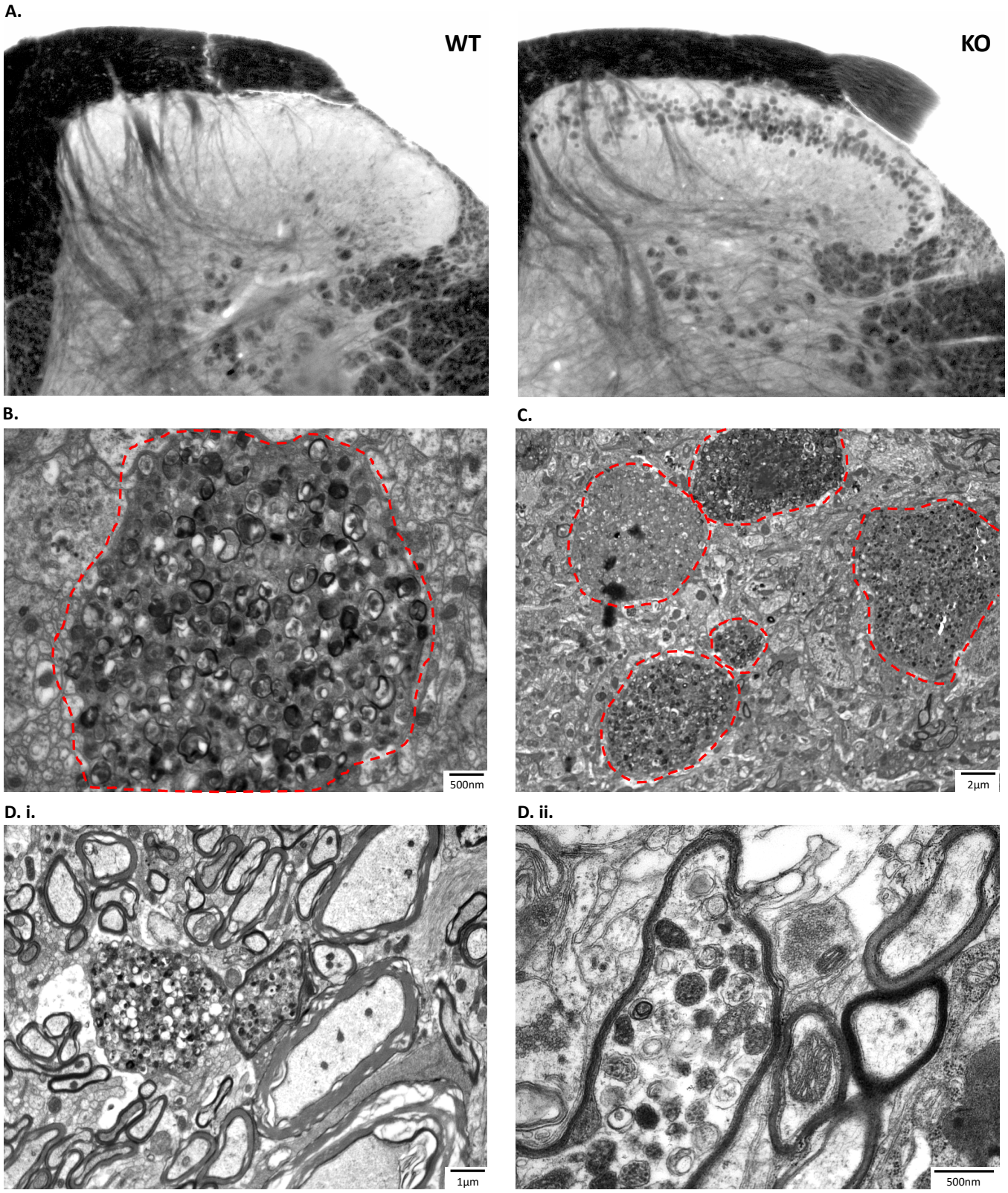

Figure 5.3 – Ultrastructural analysis of degenerative *Kcna6*^{tm1Lex} primary afferents

(A) 60µm thick osmicated sections showing lipid-rich profiles in *Kcna6*^{tm1Lex} dorsal horn. **(B, C)** Swollen terminals vary in size and electron density, and contain many small vesicular components. **(D)** Some vesicle-containing profiles originate from myelinated afferents in Lissauer's tract.

Continues overleaf…

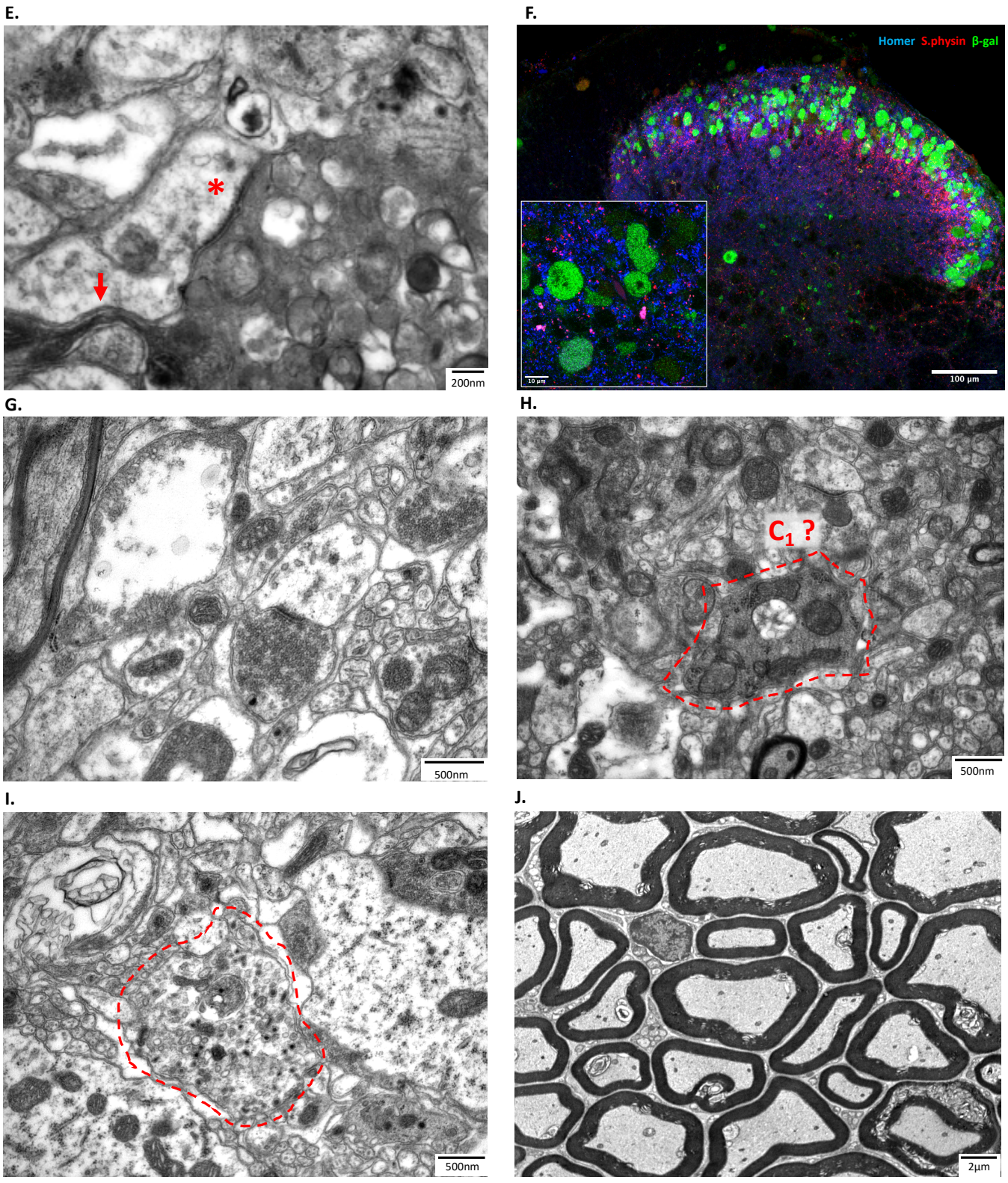

Figure 5.3 – Ultrastructural analysis of degenerative *Kcna6*^{tm1Lex} primary afferents

(E) Numerous profiles were observed adjacent to postsynaptic dendrites (asterisk) and sprouting supposed intervaricose axons (arrow), but lacked presynaptic neurotransmitter vesicles. **(F)** Immunostaining for Homer1 and synaptophysin similarly revealed frequent adjacent postsynaptic densities but absent presynaptic markers. **(G)** Some normal synapses were observed. **(H)** Presumed type 1 glomerular central boutons (C_1) originating from IB4$^+$ neurons appeared abnormal, as did peptidergic boutons containing dense-cored vesicles **(I)**. **(J)** Axons in the dorsal root were normal.

very abnormal. Some peptidergic axonal boutons (containing dense-cored vesicles) were observed, although similarly these did not look normal and potentially included vesicular pathology **Fig5.3(I)**. The dorsal root was totally unaffected **Fig5.3(J)**, so the accumulation of membranous, vesicular bodies specifically occurs once afferents have penetrated the cord.

d) *In vivo* dorsal horn physiology

Anatomical analysis of the *Kcna6*^{tm1Lex} dorsal horn had thus revealed drastic pathological degeneration of nociceptive primary afferent axon terminals. There was a stark absence or obscuration of normal presynaptic neurotransmitter-loaded vesicles in the affected boutons, so I reasoned that this was highly likely to underlie behavioural deficits in Kv1.6 knock-outs via impaired neurotransmission from first- to second-order afferent neurons. I investigated this using an *in vivo* electrophysiology preparation whereby extracellular recordings can be made from single wide dynamic range neurons (WDRs) from deep dorsal horn laminae in response to hind paw stimulation. As well as pathology in superficial laminae, there were some examples of damage to deeper terminals **Fig5.1(D)**, **Fig5.2(B)**, **Fig5.3(F)**. HRP-filled WDRs also reveal extensive dendritic processes contacting superficial laminae[11]; thus, their activity may still reflect changes to primary afferent terminals and studying this population is justified.

Wild type, *Kcna6*$^{tm1Lex/+}$ and *Kcna6*$^{tm1Lex/tm1Lex}$ WDR firing rates were characterised after 'natural' stimulation by brush, calibrated Von Frey filaments, evaporative cooling and graded temperatures of water. In all genotypes, the graded intensity of mechanical and thermal stimuli was coded in the WDR firing rate, as is expected of these neurons **Fig5.4(A, B)**. However, at the noxious end of the mechanical and thermal repertoire there were significant deficits in spike generation in both *Kcna6*^{tm1Lex} hetero- and homozygote mice following 15g Von Frey (WT 665.32 ± 81.69 spikes, HET

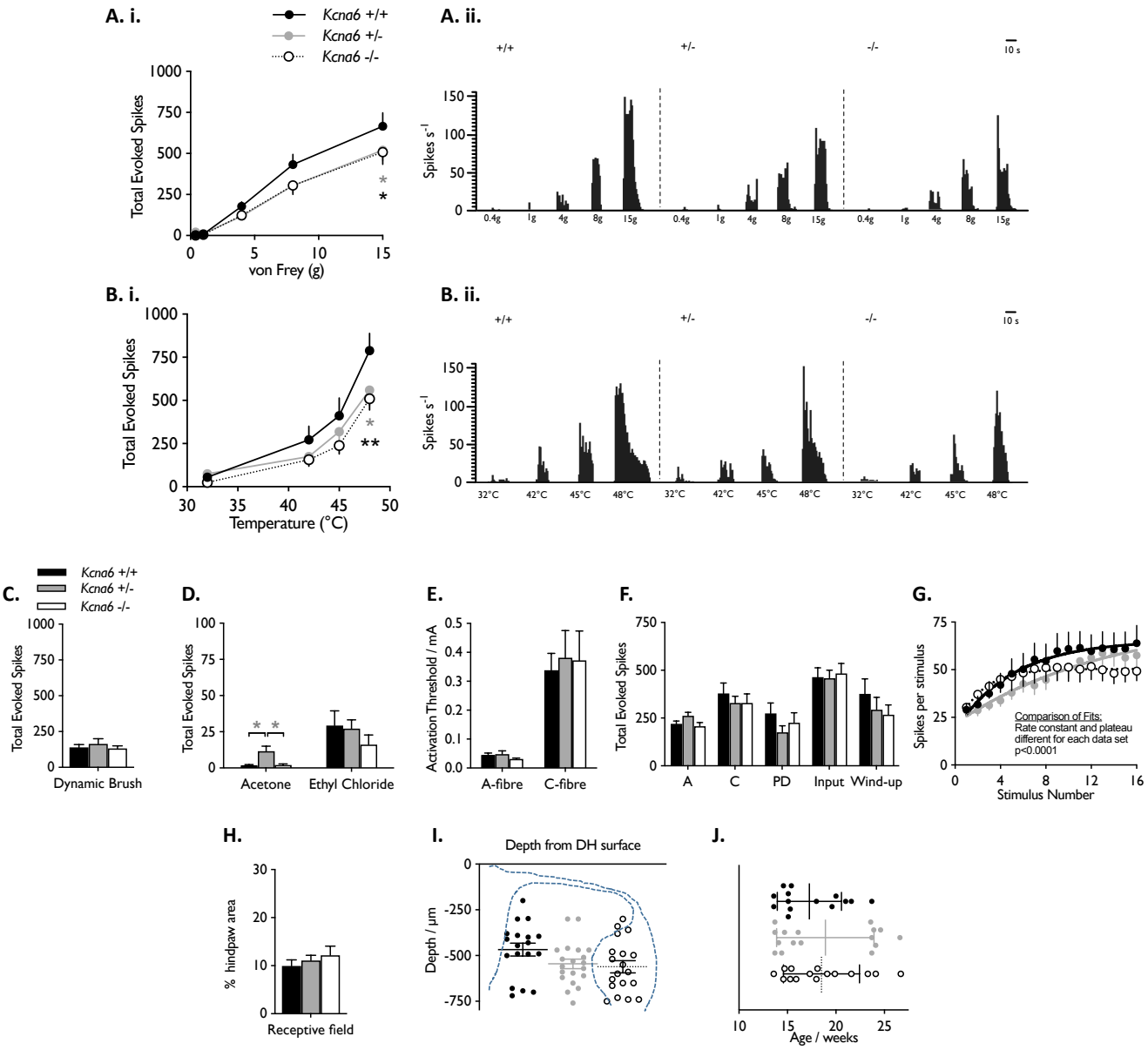

Figure 5.4 – Electrophysiological characterisation of *Kcna6*^{tm1Lex} WDR neurons

(A, B) Graded firing responses in wide dynamic range (WDR) neurons, evoked by mechanical (Von Frey) or hot water stimuli of increasing intensity applied to the hind paw.

(A.ii. & B.ii) Representative traces from single neurons. ***/**** = p<0.05/0.01 vs WT (Two-Way RM ANOVA with Dunnett's post hoc comparison test.)

(C, D) Responses evoked by dynamic application of a painter's brush, or droplets of evaporative cooling agents. ***** = p<0.05 (Ordinary One-Way ANOVA, Tukey's post hoc test)

(E) A- and C-fibre activation thresholds as determined by WDR response latency to electrical stimulation of the hind paw receptive field.

(F) Total spikes attributed to A- or C-fibres, or post-discharge (PD) as determined by WDR response latency, and attributed to input vs wind-up (see methods).

(G) Firing responses to a train of 16 identical electrical stimuli at a frequency 0.5Hz.

(H-J) Characterisation of receptive field size **(H)**, and WDR depth from the dorsal spinal cord surface **(I)**, and a graphic depicting the age of mice from which WDRs were sampled.

Group data presented as mean ± SEM in all figures except **(J)** which is mean ± SD.

520.86 ± 65.08 spikes*****, KO 508.58 ± 75.05 spikes*****, *****p<0.05 vs WT) or 48ºC heat stimulation (WT 788.76 ± 100.36 spikes, HET 560.48 ± 89.63 spikes*****, KO 510.00 ± 65.46 spikes******, ***/****p<0.05/0.01 vs WT) **Fig5.4(A, B)**. Responses to non-noxious mechanical brush stimulation did not differ between genotypes **Fig5.4(C)**. Interestingly, acetone evoked very few spikes in wild type and knock-out mice, but heterozygotes had significantly stronger responses (WT 1.71 ± 0.62 spikes, HET 11.57 ± 3.58 spikes*****, KO 2.03 ± 0.72 spikes, *****p<0.05 vs WT/KO). After the more noxious cooling assay with ethyl chloride, responses were elevated in all genotypes but did not differ from one another significantly **Fig5.4(D)**.

Electrical activation thresholds for A- and C-fibre-evoked spikes were not affected in hetero- or homozygous *Kcna6*^{tm1Lex} animals **Fig5.4(E)**, nor were there statistical differences in the total evoked spikes by either fibre class after a train of 16 electrical stimuli to the receptive field on the paw **Fig5.4(F)**. The number of spikes generated after the C-fibre latency window (termed 'post-discharge') was also not affected. While the total number of spikes attributed to 'wind-up' of WDRs (that is, the progressive increase in responsivity with each stimulus) was not different between genotypes **Fig5.4(F)**, there were some considerable differences in the kinetics of wind-up between wild types and *Kcna6*^{tm1Lex} mutants. Specifically, WDR responses in wild types followed a typical hyperbolic pattern, gradually reaching a maximal discharge rate towards the end of the 16-stimulus paradigm **Fig5.4(G)**. Knock-outs had a similar initial rate of wind-up but reached a lower plateau, while wind-up in heterozygotes formed a much more linear relationship with increasing stimuli.

I also quantified more general characteristics of the WDRs, including the receptive field size relative to hind paw area, and depth from the dorsal surface of the spinal cord. Receptive fields were similar in size across all genotypes, as was the range of sampled neuron depths **Fig5.4(H, I)**.

ii. Conclusions

a) Anatomically plausible pathology in the dorsal horn may account for behavioural hyposensitivity

The Kv1.6-null mouse strain, *Kcna6*^{tm1Lex}, presented with a striking structural abnormality within the spinal cord restricted to central, presynaptic axons and boutons of primary afferent neurons. This was visible at the light microscopy level – via osmication which revealed concentrated lipids, and via fluorescent genetic and histochemical labelling of nociceptive primary afferent populations. The fact that *Kcna6* (and the *Kcna6*^{tm1Lex} allele) were previously shown to be expressed in IB4^{+}, CGRP^{+} and TH^{+} fibres **Chapter II**, and the presence of LacZ/β-galactosidase in the damaged terminals, give confidence to the argument that this was directly related to the manipulation of the *Kcna6* locus and not some other interfering factor.

Using TEM, it was possible to analyse these profiles at a sub-micrometre scale and this unveiled some interesting properties of the degenerating terminals. Many densely-packed, lipid-delimited vesicular structures had accumulated within the swollen primary afferents. These were initially considered to be lipid droplets, but after further consideration I suggest that these structures are components of the autophagic pathway due to the frequent presence of electron dense vesicular contents, often limited by double-membranes[12–15]. There were possibly some examples of membrane whorl development, the formation of which has been described in *C. elegans* models of neurodegeneration resulting from gain-of-function mutations in epithelial sodium channel (ENaC) orthologs[16] – in which neuron swelling is also a feature. Electrochemical gradients across the neuronal plasma membrane for Na^{+} and K^{+} are reciprocal, so perhaps loss of Kv1.6 function has similar effects on osmotic balance as gain of function ENaC mutations. If this is the case, it is worth noting that expression of Kv1.6[17] and other Kv1[18] channels has been identified at presynaptic sites of CNS neurons, which may explain the specific localisation of the pathology observed here

to these central presynaptic regions. As Kv1 channels are also retained in the ER in a subunit-specific manner[19,20], this could be relevant for effects on endo/lysosome formation.

b) A physiological correlate in deep horn laminae of behavioural hyposensitivity in *Kcna6*^{tm1Lex} mice

The described abnormality was associated with loss-of-function in downstream activity of wide dynamic range dorsal horn neurons. These results must be interpreted with care. In the very simplest model, two components contribute to the responsivity of a WDR neuron – input from peripheral presynaptic neurons, whether direct (monosynaptic) or indirect (polysynaptic), and the intrinsic excitability of the WDR neuron itself. For Kv1.6 knock-out to affect the *intrinsic* electrical properties of WDRs, the gene would have to be expressed in this population. WDRs have no specific histochemical marker, but expression studies in **Chapter II** and β-galactosidase staining in **Fig5.1(A)** of this chapter showed infrequent co-localisation of *Kcna6* mRNA or β-gal reporter product with neuronal markers throughout the grey matter of the spinal cord. Therefore, with caution, one may assume that *Kcna6* is not expressed in WDRs and the loss-of-function effect of its knock-out on their response rate is a consequence of altered net input derived from primary afferents.

From immuno-staining and a major loss of type I glomerular central boutons, revealed by electron microscopy, it was apparent that IB4$^+$ fibres were morphologically the most gravely affected. This is intriguing, as there was weaker expression of *Kcna6* in IB4-binding neurons compared to peptidergic neurons **Chapter II** – although, there is admittedly no reason why the relative somal mRNA expression should *necessarily* correlate with dependence on this gene for synaptic integrity in different fibre types. However, it is also intriguing due to the evidence for the involvement of non-peptidergic fibres in mechanical, but not thermal, sensation[21] given the behavioural observations in these mice. In fact, it might be considered surprising that mechanical sensitivity

thresholds were not at all affected in the *Kcna6*^{tm1Lex} mice either in the naïve state or post-SNI **Chapter III**.

There was, however, obvious impairment of *both* mechanical and thermal processing in WDR neurons **Fig5.4(A, B)**. Whilst one cannot conclusively state that this presynaptic degenerative phenomenon *causes* the behavioural hyposensitivity in mice carrying the *Kcna6*^{tm1Lex} allele, there is evidence from paired rodent WDR recording and human psychophysical studies that WDR firing rates are positively correlated with thermal pain intensity[22]. As the reduced noxious thermal WDR response manifested behaviourally in *Kcna6*^{tm1Lex} mice, this also lends credence to the previous published work relating WDR responses to perceived pain intensity. Secondly, this might indicate that measurement of 50% mechanical withdrawal thresholds by Von Frey hairs is not a noxious assay in naïve mice. WDR firing rates at naïve 50% withdrawal forces (<1.5g, **Chapter III**) are low, and responses only differed between genotypes at more intense mechanical pressure. Perhaps behavioural differences would have been observed with a more noxious mechanical assay.

Thermal sensory deficits would be expected to arise from defective peptidergic fibre activity, which express TRP channels[4,5] capable of transducing temperature. The gross and ultrastructural effect on CGRP$^+$ fibres was more subtle, but nonetheless there were swollen profiles immunoreactive with CGRP antibodies and the lamina I neuropil appeared less densely innervated by these fibres than in wild types **Fig5.1(D)**. One cannot exclude the possibility that loss of synaptic function may either precede pathological vesicular accumulation or be entirely independent of this process. Additionally, it is important to appreciate that thermal nocifensive responses are not completely absent, but only delayed, in *Kcna6* knock-outs, so the relatively less severe effect on CGRP$^+$ fibres may still be sufficient to delay behavioural reflexes. Although thermo- and mechano-responsive fibres have historically been siloed into peptidergic and non-peptidergic categories, respectively, there is significant species-dependent overlap of IB4$^+$ and CGRP$^+$ neurons (rat >> mouse)[23], and

some 'non-peptidergic' sensory neuron subpopulations have been shown to express *Calca* (CGRP-α), and other peptides and heat-sensitive TRP channel genes such as *Trpv1*[4,5] in mice. Both CGRP$^+$ and IB4$^+$ fibre pathology may therefore contribute to thermal sensory loss-of-function.

I also presented evidence for *Kcna6* expression in TH-positive C-low threshold mechanoreceptors (C-LTMRs) in **Chapter II**. These neurons are known to be cold- as well as mechanosensitive, but recent sequencing data also demonstrated high expression of *Trpv1*[5] in this population. It is possible that these fibres, terminating in lamina II-i and lamina III directly ventral to the IB4$^+$ neuropil[24], undergo a similar degeneration, but the tyrosine hydroxylase marker is not well expressed in terminal projections so it was not possible to confirm this. Central projections of C-LTMRs can be visualised using vesicular glutamate transporter 3 (VGLUT3) immunohistochemistry[9,25], and these fibres have also been visualised using TH^{2ACreER}-dependent expression of tdTomato[24], but a cross between this mouse and *Kcna6*^{tm1Lex} was not performed in this study. Although Tafa4-positive C-LTMRs have been demonstrated forming type I glomerular structures[26], VGLUT3 immunoperoxidase labelling has been identified within type II glomerular central boutons in lamina II-i in the mouse[9], suggesting that some of these organisationally distinct structures[8,10] are formed by C-LTMR terminals within ventral lamina II. These glomeruli differ from type I central boutons in that they have "an electron-lucent and large C terminal of regular contour with less packed synaptic vesicles of more uniform diameter, more mitochondria, and sometimes neurofilaments"[10], but were scarcely found in the *Kcna6*^{tm1Lex} dorsal horn. Despite the relatively poorly defined cellular origins of glomerular central boutons, the scarcity of normal type I and II central glomeruli thus provides some evidence that C-LTMRs may be affected in the *Kcna6*^{tm1Lex} knock-outs.

b) Molecular markers of axonal injury absent in affected DRGs

Peripheral nerve or dorsal root injury results in upregulation of activating transcription factor 3[27,28] (ATF3) – which induces transcriptional changes promoting peripheral nerve repair and regeneration[28–30]. I postulated that, if primary afferent terminals were undergoing a degenerative process, ATF3 may be upregulated in the DRG of *Kcna6*^{tm1Lex} mice. Somewhat surprisingly, compared to positive control (post-SNI) or naïve wild-type DRGs there was no overt injury response in the form of ATF3 expression, despite evidence of central pathology to primary afferent terminals **Fig5.2(C)**.

c) Concluding remarks

The investigations presented in this chapter highlight the limitations of studying the peripheral nervous system in isolation – especially when using global gene knock-out strategies – and the importance of answering biological questions using methodology that is as close to *in vivo* conditions as possible. If the previous chapter's results were to stand alone, one could claim that primary afferents from Kv1.6 knock-outs were structurally intact, innervated appropriate peripheral targets, and also functionally responsive to thermal stimuli. However, the further experiments outlined in this chapter show a striking anatomical abnormality affecting the central terminals of select populations of primary afferents, with clear functional consequences in term of their ability to faithfully transmit sensory information to the central nervous system. While they of course provide insight to intrinsic excitability of sensory neurons, even *in vivo* DRG imaging assays (the merits of which have been discussed in **Chapter IV**) are neglectful of the fact that the important role of the DRG neuron does not end at the cell soma. Thus, 'negative' results at this level ought to be considered with caution, as loss- or gain-of-function phenotypes may manifest mechanistically anywhere from distal to proximal terminals.

iii. Methods

Animals

Kcna6^{tm1Lex} mice were as described in previous chapters, although at this stage the <tm1Lex> allele had been outcrossed for 5 generations to C57BL/6J mice, producing an incipient congenic B6.129S strain with >97% C57BL/6J purity. These mice were phenotypically similar to the original mice purchased on a mixed background in previous chapters.

To label primary afferent terminals within the spinal cord, this strain was interbred with a mouse strain expressing a BAC transgene encoding EGFP under the Advillin promoter – Tg(Avil-EGFP)QD84Gsat/Mmucd (MMRRC stock number 034769-UCD).

Male and female mice were used, generally >16wks old unless specified in figures.

Immunohistochemistry

Performed as in previous chapters.

Behavioural analysis

Hot plate testing was performed as in Chapter II, on 4 wild type and 4 *Kcna6*^{tm1Lex} heterozygous mice (2 male and 2 female mice from each genotype) at 50 weeks old. 3 baselines values were recorded per animal and a mean taken from these values.

Transmission electron microscopy

Adult mice received an intraperitoneal overdose of pentobarbital and were then transcardially perfused with 0.9% saline followed by a 1% PFA, 1% glutaraldehyde fixative in 0.1M phosphate buffer (PB). Spinal cords were then removed and post-fixed in the same solution for 24 hours and transferred to 0.1M PB before sectioning. From this stage, further tissue processing and imaging was kindly performed by Professor Andrew Todd and members of his laboratory at the University

of Glasgow. Qualitative interpretation regarding the appearance of identifiable glomerular structures was undertaken in consultation with Prof. Todd. 60μm sections were prepared using a vibrating-blate microtome, post-fixed with osmium tetroxide OsO_4, dehydrated and flat-embedded in epoxy resin. At this stage, some images were acquired using light microscopy. Subsequently, ultrathin sections were cut using a Diatome diamond knife and Leica Ultracut S ultramicrotome. Images were acquired at 120kV on a Philips CM100 transmission electron microscope with a Gatan OneView CMOS camera.

In vivo dorsal horn recordings

In vivo electrophysiology was performed by myself and Dr Ryan Patel in Professor Anthony Dickenson's laboratory at University College London, as previously described[31]. Both male and female wildtype, heterozygous and knockout mice were used; mean ages of animals ± standard deviation were 17.3±3.3 (WT), 14.7±1.1 (HET), and 17.1±2.5 (KO) weeks. Mice were initially anaesthetised with 3.5% v/v isoflurane delivered in 3:2 ratio of nitrous oxide and oxygen. Once areflexic, mice were secured in a stereotaxic frame and subsequently maintained on 1.5% v/v isoflurane for the remainder of the experiment (approximately 4 hours in duration). Core body temperature was maintained with the use of a homeothermic blanket and respiratory rate was visually monitored throughout. A laminectomy was performed to expose the L3-L5 segments of the spinal cord; mineral oil was then applied to prevent dehydration. Extracellular recordings were made from deep dorsal horn wide dynamic range (WDR) lamina V/VI neurons with receptive fields on the glabrous skin of the toes using 0.127 mm 2 MΩ parylene-coated tungsten electrodes (A-M Systems, Sequim, WA, USA). Searching involved light tapping of the hind paw whilst manually moving the electrode. All recordings were made at depths delineating the deep dorsal horn laminae[32], and were classified as wide dynamic range (WDR) on the basis of neuronal sensitivity to dynamic brushing (i.e. gentle stroking with a squirrel-hair brush), and noxious punctate mechanical (15g) and heat (48°C) stimulation of the receptive field.

The receptive field was then stimulated using a wider range of natural stimuli (brush, von Frey filaments – 0.4, 1, 4, 8 and 15g, and heat – 32, 42, 45 and 48°C) applied over a period of 10s per stimulus and the evoked response quantified. The heat stimulus was applied with a constant water jet onto the centre of the receptive field. Acetone and ethyl chloride (50µl) were applied to the receptive field, described previously as an evaporative innocuous cooling and noxious cooling stimulus respectively[33]. Evoked responses to room temperature water (25°C) were subtracted from acetone and ethyl chloride evoked responses to control for any concomitant mechanical stimulation during application. Natural stimuli were applied starting with the lowest intensity stimulus with approximately 40s between stimuli in the following order: brush, von Frey, cold, heat, electrical. Receptive fields were determined using a 15g von Frey. An area was considered part of the receptive field if a response of >30 action potentials over 5s was obtained. A rest period of 30s between applications was used to avoid sensitisation. Receptive field sizes are expressed as a percentage area of a standardised paw measured using ImageJ (NIH, Bethesda, MD). Electrical stimulation of WDR neurons was delivered transcutaneously via needles inserted into the receptive field. A train of 16 electrical stimuli (2ms pulses, 0.5Hz) was applied at three times the threshold current for C-fibre activation. Responses evoked by A- (0–50ms) and C-fibres (50–250ms) were separated and quantified on the basis of latency. Neuronal responses occurring after the C-fibre latency band were classed as post-discharge (PD). The input (I) and the wind-up (WU) were calculated as:

$$Input = action\ potentials\ evoked\ by\ first\ pulse \times total\ number\ of pulses$$

$$Wind\text{-}up = total\ action\ potentials\ after\ 16\ train\ stimulus - Input$$

The signal was amplified (x6000), bandpass filtered (low/high frequency cut-off 0.5/2kHz) and digitised at rate of 20kHz. Data were captured and analysed by a Cambridge Electronic Design

1401 interface coupled to a computer with Spike2 software (CED, Cambridge, UK) with post-stimulus time histogram and rate functions. In some cases where a single unit recording could not be obtained, spike sorting was performed *post hoc* with Spike2 using fast Fourier transform followed by 3-dimensional principal component analysis of waveform features for multi-unit discrimination (electrical stimulation was not performed for these neurons). One to three neurons were characterised per mouse. In total, 19 neurons were characterised from 14 wildtype mice, 21 neurons from 16 heterozygous mice, and 19 neurons from 15 knockout mice. Of these neurons, 15 per genotype were successfully stimulated transcutaneously so that electrical properties could be interrogated. *In vivo* electrophysiological procedures were non-recovery; at the end of experiments mice were terminally anesthetised with isoflurane.

Statistics

ATF3 expression – At least 4 randomly chosen fields of view were analysed from naïve DRGs dissected from 4 WT and 4 KO animals. The unit of analysis was the animal, normality was assessed with a Shapiro-Wilk test and group means were compared using an unpaired, two-tailed Student's t-test.

Hot plate behaviour – 3 baseline values were averaged per animal to produce a mean withdrawal latency. The distributions were assessed for normality with the Shapiro-Wilk test and passed except for heterozygotes at 50ºC which were affected by the maximal 20s cut-off and otherwise assumed to be sampled from a normal distribution. Means were compared via unpaired, two-tailed Student's t-test in GraphPad Prism software but were not significantly different.

Electrophysiology – in all experiments, the neuron was considered to be the experimental unit of replication. Mechanical and Heat responses were analysed by Two-Way Repeated Measures ANOVA with Dunnett's post-hoc test to compare to wild type results. Brush, cold, fibre threshold, electrical results, and receptive field were assessed for normality using the Shapiro-Wilk test. If they passed, each characteristic was assessed by One-Way ANOVA with Dunnett's or Tukey's post-

hoc test to make multiple comparisons versus wild types or between all genotypes, respectively. For characteristics which failed the normality test, a Kruskal-Wallis test was performed instead with Dunn's post-hoc multiple comparisons test. Multiplicity-adjusted p-values are reported in each case. Kinetics of wind-up were assessed by non-linear regression, fitting a one-phase association curve to each data set and comparing the rate constant and plateau between each genotype. All tests were performed in GraphPad Prism.

iv. References

1. Todd, A. J. Neuronal circuitry for pain processing in the dorsal horn. *Nat. Rev. Neurosci.* **11**, 823–836 (2010).
2. West, S. J., Bannister, K., Dickenson, A. H. & Bennett, D. L. Circuitry and plasticity of the dorsal horn - Toward a better understanding of neuropathic pain. *Neuroscience* **300**, 254–275 (2015).
3. Usoskin, D. *et al.* Unbiased classification of sensory neuron types by large-scale single-cell RNA sequencing. *Nat. Neurosci.* **18**, 145–153 (2015).
4. Zeisel, A. *et al.* Molecular Architecture of the Mouse Nervous System. *Cell* **174**, 999-1014.e22 (2018).
5. Zheng, Y. *et al.* Deep Sequencing of Somatosensory Neurons Reveals Molecular Determinants of Intrinsic Physiological Properties. *Neuron* **103**, 1–19 (2019).
6. Häring, M. *et al.* Neuronal atlas of the dorsal horn defines its architecture and links sensory input to transcriptional cell types. *Nat. Neurosci.* **21**, 869–880 (2018).
7. Hunter, D. V. *et al.* Advillin Is Expressed in All Adult Neural Crest-Derived Neurons. *eNeuro* **5**, ENEURO.0077-18.2018 (2018).
8. Gutierrez-Mecinas, M. *et al.* Immunostaining for Homer reveals the majority of excitatory synapses in laminae I-III of the mouse spinal dorsal horn. *Neuroscience* **329**, 171–181 (2016).
9. Larsson, M. & Broman, J. Synaptic Organization of VGLUT3 Expressing Low-Threshold Mechanosensitive C Fiber Terminals in the Rodent Spinal Cord. *eNeuro* **6**, ENEURO.0007-19.2019 (2019).
10. Ribeiro-Da-Silva, A. & Coimbra, A. Two types of synaptic glomeruli and their distribution in laminae I–III of the rat spinal cord. *J. Comp. Neurol.* **209**, 176–186 (1982).
11. Woolf, C. J. & King, A. E. Physiology and morphology of multireceptive neurons with C-afferent fiber inputs in the deep dorsal horn of the rat lumbar spinal cord. *J. Neurophysiol.* **58**, 460–479 (1987).
12. Eskelinen, E. L. To be or not to be? Examples of incorrect identification of autophagic compartments in conventional transmission electron microscopy of mammalian cells. *Autophagy* **4**, 257–260 (2008).
13. Eskelinen, E. L. & Kovács, A. L. Double membranes vs. lipid bilayers, and their significance for correct identification of macroautophagic structures. *Autophagy* **7**, 931–932 (2011).
14. Eskelinen, E. L., Reggiori, F., Baba, M., Kovács, A. L. & Seglen, P. O. Seeing is believing: The impact of electron microscopy on autophagy research. *Autophagy* **7**, 935–956 (2011).
15. Klionsky, D. J., Eskelinen, E. L. & Deretic, V. Autophagosomes, phagosomes, autolysosomes, phagolysosomes, autophagolysosomes... Wait, I'm confused. *Autophagy* **10**, 549–551 (2014).
16. Hall, D. H. *et al.* Neuropathology of degenerative cell death in Caenorhabditis elegans. *J. Neurosci.* **17**, 1033–1045 (1997).
17. Fulton, S. *et al.* Contribution of Kv1.2 voltage-gated potassium channel to D2 autoreceptor regulation of axonal dopamine overflow. *J. Biol. Chem.* **286**, 9360–72 (2011).
18. Wang, H., Kunkel, D. D., Schwartzkroin, P. A. & Tempel, B. L. Localization of Kv1.1 and Kv1.2, two K channel proteins, to synaptic terminals, somata, and dendrites in the mouse brain. *J. Neurosci.* **14**, 4588–99 (1994).
19. Manganas, L. N. & Trimmer, J. S. Subunit composition determines Kv1 potassium channel surface expression. *J. Biol. Chem.* **275**, 29685–29693 (2000).
20. Misonou, H. & Trimmer, J. S. Determinants of Voltage-Gated Potassium Channel Surface Expression and Localization in Mammalian Neurons. *Crit. Rev. Biochem. Mol. Biol.* **393**,

125–145 (2004).
21. Cavanaugh, D. J. *et al.* Distinct subsets of unmyelinated primary sensory fibers mediate behavioral responses to noxious thermal and mechanical stimuli. *Proc. Natl. Acad. Sci. U. S. A.* **106**, 9075–80 (2009).
22. Sikandar, S., Ronga, I., Iannetti, G. D. & Dickenson, A. H. Neural coding of nociceptive stimuli - From rat spinal neurones to human perception. *Pain* **154**, 1263–1273 (2013).
23. Price, T. J. & Flores, C. M. Critical Evaluation of the Colocalization Between Calcitonin Gene-Related Peptide, Substance P, Transient Receptor Potential Vanilloid Subfamily Type 1 Immunoreactivities, and Isolectin B4 Binding in Primary Afferent Neurons of the Rat and Mouse. *J. Pain* **8**, 263–272 (2007).
24. Abraira, V. E. *et al.* The Cellular and Synaptic Architecture of the Mechanosensory Dorsal Horn. *Cell* **168**, 295-310.e19 (2016).
25. Seal, R. P. *et al.* Injury-induced mechanical hypersensitivity requires C-low threshold mechanoreceptors. *Nature* **462**, 651–655 (2009).
26. Kambrun, C. *et al.* TAFA4 Reverses Mechanical Allodynia through Activation of GABAergic Transmission and Microglial Process Retraction. *CellReports* **22**, 2886–2897 (2018).
27. Tsujino, H. *et al.* Activating transcription factor 3 (ATF3) induction by axotomy in sensory and motoneurons: A novel neuronal marker of nerve injury. *Mol. Cell. Neurosci.* **15**, 170–182 (2000).
28. Lindå, H., Sköld, M. K. & Ochsmann, T. Activating transcription factor 3, a useful marker for regenerative response after nerve root injury. *Front. Neurol.* **MAY**, 1–6 (2011).
29. Pearson, A. G. *et al.* ATF3 enhances c-Jun-mediated neurite sprouting. *Mol. Brain Res.* **120**, 38–45 (2003).
30. Seijffers, R., Mills, C. D. & Woolf, C. J. ATF3 Increases the Intrinsic Growth State of DRG Neurons to Enhance Peripheral Nerve Regeneration. *J. Neurosci.* **27**, 7911–7920 (2007).
31. Dawes, J. M. *et al.* Immune or Genetic-Mediated Disruption of CASPR2 Causes Pain Hypersensitivity Due to Enhanced Primary Afferent Excitability. *Neuron* **97**, 806–822 (2018).
32. Watson, C., Paxinos, G., Kayalioglu, G. & Heise, C. Atlas of the Rat Spinal Cord. in *The Spinal Cord* 238–306 (Academic Press, 2009). doi:10.1016/B978-0-12-374247-6.50019-5
33. Leith, J. L., Koutsikou, S., Lumb, B. M. & Apps, R. Spinal Processing of Noxious and Innocuous Cold Information: Differential Modulation by the Periaqueductal Gray. *J. Neurosci.* **30**, 4933–4942 (2010).

Chapter VI

Contributions of *Kcna6* loss vs. *lacZ* expression to the *Kcna6* ^{tm1Lex} phenotype

Degenerative lipid accumulation in central nociceptor terminals and thermal hyposensitivity are wholly unexpected findings in a Kv1 channel knock-out model. Although *lacZ*/*neo* reporter mouse strains such as *Kcna6*^{tm1Lex} are commonplace and the function of the β-galactosidase or neomycin phosphotransferase product is assumed to be negligible, they suffer nonetheless from the limitation that in this system there are multiple independent variables. Observed phenotypes cannot truly be attributed to, in this case for example, the loss of Kv1.6 as opposed to the gain of exogenous β-galactosidase and/or neomycin phosphotransferase. They are, in essence, combined knock-out/knock-in models as opposed to 'clean' knock-outs.

Considering the abundance of immunoreactive *lacZ* product in the degenerated afferent boutons **Chapter V**, I queried whether expression of this commonly employed reporter cassette was contributing to the striking phenotype in *Kcna6*^{tm1Lex} mice. To delineate which aspects of the phenotype might be caused by *Kcna6* knock-out or *lacZ* expression, or whether both of these conditions are required, I acquired and created novel cohorts of mice: an alternative ('clean', *lacZ*-negative) Kv1.6 knock-out strain, and a cohort in which *lacZ* expression is conditionally driven in nociceptors – shown to express *Kcna6* **Chapter II** and undergo central degeneration in the *Kcna6*^{tm1Lex} knock-out model **Chapter V**.

The alternative Kv1.6 knock-out, *Kcna6*$^{em1(IMPC)J}$/Mmjax, features a Cas9 endonuclease-mediated 1,565 base pair deletion in exon 1, resulting in a frame shift and altered amino acid sequence after the 7th residue and a predicted premature stop codon at residue 61 (*Mus musculus* wild type Kv1.6

comprises 529 amino acids). There is no insertion of an external transgene in this knock-out targeting strategy. As such, this strain serves as a control for potential β-galactosidase effects in the *Kcna6*^{tm1Lex} mouse, enabling detection of behavioural and *in vitro* physiological phenotypes resulting solely from Kv1.6 loss.

In a similar effort to determine effects of exogenous β-galactosidase in *Kcna6*-positive DRG populations, I have conditionally expressed *lacZ* in the nociceptor populations affected in the *Kcna6*^{tm1Lex} mouse. The *Gt(ROSA)26Sor*^{tm1Sor}*/J* mouse (henceforth termed R26R^{lacZ}) is a conditional-ready strain carrying a *loxP–neo–polyA–loxP–lacZ* cassette in the ubiquitously expressed ROSA26 locus[1]. Thus, there is ubiquitous expression of neomycin phosphotransferase (*neo*), followed by a *polyA* tail, which ordinarily prevents read-through transcription of *lacZ*. The *neo–polyA* sequence is flanked by *loxP* sites, so Cre-mediated recombination excises this region and results in expression only of *lacZ*. I crossed this reporter mouse with a strain constitutively expressing Cre recombinase knocked into the Nav1.8 locus[2,3], and therefore active in the majority of nociceptive DRG neurons and some low-threshold populations[4]. Via this approach, I was able to study the consequences of *neo* or *lacZ* expression in DRG populations that normally express *Kcna6*, but independently of *Kcna6* knock-out.

The reach of this chapter was constrained by time, but I aimed to test the hypothesis that expression of exogenous LacZ drives the anatomical pathology affecting primary afferent central terminals in *Kcna6*^{tm1Lex} mice, by transgenic cross-breeding to introduce LacZ into Nav1.8$^{Cre/+}$ nociceptors. With this in mind, I also aimed to compare behavioural and physiological phenotypes of the two described *Kcna6* knock-out mice – one with and one without exogenous LacZ.

i. Results

a) LacZ is responsible for the aberrant *Kcna6*^{tm1Lex} primary afferent terminal morphology

Of all observed phenotypic features of the *Kcna6*^{tm1Lex} mouse, the effect on central afferent terminals was considered the most likely, if any, to be mediated via some interaction with exogenous β-galactosidase. Spinal cord tissue was collected from homozygous *Kcna6*$^{em1(IMPC)J}$ mice aged >15 weeks, by which time point dorsal horn pathology had fully developed in *Kcna6*^{tm1Lex} homozygotes. However, there was no sign of a similar effect on primary afferents **Fig6.1(A)**. The superficial neuropil appeared normal, with dense peptidergic and non-peptidergic fibre reactivity in laminae I and II. More tissue was collected from 6-month old homozygous mice and there was still no evidence of IB4 neuron degeneration (data not shown).

Similarly, 17-week-old Nav1.8$^{+/+}$;ROSA$^{R26R/+}$ mice, which express the neomycin phosphotransferase gene (*neo)* globally, had no central terminal features resembling the *Kcna6*^{tm1Lex} mouse **Fig6.1(B)**. In contrast, age-matched Nav1.8$^{Cre/+}$;ROSA$^{R26R/+}$ littermates expressed *lacZ* in Nav1.8-positive neurons – including IB4^{+} and CGRP^{+} nociceptors – and presented with clearly swollen nociceptor terminals containing β-galactosidase in the superficial dorsal horn laminae **Fig6.1(C)**. Overexpression of exogenous *lacZ* is therefore sufficient to drive a degenerative process affecting the central presynaptic terminals of sensory neurons, and this effect may be present in other transgenic animals where exogenous *lacZ* is expressed.

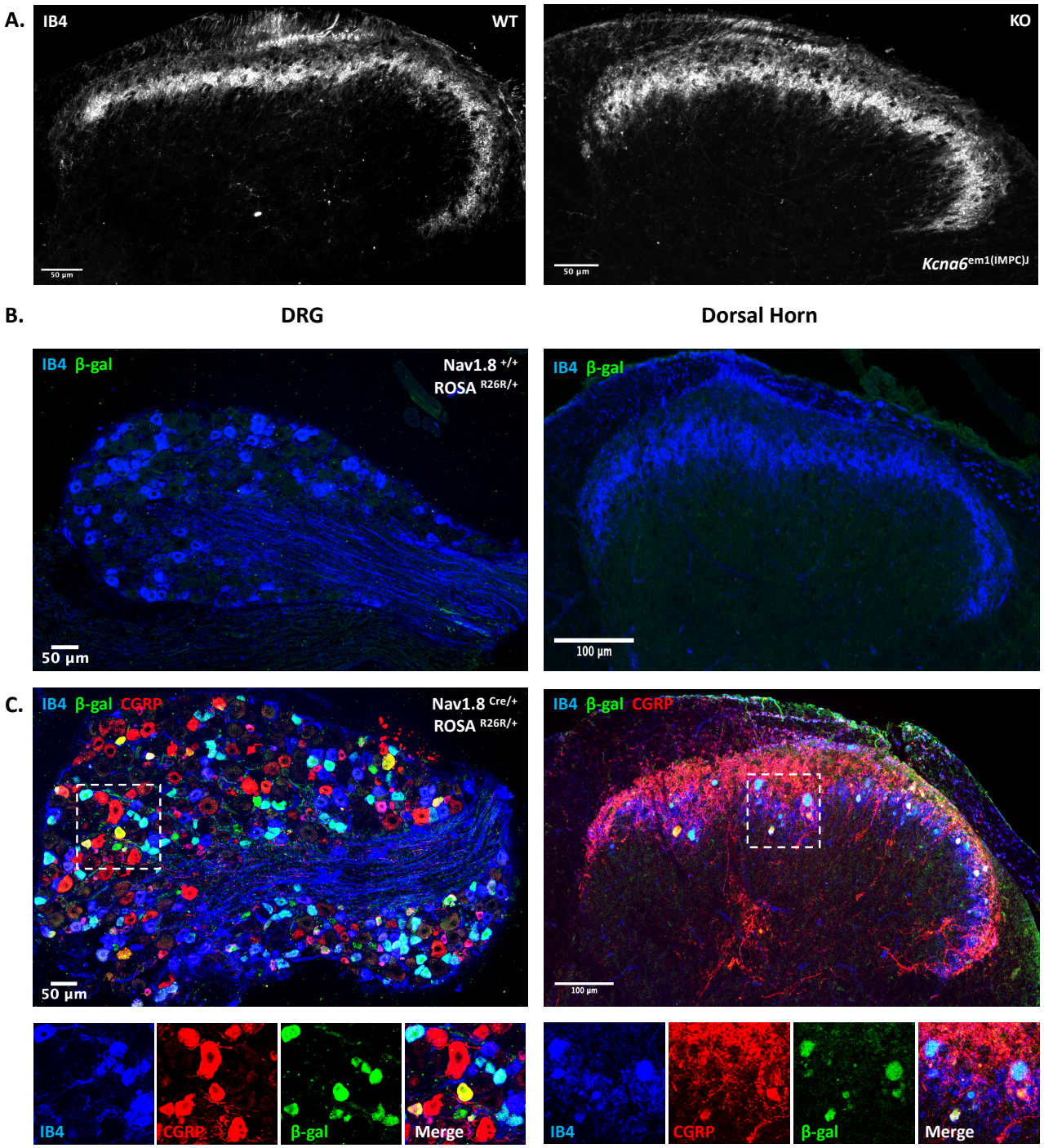

Figure 6.1 – Consequences of independent *Kcna6* deletion or *lacZ* expression on nociceptor terminals

(A) Comparison of IB4 central terminal staining in *Kcna6*$^{em1(IMPC)J}$ homozygote knock-outs and wild-type littermates reveals normal morphology

(B) No Cre-mediated *lacZ* expression in Nav1.8 Cre-negative mice expressing the R26R reporter allele. IB4 terminals are again normal in these mice expressing *neo* globally.

(C) In mice carrying one R26R allele and one Nav1.8 Cre allele, *lacZ* is expressed in small diameter, IB4^{+} and CGRP^{+} DRG neurons. Swollen nociceptor terminals containing β-galactosidase are clearly visible in the superficial laminae.

Images in **(B)** and **(C)** are paired DRG and dorsal horn sections from the same animals.

b) 'Clean' *Kcna6*$^{em1(IMPC)J}$ knock-outs also display hyposensitive behavioural tendencies

The *Kcna6*$^{em1(IMPC)J}$ mouse line was subjected to an array of sensorimotor behavioural assays. On the exploratory open field assay, homozygous knock-out mice developed a trend of reduced environmental exploration over recurrent baseline tests, as measured by movement across gridlines and hind-limb rearing episodes in a 3-minute period **Fig6.2(A)**. Responses were somewhat similar to the *Kcna6*^{tm1Lex} colony in that there was no difference in motor performance, or mechanical sensitivity **Fig6.2(B, C)**. In this instance, additional behavioural tests were performed, including a mechanical 'pin-prick' assay considered to be more noxious than Von Frey stimulation, and a noxious cooling assay involving application of dry ice to the hind-paw[5], but knock-outs did not differ in withdrawal latency to either **Fig6.2(D, E)**.

Unlike *Kcna6*^{tm1Lex} mice, withdrawal latency to Hargreaves stimulation or at 50°C was not altered in *Kcna6*$^{em1(IMPC)J}$ homozygotes **Fig6.2(F, G)**. However, these *lacZ*-negative homozygous knock-out mice were hyposensitive at 53°C, although the effect was milder (KO 11.12±0.52s*****, HET 9.33±0.41s, WT 9.28±0.43s, *****$p<0.05$ vs WT) **Fig6.2(H)**. The afferent populations stimulated by such noxious heat paradigms ostensibly include those which express Trpv1[6], the 'receptor' for temperatures above the noxious threshold of 43°C that is also activated by capsaicin[7]. To test if there was hyposensitivity generally across modalities in Trpv1$^+$ fibres, not just evoked by heat, mice were also injected with capsaicin to the dermis of the hind-paw, to stimulate Trpv1-expressing neurons. Most overt behavioural responses occurred within the first minute after injection, and heterozygous and homozygous *Kcna6*$^{em1(IMPC)J}$ mice were hyposensitive with a gene dosage trend at this time point (duration of responses: KO 20.06±4.65s*******, HET 23.45±4.39s*****, WT 30.76±2.19s, *****/*******$p<0.05/0.001$ vs WT) **Fig6.2(I)**. Apart from a very minor delay to the 2nd phase of formalin-induced behaviour **Fig6.2(J)**, which is not believed to be of much genuine significance, there were no major differences in the magnitude of the formalin-evoked response.

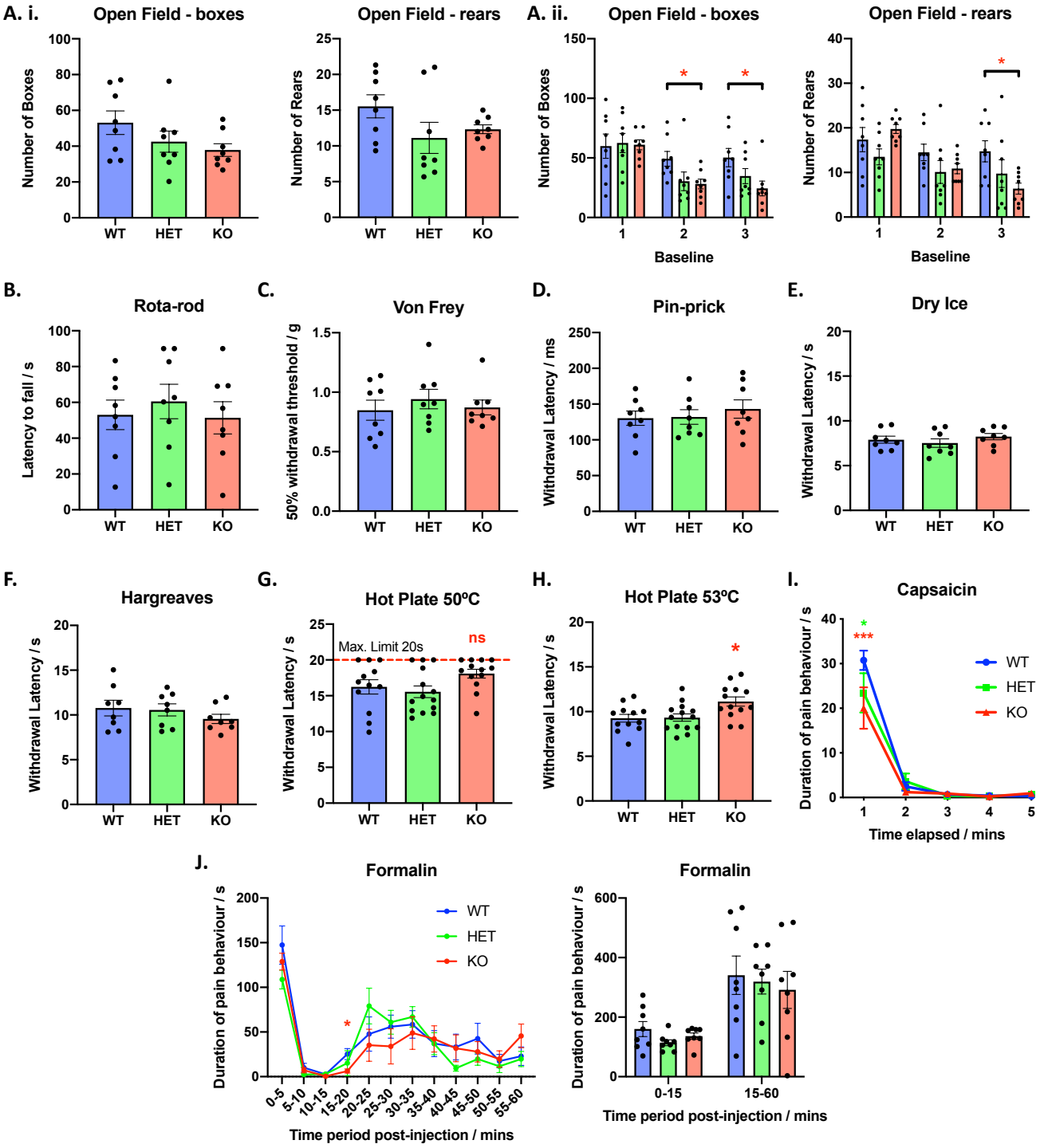

Figure 6.2 – Sensorimotor behaviour in *Kcna6*$^{em1(IMPC)J}$ knock-out mice

(A) Measurement of exploratory behaviour (gridline crosses and rearing episodes) averaged across 3 baselines **(i)**, and separated by baselines **(ii)** to reveal learning processes.
(B-H) Motor performance on Rota-rod **(B)**, and withdrawal threshold or latency to plantar hind-paw stimulation by Von Frey **(C)**, pin-prick **(D)**, dry ice **(E)**, Hargreaves **(F)** and hot plate **(G, H)**. **(A-F)** n = 8 WT, 8 HET, 8 KO; **(G, H)** n = 12 WT, 14 HET, 13 KO, mean ± SEM *=p<0.05 vs. WT by Two-Way RM ANOVA **(A.ii.)** or One-Way ANOVA **(H)** with Dunnett's multiple comparisons test.
(I, J) Pain-related behavioural responses to intraplantar injection of capsaicin and formalin. */***=p<0.05/0.001 vs WT by Two-Way RM ANOVA with Dunnett's multiple comparisons test. n = 7 WT, 10 HET, 7 KO **(I)** or n = 8 WT, 8 HET, 8 KO **(J)**, mean ± SEM

Kcna6$^{em1(IMPC)J}$ carriers were also tested on a thermal gradient assay; the apparatus is depicted in **Fig6.3(A)**. For 30mins, mice were allowed to freely explore a 1.25m long aluminium corridor connecting a hot and cold plate. There was a notable light gradient ranging from 110 lux in the middle of the track approximately 70 lux at either end, caused by shading from the apparatus end walls. This had a significant impact on animal behaviour, as mice formed an obvious preference for the darker, more sheltered ends of the corridor when the track was maintained at room temperature **Fig6.3(B)**. The hot and cold plates enable the establishment of a stable, linear temperature gradient between 5-54ºC **Fig6.3(C)**. The extremities are apparently perceived as aversive as the innate preference for the shaded ends is removed when temperature becomes the dominant environmental stimulus, with most time being spent at innocuous, warm temperatures around 29ºC **Fig6.3(D)**. A comparison of Lorentzian fits applied to the data showed that the centres of temperature preference did not vary between genotypes (WT 28.65ºC (27.96 – 29.35), HET 29.73ºC (29.15 – 30.31), KO 29.49ºC (28.35 – 30.32), mean (95% CI), p = 0.0693). Although time spent in zone 6 (centre – 36.3ºC) and zone 8 (centre – 30.7ºC) was significantly elevated for homozygotes and heterozygotes, respectively, when analysed by Two-Way ANOVA, this effect was mostly driven by one or two exceptional animals, which have still been included as there is no biological or procedural reason why they are not valid behavioural observations.

The number of entries into each temperature zone was also analysed, with a peak at a similar temperature around 29ºC for each genotype **Fig6.3(E)**. Unlike with the time spent in each zone, which was self-limiting due to the 30-minute restriction, there was no upper limit to the number of zone entries as this reflects exploratory activity, and therefore the significant reduction in homozygotes at zones 9 (centre – 27.9ºC) and 10 (centre – 25.3ºC) can also be considered a reduced motivation to explore the environment – mirroring open field assay data **Fig6.2(A)**. The sensitivity of the thermal gradient apparatus to detect changes in thermal sensation was tested on a small cohort (n=4) of *Kcna6*^{tm1Lex} homozygous mice that, having been out-crossed to a pure C57BL/6J

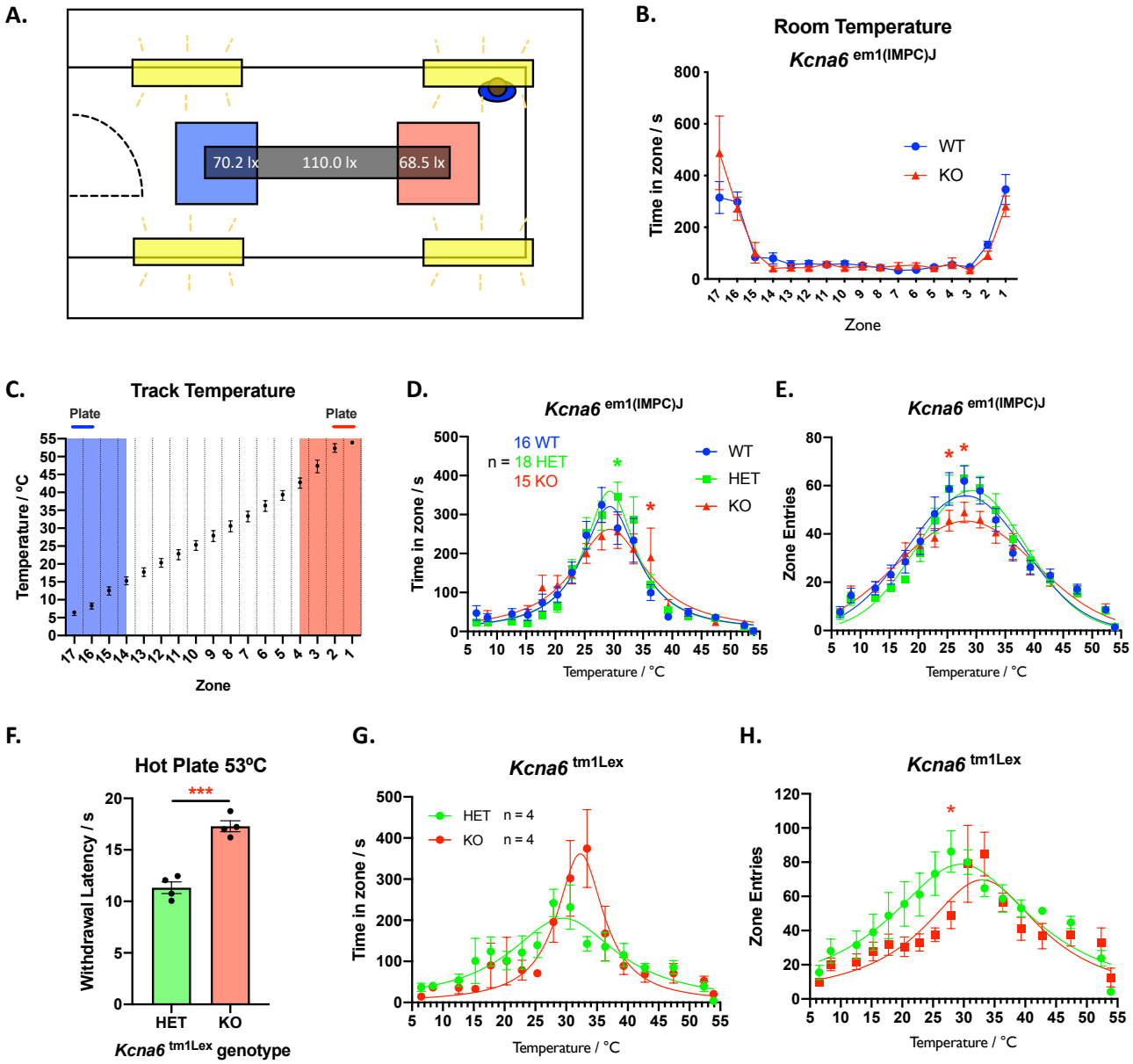

Figure 6.3 – Comparison of Kv1.6 knock-out preference formation on a thermal exploration gradient

(A) The thermal gradient apparatus consists of two plates with independent temperature control, joined by a metal track. The room was lit evenly but the track had a centre-weighted light intensity gradient due to shading. The experimenter was generally present in one of the four corners of the room.
(B) When neither plate was switched on, mice prefer the darker ends of the track over a 30min period (n = 8 WT, 7 KO, mean ± SEM)
(C) A linear thermal gradient between 5-54°C is achieved by switching on the plates (mean ± range from 8 recordings)
(D) Amount of time spent at and number of entries into **(E)** each temperature zone over a 30min period (n = 16 WT, 18 HET, 15 KO, mean ± SEM) *=p<0.05 vs WT after Two-Way ANOVA with Dunnett's multiple comparison test. Lorentzian **(D)** or Gaussian **(E)** non-linear regression fit applied to the data revealed no differences in mean temperature preference.
(F) After back-crossing onto a C57Bl6/J background, homozygote *Kcna6*^{tm1Lex} mice were still hyposensitive at 53°C and serve as a good positive control population to test the sensitivity of the thermal gradient (n = 4 HET, 4 KO, mean ± SEM) ***=p<0.001 after unpaired, two-tailed Student's t-test
(G, H) *Kcna6*^{tm1Lex} knock-outs have a more pronounced shift in thermal preference towards higher temperature compared to heterozygous littermates, as indicated by Lorentzian non-linear regression. *=p<0.05 vs HET after Two-Way ANOVA with Sidak's post-hoc multiple comparisons test.

background, were still markedly hyposensitive on the 53ºC hot plate compared to heterozygous littermates (n=4) **Fig6.3(F)**. Despite small sample numbers, a more obvious trend towards warmer preferred temperatures was observed in this strain (centre of peak: HET 29.52ºC (27.78 – 31.30), KO 32.29ºC (31.35 – 33.20), mean (95% CI), p = 0.0239) **Fig6.3(G)**. Similar trends were observed in terms of temperature zone exploration **Fig6.3(H)**.

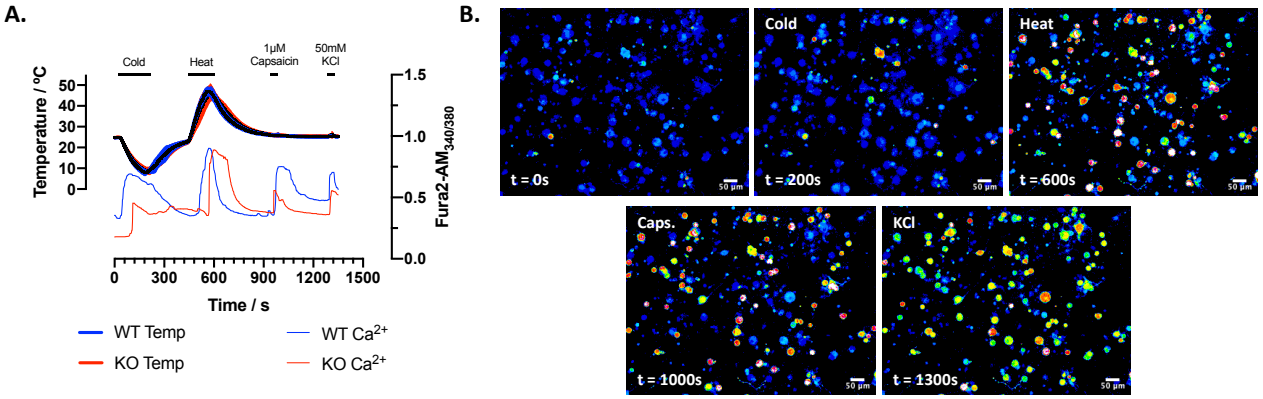

C. i.

Heat	Caps	Cold	WT	KO
+	–	–	10.18 %	8.50 %
–	+	–	4.43 %	1.96 %
–	–	+	0.44 %	0.49 %
+	+	–	49.56 %	42.81 %
+	–	+	1.11 %	0.49 %
–	+	+	0.66 %	0.49 %
+	+	+	6.64 %	2.61 %
–	–	–	26.99 %	42.65 %
67.48 %	61.28 %	8.85 %	WT	
54.41 % ****	47.88 % ****	4.09 % **	KO	

C. ii.

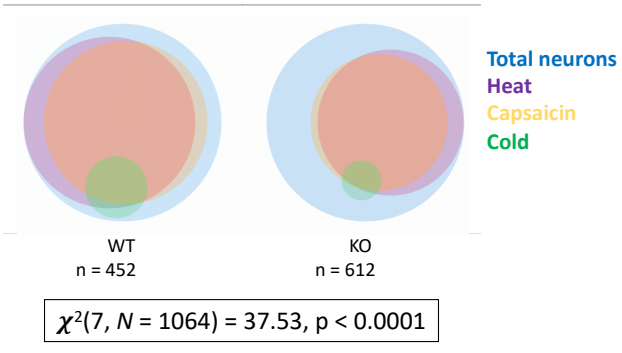

Figure 6.4 – *In vitro* DRG Ca^{2+} responses to heat, capsaicin, and cold in *Kcna6*$^{em1(IMPC)J}$ knock-outs

(A,B) A more extensive calcium imaging protocol was used on dissociated DRGs from the *lacZ*-negative *Kcna6* knock-out line and littermate controls, involving cooling from 24-6°C, passive warming back to room temperature before heating to 50°C and a passive cooling phase. Subsequently, neurons were challenged with 1µM capsaicin and 50mM KCl.
(C) There were 8 possible outcomes for responsivity of neurons (by definition KCl-sensitive) to the 3 challenge stimuli. A chi-squared test was performed with 7 degrees of freedom to test for an association between genotype and raw counts relating to the percentages highlighted in green **(i)**. Proportional Venn diagrams were produced to depict overlap between populations based on these responses **(ii)**.

c) *In vitro* Ca^{2+} responses of *Kcna6*$^{em1(IMPC)J}$ DRG neurons to thermal and chemical challenges

As there was still some evidence for a thermal behavioural phenotype in this new Kv1.6 knock-out mouse and novel evidence of hyposensitivity to capsaicin, even with intact nociceptive presynaptic boutons, primary afferent function was once again interrogated via *in vitro* Ca^{2+} imaging of dissociated DRG neurons. The stimulation paradigm was more rigorous than that used previously for *Kcna6*^{tm1Lex} DRGs – robust calcium transients were evoked by consecutive cooling, heating and application of 1μM capsaicin and 50mM KCl, with all 4 responses occasionally present in the same neuron **Fig6.4(A, B)**. This protocol enabled identification of neurons with overlapping and non-overlapping response properties **Fig6.4(C)**. A significant chi-squared test (χ^2 (7d.f., N = 1064) = 37.53, $p < 0.0001$) revealed an association between genotype and likelihood of response to the various combinations of stimuli. Furthermore, comparing the number of heat-sensitive to heat-insensitive neurons between genotypes (WT – 305 : 147; KO – 333 : 279) by a two-sided Fisher's exact test revealed a significant reduction ($p < 0.0001$) in knock-outs. The same was true for the proportion of capsaicin responders (WT – 277 : 175; KO – 293 : 319, $p < 0.0001$) and cold responders (WT – 40 : 412; KO – 25 : 587, $p = 0.0017$).

Comparing activation temperatures of heat-activated neurons, it was again evident that Kv1.6 knock-out neurons were on average activated by lower temperatures, owing to a greater proportion of neurons in the 30-40ºC range and a smaller proportion at the extreme noxious range **Fig6.5(A.i.)**. The distributions of amplitude and area under the curve (AUC) from heat-evoked responses were also reduced **Fig6.5(A.ii-iii.)** and further analysis revealed that this effect was driven mostly by reduction in amplitude of cells responding between 30-45ºC **Fig6.5(D)**. The vast majority of heat-sensitive neurons also responded to capsaicin, indicated in **Fig6.4**. Interestingly, these heat-sensitive cells which subsequently responded to capsaicin, and by inference express the noxious heat receptor Trpv1, were activated by a broad range of temperatures between 22-51ºC in

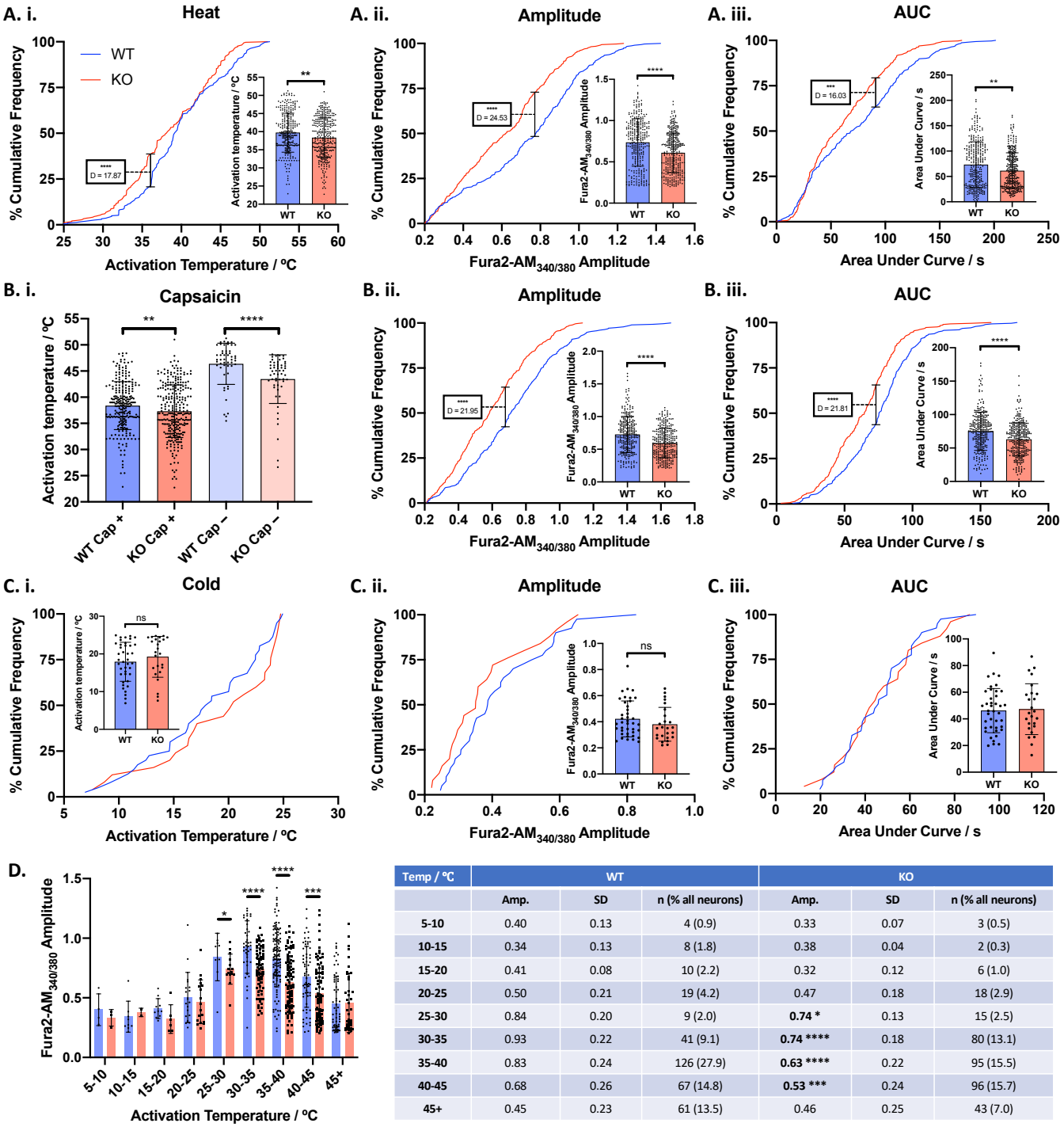

Temp / °C	WT			KO		
	Amp.	SD	n (% all neurons)	Amp.	SD	n (% all neurons)
5-10	0.40	0.13	4 (0.9)	0.33	0.07	3 (0.5)
10-15	0.34	0.13	8 (1.8)	0.38	0.04	2 (0.3)
15-20	0.41	0.08	10 (2.2)	0.32	0.12	6 (1.0)
20-25	0.50	0.21	19 (4.2)	0.47	0.18	18 (2.9)
25-30	0.84	0.20	9 (2.0)	**0.74** *	0.13	15 (2.5)
30-35	0.93	0.22	41 (9.1)	**0.74** ****	0.18	80 (13.1)
35-40	0.83	0.24	126 (27.9)	**0.63** ****	0.22	95 (15.5)
40-45	0.68	0.26	67 (14.8)	**0.53** ***	0.24	96 (15.7)
45+	0.45	0.23	61 (13.5)	0.46	0.25	43 (7.0)

Figure 6.5 – *In vitro* DRG Ca^{2+} responses to heat, capsaicin, and cold in *Kcna6*$^{em1(IMPC)J}$ knock-outs

(A) Activation temperature **(i)** and the amplitude **(ii)** and area under the curve **(iii)** of heat-evoked calcium responses (n = 305 of 452 WT and 333 of 612 KO neurons from N = 2 mice per genotype)
(B) Activation temperatures of heat-sensitive neurons from **(A)** which did or did not subsequently respond to capsaicin stimulation **(i)**, and the amplitude **(ii)** and area under the curve **(iii)** of all capsaicin responses (n = 293 of 452 WT and 277 of 612 KO neurons from N = 2 mice per genotype)
(C) Activation temperature **(i)** and the amplitude **(ii)** and area under the curve **(iii)** of cold-evoked calcium responses (n = 40 of 452 WT and 25 of 612 KO neurons from N = 2 mice per genotype)
(D) Reduction of heat response amplitude occurred mostly in neurons activated between 25-45°C
Data presented as mean ± SD plus individual neurons. ***/**/***/****** = p<0.05/0.01/0.001/0.0001 with Mann-Whitney (bars) or Kolmogorov-Smirnov test (c. frequency)

wild types and knock-outs alike **Fig6.5(B.i.)**. Meanwhile, the approximately 10% of neurons that were heat-sensitive and capsaicin-insensitive had a much higher activation threshold on average, typically well into the noxious range. The general trend towards lower activation temperatures in Kv1.6 knock-outs was present in both the capsaicin-sensitive and -insensitive populations. Analysis of the response magnitude in all capsaicin-sensitive cells was also performed, including those which either did or did not respond to some combination of thermal stimuli. In a similar fashion to heat responses, there was a reduction of capsaicin response amplitude and AUC in knock-out neurons **Fig6.5(B.ii-iii)**. Cold sensitivity appeared to be preserved, as there were no significant alterations in the distribution of activation temperatures or the magnitude of cooling-evoked responses **Fig6.5(C.i-iii.)**.

	Kcna6^{tm1Lex}	*Kcna6*$^{em1(IMPC)J}$	Nav1.8^{LacZ}	*Kcna6*^{tm1Lex}; Advillin^{EGFP}
ANATOMY				
Primary afferent terminal degeneration?	++	-	+	++
NAIVE				
Open field exploration	=	↓		
Rota-rod	=	=		
Beam test	=	=		
Von Frey	=	=		
Pin prick	n/a	=		
Cold plantar test	n/a	=		
Hargreaves	↓	=		
Hot Plate	↓↓	↓		
Formalin	↑	=		
Capsaicin	n/a	↓		
Thermal preference	? warm shift (n=4)	=		
NEUROPATHIC				
Sural nerve (SNI) hypersensitivity	=	n/a		
Neuroma hypersensitivity	↑↑	n/a		

Table 6.1 – Comparison of behavioural and anatomical phenotypes between transgenics

This thesis has included phenotyping work on 4 transgenic mouse strains. A summary of the relevant anatomical and behavioural phenotypes is provided.

↑ augmented response relative to WT
↓ diminished response relative to WT
= similar response to WT

ii. Conclusions

a) Confirmation of neurotoxic effects mediated by LacZ overexpression

The acquisition of a second Kv1.6 knock-out mouse strain has proven to be an important step towards understanding the contribution of this channel to sensory neuron function. Murine *Kcna6* has a relatively simple genetic structure, with 2 exons – only one of which contains a protein-coding region. In both global knock-out strategies, very similar regions of exon 1 were removed (bp 751-2390 in *Kcna6*^{tm1Lex} and bp 773-2337 in *Kcna6*$^{em1(IMPC)J}$), which results in complete or near-complete ablation of the coding sequence (bp 751-2340). It would not be unreasonable to assume that the two mouse strains – both on C57BL/6J backgrounds – would have the same phenotype. However, the observation that primary afferent terminals did not undergo the same process of degeneration in *Kcna6*$^{em1(IMPC)J}$ carriers **Fig6.1(A)** as in *Kcna6*^{tm1Lex} knock-outs raised concerns over the two different knock-out strategies. The <tm1Lex> targeting vector (Lexicon Pharmaceuticals, Inc. – previously Lexicon Genetics, Inc.) was used to produce a collection of 53 global knock-out mice strains for the Knockout Mouse Project (KOMP)[8,9] via gene trap homologous recombination introducing a selection cassette containing *lacZ* and *neo* sequences, all of which are available at (www.mmrrc.org/catalog/StrainCatalogSearchForm.php?jboEvent=Search&SourceCollection=Lexicon). The gene trap technique has been reviewed previously[10,11] and used extensively. This particular example results in expression of LacZ (β-galactosidase) and NeoR (neomycin phosphotransferase). This key feature distinguishes the two mouse lines from one another, as the *Kcna6*$^{em1(IMPC)J}$ allele was produced by Cas9 endonuclease excision and no exogenous genetic material was inserted to the locus.

There was therefore a strong possibility that either the neomycin resistance cassette *neo* or the *lacZ* reporter cassette were responsible for the pathological changes to nociceptor terminal boutons in

the dorsal horn. I made use of the *Gt(ROSA)26Sor*^{tm1Sor}*/J* mouse to conditionally express *lacZ* in nociceptors by breeding this line with a Nav1.8-Cre mouse to compound heterozygosity. The rationale for using Nav1.8-Cre[2,3] was that expression of this gene is restricted to peripheral sensory neuron populations that have significant overlap with *Kcna6* expression. This has been demonstrated by Nav1.8-Cre-mediated expression of tdTomato in ~75% of lumbar DRG profiles (>90% of nociceptors and ~40% of LTMRs)[4], and by single-cell RNA sequencing[12,13]. *Kcna6* was also recently reported to have 9-fold expression enrichment in FACS-sorted Nav1.8-Cre (tdTomato^{+}) versus Nav1.8-negative, cold-sensitive neurons[14]. The *Gt(ROSA)26Sor*^{tm1Sor}*/J* mouse alone also had additional utility in this scenario as it ubiquitously expresses *neo* in the absence of Cre recombinase[1], so it was possible to segregate the effects of the two reporter sequences expressed together in the *Kcna6*^{tm1Lex} line.

As expected, only Cre-positive mice expressed LacZ in DRG neurons **Fig6.1(B, C)**. This expression has not yet been quantified but was confined to subsets of IB4- and/or CGRP-positive neurons. However, it did not appear as though the reported[4] >90% of Cre-positive nociceptor profiles were immunoreactive for β-galactosidase. In particular, only very few CGRP-immunoreactive profiles co-localised with the reporter. The apparent inefficiency of Cre-recombination compared to previous reports[4] may simply reflect poor antibody detection of the product in the remaining LacZ-negative nociceptor profiles, especially considering these mice were only heterozygous carriers of the R26R^{lacZ} reporter allele. Nevertheless, the consequence of this *lacZ* expression, versus *neo* expression in Cre-negative mice, for nociceptive terminals was clear. In Nav1.8-Cre mice, grossly enlarged IB4^{+}/LacZ^{+} boutons were visible by fluorescence microscopy in lamina II, as well as a smaller number of enlarged CGRP^{+}/LacZ^{+} boutons in lamina I/II-o **Fig6.1(C)**. The morphology very closely matched that of the *Kcna6*^{tm1Lex} dorsal horn. This exact strain was in fact made before, but the effect was not reported[3]. There is now compelling evidence

for direct, site-specific toxicity of exogenous LacZ to primary afferent presynaptic terminals and resolution to some questions raised by the *Kcna6*^{tm1Lex} CNS phenotype.

Moreover, this result also has far-reaching implications for the interpretation of the extensive body of research that has involved the use of exogenous *lacZ* insertion to achieve deletion and/or to report gene expression. In addition to the >50 other <tm1Lex> knock-out mice harbouring the same cassette affecting *Kcna6*^{tm1Lex}, the original publication describing Cre-dependent *lacZ* reporter *Gt(ROSA)26Sor*^{tm1Sor}*/J* has in excess of 3000 citations[1] – a large proportion of which have presumably used this genetic technology to report Cre-recombinase expression. Of course, knock-out mice containing *lacZ* are not limited to those containing <tm1Lex> alleles, but probably exist in the hundreds if not thousands. In fact, a keyword search for "lacZ" on the International Mouse Strain Resource (IMSR) database yielded 1049 mouse strain results (http://www.findmice.org/summary?query=lacz&states=Any&_states=1&types=Any&_types=1&repositories=Any&_repositories=1&_mutations=on). Unfortunately, as only structural analysis has been performed on the Nav1.8$^{Cre/+}$;ROSA$^{R26R/+}$ mice, it is currently impossible to directly determine functional consequences of nociceptor terminal degeneration, such as behavioural or dorsal horn electrophysiological phenotypes. These experiments would ideally be performed as part of a continuation of this project but have been limited by time constraints. However, structural change begets functional change, and with TEM imaging the swollen boutons of LacZ^{+} terminals were seemingly devoid of pre-synaptic vesicular machinery **Chapter V**, so it is likely that there is a downstream effect on neurotransmission. Some literature exists to suggest that structural and functional changes may occur as a result of *lacZ* expression in other CNS neuronal populations[15].

b) Milder behavioural phenotypes in *Kcna6* knock-outs with intact primary afferent terminals

On the other hand, it has been possible to parse out which contributions the knock-out of Kv1.6 actually made to the original *Kcna6*^{tm1Lex} phenotype. Studying the 'clean' knock-out strain, *Kcna6*$^{em1(IMPC)J}$, revealed a remarkably similar phenotypic profile considering the absence of dorsal horn pathology. As in the first knock-out line, some of the behavioural data regarding mechanical and cold stimuli applied focally to the hind-paw was unchanged. It interesting that cold sensation was unaffected, as α-dendrotoxin (α-DTx)-sensitive Kv1.1/1.2/1.6 currents are known to be important regulators of excitability in cold-activated neurons[16]. The loss of this brake current, I_{KD}, in DRG neurons after nerve injury contributes to cold allodynia[17]. It is also interesting that pin-prick responses were unaltered, given that *Kcna6* expression was high in myelinated peptidergic DRG nociceptors, of which 30% express the Neuropeptide Y receptor-2, *Npy2r*, and convey pin-prick sensation.

However, homozygous *Kcna6*$^{em1(IMPC)J}$ knock-outs did retain the phenotype of hyposensitivity to noxious heat stimulation. This was less obvious than in the previous *Kcna6*^{tm1Lex} line – responses to the Hargreaves and 50ºC hot plate tests were comparable to wild type littermates, and despite reaching significance the delayed withdrawal latency to 53ºC stimulation was not as pronounced **Fig6.2(F-H)**. Nonetheless, these mice were also significantly less responsive to intradermal injection of capsaicin to the hind-paw **Fig6.2(I)**. Interestingly, Kv1.6 knock-outs also showed some deficits on the open field test **Fig6.2(A)**. This is considered to be a cognitive behavioural assay reflecting anxiety-related behaviour, although it is difficult to state whether reduced exploration is due to increased 'anxiety', or simply enhanced learning of the environment, as deficits were only observed after multiple test sessions **Fig6.2(A.ii.)**.

Sensory perception and locomotor activity in such assays involve many complex CNS circuits, but it has been demonstrated recently that developmental deletion of an autism candidate gene *Mecp2* in the peripheral somatosensory system alone can cause deficits in open field exploration[18]. Peripheral replacement of the same gene on a global *Mecp2* $^{+/-}$ background via Advillin-Cre was sufficient to restore normal behaviour. Similarly, Nav1.8-Cre deletion of another autism-related gene *Shank3* (present in primary sensory neurons and their synaptic terminals, as well as widely in the CNS) resulted in hyposensitivity to noxious heat and capsaicin via dysregulation of its direct molecular interactor Trpv1[19]. The phenotypes of both peripherally-restricted knock-outs closely matched those of global knock-outs in the equivalent genes. Therefore, although the model presented here features global *Kcna6* deletion, it is still plausible that the behavioural phenotypes relate to mechanisms originating in the peripheral nervous system.

Whilst there was an effect of the *Kcna6*$^{em1(IMPC)J}$ allele on heat withdrawal thresholds and capsaicin sensitivity, the results from thermal preference testing were underwhelming and showed no significant alteration in peak temperature preference, or time spent at and entries to noxious temperature zones **Fig6.3(D)**. This apparent paradox is not unprecedented – even Trpa1/Trpm3/Trpv1 triple knock-out mice with severely impaired thermal sensitivity (>75% exhibit zero withdrawal responses to hot plate temperatures reaching 57ºC) form a bell-shaped preference curve identical to wild types on the same thermal gradient apparatus used here[20]. Of course, the formation of place preference is likely to be partly induced by warmth-induced positive affect as well, which may provide an explanation for the persistence of place preference in such knock-out studies. However, these results are indicative that the field should avoid reliance on reflexive withdrawal as a measure of pain; apparently, reduced ability to engage spinal reflex circuits does not preclude the overall sensation of aversiveness elicited by noxious stimuli. The converse is also true – using the same thermal gradient, silencing amygdalar neurons activated by nociception

removed the aversive quality of noxious temperature zones, while having no effect on reflexive thresholds[21].

c) Cellular temperature sensing in DRG neurons is affected by *Kcna6* knock-out

In order to study *Kcna6*$^{em1(IMPC)J}$ sensory neurons in isolation, I again turned to calcium imaging of dissociated DRG neurons. Both wild type and homozygous knock-out DRGs included neurons responding *in vitro* to cold, heat, and capsaicin – and all combinations of the three. Estimates of sensory neurons that respond to thermal stimuli are lacking, although one observation from dissociated trigeminal ganglion neurons suggests a figure of 45-70% for sensitivity to 45ºC heat[20]. The protocol used in this chapter provided an opportunity to quantify sensors of thermal stimuli and relate this to functional Trpv1 expression. In this chapter, I demonstrated that 68.6% (310/452) of wild-type sensory neurons were thermally sensitive, responding during either the cooling (1.1% – 5/452) or heating ramp (59.7% – 270/452), or both (7.7% – 35/452) **Fig6.4 & Fig6.5**. Compared to results in **Chapter IV**, the proportion of heat-sensitive wild-type neurons was increased from ~40% to 67.5% (305/452). However, the protocol performed in **Chapter IV** failed to reach temperatures above 45ºC, whereas in this case the maximum temperature reached was just in excess of 50ºC and a considerable proportion (13.5% – 61/452) of neurons were activated within this additional 5ºC window **Fig6.5(D)**. Of course, there are potentially additional heat-sensitive neurons activated above even the 50ºC threshold, which were not accounted for in this experiment. For the same reason, the proportion of cold-sensitive neurons (8.9% – 40/452) is very likely to be an underestimate as the lowest temperatures achieved were 6ºC. The proportion of cold sensitive neurons *in vitro* was previously quoted as 8%[17] up to 25%[22], although the stimulation paradigms used a cooling ramp from 36-18ºC or 30-10ºC and sampled from DRGs and trigeminal ganglia, respectively, so these are not directly comparable.

Capsaicin responses were present in 67.5% of neurons – higher than prior estimates of ~40%, but this previous report used a 3-fold weaker (300nM capsaicin) stimulus and only sampled lumbar DRGs[23]. The analysis presented in this chapter included DRGs indiscriminately from all spinal regions, and there is known variation in proportions of Trpv1-expressing neurons at different DRG levels; for example, an over-representation in colonic compared to epidermal afferents[24]. It was interesting that a small proportion (< 5%) of wild-type neurons responded to capsaicin but neither heat nor cold, suggesting that functional Trpv1 expression is not a guarantee of thermal sensitivity. The capsaicin-sensitive neurons which were heat responsive had a mean activation temperature of 38.38ºC within an unexpectedly wide range from 28.87 – 48.38ºC, with 85% (109/141) of these neurons activating below the Trpv1 'activation threshold' of 43ºC **Fig6.5(B.i.)**. It is unfortunately not possible to assert that this is the same *in vivo*. It is possible that the warm-sensing cells are sensitised to capsaicin *in vitro*, for example mediated by receptor sensitisation, *de novo* gene expression, or by nerve growth factor (NGF), which is present in the culture medium and increases Trpv1 membrane expression[25]. Conversely, the heat-sensitive, capsaicin-insensitive neurons were activated between 35.46 – 51.26ºC (mean 46.39ºC, with 39/51 or 73% above 43ºC). The concept of extreme heat being transduced by Trpv1-independent means is not new[26], but these results satisfyingly complement original observations that $Trpv1^{-/-}$ mice retain DRG responses to high temperature stimulation but lose responses to moderate heat[27].

How does the loss of Kv1.6 affect the described response parameters? Across cold, heat, and capsaicin-sensitivity there was a general reduction in the proportion of responsive neurons **Fig6.4(C)**. In terms of remaining cold sensitive neurons, there was no effect on the distribution of activation temperatures, or magnitude of cold-evoked calcium responses **Fig6.5(C)**. This correlates well with behavioural outcomes **Fig6.2(E) & Fig6.3**, and suggests that the I_{KD} current is carried by Kv1.1/1.2-containing channels and not Kv1.6, because blockade of I_{KD} by α-DTx or 4-AP shifts activation temperature of cold-activated neurons towards warmer temperatures[16,17].

This is also predicted by comparison of Kv1 channel expression in TRPM8 neurons – *Zeisel et al. (2018)* used expression of cold-transducing channel TRPM8 to define 3 of their 17 DRG subpopulations, in which expression of the α-DTx-sensitive Kv1 subunits is Kv1.2 >> Kv1.6 > Kv1.1 **Chapter II (Table 2.1)**. The likely candidate for I_{KD} is therefore Kv1.2-dominant channels.

The distribution of heat activation temperatures very closely mirrored the data collected from *Kcna6*^{tm1Lex} mouse in **Chapter IV**. As depicted in **Fig6.5(A.i.)**, the cumulative frequency distribution compared to wild-types is almost identical to the pattern observed in *Kcna6*^{tm1Lex} knock-outs, with an increased proportion of neurons activated between 30-40ºC but similar proportion between 40-45ºC. Whereas the heat curve ended at 45ºC in **Chapter IV**, in this chapter one can additionally see from **Fig6.5(A.i.)** and **Fig6.5(D)** that *Kcna6*$^{em1(IMPC)J}$ knock-outs also have 6.5% fewer neurons than wild-types activated by >45ºC. So, perhaps the shift observed in average activation temperature is mediated by the loss of a population of neurons activating above this temperature, rather than a generic mechanism broadly reducing the activation temperature for all neurons. This shift was especially but not exclusively apparent in capsaicin-insensitive neurons **Fig6.5(B.i.)**. In this case, the apparent 5-6% reduction of unmyelinated $CGRP^+$ profiles in *Kcna6*^{tm1Lex} DRG sections could be important **Chapter IV (Fig4.2)**. One explanation of heat hyposensitivity in mice ubiquitously lacking Kv1.6 is therefore developmental loss of a small population of noxious heat receptors. DRGs from *Kcna6*$^{em1(IMPC)J}$ knock-outs will be analysed to see if this effect is consistent across strains.

There was, however, a significant reduction in the $[Ca^{2+}]_i$ peak amplitude and area under the curve of both heat- (particularly between 30-45ºC) and capsaicin-evoked responses, indicating that an unidentified cellular mechanism may also contribute to the behavioural phenotype. Despite reaching significance on population-based statistical tests combining data from two animals per genotype, and trends consistent with the *Kcna6*^{tm1Lex} results where n = 3 animals per genotype

Chapter IV, the effects observed in the *Kcna6*$^{em1(IMPC)J}$ would still benefit from repetition in more biological replicates to have confidence regarding reproducibility.

d) Concluding remarks

Overall, this chapter has demonstrated a danger of using the exogenous reporter allele *lacZ* in neuroscience research, and potentially other fields, owing to its toxicity when present in sensory nerve terminals. The downstream consequences of this are uncertain, as Kv1.6 knock-outs without *lacZ* share some phenotypic features with Kv1.6 knock-outs expressing *lacZ* in terms of behaviour and DRG sensitivity to stimuli. The complete overlap between modalities affected *in vivo* and in DRGs *in vitro* provides evidence for a peripheral mechanism of thermal hyposensitivity in both *Kcna6*^{tm1Lex} and *Kcna6*$^{em1(IMPC)J}$ strains, but *lacZ*-mediated neurodegeneration cannot be dismissed as a confounding and exacerbating factor in *Kcna6*^{tm1Lex} knock-out mice.

iii. Methods

N.B. Histochemical and other behavioural experiments not listed here were performed as described in previous chapters

Animals

All animals were bred, maintained, and tested in compliance with the Animals (Scientific Procedures) Act 1986, under UK Home Office project license number P1DBEBAB9 held by Professor David Bennett at the University of Oxford.

Kcna6$^{em1(IPMC)J}$ animals were purchased (MMRRC stock number 042391-JAX) and maintained on a C57Bl6 background. The nature of the mutation is Cas9-mediated excision of the sole coding region, leaving the initial 7 residues intact and resulting in frame shift and premature STOP codon. Homozygous conditional-ready *Gt(ROSA)26Sor*^{tm1Sor}*/J* mice[1] were gifted kindly by Prof Shankar Srinivas (DPAG, University of Oxford) to serve as founders of the Nav1.8^{lacZ} colony by crossing with in-house heterozygous Nav1.8-Cre mice (gifted by Prof John Wood, University College London)[2,3], producing compound heterozygotes expressing one *lacZ* allele at the ROSA26 locus in Nav1.8-positive neurons.

Immunohistochemistry

Spinal cords of *Kcna6*$^{em1(IMPC)J}$ homozygotes, their wild-type littermates, and Nav1.8-Cre-negative and Cre-positive animals were analysed to ascertain whether Kv1.6 knock-out, or *neo* or *lacZ* cassettes were harmful to nociceptor terminals. Tissue was harvested as described in other chapters, from >15-week-old mice to allow for the progressive development observed previously in **Chapter V**. Images in **Fig6.1** were acquired from tissue derived from female 15 to 17-week-old *Kcna6*$^{em1(IMPC)J}$ or Nav1.8^{lacZ} mice, but the same effects were observed in male tissue.

Behavioural assays

Age- and sex-matched male and female *Kcna6*$^{em1(IMPC)J}$ mice underwent behavioural testing between the ages of 8-18 weeks old. Age- and sex-matched wild-type littermates served as controls. Animals were habituated to any novel environmental stimuli prior to behavioural testing. The experimenter was blinded to genotype until all behavioural testing had been completed. Data from left and right paws on the pin-prick and cold plantar (dry ice) assay were combined to produce one average.

a) Pin-prick

Animals were temporally housed individually in plexiglass chambers on a grille used for Von Frey testing. A sharp pin was fixed to the filament of a 2.0g Von Frey hair and used to provide noxious punctate stimulation to left and right hind-paws. Withdrawal reflexes were filmed from below using an iPhone8 in slo-mo mode (720p, 240fps) such that still frames are ~4ms apart. The withdrawal latency was derived post-hoc by scrolling through frames from the time of contact with the paw to withdrawal. Two or occasionally three stimuli were applied to each paw on three separate baseline testing days, from which a mean baseline latency was calculated.

b) Dry ice (cold plantar assay)

This assay has been described in detail previously[5]. Briefly, mice were housed individually in plexiglass chambers on a 5mm borosilicate glass surface. Crushed dry ice pellets were compacted into a syringe with the tapered end cut off, such that the dry ice could be applied to the glass evenly beneath the hind-paw. A stopwatch was used to time the withdrawal latency. Mice received 3 or occasionally 4 stimuli per hind-paw on 3 baseline occasions, from which a mean baseline withdrawal latency was calculated.

c) Intradermal capsaicin

Animals received a 10µl intradermal injection of 500µM capsaicin (Sigma M2028, 1.5µg in 10µl sterile 0.9% saline with 1% v/v ethanol and 0.5% v/v Tween-20) to the plantar left hind paw as described previously[28]. Pain-related paw scratching, biting, licking and shaking behaviour was monitored and recorded per minute over a 5-minute period immediately following injection.

d) Thermal gradient assay

Mice were tested on a thermal gradient apparatus (Bioseb) comprising a 1.25m long aluminium track connecting two hot/cold plates. A stable linear temperature gradient from ~5-54ºC was established when plates were switched on, as measured by a Pro-Surface Thermapen contact thermometer (Electronic Temperature Instruments, Ltd.). The track was monitored from above by a webcam, which fed into AnyMaze software for operator-independent animal tracking and analysis of time spent in and entries to 17 equally sized zones drawn inside the software interface. The temperature was recorded from the centre point of each zone. Mice were placed in the centre of the track at the start of the test and allowed to explore the gradient freely for 30mins.

In vitro Ca^{2+} imaging

DRG dissociation, culture, and calcium imaging was performed in essentially the same manner as in **Chapter IV**, from 15-week-old male mice. The stimulation protocol differed, and was as follows: 0-30s baseline recording; 30-200s cooling phase from 24ºC – 6ºC; 200-450s passive warming to room temperature, 450-600s heating phase from 24ºC – 51ºC, 600-950s passive cooling to room temperature; 950-980s 1µM capsaicin; 980-1290s washout; 1290-1320s 50mM KCl; 1320-1350s washout. Unbiased analysis was performed using the custom MATLAB script introduced in **Chapter IV**.

Statistics

Behaviour – The unit of biological replication is the animal, with n values for individual experiments indicated in figure legends. Data were assessed for normality using the Shapiro-Wilk test and analysed using One-Way ANOVA or Two-Way (Repeated Measures) ANOVA with Dunnett's post-hoc multiple comparisons test to compare HET or KO to WT. Thermal gradient results have previously been analysed by Ordinary Two-Way ANOVA[29], so this analysis was also performed here with Dunnett's (3 groups) or Sidak's (2 groups) multiple comparisons test. However, this form of analysis assumes sphericity, which is not always the case for each temperature zone. A preferred method was employed, consisting of non-linear regression analysis taking into account all replicate data points, followed by comparison of fits between genotypes. For each experiment GraphPad Prism was used to decide a preferred model between Gaussian and Lorentzian distributions and is the result indicated in figure legends. Curve parameters were compared and quoted with 95% confidence intervals.

Calcium imaging – neurons were combined from 2 WT and 2 KO animals, with 3 or 4 coverslips imaged per mouse. The combined n = 452 WT and 612, where the unit of replication is the neuron. Raw counts of neurons defined by their stimulus response properties were compared between genotypes by Chi-squared test (across all combinations, 7 d.f.) or by two-sided Fisher's exact test (for each comparison of total heat- or capsaicin- or cold-sensitive vs insensitive). As in **Chapter IV**, other parameters such as activation temperature, amplitude, and AUC were not normally distributed so comparisons between genotypes were made by Mann-Whitney and Kolmogorov-Smirnov tests.

All statistical tests were performed in GraphPad Prism software. Venn diagrams were drawn using a free online tool available at (https://www.meta-chart.com/venn).

iv. References

1. Soriano, P. Generalized lacZ expression with the ROSA26 Cre reporter strain. *Nat. Genet.* **21**, 70–71 (1999).
2. Nassar, M. A. *et al.* Nociceptor-specific gene deletion reveals a major role for Nav1.7 (PN1) in acute and inflammatory pain. *Proc. Natl. Acad. Sci.* **101**, 12706–12711 (2004).
3. Stirling, L. C. *et al.* Nociceptor-specific gene deletion using heterozygous Nav1.8-Cre recombinase mice. *Pain* **113**, 27–36 (2005).
4. Seal, R. P. *et al.* Nav1.8 expression is not restricted to nociceptors in mouse peripheral nervous system. *Pain* **153**, 2017–2030 (2012).
5. Brenner, D. S., Golden, J. P. & Gereau IV, R. W. A novel behavioral assay for measuring cold sensation in mice. *PLoS One* **7**, (2012).
6. Cavanaugh, D. J. *et al.* Distinct subsets of unmyelinated primary sensory fibers mediate behavioral responses to noxious thermal and mechanical stimuli. *Proc. Natl. Acad. Sci. U. S. A.* **106**, 9075–80 (2009).
7. Cao, E., Cordero-Morales, J. F., Liu, B., Qin, F. & Julius, D. TRPV1 Channels Are Intrinsically Heat Sensitive and Negatively Regulated by Phosphoinositide Lipids. *Neuron* **77**, 667–679 (2013).
8. Bahcall Niemitz, E., Packer, A., and Vogan, K., O. NIH acquires knockout mice. *Nat. Genet.* **37**, 1167 (2005).
9. Austin, C. P. *et al.* The Knockout Mouse Project. *Nature Genetics* **36**, 921–924 (2004).
10. Stanford, W. L., Cohn, J. B. & Cordes, S. P. Gene-trap mutagenesis: Past, present and beyond. *Nature Reviews Genetics* **2**, 756–768 (2001).
11. Friedel, R. H. & Soriano, P. Gene Trap Mutagenesis in the Mouse. *Methods Enzymol.* **477**, 243–269 (2010).
12. Zeisel, A. *et al.* Molecular Architecture of the Mouse Nervous System. *Cell* **174**, 999-1014.e22 (2018).
13. Zheng, Y. *et al.* Deep Sequencing of Somatosensory Neurons Reveals Molecular Determinants of Intrinsic Physiological Properties. *Neuron* **103**, 1–19 (2019).
14. Luiz, A. P. *et al.* Cold sensing by Nav1.8-positive and Nav1.8-negative sensory neurons. *Proc. Natl. Acad. Sci.* 201814545 (2019). doi:10.1073/pnas.1814545116
15. Reichel, J. M. *et al.* Beware of your Cre-Ation: lacZ expression impairs neuronal integrity and hippocampus-dependent memory. *Hippocampus* **26**, 1250–1264 (2016).
16. Madrid, R., De La Peña, E., Donovan-Rodriguez, T., Belmonte, C. & Viana, F. Variable threshold of trigeminal cold-thermosensitive neurons is determined by a balance between TRPM8 and Kv1 potassium channels. *J. Neurosci.* **29**, 3120–3131 (2009).
17. González, A. *et al.* Role of the excitability brake potassium current I KD in cold allodynia induced by chronic peripheral nerve injury. *J. Neurosci.* **37**, 3553–16 (2017).
18. Orefice, L. L. L. *et al.* Peripheral Mechanosensory Neuron Dysfunction Underlies Tactile and Behavioral Deficits in Mouse Models of ASDs. *Cell* **166**, 299–313 (2016).
19. Han, Q. *et al.* SHANK3 Deficiency Impairs Heat Hyperalgesia and TRPV1 Signaling in Primary Sensory Neurons. *Neuron* **92**, 1–15 (2016).
20. Vandewauw, I. *et al.* A TRP channel trio mediates acute noxious heat sensing. *Nature* **555**, 662–666 (2018).
21. Schnitzer, M. J. *et al.* An amygdalar neural ensemble that encodes the unpleasantness of pain. *Science (80-.).* **363**, 276–281 (2019).
22. Karashima, Y. *et al.* TRPA1 acts as a cold sensor in vitro and in vivo. *Proc. Natl. Acad. Sci. U. S. A.* **106**, 1273–1278 (2009).
23. Teichert, R. W. *et al.* Functional profiling of neurons through cellular neuropharmacology. *Proc. Natl. Acad. Sci. U. S. A.* **109**, 1388–95 (2012).

24. Hockley, J. R. F. *et al.* Single-cell RNAseq reveals seven classes of colonic sensory neuron. *Gut* **68**, 633–644 (2019).
25. Zhang, X., Huang, J. & McNaughton, P. A. NGF rapidly increases membrane expression of TRPV1 heat-gated ion channels. *EMBO J.* **24**, 4211–4223 (2005).
26. Nagy, I. & Rang, H. Noxious heat activates all capsaicin-sensitive and also a sub-population of capsaicin-insensitive dorsal root ganglion neurons. *Neuroscience* **88**, 995–997 (1999).
27. Caterina, M. J. *et al.* Impaired nociception and pain sensation in mice lacking the capsaicin receptor. *Science (80-.).* **288**, 306–313 (2000).
28. Dawes, J. M. *et al.* Immune or Genetic-Mediated Disruption of CASPR2 Causes Pain Hypersensitivity Due to Enhanced Primary Afferent Excitability. *Neuron* **97**, 806–822 (2018).
29. Urien, L. *et al.* Genetic ablation of GINIP-expressing primary sensory neurons strongly impairs formalin-evoked pain. *Sci. Rep.* **7**, 43493 (2017).

Chapter VII

Discussion

The work in this thesis has sought to elucidate the contributions of the potassium channel α-subunit Kv1.6 to somatosensory function. This has been complicated by the somewhat discrepant phenotypes of *Kcna6*^{tm1Lex} and *Kcna6*$^{em1(IMPC)J}$ knock-out mouse strains, with the most notable anomaly being neurodegenerative processes in primary afferent terminals specifically relating to expression of the LacZ-containing <tm1Lex> allele. The results of each line of experimental enquiry have been discussed in detail within each chapter, but it is important to place these conclusions in context with each other and with prior research in the wider field of pain. This discussion will review the fundamental insights that have been gained regarding primary afferent and dorsal horn physiology and function.

i. LacZ/β-gal toxicity suggests a role for gangliosides in presynaptic boutons

Numerous hypotheses were generated to account for the anatomical findings in the *Kcna6*^{tm1Lex} dorsal horn. It was tempting to dismiss this feature as a peculiar sequela resulting from, potentially, an undue effect of the allele insertion on other neighbouring or distant genetic loci. Many transgenic mouse lines inexplicably fail to manifest in their intended manner, or present differently depending on genetic background, emphasising our incomplete understanding of the genome and its regulation[1]. The intense immunoreactivity for LacZ in degenerating *Kcna6*^{tm1Lex} afferent terminals **Chapter IV**, and the specificity of the effect on neuronal populations known to express *Kcna6*, provided a clue the that the *Kcna6*^{tm1Lex} allele itself was key in initiating the neurodegeneration, as opposed to an off-target genetic abnormality – which might be less discriminating. However, a

pathological role of LacZ in the aetiology of this condition was still unclear, as cytoplasmic immunoreactivity in distended neuron terminals was expected from a reporter designed with no subcellular targeting mechanism – analogous to cell tracing by cytoplasmic expression of unconjugated tdTomato or GFP, for instance.

A LacZ-mediated mechanism became more apparent with the absence of primary afferent degeneration in the *lacZ*-negative Kv1.6 knock-out mouse, *Kcna6*$^{em1(IMPC)J}$, and was left in little doubt when the same structural degeneration of central afferent terminals was observed in Nav1.8-Cre; R26R^{lacZ} mice **Chapter VI**. Technically, the Nav1.8^{lacZ} mouse expresses the reporter on a Nav1.8 heterozygous background, due to the knock-in of Cre recombinase, so an interaction of *lacZ* expression with a secondary genetic insult to ion channel genes cannot be ruled out mechanistically, as with *Kcna6*^{tm1Lex} knock-outs. However, this is considered highly unlikely as Nav1.8$^{Cre/+}$ mice are otherwise phenotypically normal[2].

A unifying feature of these enlarged profiles, revealed by electron microscopy, was an abundance of lipid-rich organelles thought to represent components of the endo-/lyso-/autophagosome pathway involved in plasma membrane turnover. Complex gangliosides – sialic acid-containing glysosphingolipids – are a major component of mammalian cell membranes and are composed of an oligosaccharide chain covalently bonded to a ceramide lipid. Through progressive cleavage steps occurring at different stages of the endo/lysosomal pathway, terminal glycoside residues are successively removed in the catabolism and recycling of these membrane components[3]. Neurons chiefly synthesise a- and b-series gangliosides including GM1, the cleavage of which to GM2 is achieved by GM1 β-galactosidase removing a terminal β-galactose residue. Loss of function mutations affecting either GM1 β-galactosidase or the group of enzymes that catabolise GM2 (β-hexosaminidases) result in fatal neurodegenerative lysosomal storage disorders (reviewed very

recently[3]) featuring accumulation of the substrates GM1 and GM2, respectively, in neuronal lysosome structures.

Complex gangliosides are known for their structural role in axon-Schwann cell interaction[4], where they are an antigenic target of autoantibodies in demyelinating neuropathies[5]. The results presented here indicate that GM1/2 gangliosides or appropriate endo/lysosomal function may also play an important role in stabilising and maintaining the structural integrity of central primary afferent terminals as well. I suggest that overexpression of exogenous β-galactosidase via the *lacZ*-containing <tm1Lex> and R26R alleles has caused a GM2 gangliosidosis restricted to neurons expressing these alleles, via excessive hydrolysis of GM1 gangliosides that may produce a quantity of GM2 substrate sufficient to overwhelm downstream β-hexosaminidases. It is also possible that exogenous LacZ has a dominant-negative effect on endogenous β-galactosidase, causing GM1 gangliosidosis, although the *Glb1* gene is reportedly expressed very weakly in mouse DRG neurons[6] and β-galactosidase was not detectable via immunohistochemistry in wild type dorsal root ganglia **Chapter II**. It is unlikely that a generic effect of exogenous protein overexpression is responsible, as other primary afferent reporter mice such as Advillin^{EGFP} or Mrgprd^{YFP} mice do not share these features[7,8].

In both GM1 and GM2 gangliosidoses, accumulation of gangliosides induces the formation of 'meganeurites' or 'ballooned' neurons[3], visible by Golgi-staining in feline models[9,10] but also present in post-mortem brain tissue from human patients[11]. Ultrastructurally, these meganeurites contain electron-dense membranous whorls and lysosome-like structures[9,10,12–14], which bear remarkable similarity to swollen terminals of *Kcna6*^{tm1Lex} afferents viewed by electron microscopy **Chapter V**. In the feline model it was suggested that, controlling for age, meganeurites were more prevalent in GM2 than GM1 gangliosidosis[12,13]. GM2 gangliosidoses, including Tay-Sachs disease and Sandhoff

disease, have an early onset, although there are variants which have a delayed onset and reduced severity – which correlate with improved catabolic GM2 clearance[3,11,15]. This is analogous to the delayed onset and milder nature of pathology in *Kcna6*^{tm1Lex} heterozygotes and Nav1.8^{lacZ} mice, which only had one copy of the *lacZ* allele **Chapter V & VI**. Another feature of GM2 gangliosidosis, demyelination, is in part mediated by activated microglia[16], which were also detected in close apposition to swollen *Kcna6*^{tm1Lex} profiles **Chapter V**.

Despite the fact that LacZ protein was detectable in distal nerve terminals innervating the skin **Chapter IV**, structural abnormalities were only ever observed in central afferent axons, specifically once they had penetrated the spinal cord. This is curious and accentuates the polarised structure and function of sensory neurons. It remains unclear why presynaptic axons were affected specifically, but there is some evidence that neurotransmitter release is dependent on effective lysosomal function. In cerebellar granule cells, activity-dependent release of the synaptic organiser[17] cerebellin (Cbln1) from lysosomes is required for the initiation and maintenance of glutamatergic synaptic integrity[18]. Following its exocytosis, Cbln1 integrates with the plasma membrane and accumulates at pre-synaptic boutons; this is permissive of glutamatergic synapse formation by directly linking presynaptic neurexin to postsynaptic glutamate receptors[18]. *Cbln1* is expressed in a subset of non-peptidergic sensory neurons, according to single-cell RNA sequencing[6]. This is a speculative extrapolation, but if a similar mechanism of synaptic plasticity exists in the pseudo-unipolar primary nociceptor, one could conceive of how lysosomal overload or dysfunction in primary afferent gangliosidoses might have specific consequences for synapse-forming central boutons versus peripheral terminals.

While there was evidence of CGRP-immunoreactive meganeurites in both LacZ reporter lines, the most severe impact was consistently seen in IB4-binding neurons. This is interesting, as both subpopulations displayed comparable expression of LacZ in DRG tissue from *Kcna6*^{tm1Lex} mice,

and *Kcna6* expression was in fact weaker in IB4 neurons compared to CGRP neurons in wild type DRGs **Chapter II**. Apart from a small degree of overlap in mice[19], these two fibre types differ at molecular genetic[6,20], structural (central[21–23] and peripheral[22]), and functional[24] levels. In the context of peripheral nerve injury, transient central terminal retraction occurs in non-peptidergic $IB4^+$ fibres, but not peptidergic $CGRP^+$ fibres[25]. Clearly the synaptic development and maintenance of these two subpopulations is orchestrated by distinct processes, so perhaps the enhanced potency of LacZ in $IB4^+$ fibres reflects an increased susceptibility of non-peptidergic neurons to disturbance of complex ganglioside biochemistry or lysosomal function. In fact, the very definition of an 'IB4-binding' neuron relies upon binding of the plant lectin IB4 to terminal α-galactose residues on glycolipids[26,27]. Whilst peptidergic neurons contain the enzymes necessary for IB4 epitope synthesis[28], they generally do not bind IB4 – suggesting differential glycolipid regulation. Ultimately, the effect of LacZ expression will depend on the native species of ganglioside present in neuronal cell membranes, which varies among populations[29,30].

* * *

The tendency to assume that exogenous *lacZ* cassettes are inert in transgenic animals is surprising. In fact, the ability to detect its expression via X-GAL staining even relies upon functional enzymatic activity. Careful interpretation of previous research using the LacZ reporter protein is advised. For instance, knock-out of brain-derived neurotrophic factor (BDNF) via *lacZ* insertion resulted in reduced dendritic complexity in cortical neurons[31], which is a known feature of neurons lacking glycosphingolipids[32]. One publication warning of unwanted LacZ side-effects featured conditional expression of the $R26R^{lacZ}$ reporter allele in cortical glutamatergic neurons, and also observed defects in dendritic complexity, but not when expressing ChR2-YFP[33].

The BDNF^{lacZ} mouse was also used to report conditional knock-out of BDNF in primary afferent neurons via Advillin-Cre recombination in adulthood[34]. This induced LacZ expression in sensory neurons under the endogenous BDNF promoter, which was predominantly active in non-nociceptive NF200^{+} neurons. Although some CGRP^{+} and IB4^{+} neurons were LacZ immunoreactive, there was no signs of LacZ expression or meganeurite development in either the superficial or deep dorsal horn. Induction in adulthood may simply delay the onset of primary afferent degeneration, or the timing of *lacZ* expression may be important throughout development, when the delicate balance of glycosphingolipid species is known to determine neuronal differentiation[35]. However, adult expression of *lacZ* alone in cortical neurons is still sufficient to cause structural and behavioural phenotypes[33].

Equally, the nature of the specific LacZ protein expressed and its subcellular localisation appears to affect its toxicity, as nuclear-localised (nLacZ) expressed in primary afferent populations apparently does not initiate central terminal degeneration[36]. It is unclear whether other fusion proteins such as tau-LacZ retain their toxicity. A number of publications have used expression of such proteins in sensory neurons[37,38], using X-GAL staining for visualisation. While nothing untoward was reported by the authors, careful inspection of figures does seem suggestive that similar swollen structures are present in the substantia gelatinosa[38] and in CNS structures[37] expressing tau-LacZ, although without neuronal counterstaining it is admittedly difficult to be confident in this assertion. With hindsight it is clear that X-GAL staining was indeed capable of identifying LacZ^{+} degenerative boutons in *Kcna6*^{tm1Lex} spinal cord tissue, but initially this was misidentified as cell body staining due to the lack of counterstaining **Chapter II**. The spatiotemporal context of LacZ expression should therefore be taken into consideration, but arguably the use of exogenous *lacZ* cassettes in mice should in general be avoided.

ii. Insights into thermal sensation

This study has sought to define a role for Kv1.6 in pain and somatosensation. Behavioural phenotypes of Kv1.6 knock-out mice prompted an investigation into primary afferent sensitivity to thermal stimuli. In conducting a comprehensive analysis of thermal sensitivity *in vitro*, I have found some interesting consequences of genetic Kv1.6 deletion, but I have also been able to make novel inferences regarding wild type thermo-sensation in distinct afferent populations. Estimations of thermal sensitivity in the sensory ganglia (that is to say the proportion of neurons responsive to thermal stimuli) are frequently based on calcium imaging, due to its high-throughput capabilities, but vary widely in their assertions. This variance is most likely due to differing experimental contexts (*in vitro* versus *in vivo*) and designs, including the 'holding temperature' for *in vitro* experiments, stepping versus ramp protocols, the temperature limits at heat or cold extremes, and quantitative definitions of a *bona fide* heat response.

The calcium imaging protocol employed in **Chapter VI** was more extensive than in **Chapter IV**, covering a temperature range from approximately 6ºC to 51ºC with heating or cooling ramps beginning at a holding temperature of 24ºC (ambient room temperature). The data collected from this experiment declare that 65-70% of DRG neurons throughout all spinal levels responded to warmth or heat. A very similar ramp protocol from 25-48ºC only yielded responses in 30% of dissociated wild type DRG neurons[39]. Meanwhile, other *in vitro* experiments have reported sensitivity to 43ºC stimulation in 80% of DRG or TG neurons[40], while yet others reported values of 50-60% after 45ºC stimulation[41]. The latter publication convincingly demonstrated that the TRP channels Trpv1, Trpm3, and Trpa1 have mostly overlapping expression in sensory neurons, are each independently capable of transducing heat, and are individually sufficient for withdrawal responses to noxious heat, using double and triple knock-out mice and pharmacological manipulation of these channels[41].

While they may offer a closer approximation of normal neuronal activity, *in vivo* calcium imaging protocols are not without their own limitations, and still produce contrasting results depending on stimulation paradigms and methods of quantitation. A recent publication by *Emery et al. (2016)* selected mechanically responsive neurons and stated that the majority of these neurons were not also thermosensitive[42]. However, thermal stimulation was achieved by paw submersion, which will have evoked activity in many neurons with non-overlapping receptive fields with the mechanically probed region. These neurons were thus not assessed for mechanosensitivity, so there was likely to be an unintended selection bias and misrepresentative calculations using mechanical sensitivity as the denominator. Instead, calculating the percentage of thermosensitive neurons (the denominator) that also exhibited mechanical sensitivity in the same receptive field, *Chisholm et al. (2018)* subsequently reported a high degree of polymodality among DRG neurons *in vivo*[43].

Another recent publication by *Wang et al. (2018)* imaged thousands of adult lumbar DRG neurons *in vivo* in mice that had received early postnatal intraplantar delivery of viral constructs to transduce sensory neurons with the calcium indicator GCaMP6s[44]. The authors identified polymodality in half of all DRG neurons, corroborating previous results[43] from *Chisholm et al.* and most likely confirming that polymodality is an intrinsic property of many sensory neurons *in vivo*, not simply induced by the dissociation process for *in vitro* experiments, as was suggested by *Emery et al.*[42]. *Wang et al.* also demonstrated that in all neurons the magnitudes of Ca^{2+} transients correlate linearly with the number of electrical stimuli applied to evoke neuronal firing – an important validation for the interpretation of Ca^{2+} signals as a proxy for neuronal activity.

According to *Wang et al.*, 45% of neurons responded to heating steps from 25ºC to 38, 43 or 50ºC, and 15% responded to cooling steps from 32ºC to 20, 15 or 6ºC [44]. Six percent of neurons responded to both cold and heat, which supports the data collected in **Chapter VI** of this thesis (quoting a value of 7-8%), although the authors' estimates of sole heat and cold sensors differed

from my own, which could reflect a sensitisation artefact *in vitro*. Interestingly, approximately 15% of large-diameter neurons respond to 50ºC heat[44], implying that a population of Aβ afferents may partly convey noxious heat sensation (perhaps relating to rapid reflex withdrawal from extreme heat sources), but this was not commented on by the authors. A virtue of *in vivo* imaging is the ability to record from the same neurons after multiple thermal stimuli without jeopardising neuron viability. *Wang et al.* found that many neurons could be activated at multiple temperature steps, and that hotter absolute temperature was encoded by increased response magnitude in these neurons, as well as sequential recruitment of activity in neurons with higher activation thresholds.

At first, this seems to contrast with the results in **Chapter VI**, where I observed a negative correlation between activation temperature and maximal response amplitude (neurons with higher activation temperatures generally had smaller amplitudes). However, this discrepancy could be explained by subtle differences between the two stimulation protocols. Using a ramp protocol, the activation temperature in **Chapter VI** was designated as the temperature at which a neuron first responded to heat – its minimal activation threshold. The observations of *Wang et al.* imply that heat-sensitive neurons have a temperature bandwidth within which they exhibit graded responses (probably due to increased open probability of individual heat transducers and overlapping expression of transducers of different temperatures). If this is the case, neurons with lower activation temperatures may be repeatedly and increasingly activated as a temperature ramp protocol rises above their minimum threshold and potentially opens various transduction channels in sequence. Evidence for functional co-expression of Trpm2-mediated, warmth-induced currents with Trpv1 and Trpm3 channels was described by *Tan & McNaughton (2016)*[45]. The temporal resolution of the ramp heating protocol may not enable the separation of the Ca^{2+} signal into discrete responses, so a large cumulative calcium signal comprising numerous superimposed activation responses may occur in such scenarios. This would result in a larger amplitude for warm-sensing neurons, and a smaller amplitude for noxious heat receptors that will have only been

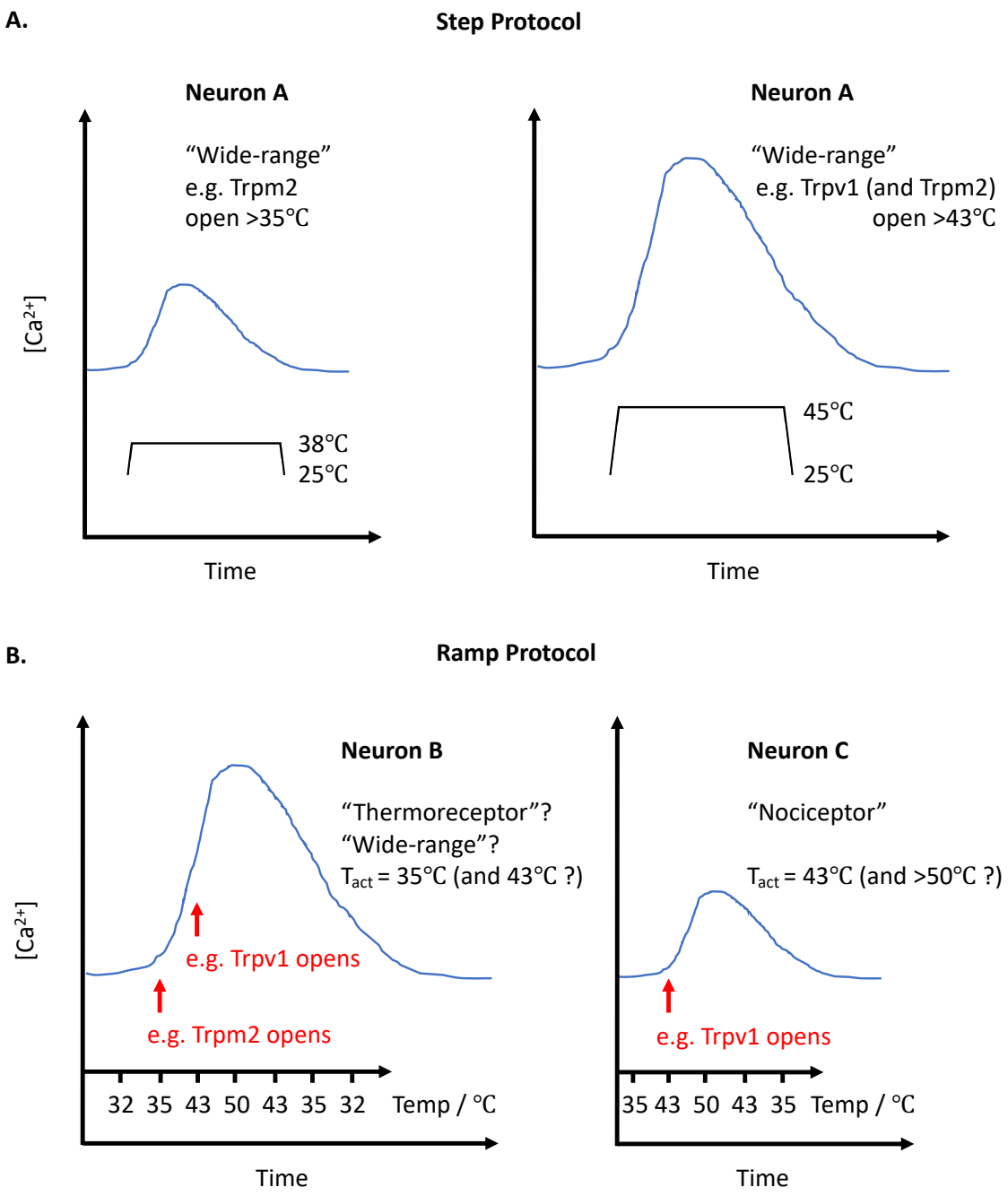

Figure 7.1 – Choice of heating protocol and consequences for Ca^{2+} response amplitude

(A) Heat **step** protocol used by *Wang et al.* identifies "wide-range warm/heat neurons" that encode increased temperature as greater response magnitude, potentially via opening of multiple transduction channels co-expressed in the same neuron.
(B) Relatively slower heat **ramp** protocol potentially opens multiple transduction channels in sequence in the same neuron during the same overall calcium response, resulting in a large-amplitude calcium signal (Neuron B). Amplitude of 'nociceptor' response, which may also encode temperature as response magnitude but within a hotter bandwidth, is limited by the upper extreme of the ramp (Neuron C). Regardless, activation temperature (T_{act}) is recorded as the lowest temperature at which each neuron begins to respond.

excited at the lower end of their temperature bandwidth by this heat ramp. The differences between protocols and effects on interpretation of results are depicted in **Fig7.1**.

One implication of this hypothesis is that some heat nociceptors may also have the capability of encoding non-noxious heat. Direct evidence of this was presented in **Chapter VI**. As described previously, Trpv1 has been identified as a key candidate underlying noxious heat sensation. Its activation temperature conveniently lies around the temperature threshold for noxious sensation, 43ºC (although 'activation temperature' is a misnomer; channel activation is a gradual process and temperature dependence is best described as a Q_{10} ratio of channel gating, eloquently explained by *Vriens, Nilius & Voets (2014)*[46]).

By chemically activating $Trpv1^+$ neurons *in vitro* with capsaicin following cold/heat ramps, it was possible to determine cold sensitivity and the minimum heat activation threshold in a population classically defined as heat nociceptors **Chapter VI**. Perhaps surprisingly, approximately 10% of capsaicin-sensitive neurons responded to cold, with most of these neurons also responding to heat, which complicates the idea of a 'labelled line' in the periphery. Seven per cent of capsaicin responders were not responsive to either cold or heat, suggesting that Trpv1 expression is not a guarantee of thermal sensitivity in sensory neurons. As expected, the majority (90%) of capsaicin-sensitive neurons did also respond to heating. However, the minimal activation temperature for most of these neurons was considerably below 43ºC, which signifies the existence of thermoreceptors with signalling roles for both innocuous and noxious stimuli. Such neurons were previously identified by *Wang et al. (2018)*[44] and *Tan & McNaughton (2016)*[45], and are described in **Fig7.1**.

* * *

It is clear from published literature[39,44] as well as **Chapters IV & VI** that the majority of thermosensitive sensory neurons respond in the 35-50ºC range, with very few neurons activated by ramps through mild or ambient temperatures. This is interesting as it implies that sensation of ambient temperature may arise from a relative paucity of afferent neuronal input. In some ways this is intuitive – in most scenarios, we do not consciously perceive ambient temperature, but we are soon aware of uncomfortable heat or cold, and equally we consciously derive pleasure from innocuous warmth. For tactile sensation, this is a well observed and intuitive phenomenon; in the absence of a physical stimulus mechanoreceptors are not activated and we simply do not perceive touch. However, unlike with tactile somatosensation, all parts of the body are always exposed to a thermal stimulus and the encoding of absolute temperature is still poorly understood. The results presented in this thesis suggest that temperature sensation might operate via a thermostatic mechanism, whereby ambient temperature (which could be considered an absence of temperature causing either discomfort or pleasure) is encoded peripherally by a dearth of primary afferent activation. When external temperature varies beyond the ambient window, afferent neurons appear to become activated to signify the salience of the stimulus, whether it has a pleasurable or aversive quality. This seems an evolutionarily appropriate mechanism when one also considers the homeostatic nature of the thermoregulatory functions of the autonomic nervous system occurring downstream of temperature sensation.

* * *

Lastly, it has become clear through studying Kv1.6 knock-out mice that the sensation of heat in mice is in part dependent on appropriate expression of this channel. Two independently produced Kv1.6 knock-out strains both had significantly delayed withdrawal responses to 53ºC noxious heat, and displayed hypoexcitability in heat-sensitive peripheral sensory neurons. Hypothetical mechanisms for these traits are outlined in the following section.

iii. Why are Kv1.6 knock-out mice hyposensitive to noxious thermal stimuli?

Kcna6 is expressed throughout the nervous system[6]. Of course, in two global Kv1.6 knock-out strategies, there are myriad explanations for hyposensitive behavioural traits. However, hyposensitivity and alteration of thermal activation thresholds were features of dissociated Kv1.6 knock-out sensory neurons from both mouse lines, with the same modality specificity as the hyposensitive behavioural data. While *Kcna6*^{tm1Lex} mice were more markedly hyposensitive to heat than *Kcna6*$^{em1(IMPC)J}$ mice, if one considers that synaptic boutons in the former were rendered highly dysfunctional, the discrepancy between these two lines is akin to those frequently observed between gene knock-out and fibre ablation studies, such as with Trpv1$^{-/-}$ versus Trpv1 fibre ablation[24,47]. The loss of Trpv1 fibres, which may contain other heat transducers besides Trpv1, has a more potent impact on noxious thermal sensation than the loss of Trpv1 channels within these fibres. In *Kcna6*^{tm1Lex} afferent fibres, which overlap considerably (if not completely) with Trpv1 afferents[6,48], the effective loss or reduction of synaptic transmission evidenced by bouton degeneration and reduced WDR neuron responses **Chapter V** would predictably result in more significant thermal deficits than *Kcna6* knock-out alone.

These observations intimate that a primary afferent mechanism might be responsible for reduced sensitivity to heat and capsaicin in Kv1.6 knock-outs. Nevertheless, they do not offer a satisfactory physiological mechanism through which Kv1.6 loss would result in sensory neuron hypoexcitability. Most known functions of Kv1 channels would instead point to a hypersensitive phenotype upon removal of Kv1.6. Indeed, absence of Kv1.6 in the wake of peripheral nerve injury seems to maintain persistent mechanical hypersensitivity **Chapter III**, while its upregulation in wild type animals promotes the restoration of normal sensory thresholds and reduces spontaneous electrical discharge in injured nerve fibres[49]. Blockade of Kv1 currents in non-peptidergic nociceptors isolated from Mrgprd-GFP mice (where Kv1.6 is enriched and is the major Kv1

subunit) also increased the maximal action potential firing rate of these neurons substantially[48]. The channel's acute effect on membrane excitability thus appears to involve limitation of excitability, falling in line with canonical Kv1 channel properties in sensory neurons[50,51]. Some hypothetical explanations for the phenotypes of both Kv1.6 knock-out mice are outlined below.

a) Genetic compensation as a driver of hyposensitivity

Genetic loss of Kv1.6 could result in a compensatory upregulation of other VGKCs. Two recent papers have begun to address the oft-noted anecdotal phenomenon that loss of a gene can lead to compensatory upregulation of its paralogs[52,53] and absence of a phenotype. Under some circumstances at least, the process appears to be dependent on degradation of mRNA transcripts with premature stop codons, from the gene in question, by mRNA surveillance and quality control machinery. Given the abundance of VGKC genes, including Kv1 genes, if such a process was to occur after Kv1.6 knock-out the so-called genetic compensation response might be of sufficient strength and breadth to produce a Kv1 overexpression phenotype. However, quantitative RT-PCR of brain-derived RNA in *Kcna6*^{tm1Lex} mice revealed no change in *Kcna1* or *Kcna2* mRNA compared to wild type mice **Chapter II**. On balance, this is an unlikely explanation for hyposensitivity in Kv1.6 knock-outs.

b) Subunit stoichiometry: Kv1.6 loss could produce Kv1 gain-of-function

It is not entirely unprecedented for knock-out of a delayed rectifier Kv1 subunit to present with some features of hypoexcitability. In Kv1.2-null mice, while an overall phenotype of hyperexcitability is made clear by frequent seizures, auditory neurons of the medial nucleus of the trapezoid body (MNTB) were, surprisingly, hypoexcitable in slice preparations[54]. This contrasted with markedly hyperexcitable auditory MNTB neurons from Kv1.1-null mice observed by the same

authors[55]. This hypoexcitability in Kv1.2$^{-/-}$ neurons was caused by paradoxically increased Kv1 currents, with a negative shift in their half maximal activation potential[54]. The subunit stoichiometry of heteromeric Kv1 channels has a significant influence on activation thresholds, with Kv1.2 channels promoting a more depolarised activation potential than Kv1.1[56], and Kv1.6 a still more depolarised activation potential[57] ($V_{0.5max}$ for homomeric channels: Kv1.1 -33mV, Kv1.2 -26mV, Kv1.6 -17mV).

Therefore, knock-out of Kv1.6 in sensory neurons could result in over-representation of Kv1.1/1.2 subunits and reduced neuronal excitability. This would be easily tested with basic patch-clamp electrophysiology of dissociated DRG neurons in wild types and knock-outs, as there would be an expected increase in rheobase if Kv1 channels were active at more hyperpolarised potentials. Excessive activation of Kv1 currents could also explain the reduction in heat and capsaicin-evoked Ca^{2+} response amplitudes and AUC associated with Kv1.6 knock-outs **Chapter IV & VI**. The contribution of specific Kv1 heteromers to DRG electrophysiological parameters could be investigated further with the growing availability of subunit-specific antagonists[58–60], including some toxins which even have substantial selectivity for asymmetric heteromers containing three Kv1.2 and one Kv1.1/1.6 subunits[61]. Due to time constraints, such experiments have not been performed, but would provide a good foundation for future work.

c) <u>Generic effect on thermosensitive primary afferents</u>

A recent study of nociception in a mouse model of diabetes reported significant thermal hyposensitivity in male *Ins2* $^{+/Akita}$ mice[39]. Interestingly, cultured DRG neurons from these mice also had shift towards cooler activation temperatures, and a reduction in Ca^{2+} response amplitude. Again, there were no investigations into the mechanism by which this occurs, so it is not possible to postulate the involvement of a shared pathway between the *Ins2* $^{+/Akita}$ mouse and Kv1.6 knock-

outs. It does remain interesting that, in two independent mouse models, an entire population shift in heat activation threshold and response amplitude *in vitro* correlates with heat hyposensitivity *in vivo*. This supports the concept that *Wang et al. (2018)* suggested, regarding the importance of response amplitude as well as the number of activated neurons in coding heat sensation[44], and supports primary afferent hypoexcitability as a cause for thermal hyposensitivity in global Kv1.6$^{-/-}$ mice. Future work might investigate the acute effects of Kv1.6 blockade on thermal activation of DRG neurons, by extension of the calcium imaging protocol used in this thesis to include temperature ramps pre-/post-application of Kv1.6-specific conotoxins[59]. The assumption is that acute Kv1.6 blockade does not affect heat sensation, however, as direct application of α-DTx to the hind paw only evokes behavioural cold hypersensitivity (through I_{KD} blockade) but not heat hyposensitivity[62].

d) Developmental loss of a thermosensitive DRG subpopulation

The results in this thesis have provided some evidence for a mechanism involving aberrant DRG development or maintenance. *Kcna6*^{tm1Lex} mice appeared to have a small (6%) reduction in the proportion of CGRP immunoreactive profiles in lumbar DRGs **Chapter IV**. This phenotype has not been assessed in the *Kcna6*$^{em1(IMPC)J}$ knock-out mouse, but this is a priority for further experiments. Interestingly, using a calcium imaging protocol with more noxious maximal temperatures, there was a corresponding loss of heat-activated neurons **Chapter VI**. Presently it cannot be confirmed that this represents a similar absence of CGRP^{+} neurons. The loss observed in *Kcna6*^{tm1Lex} mice also cannot yet be attributed to an actual reduction of total DRG neurons versus an alteration in developmental fate, but there are techniques available involving tissue clearing and whole-DRG imaging that would enable this analysis to be performed[63].

iv. Conclusion

To summarise, this thesis has provided a thorough characterisation of potassium channel Kv1.6 in the sensory nervous system. Its expression has been visualised *in situ*, confirming emerging reports that this channel subunit is among the highest expressed potassium channel subunits in mouse nociceptors[48]. Two independent Kv1.6 knock-out mice displayed behavioural hyposensitivity to noxious thermal stimuli, as well as deficits in DRG neuron calcium responses to thermal stimulation. Together, these results have identified a novel role for Kv1.6 in noxious thermal sensation. An exacerbated phenotype and pathological structural degradation of synapses in the *Kcna6*^{tm1Lex} mouse line, carrying a recombinant *lacZ* allele, calls into question the utility of recombination with such reporter cassettes as a means of gene ablation, and warns against a naïve assumption that all effects observed in knock-out mice relate to gene deletion. This has broad implications for neuroscience research given the continued widespread use of transgenic mice carrying exogenous *lacZ* cassettes. The exact mechanism through which Kv1.6 genetic knock-out acts to impede detection of noxious thermal stimuli remains unclear, but some postulations are described in **Fig7.2**, including developmental loss of thermosensitive nociceptive populations or shifts in subunit stoichiometry resulting in hypoexcitability.

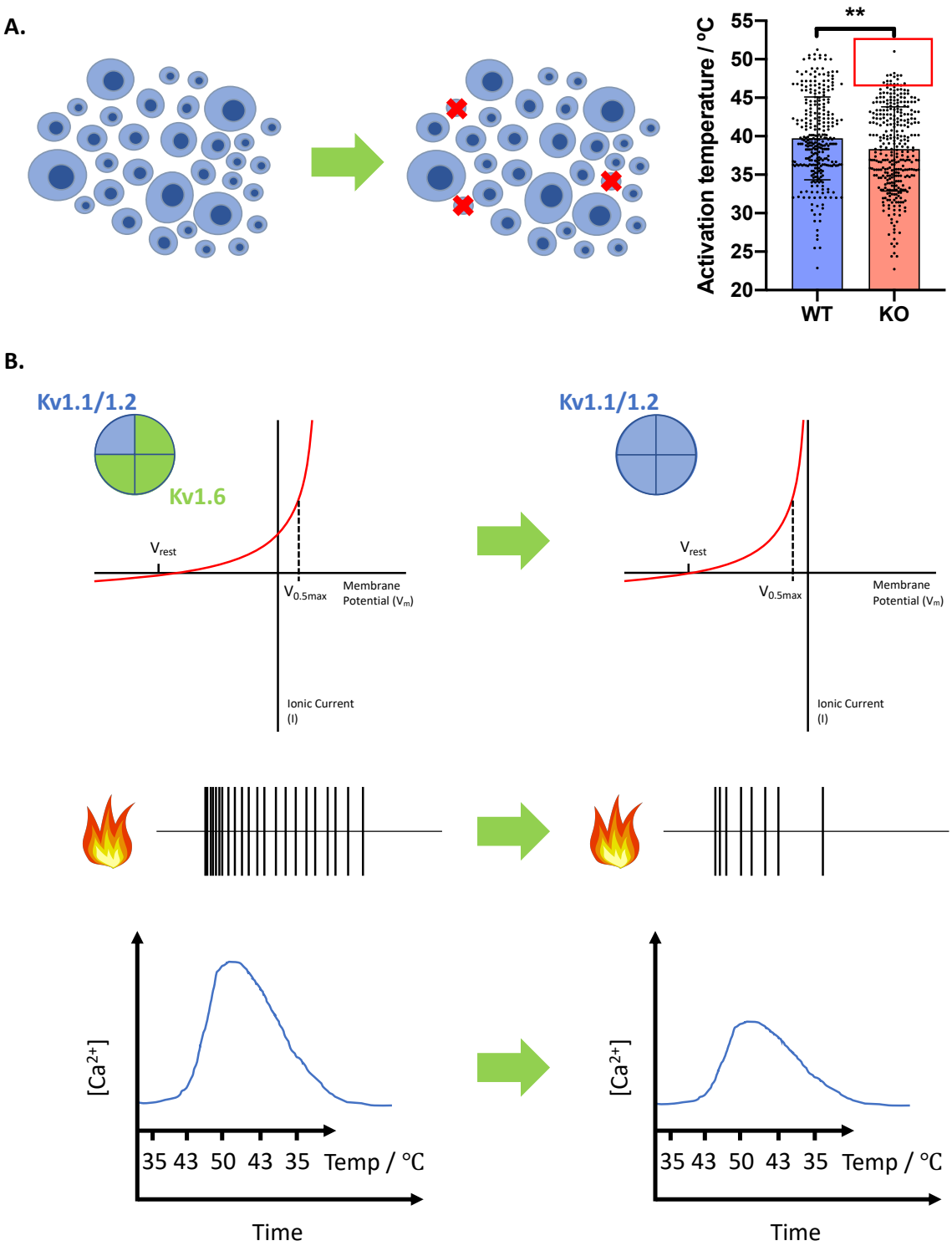

Figure 7.2 – Potential mechanisms for thermal hyposensitivity in Kv1.6 knock-out mice

(A) Absence of Kv1.6 during development could result in aberrant differentiation of certain thermo-sensitive DRG populations responsive to high temperatures.
(B) Loss of Kv1.6 subunits in nociceptors may mean that the resultant Kv1 channels are primarily composed of Kv1.1/1.2 subunits, with more hyperpolarised half maximal activation potentials. Such channels would more readily provide repolarising counter-currents in response to sub- and supra-threshold stimuli, causing primary afferent hypoexcitability, which may manifest as decreased firing rate and reduced calcium influx.

v. References

1. Lariviere, W. R., Chesler, E. J. & Mogil, J. S. Transgenic studies of pain and analgesia: mutation or background genotype? *J. Pharmacol. Exp. Ther.* **297**, 467–473 (2001).
2. Stirling, L. C. *et al.* Nociceptor-specific gene deletion using heterozygous Nav1.8-Cre recombinase mice. *Pain* **113**, 27–36 (2005).
3. Breiden, B. & Sandhoff, K. Lysosomal Glycosphingolipid Storage Diseases. *Annu. Rev. Biochem.* **88**, 461–485 (2019).
4. Susuki, K. *et al.* Gangliosides contribute to stability of paranodal junctions and ion channel clusters in myelinated nerve fibers. *Glia* **55**, 746–757 (2007).
5. Fehmi, J., Scherer, S. S., Willison, H. J. & Rinaldi, S. Nodes, paranodes and neuropathies. *J. Neurol. Neurosurg. Psychiatry* **89**, 61–71 (2018).
6. Zeisel, A. *et al.* Molecular Architecture of the Mouse Nervous System. *Cell* **174**, 999-1014.e22 (2018).
7. Hunter, D. V. *et al.* Advillin Is Expressed in All Adult Neural Crest-Derived Neurons. *eNeuro* **5**, ENEURO.0077-18.2018 (2018).
8. Olson, W. *et al.* Sparse genetic tracing reveals regionally specific functional organization of mammalian nociceptors. *Elife* **6**, 1–26 (2017).
9. Purpura, D. P. & Baker, H. J. Meganeurites and other aberrant processes of neurons in feline GM1-gangliosidosis: A golgi study. *Brain Res.* **143**, 13–26 (1977).
10. Walkley, S. U., Wurzelmann, S. & Purpura, D. P. Ultrastructure of neurites and meganeurites of cortical pyramidal neurons in feline gangliosidosis as revealed by the combined Golgi-EM technique. *Brain Res.* **211**, 393–398 (1981).
11. Sandhoff, K. & Harzer, K. Gangliosides and gangliosidoses: Principles of molecular and metabolic pathogenesis. *J. Neurosci.* **33**, 10195–10208 (2013).
12. Purpura, D. P., Pappas, G. D. & Baker, H. J. Fine structure of meganeurites and secondary growth processes in feline GM1-gangliosidosis. *Brain Res.* **143**, 1–12 (1978).
13. Walkley, S. U., Baker, H. J. & Rattazzi, M. C. Initiation and growth of ectopic neurites and meganeurites during postnatal cortical development in ganglioside storage disease. *Dev. Brain Res.* **51**, 167–178 (1990).
14. Sango, K. *et al.* Mouse models of Tay–Sachs and Sandhoff diseases differ in neurologic phenotype and ganglioside metabolism. *Nat. Genet.* **11**, 170–176 (1995).
15. Leinekugel, P., Michel, S., Conzelmann, E. & Sandhoff, K. Quantitative correlation between the residual activity of β-hexosaminidase A and arylsulfatase A and the severity of the resulting lysosomal storage disease. *Hum. Genet.* **88**, 513–523 (1992).
16. Ogawa, Y. *et al.* Improvement in dysmyelination by the inhibition of microglial activation in a mouse model of Sandhoff disease. *Neuroreport* **29**, 962–967 (2018).
17. Hirai, H. *et al.* Cbln1 is essential for synaptic integrity and plasticity in the cerebellum. *Nat. Neurosci.* **8**, 1534–1541 (2005).
18. Ibata, K. *et al.* Activity-Dependent Secretion of Synaptic Organizer Cbln1 from Lysosomes in Granule Cell Axons. *Neuron* **102**, 1184-1198.e10 (2019).
19. Price, T. J. & Flores, C. M. Critical Evaluation of the Colocalization Between Calcitonin Gene-Related Peptide, Substance P, Transient Receptor Potential Vanilloid Subfamily Type 1 Immunoreactivities, and Isolectin B4 Binding in Primary Afferent Neurons of the Rat and Mouse. *J. Pain* **8**, 263–272 (2007).
20. Usoskin, D. *et al.* Unbiased classification of sensory neuron types by large-scale single-cell RNA sequencing. *Nat. Neurosci.* **18**, 145–153 (2015).
21. McNeill, D. L., Coggeshall, R. E. & Carlton, S. M. A light and electron microscopic study of calcitonin gene-related peptide in the spinal cord of the rat. *Exp. Neurol.* **99**, 699–708 (1988).

22. Zylka, M. J., Rice, F. L. & Anderson, D. J. Topographically distinct epidermal nociceptive circuits revealed by axonal tracers targeted to Mrgprd. *Neuron* **45**, 17–25 (2005).
23. Ribeiro-Da-Silva, A. & Coimbra, A. Two types of synaptic glomeruli and their distribution in laminae I–III of the rat spinal cord. *J. Comp. Neurol.* **209**, 176–186 (1982).
24. Cavanaugh, D. J. *et al.* Distinct subsets of unmyelinated primary sensory fibers mediate behavioral responses to noxious thermal and mechanical stimuli. *Proc. Natl. Acad. Sci. U. S. A.* **106**, 9075–80 (2009).
25. Bailey, A. L. & Ribeiro-Da-Silva, A. Transient loss of terminals from non-peptidergic nociceptive fibers in the substantia gelatinosa of spinal cord following chronic constriction injury of the sciatic nerve. *Neuroscience* **138**, 675–690 (2006).
26. Goldstein, I. J. & Winter, H. G. The Griffonia simplicifolia I-B4 isolectin. A probe for alpha-D-galactosyl end groups. *Subcell. Biochem.* **32**, 127–41 (1999).
27. Fullmer, J. M., Riedl, M. S., Higgins, L. & Elde, R. Identification of some lectin IB4 binding proteins in rat dorsal root ganglia. *Neuroreport* **15**, 1705–1709 (2004).
28. Fullmer, J. H., Riedl, M., Williams, F. G., Sandrin, M. & Elde, R. Enzymes that synthesize the IB4 epitope are not sufficient to impart IB4 binding in dorsal root ganglia of rat. *J. Comp. Neurol.* **501**, 70–82 (2007).
29. Svennerholm, L. *et al.* Gangliosides and allied glycosphingolipids in human peripheral nerve and spinal cord. *Biochim. Biophys. Acta (BBA)/Lipids Lipid Metab.* **1214**, 115–123 (1994).
30. Chiba, A., Kusunoki, S., Obata, H., Machinami, R. & Kanazawa, I. Ganglioside composition of the human cranial nerves, with special reference to pathophysiology of Miller Fisher syndrome. *Brain Res.* **745**, 32–36 (1997).
31. Gorski, J. A., Zeiler, S. R., Tamowski, S. & Jones, K. R. Brain-derived neurotrophic factor is required for the maintenance of cortical dendrites. *J. Neurosci.* **23**, 6856–6865 (2003).
32. Jennemann, R. *et al.* Cell-specific deletion of glucosylceramide synthase in brain leads to severe neural defects after birth. *Proc. Natl. Acad. Sci.* **102**, 12459–12464 (2005).
33. Reichel, J. M. *et al.* Beware of your Cre-Ation: lacZ expression impairs neuronal integrity and hippocampus-dependent memory. *Hippocampus* **26**, 1250–1264 (2016).
34. Dembo, T., Braz, J. M., Hamel, K. A., Kuhn, J. A. & Basbaum, A. I. Primary Afferent-Derived BDNF Contributes Minimally to the Processing of Pain and Itch. *eneuro* **5**, ENEURO.0402-18.2018 (2018).
35. Russo, D. *et al.* Glycosphingolipid metabolic reprogramming drives neural differentiation. *EMBO J.* **37**, e97674 (2018).
36. Cavanaugh, D. J. *et al.* Restriction of Transient Receptor Potential Vanilloid-1 to the Peptidergic Subset of Primary Afferent Neurons Follows Its Developmental Downregulation in Nonpeptidergic Neurons. *J. Neurosci.* **31**, 10119–10127 (2011).
37. Gordon, A. *et al.* Expression of Cntnap2 (Caspr2) in multiple levels of sensory systems. *Mol. Cell. Neurosci.* **70**, 42–53 (2016).
38. Hu, C. *et al.* A useful transgenic mouse line for studying the development of spinal nociceptive circuits. *Neurosci. Lett.* **450**, 211–216 (2009).
39. Vastani, N. *et al.* Impaired nociception in the diabetic Ins2 +/Akita mouse. *Diabetes* **67**, 1650–1662 (2018).
40. Vriens, J. *et al.* TRPM3 Is a Nociceptor Channel Involved in the Detection of Noxious Heat. *Neuron* **70**, 482–494 (2011).
41. Vandewauw, I. *et al.* A TRP channel trio mediates acute noxious heat sensing. *Nature* **555**, 662–666 (2018).
42. Emery, E. C. *et al.* In vivo characterization of distinct modality-specific subsets of somatosensory neurons using GCaMP. *Sci. Adv.* **2**, e1600990–e1600990 (2016).
43. Chisholm, K. I., Khovanov, N., Lopes, D. M., La Russa, F. & McMahon, S. B. Large scale in vivo recording of sensory neuron activity with GCaMP6. *eNeuro* **5**, e0417-17.2018 1–14

(2018).
44. Wang, F. *et al.* Sensory Afferents Use Different Coding Strategies for Heat and Cold. *Cell Rep.* **23**, 2001–2013 (2018).
45. Tan, C. H. & McNaughton, P. A. The TRPM2 ion channel is required for sensitivity to warmth. *Nature* **536**, 460–463 (2016).
46. Vriens, J., Nilius, B. & Voets, T. Peripheral thermosensation in mammals. *Nature Reviews Neuroscience* **15**, 573–589 (2014).
47. Caterina, M. J. *et al.* Impaired nociception and pain sensation in mice lacking the capsaicin receptor. *Science (80-.).* **288**, 306–313 (2000).
48. Zheng, Y. *et al.* Deep Sequencing of Somatosensory Neurons Reveals Molecular Determinants of Intrinsic Physiological Properties. *Neuron* **103**, 1–19 (2019).
49. Calvo, M. *et al.* Altered potassium channel distribution and composition in myelinated axons suppresses hyperexcitability following injury. *Elife* **5**, 1–26 (2016).
50. Glazebrook, P. A. *et al.* Potassium channels Kv1.1, Kv1.2 and Kv1.6 influence excitability of rat visceral sensory neurons. *J. Physiol.* **541**, 467–482 (2002).
51. Chi, X. X. & Nicol, G. D. Manipulation of the potassium channel Kv1.1 and its effect on neuronal excitability in rat sensory neurons. *J. Neurophysiol.* **98**, 2683–2692 (2007).
52. El-Brolosy, M. A. *et al.* Genetic compensation triggered by mutant mRNA degradation. *Nature* **568**, 193–197 (2019).
53. Ma, Z. *et al.* PTC-bearing mRNA elicits a genetic compensation response via Upf3a and COMPASS components. *Nature* **568**, 259–263 (2019).
54. Wang, H., Kunkel, D. O., Schwartzkroin, P. A. & Tempel, B. L. Localization of Kv1.1 and Kv1.2, two K channel proteins, to synaptic terminals, somata, and dendrites in the mouse brain. *J. Neurosci.* **14**, 4588–4599 (1994).
55. Brew, H. M., Hallows, J. L. & Tempel, B. L. Hyperexcitability and reduced low threshold potassium currents auditory neurons of mice lacking the channel subunit Kv1.1. *J. Physiol.* **548**, 1–20 (2003).
56. Akhtar, S., Shamotienko, O., Papakosta, M., Ali, F. & Oliver Dolly, J. Characteristics of brain Kv1 channels tailored to mimic native counterparts by tandem linkage of α subunits. Implications for K+ channelopathies. *J. Biol. Chem.* **277**, 16376–16382 (2002).
57. Grupe, A. *et al.* Cloning and expression of a human voltage-gated potassium channel. A novel member of the RCK potassium channel family. *EMBO J.* **9**, 1749–1756 (1990).
58. Imperial, J. S. *et al.* A novel conotoxin inhibitor of Kv1.6 channel and nAChR subtypes defines a new superfamily of conotoxins. *Biochemistry* **45**, 8331–8340 (2006).
59. Imperial, J. S. *et al.* Tyrosine-rich conopeptides affect voltage-gated K+ channels. *J. Biol. Chem.* **283**, 23026–23032 (2008).
60. Leipold, E. *et al.* Subtype-specific block of voltage-gated K+ channels by μ-conopeptides. *Biochem. Biophys. Res. Commun.* **482**, 1135–1140 (2017).
61. Cordeiro, S. *et al.* Conotoxin κM-RIIIJ, a tool targeting asymmetric heteromeric Kv1 channels. *Proc. Natl. Acad. Sci. U. S. A.* **116**, 1059–1064 (2019).
62. Madrid, R., De La Peña, E., Donovan-Rodriguez, T., Belmonte, C. & Viana, F. Variable threshold of trigeminal cold-thermosensitive neurons is determined by a balance between TRPM8 and Kv1 potassium channels. *J. Neurosci.* **29**, 3120–3131 (2009).
63. West, S. J. & Bennett, D. L. StereoMate: A Stereological and Automated Analysis Platform for Assessing Histological Labelling in Cleared Tissue Specimens. *bioRxiv* 648337 (2019). doi:10.1101/648337

Appendix

Antibodies

Antigen	Host / Conjugate	Source / RRID	Dilution	Used in:
		Primary Antibodies		
ATF3	Rabbit	Santa Cruz (sc188) RRID: AB_2258513	1:500	Ch.4, Ch.5
β-III tubulin	Mouse	Sigma-Aldrich (T8578) RRID: AB_1841228	1:500	Ch.5
β-gal (*E.coli*)	Chicken	Abcam (ab9361) RRID: AB_307210	1:500	Ch.2, Ch.4, Ch.5, Ch.6
CGRP	Sheep	Enzo Life Sciences (BML-CA1137) RRID: AB_2050885	1:500	Ch.2, Ch.4, Ch.5
CGRP	Rabbit	Peninsula Laboratories (T-4032) RRID: AB_2313775	1:500	Ch.6
IB4	(biotinylated)	Sigma-Aldrich (LT-2140) RRID: AB_2313663	1:200	Ch.2, Ch.4, Ch.5, Ch.6
FLAG	Rabbit	Sigma-Aldrich	1:500	Ch.2
GFAP	Mouse	Sigma-Aldrich	1:500	Ch.5
Glutamine Synthetase	Rabbit	Sigma-Aldrich (G2781) RRID: AB_259853	1:1000	Ch.2
Homer1	Goat	Frontier Institute RRID: AB_2631104	1:500	Ch.5
IBA1	Rabbit	Abcam (ab178847)	1:500	Ch.5
NeuN	Chicken	Millipore (ABN91) RRID: AB_11212808	1:500	Ch.2, Ch.4, Ch.5
NeuN	Rabbit	Abcam (ab177487) RRID: AB_2532109	1:500	Ch.5
Neurotrace (red)	n/a	Life Technology (N21482) RRID: AB_2620170	1:100	Ch.4, Ch.5
Neurotrace (blue)	n/a	Life Technology (N21479)	1:100	Ch.4
NF200	Mouse	Sigma-Aldrich (N-0142) RRID: AB_477257	1:500	Ch.2, Ch.4
PAX2	Rabbit	ThermoFisher Scientific (71-6000) RRID: AB_2533990	1:200	Ch.5
PGP9.5	Rabbit	Ultraclone (discontinued)	1:500	Ch.4
Synaptophysin	Rabbit	Frontier Institute RRID: AB_2571842	1:500	Ch.5
TH	Sheep	Millipore (AB1542) RRID: AB_90755	1:200	Ch.2, Ch.4

Antigen	Host / Conjugte	Source	Dilution	RRID
		Secondary Antibodies		
Biotin	Streptavidin / Pacific Blue	ThermoFisher Scientific (S11222)	1:500	
Chicken IgG	Goat / Alexa488	ThermoFisher Scientific (A-11039)	1:500	AB_253409
Chicken IgG	Goat / Alexa546	ThermoFisher Scientific (A-11040)	1:500	AB_2534097
Goat IgG	(biotinylated)	Vector Laboratories (BA-9500)	1:200	AB_2336123
Mouse IgG	Goat / Pacific Blue	ThermoFisher Scientific (P-31582)	1:500	AB_10374586
Mouse IgG	Donkey / Alexa488	ThermoFisher Scientific (A-21202)	1:500	AB_141607
Rabbit IgG	Donkey / Cy3	Jackson Immunoresearch Labs (711-166-152)	1:500	AB_2313568
Rabbit IgG	Donkey / Alexa488	ThermoFisher Scientific (A-21206)	1:500	AB_2535792
Rabbit IgG	Goat / Pacific Blue	ThermoFisher Scientific (P-10994)	1:500	AB_2539814
Sheep IgG	Donkey / Alexa488	ThermoFisher Scientific (A-11015)	1:500	AB_2534082

RT-qPCR Primers

Gene	Description	Fwd (5'-3')	Rev (5'-3')	Used in:
Kcna6 #1	Coding sequence	TGGCGAGGATGAGAAACCAC	TACTGAGACGATGGCGATGC	Ch.2
Kcna6 #2	Coding sequence	CCAGCTTCGACGCTATCCTT	TGGTTTCTCATCCTCGCCAC	Ch.2
Kcna6 #3	Exon-spanning	TCTTGCCTCTGAGGGTTGTG	CGGCTGAGTTATTCAGTGGGG	Ch.3
Kcna1	Exon-spanning	TTACCCTGGGCACGGAGATA	ACACCCTTACCAAGCGGATG	Ch.2
Kcna2	Exon-spanning	CATCTGCAAGGGCAACGTCAC	CCTTTGGAAGGAAGGAGGCA	Ch.2
Hprt1	Exon-spanning	GTCCTGTGGCCATCTGCCTAG	TGGGGACGCAGCAACTGACA	Ch.2, Ch.3
Gapdh	Exon-spanning	TGTGTCCGTCGTGGATCTGA	TTGCTGTTGAAGTCGCAGGAG	Ch.2